C. ELEGANS AS A PLATFORM TO CHARACTERIZE GENES AND THERAPEUTICS AFFECTING GENOME STABILITY

by

Bin Ye

B.Sc., Xiamen University, 2014

A THESIS SUBMITTED IN PARTIAL FULFILLMENT OF

THE REQUIREMENTS FOR THE DEGREE OF

DOCTOR OF PHILOSOPHY

in

THE FACULTY OF GRADUATE AND POSTDOCTORAL STUDIES

(Genome Science and Technology)

THE UNIVERSITY OF BRITISH COLUMBIA

(Vancouver)

December 2019

The following individuals certify that they have read, and recommend to the Faculty of Graduate and Postdoctoral Studies for acceptance, the dissertation entitled:

C. elegans as a platform to characterize genes and therapeutics affecting genome stability

submitted by Bin Ye in partial fulfillment of the requirements for

the degree of Doctor of Philosophy

in Genome Science and Technology

Examining Committee:

Philip Hieter, Medical Genetics
Supervisor

Stefan Taubert, Medical Genetics
Supervisory Committee Member

Michel Roberge, Biochemistry & Molecular Biology
Supervisory Committee Member

Peter Lansdorp, Medical Genetics
University Examiner

Don Moerman, Zoology
University Examiner

Additional Supervisory Committee Members:

Samuel Aparicio, Pathology
Supervisory Committee Member

Supervisory Committee Member

ABSTRACT

Genome stability is essential for survival in all living organisms. Perturbations of genome stability can lead to cancer and other diseases in human. Dysfunction of genome care-taking genes and exposure to external genotoxins are the two major drivers of genomic instability. Here, we used a model organism, *C. elegans* to study these factors and how they interact to affect genome stability. We first generated a chemi-genetic interaction map as a preliminary reference for characterizing genes and agents. From there, we elucidated the mechanisms of action for an emerging anticancer therapeutic CX-5461. CX-5461 turned out to be a multi-modal agent that exhibits genotypic sensitivity, mutagenicity and photosensitivity. Next, we identified a few genetic interactions within and between double-strand break repair pathways in *C. elegans*, which have implications in the response to both endogenous and exogenous DNA damage. We also characterized a less-understood gene SMRC-1, an annealing helicase. Loss of SMRC-1 results in copy number variations, and SMRC-1 is synthetic lethal with a number of DNA damage response genes. Our work concludes that *C. elegans* is a great platform to untangle the sophisticated complexity in genome maintenance, and provide meaningful insights for prospective anticancer therapeutic development.

LAY SUMMARY

It is critical for all living organisms to faithfully maintain and pass down genetic information encoded in their DNA. This involves a mechanism called genome stability maintenance. Failure to maintain genome stability can lead to dire consequences, such as cancers in human. Here, we are using the nematode worm to study factors that can affect this mechanism. Many genes that function in worms have similar roles in humans, and worms are easier to maneuver, making them a great platform for biomedical research. In this study, we characterized genes and therapeutics that can affect genome stability maintenance and how these two factors interact. This provides insights that can shed light on future development of anticancer therapy.

PREFACE

Part of the research described in Chapter 3 was published in "Hong Xu, Marco Di Antonio, Steven McKinney, Veena Mathew, Brandon Ho, Nigel J. O'Neil, Nancy Dos Santos, Jennifer Silvester, Vivien Wei, Jessica Garcia, Farhia Kabeer, Daniel Lai, Priscilla Soriano, Judit Banath, Derek S. Chiu, Damian Yap, Daniel D. Le, Frank B. Ye, Anni Zhang, Kelsie Thu, John Soong, Shu-chuan Lin, Angela Hsin Chin Tsai, Tomo Osako, Teresa Algara, Darren N. Saunders, Jason Wong, Jian Xian, Marcel B. Bally, James D. Brenton, Grant W. Brown, Sohrab P. Shah, David Cescon, Tak W. Mak, Carlos Caldas, Peter C. Stirling, Phil Hieter, Shankar Balasubramanian & Samuel Aparicio (2017). CX-5461 is a DNA G-quadruplex stabilizer with selective lethality in BRCA1/2 deficient tumours. Nature communications *8*, 14432". The paper was designed and written by Dr. Hong Xu, Dr. Marco Di Antonio, Dr. Veena Mathew, Dr. Nigel J. O'Neil, Dr. Sohrab P. Shah, and Dr. Samuel Aparicio. Frank Bin Ye contributed to the *C. elegans* experiments in the paper, and a small fraction of Figure 2.2 was used to generate figures in the publication.

The research described in Chapter 2 and 3 will be submitted as "Frank B. Ye, Akil Hamza, Tejomayee Singh, Stephane Flibotte, Samuel Aparicio, Philip Hieter, Nigel J. O'Neil. *C. elegans* as a platform to characterize the anti-cancer therapeutic CX-5461". The paper was designed and co-written by Frank Bin Ye, Dr. Nigel J. O'Neil and Dr. Philip Hieter. Frank Bin Ye performed most of the experiments. Dr. Stephane Flibotte performed the bioinformatic analysis on sequencing data. Dr. Akil Hamza performed the yeast experiments, and Tejomayee Singh performed the mammalian cell experiments.

The research described in Chapter 4 and 5 was designed and performed mostly by Frank Bin Ye, and will be submitted for two future publications. The bioinformatic analysis of sequencing data was performed by Dr. Stephane Flibotte.

TABLE OF CONTENTS

LIST OF TABLES

LIST OF FIGURES

LIST OF ABBREVIATIONS & ACRONYMS

ATM	Ataxia telangiectasia mutated
ATR	Ataxia telangiectasia and RAD3-related
BTR	BLM–RMI–TOP3α
CDK	Cyclin-dependent kinase
CNV	Copy number variation
CPT	Camptothecin
CRISPR	Clustered regularly interspaced short palindromic repeats
DAPI	4',6-diamidino-2-phenylindole dihydrochloride
DDA	DNA damaging agent
Del	Deletion
DMSO	Dimethyl sulfoxide
DNA	Deoxyribonucleic acid
DNA-PK	DNA-dependent protein kinase
DSB	Double-strand break
dsDNA	Double-stranded DNA
Dup	Duplication
EMS	Ethyl methanesulfonate
ENU	N-ethyl-N-nitrosourea
ETOP	Etoposide
FA	Fanconi anemia
FS	Frame shift
G4	G quadruplex
GG-NER	Global genome nucleotide excision repair
H_2DCFDA	2',7'-dichlorodihydrofluorescein diacetate
HDR	Homology-directed repair
Him	High incidence of males
HPRT	Hypoxanthine phosphorybosyl transferase
IC50	Half maximal inhibitory concentration

ICL	Interstrand crosslink
IDL	Insertion/deletion loop
Inv	Inverstion
M-Z-	Maternally negative and zygotically negative
M+Z-	Maternally positive and zygotically negative
MBN	Mung bean nuclease
MGMT	O^6-methylguanine-DNA methyltransferase
MH	Microhomology
MMEJ	Microhomology-mediated end joining
MMP	Million mutation project
MMR	Mismatch repair
MNM	Multi-nucleotide mutation
NER	Nucleotide excision repair
NGI	Negative genetic interaction
NGM	Nematode growth media
NHEJ	Non-homologous end joining
Ola	Olaparib
PARP	Poly (ADP-ribose) polymerase
PCR	Polymerase chain reaction
ROS	Reactive oxygen species
SDSA	Synthesis dependent strand annealing
SEM	Standard error of the mean
shRNA	Small hairpin RNA
SIOD	Schimke immuno-osseous dysplasia
SL	Synthetic lethality or synthetic lethal
SNV	Single nucleotide variation
SS	Synthetic sickness of synthetic sick
SSB	Single-strand break
ssDNA	Single-stranded DNA

TC-NER	Transcription-coupled nucleotide excision repair
TFIIH	Transcription factor II H
TLS	Translesion synthesis
TMP	Trimethylpsoralen
Trans	Translocation
UV	Ultra-violet
WT	Wild-type

ACKNOWLEDGEMENTS

I thank my supervisor Dr. Philip Hieter for his guidance, support and patience during my graduate studies. I am deeply indebted to Dr. Nigel O'Neil for his generous mentorship, which was crucial to my graduate training.

I thank my committee members, Dr. Samuel Aparicio, Dr. Stefan Taubert, and Dr. Michel Roberge. Their scientific input and suggestions were helpful for my thesis.

I thank all the members in Hieter Lab, present and past, Dr. Melanie Bailey, Dr. Akil Hamza, Leanne Amitzi, Tejomayee Singh, Rafaela Marodin, Anthony Oppedisano, Walid Omar, Maureen Driessen, Dr. Supipi Duffy, Megan Kofoed, Sidney Ang, and Sivan Reytan. I am grateful for the fun and chats that helped me get through my graduate study.

I also thank the friends I have met in Vancouver and Canada that made my graduate study experience a memorable one.

I acknowledge scholarship support from the Genome Science and Technology Program, Mitacs Inc., St John's College, and the University of British Columbia.

Thanks to my parents for their enduring support throughout the degree.

DEDICATION

To my parents for their continual support.

CHAPTER 1: INTRODUCTION

1.1 Genome stability and cancer

Mechanisms that ensure genome stability are critical for the faithful transmission of genetic information to daughter cells upon cell division. To maintain genome stability, organisms have evolved a complex maintenance system to safeguard and protect the genome against both endogenous and exogenous factors that could affect its integrity. Genome integrity is essential for normal cell growth and development, and the perturbation of genome stability can lead to cancer and other diseases (Aguilera and Garcia-Muse, 2013; Jeggo et al., 2016; Negrini et al., 2010).

An increasing body of evidence supports genome instability as an enabling characteristic of carcinogenesis (Hanahan and Weinberg, 2011). Genome instability drives genetic diversity by the sequential accumulation of genetic alterations. These genetic alterations range from structural and numerical chromosomal changes, which result in partial gain or loss of chromosomes and chromosomal rearrangements, to single nucleotide variations at the base level. These genetic alterations increase the probability of acquiring a set of mutations that promote tumor initiation and development (Sieber et al., 2003; Stratton et al., 2009).

Genome instability enables cancer cell evolution, but there is a limit to the amount of genome instability that cancer cells can withstand (Andor et al., 2017). This is because cancer cells have a reduced set or downregulation of genome maintenance genes, which in effect represents a sub-lethal loss-of-function of processes that in aggregate are essential for cell viability (Helleday et al., 2008; Jeggo et al., 2016). Cancer cells are often sensitized to DNA damaging agents that

further increase genomic instability (Cheung-Ong et al., 2013). For example, the platinum-based compounds such as cisplatin, can crosslink DNA and cause DNA lesions (Deans and West, 2011). Cancer cells defective in homology-directed repair (HDR) are unable to resolve cisplatin-induced DNA damage which results in cell death (Helleday, 2010). Therefore, genome instability drives tumorigenesis but it can also be exploited for anticancer treatment.

The key to providing more informed anticancer therapy is a better understanding of the causes and effects of genome instability. Although it is not always clear how genome instability arises, dysfunction of genome maintenance genes and exposure to external genotoxins are two major causes of genomic instability (Aguilera and Garcia-Muse, 2013). Therefore, characterizing how genome stability genes and genotoxic agents affect genome stability is crucial to the development of anticancer strategies.

1.2 Genes that Affect Genome Stability

Cells have a sophisticated system dedicated to maintaining genome stability involving a plethora of interconnected genes. These genes encompass a wide range of biological processes, from maintaining normal DNA metabolism, responding to DNA damage, to mediating the segregation of chromosomes to daughter cells during cell division. This thesis focuses on those genes required for normal DNA metabolism and the DNA damage response. Here, we catalog some of the genes and processes that were investigated as part of this thesis and provide brief phenotypic descriptions of relevant mutations in the model organism *Caenorhabditis elegans.*

1.2.1 DNA metabolism genes

Under normal conditions, many genes are required for DNA metabolism, such as DNA replication and transcription. These genes encode protein products that are directly involved in replication and transcription, such as helicases and polymerases, as well as genes that regulate replication and transcription, such as chromatin modifiers. Disrupting these genes often has a negative effect on DNA metabolism. For example, defects in polymerase can result in a compromised fidelity of replication, while loss of certain helicases can increase the risk of mutations (London et al., 2008). Among DNA metabolism genes, many have been found dysregulated in cancer. For instance, many cancers have upregulated RecQ-family helicases (Futami et al., 2010; Su et al., 2010), making them potential biomarkers and targets for anticancer drugs.

1.2.2 DNA damage response genes

DNA damage response genes safeguard the genome by counteracting DNA damage, which if not resolved could lead to genome instability. In most cases, the response to DNA damage is a multi-step process: recognition of damage, cell cycle arrest, repair or bypass of lesions, activation of apoptosis if the damage cannot be repaired, and restart of the cell cycle. Perturbation of any step in the DNA damage response could affect the resolution of DNA lesions and contribute to genome instability.

DNA damage checkpoints

DNA damage checkpoints initiate a cascade of signalling responses in response to DNA damage. DNA damage checkpoint genes initiate cell cycle arrest and activate and recruit DNA repair proteins to sites of DNA damage. Two major DNA damage checkpoint pathways are ataxia

telangiectasia mutated (ATM)-dependent signalling and ataxia telangiectasia and RAD3-related (ATR)-dependent signaling. Both ATM and ATR can regulate cyclin-dependent kinases (CDKs) to arrest the cell cycle to allow time for DNA repair proteins to resolve the damage (Blackford and Jackson, 2017; Yang et al., 2003). If DNA damage exceeds the ability to repair, cells activate p53-dependent apoptosis (Nowsheen and Yang, 2012). In *C. elegans,* ATM-1 and ATR-1 are activated in response to replication stress or double-strand breaks to induce cell cycle arrest (Garcia-Muse and Boulton, 2005). ATM-1 and ATR-1 also play a role in regulating the resolution of meiotic crossovers in *C. elegans* (Li and Yanowitz, 2019). Loss of *atm-1* in *C. elegans* results in genome instability and telomeric defects (Jones et al., 2012).

DNA repair pathways

Cells have a number of DNA repair pathways that respond to different types of DNA lesions to maintain genome stability and fidelity (Ciccia and Elledge, 2010). Homology-directed repair (HDR), non-homologous end joining (NHEJ), and microhomology-mediated end joining (MMEJ) respond to double-strand breaks (DSBs) (Ceccaldi et al., 2016a). Nucleotide excision repair (NER) removes bulky lesions such as thymine dimers and photoproducts (Marteijn et al., 2014). The Fanconi Anemia (FA) repair pathway resolves DNA interstrand crosslinks (Deans and West, 2011). Here, we give a brief overview of the different DNA repair pathways.

1.2.3 DNA repair pathways

Nucleotide excision repair (NER)

NER can repair a wide range of DNA lesions that alter DNA structure, such as bulky chemical adducts, Ultra-violet (UV)-induced thymine dimers and interstrand crosslinks. There are two kinds of NER, global genome NER (GG-NER) and transcription-coupled NER (TC-NER). The

two kinds of NER differ in how the lesions are first recognized. In GG-NER, the lesion is detected by XPC, a protein that binds to distorted DNA (Sugasawa et al., 2001), whereas in TC-NER, the lesion stalls RNA polymerase II, which then recruits a number of proteins, including CSA, CSB and XPA (Marteijn et al., 2014). Then, XPC or XPA recruits the transcription factor II H (TFIIH) complex, and the two helicases within TFIIH further open up the double helix containing the lesion. The strand containing the lesion is then excised by the endonucleases XPF–ERCC1 and XPG, resulting in a 22-30 nucleotide gap. The gap is filled by a DNA polymerase, which could sometimes be error-prone translesion polymerases such as POLK and POLH (Figure 1.1) (Marteijn et al., 2014; Zheng et al., 2003). In *C. elegans,* loss of NER results in hypersensitivity to UVC radiation and DNA crosslinks in a developmentally dependent manner (Astin et al., 2008; Wilson et al., 2017).

Mismatch repair (MMR)

MMR repairs mis-paired bases and insertion/deletion loops (IDLs) (Pena-Diaz and Jiricny, 2012) . The MMR pathway initiates with MutSα (MSH2-MSH6) binding to a mismatch, followed by binding MutSβ (PSM2-MLH1). Then, MutSα is activated by PCNA to incise the newly-synthesized strand, creating a nick that is further processed by exonuclease EXO1 to form a gap up to 150 bp (Kunkel and Erie, 2015; Pena-Diaz and Jiricny, 2012). The gap is filled by a DNA polymerase and a ligase (Figure 1.1). In *C. elegans,* some mismatch repair mutants exhibit genome instability and mutation accumulation (Degtyareva et al., 2002; Tijsterman et al., 2002). In contrast, the germ line-specific MutS mismatch repair mutant, *him-14* is defective in meiotic crossing over (Zalevsky et al., 1999).

Homology-directed repair (HDR)

HDR, NHEJ and MMEJ all repair DSBs. The HDR is an error-free repair pathway as it uses homologous DNA as a template for repair. HDR initiates the DSB repair by resecting the ends carried out by MRE11 and CtIP endonucleases, generating two free 3' overhangs. The free 3' overhangs can be further resected by helicases or exonucleases (i.e., CtIP, DNA2, BLM, WRN, and EXO1) (Ceccaldi et al., 2016a). The single-stranded DNA associates with the single-stranded DNA (ssDNA) binding protein RPA; this allows BRCA2-mediated recruitment of RAD51 to displace RPA and form RAD51 filaments. RAD51 filaments catalyze the search for homology and subsequent invasion into the homologous sequences on the sister chromatid or the homologous chromosome, forming a displacement D-loop. DNA synthesis occurs spanning the original break site. Finally, the D-loop is resolved by endonucleases or dissolvases such as MUS81 or the BTR complex (BLM–RMI–TOP3α) (Wright et al., 2018) (Figure 1.1). HDR is a multifaceted repair process with several steps. There are variations on how HDR can resolve the DSBs, which are dictated by the nature of the DSB and the available repair proteins. Variants include: synthesis dependent strand annealing (SDSA), break induced replication repair, and homologous recombination (Verma and Greenberg, 2016). In *C. elegans,* homologous recombination is essential for meiosis, and therefore, survival (Saito and Colaiacovo, 2017). Loss of function mutations affecting key HDR homolog genes, such as *brc-2* (*C. elegans* homolog of human BRCA2*)* and *rad-51* (*C. elegans* homolog of human RAD51*),* cannot be maintained (Alpi et al., 2003; Martin et al., 2005). However, several non-essential HDR genes can be mutated and maintained such as *brc-1* (*C. elegans* homolog of human BRCA1*), brd-1* (*C. elegans* homolog of human BARD1) and *rfs-1* (*C. elegans* homolog of human RAD51C*)*.

Non-homologous end-joining (NHEJ)

In contrast to HDR, the NHEJ pathway does not use a template to repair DSBs and therefore does not need to resect the broken DNA ends. NHEJ mediates the ligation of two non-resected blunt DNA ends. The KU70/80 heterodimer binds to the blunt DSB ends. Next, DNA-dependent protein kinases (DNA-PKs) are recruited along with other end-processing factors to keep the two ends in close proximity. Finally, the DNA ligase LIG4 catalyzes the DNA-end ligation (Panier and Boulton, 2014) (Figure 1.1). In *C. elegans,* loss of NHEJ results in sensitivity to ionizing radiation in somatic cells (Clejan et al., 2006). Inappropriate NHEJ of meiotic DSBs in the *C. elegans* germ line is prevented by the COM-1 protein, and loss of COM-1 leads to deleterious NHEJ of meiotic DSBs (Lemmens et al., 2013). This illustrates the importance of interplay between different repair pathways to ensure genome stability.

Microhomology-mediated end-joining (MMEJ)

MMEJ was discovered in recent years (Deriano and Roth, 2013). As in HDR, the MMEJ pathway requires resection of the DSB ends by MRE11 and CtIP (Truong et al., 2013). In contrast to HDR, MMEJ only requires a microhomology, which can be as small as 1 nucleotide, for DSB repair (Koole et al., 2014). When the resected ends anneal with microhomology via complementary base pairing, the flanking single-stranded regions are filled in by polymerase theta POLQ (Figure 1.1). Finally, DNA ends are ligated by DNA ligases LIG1 or LIG3 (Sfeir and Symington, 2015). Since MMEJ anneals micro-homologous sequences within the resected DSB ends before joining, this often results in deletions surrounding the original DSBs (Sfeir and Symington, 2015). In *C. elegans,* POLQ-1 is required for the interstrand crosslink (ICL) repair (Muzzini et al., 2008) and the bypass of G-quadruplex (G4) structures that form in the absence of the *C. elegans FANCJ* homolog, *dog-1* (Koole et al., 2014).

Translesion synthesis (TLS) Bypass

Translesion synthesis does not repair DNA lesions. It incorporates nucleotides opposite the site of DNA damage to allow replicative bypass at the expense of low fidelity replication. The bypass often involves several polymerase-switching processes, including the dissociation of the replicative polymerase from the replication fork, the recruitment of the TLS polymerase to the fork, and subsequent displacement of the TLS polymerase with a replicative polymerase. The switch is regulated by posttranslational modifications, such as monoubiquitylation of PCNA in response to DNA damage that displaces replicative polymerase with the TLS polymerase, and ubiqtuitylation of TLS polymerases for removal (Figure 1.1) (Friedberg et al., 2005; Zhao and Washington, 2017). TLS polymerases Rev1, Pol ζ and Pol η are conserved from yeast to human (Sale, 2013). TLS polymerases in *C. elegans* protect against a wide range of DNA damaging agents (Roerink et al., 2012).

Fanconi anemia (FA) Pathway

The FA pathway repairs DNA interstrand crosslinks by coordinating a number of different repair pathways. The canonical FA pathway starts with damage recognition by FANCM during DNA replication. FANCM mediates the regression of both replication forks and recruits the FA core complex, including FANCA, FANCB, FANCC, FANCE, FANCF, FANCG and FANCL, which then monoubiquitylates FANCD2-FANCI. Monoubiquitylated FANCD2 recruits the nucleases FAN1, MUS81 and XPF that incise both ends of the lesion on one strand, unhooking the crosslink. Following that, the nascent strand opposite to the unhooked ICL is extended by a translesion polymerase, whereas the DSB induced by the incision is repaired by HDR (Figure 1.1) (Ceccaldi et al., 2016b; Deans and West, 2011). *C. elegans* appears to lack the core complex

components but does have homologs of *FANCM*, *FANCJ* and *FANCD2-FANCI*, which when mutated result in sensitivity to interstrand crosslinking agents (Youds et al., 2009).

1.2.4 The interplay between DNA repair pathways

Different repair pathways have lesion specificity, but some pathways are functionally compensatory. For example, HDR, NHEJ and MMEJ all repair DSBs, and pathway usage depends on the nature of the DSB, the cell cycle stage, and the availability of repair templates. Much of this repair pathway choice is mediated by the antagonistic relationship between the proteins 53BP1 and BRCA1 that affects end resection (Hustedt and Durocher, 2016; Panier and Boulton, 2014). It has recently been shown that the shieldin complex acts as an effector of 53BP1 in DSB-repair pathway choice by preventing DSB end resection (Gupta et al., 2018; Noordermeer et al., 2018).

The interplay between DNA repair pathways is particularly important in cancer because repair mechanisms are often dysregulated, and the reduced replication and repair fidelity can generate greater genetic diversity. For example, upregulation of an error-prone repair mechanism like MMEJ has been found to be common in breast cancer and is associated with poor clinical outcomes (Higgins et al., 2010; Lemee et al., 2010). Dysregulated DNA repair mechanisms could result in a compromised capability to deal with intrinsic DNA lesions as well external chemical insults, which can be exploited for anticancer therapy (Nickoloff et al., 2017).

Much work has focused on exploiting the DNA damage response to treat cancer (Nickoloff et al., 2017). An emerging approach is to exploit the concept of synthetic lethality (SL). DNA repair deficiencies in cancer can be made intolerable by inhibiting parallel functional DNA repair

pathways (Chan and Giaccia, 2011; O'Neil et al., 2017). One successful example is PARP (Poly (ADP-ribose) polymerase) inhibitors, which have been approved to treat *BRCA1/2*-deficient breast and ovarian cancer patients (Lord et al., 2015; Tutt et al., 2010). The knowledge of mechanism underlying the SL between *BRCA1/2* and *PARP* is still incomplete. Early work showed that co-inhibition of two parallel repair pathways (HDR and single-strand break repair) resulted in cell death (Fong et al., 2009). More recent work argued that PARP inhibitors induced trapping of PARP on the DNA that required functional HDR to bypass (Hopkins et al., 2015).

A major challenge for targeting genome instability in tumors is that the genome instability causes tumor evolution that can rewire DNA repair pathways and acquire resistance to therapy. It has been shown that loss of factors that regulate the NHEJ repair mechanism can restore HDR and confer resistance to PARP inhibitors in Brca1-/- cells (Bouwman et al., 2010; Bunting et al., 2012; Bunting et al., 2010). Therefore, some genetic alterations provide an opportunity for anticancer therapeutic targets, while others can result in resistance. Identifying the genetic vulnerabilities that positively and negatively affect genome stability is useful for developing new therapeutic approaches.

1.3 Carcinogens and therapeutics that affect genome stability

1.3.1 Carcinogens

Cancer can also be driven by exogenous factors. These factors, also known as carcinogens, promote tumorigenesis, often by causing genetic changes or mutations though interaction with DNA. For instance, individuals that have used aristocholic acid as part of traditional medicine are at high risk of liver and urothelial cancers, as aristocholic acid can form covalent bonds with

DNA resulting in mutagenic lesions and genome instability (Arlt et al., 2002; Rosenquist and Grollman, 2016). Other nonchemical carcinogens, such as X-rays, or ultraviolet light, can also produce DNA damage, which if not appropriately resolved could result in mutations.

1.3.2 Therapeutics

Counterintuitively, many anticancer therapeutics used to treat cancer patients negatively affect genome stability. The mutagenic activity of an anticancer therapeutic can be either its primary mode-of-action or a side-effect (Allan and Travis, 2005). Cancer cells often have DNA damage response or cell cycle regulatory defects that make them more sensitive to DNA damaging agents. This can result in a greater therapeutic index for DNA damaging agents in cancer cells compared to non-cancer cells. Consideration of the mutagenic effects of therapeutics is critical in developing anticancer strategies because these mutagenic therapeutics increase the risk of developing a secondary cancer in patients. One example is Hodgkin lymphoma patients, who have an increased chance of developing lung cancer after they receive ionizing radiation for treatment (Gilbert et al., 2003). In particular, ionizing radiation generates DSBs, which are toxic to cells, making it an effective anticancer treatment; however, error-prone repair of ionizing radiation-induced DSBs can create new sources of genome instability. Furthermore, the landscape of DNA repair competence can vary greatly post-treatment. Cells that escape a treatment may have developed new mutations that confer therapeutic resistance.

Although anticancer therapeutics can cause genome instability that promotes the development of secondary tumors or confers resistance, the overall benefit of DNA damaging therapeutics is evident in the wide-range of common DNA damaging anti-cancer therapeutics. Hence, the key to

improving DNA damaging therapeutics is a better understanding of how different cancer-associated genotypes respond to specific therapeutic agents to develop genotype-specific anticancer therapies that improve efficacy and eliminate or limit ineffective or harmful treatments.

1.4 Investigating genome instability

As mentioned above, genome stability is affected by intrinsic and extrinsic factors. Decades of effort have been devoted into developing platforms and methods to study the causes and effects of genome instability. In general, the causes and effects of the genome instability are conserved across species. DSBs, single nucleotide mutations, and chromosome rearrangements are common outcomes observed in bacteria to yeast to humans. In general, the processes that maintain genome stability are highly conserved. In some instances, the specific players may be different but the overall maintenance and repair processes are remarkably similar.

1.4.1 Assays for measuring genome instability: micronuclei test to HPRT assay

Assays for genome instability can be physical assays that measure chromosomal aberrations, such as the micronuclei assay which detects micronuclei formation, or the comet assay which detects DNA breaks. These assays allow direct visualization of genomic alterations events but are labor-intensive and thus challenging to conduct in a high-throughput manner. Other assays have been developed to look for phenotypic changes in colonies or cells. The most commonly used genotoxicity assay is the bacteria-based Ames test, which can assess the mutagenicity of chemicals and chemotherapeutics (Ames et al., 1973; Mortelmans and Zeiger, 2000; Wang et al., 2009). However, bacteria have different cellular conditions as compared to human cells. Despite

some conserved DNA repair pathways between bacteria and eukaryotes such as MMR, bacteria lack many genome stability maintenance mechanisms that eukaryotes use in response to a mutagen, which can result in false negatives when assessing mutagenicity. Yeast-based genotoxicity tests have been developed by taking advantage of auxotrophic selection to screen mutants that acquire genotoxin-induced mutations. These yeast-based tests can assay genotoxins that induce various genome alterations, including gene deletion, gene conversion and mitotic recombination events (Schafer et al., 2008). Furthermore, hypoxanthine phosphorybosyl transferase (HPRT) mutagenesis assay offers a genotoxicity test in mammalian cell lines (Johnson, 2012). In these cell-based tests, the clonal population that have acquired the genotoxin-induced mutations can be sequenced to elucidate the genotypes or genetic changes. However, all these assays rely largely on the generation of mutations in single reporter genes that result in detectable phenotypic changes. This severely limits the spectrum of mutations that can be detected by these methods.

1.4.2 Defining the genome stability gene spectrum

Large-scale screens have attempted to identify all the genes required for genome maintenance. Yeast has provided an excellent screening platform to identify genome maintenance genes, because of its low cost and easy manipulation as well available knockout mutant collections. A set of assays have been developed in yeast to conduct comprehensive screens for genome stability genes. In particular, these assays are able to detect increased rates of chromosome mis-segregation, gross chromosomal rearrangement, loss of heterozygosity, and gene conversion (Stirling et al., 2011; Yuen et al., 2007). Many genome maintenance genes identified in yeast screens are conserved in humans (Stirling et al., 2011; Yuen et al., 2007). Later work has

complemented the gene lists and uncovered genes that caused genome instability when overexpressed (Duffy et al., 2016). These findings have implications for developing therapeutic strategies when combined with synthetic lethal or synthetic dosage lethal screens (Duffy et al., 2016; McLellan et al., 2012).

Advances in cell culture, and RNAi-based gene knock-down approaches have made large-scale screening possible in human cancer cell lines. Large scale RNAi screens using mammalian cell lines have delineated genes and cellular processes required for genome integrity. Several have used DNA damage response markers (e.g. phospho-H2AX antibody) as a readout to identify key pathways mediating genome maintenance (Kavanaugh et al., 2015; Paulsen et al., 2009). Some screens further identified the therapeutic-sensitive and -resistant genotypes in multiple cancer cell lines (Barretina et al., 2012; Basu et al., 2013; Garnett et al., 2012). This is meaningful for better understanding the interaction between genotypes and therapeutics, and providing insights of the mechanisms of anti-cancer therapeutics and biology of genome care-taking genes. However, the complex heterogeneous genetic background of cancer cells and the inherent genome instability of these lines can confound the analysis.

Recently, the emergence of the genome-editing technology CRISPR (clustered regularly interspaced short palindromic repeats) has made it possible to conduct more powerful and complete loss-of-function genetic screens. Moreover, further advances in sequencing technology enables an economic approach to sequence the genome. CRISPR and advanced sequencing technology has accelerated the era of high-throughput genome-wide screens. For instance, a CRISPR knockout screen for resistance to the DNA Topoisomerase II inhibitor etoposide has

successfully identified *TOP2A* and *CDK6* (Wang et al., 2014), while another CRISPR screen identified new factors that mediate resistance to the PARP inhibitor olaparib (Zimmermann et al., 2018).

1.4.3 Mutational signatures

Advances in next-generation sequencing, have also made it possible to directly characterize the mutational footprints associated with genome stability, including genomic instability caused by loss of function of genome maintenance genes or by treatment with genotoxic agents. Mutational footprints are informative, because they are the visible by-products of the interactions between DNA damage and DNA repair mechanisms. Unique mutational footprints are also known as mutational signatures. Whole-genome sequencing analysis of cells or strains lacking specific repair mechanism can provide mutational signatures associated with repair deficiencies (Meier et al., 2014; Segovia et al., 2017; Serero et al., 2014). Several studies have revealed deep mutational signatures in various cancers and their association with genetic deficiencies and carcinogen exposure (Alexandrov et al., 2013; Roberts et al., 2013). These mutational signature catalogs can be informative for assigning genetic deficiencies or mutagen exposures to newly sequenced tumors. For instance, a tumor with a mutational signature containing a large number of substitutions and small insertions or deletions is likely to be defective in DNA mismatch repair, while another tumor could have a signature consistent with ultraviolet-light-induced mutations. Recently, Kucab and colleagues elucidated comprehensive mutational signatures of a number of carcinogens and anticancer therapeutics (Kucab et al., 2019). This lays the foundation for therapy-induced mutational signatures in human stem cells that provides key insights into the mechanisms of mutagenesis.

Mutational signatures are, however, limited to those that do not cause severe effects on viability. Mutational signatures involving large chromosomal alterations that result in copy number variations (CNVs) are underrepresented because large CNVs, unlike point mutations, tend to be infrequent in cell populations because of the negative selection against such deleterious genomic changes (Gordon et al., 2012). In addition, there are limitations of short read sequencing in finding large structural chromosomal alterations (Pollard et al., 2018). Nonetheless, mutational signatures provide valuable information for the understanding of DNA damaging factors in cancer etiology with potential implications for prevention and treatment.

1.5 *C. elegans* as a platform to study factors affecting genome stability

Studies in yeast and mammalian cells provide useful insights into how genes and therapeutics affect genome stability. However, there are limitations associated with yeast and mammalian cell line experiments. For instance, yeast lack many DNA damage response and repair genes such as *PARP* or *BRCA1*, and genetic heterogeneity in mammalian cell lines can confound the analysis of interactions between genotypes and therapeutics. Here, we are using a model organism, *Caenorhabditis elegans* to address these limitations. *C. elegans* is a multicellular invertebrate animal that combines the technical advantages of a microorganism (such as yeast) with greater biological complexity and a gene complement more akin to human. The nematode model was first proposed by Nobel Laureate Sydney Brenner in the early 1960s to be employed as a model for studying developmental biology and neurobiology (Goldstein, 2016). *C. elegans* feeds on bacteria and is easy and inexpensive to culture in the laboratory. *C. elegans* adults are only about 1mm long and 0.1mm in width, and it only takes three days for *C. elegans* to develop from a fertilized oocyte to a multicellular adult nematode worm. Availability of both hermaphrodites

and males makes genetic manipulations quick and simple. Over the past decades, its simplicity, small size, relatively small genome, evolutionarily conserved mechanisms, and suite of experimental tools have made *C. elegans* an instrumental platform for elucidating biological processes implicated in human diseases, including cancer (Corsi et al., 2015).

C. elegans can be used to study genes required for genome stability to gain insights into human cancer. Genome maintenance mechanisms are well conserved between *C. elegans* and human, and the majority of human genome stability-associated genes have homologs in *C. elegans*. For example, *C. elegans* homologs of the cancer-associated *BRCA1* and *BRCA2* genes have been identified and shown to be required for DNA repair, whereas no homologs are present in the yeast *S. cerevisiae* (Boulton et al., 2004; Martin et al., 2005). There are near isogenic *C. elegans* mutant strains available for most genes, including many well-characterized DNA replication and repair mutants. This provides a powerful resource for studying the biology of genome stability genes. *C. elegans* is multicellular and therefore has many more sophisticated phenotypes that can be associated with genome instability, including brood size, embryo survival, frequency of spontaneous males, and animal morphologies. There are many tools available for *C. elegans* such as genetic balancers that suppress meiotic recombination and allow for sterile or lethal mutations to be maintained. Genetic balancers can be used to capture and maintain lethal mutations (such as complex chromosomal rearrangements and CNVs) that tend to be lost in mutagenesis screens or mutational signature analysis in mammalian cells. *C. elegans* has a relatively small genome (~100Mb), and thus it is more economical to conduct deep whole-genome sequencing than mammalian cells.

C. elegans can also be used to study the effect of chemicals or environmental factors on genome stability (Craig et al., 2012; Shin et al., 2019). These assays rely on the phenotypic changes such as embryo viability or spontaneous male frequency to identify whether an agent increases genome instability. Combining chemical sensitivity studies with different genome stability mutants allows the identification of anticancer chemi-genetic interactions. This can add to the knowledge of genotypic dependencies, mechanisms of therapeutics, and insights into anticancer treatment.

C. elegans has also proven useful for determining mutational frequencies (Denver et al., 2005; Rosenbluth et al., 1983; Rosenbluth et al., 1985). There is a large body of research in *C. elegans* that has revealed distinct mutational signatures related to different carcinogens and DNA repair deficiencies (Meier et al., 2014; Meier et al., 2018; van Schendel et al., 2016). For instance, self-propagating *C. elegans* MMR mutants (*pms-2* and *mlh-1*) exhibited extremely high base substitutions and 1-bp insertions or deletions, recapitulating the mutational signatures observed in MMR-deficient cancer samples (Meier et al., 2018). Examples such as these demonstrate the evolutionary conservation between *C. elegans* and human, highlighting the potential of *C. elegans* research to gain an understanding of human diseases associated with genome stability.

A good example of the utility of *C. elegans* in exploring genome instability is the study of the *C. elegans FANCJ* homolog, *dog-1*. The *dog-1* mutants display occasional specific morphological defects, such as notched-head, molting defects, and the Dumpy phenotype (Cheung et al., 2002). These specific phenotypes were mapped, and PCR-based sequencing analysis of these *dog-1*-induced mutations revealed that all were caused by genetic alterations in poly-guanine tracts,

suggesting that DOG-1 was required to maintain poly-guanine tracts in the genome (Cheung et al., 2002). The *dog-1* mutants are sensitive to DNA damaging agents that create interstrand crosslinks (Youds et al., 2008), which is consistent with the role of the human *dog-1* homolog *FANCJ*, a member of the Fanconi Anemia repair pathway (Bridge et al., 2005). Using the genetic balancer *eT1*, a reciprocal translocation of half of chromosome III and half of chromosome V, a *dog-1*-induced mutation screen identified complex chromosomal rearrangement events and CNVs in the absence of *dog-1* (Zhao et al., 2008). These chromosomal rearrangements often resulted in lethality in mammalian cells, but were able to be maintained using *eT1* balancer in *C. elegans*. Further genetic interaction and whole-genome sequencing studies revealed that these *dog-1*-induced poly-guanine deletions were mediated by polymerase theta (Koole et al., 2014).

1.6 Research objectives

Cancer is driven by genetic and environmental factors. These genetic and environmental factors can also enhance or suppress the efficacy of anti-cancer therapeutics. Key to the adoption of targeted anticancer therapies is a better understanding of the interactions between therapeutic agents and the tumor genotype and environment. Here, we used *C. elegans* to explore how genes, therapeutics and their interactions affect genome stability. The first aim of this thesis is to generate a chemi-genetic interaction map for well-characterized therapeutics or genotoxic agents in *C. elegans* (Chapter 2), which can be used as a reference for investigating new anticancer therapeutics. We then applied the chemi-genetic interaction map to further investigate the mechanism of action for an emerging anticancer therapeutic agent, CX-5461 (Chapter 3). The second aim is to use *C. elegans* to characterize genetic interactions within and between DSB repair pathways under different conditions, since DSB repair is a process often dysregulated in

cancer (Chapter 4). The third aim is to study the biology of a less understood genome stability gene, the annealing helicase, SMRC-1 (Chapter 5). We characterized the mutational signature of loss of SMRC-1 and identified novel genetic interactions with SMRC-1.

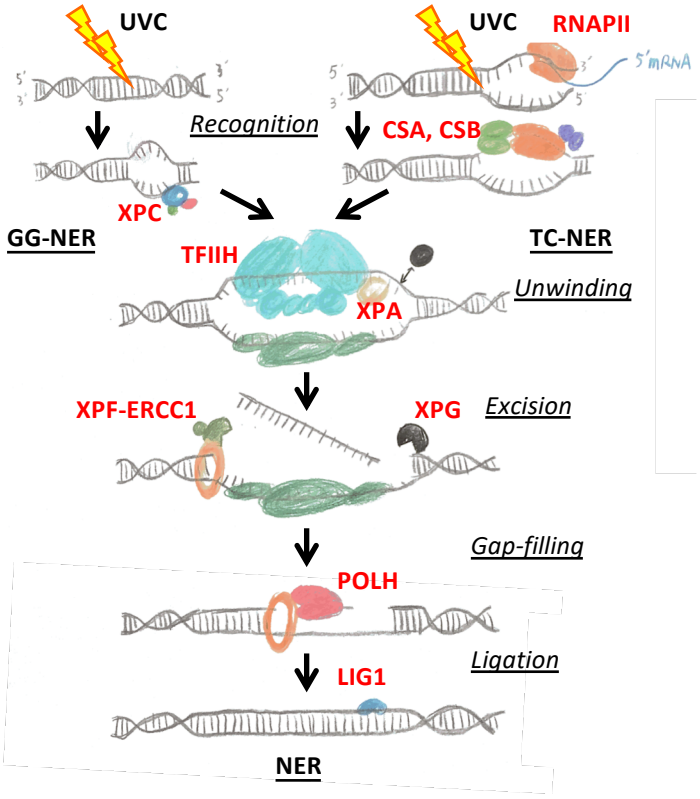
UVC
UVC
RNAPII
5'mRNA
Recognition
CSA, CSB
XPC
GG-NER
TC-NER
TFIIH
Unwinding
XPA
XPF-ERCC1
XPG
Excision
Gap-filling
POLH
Ligation
LIG1
NER

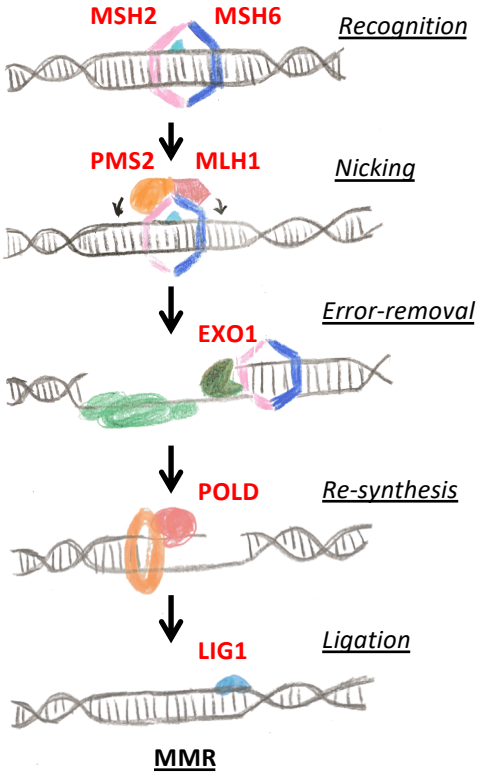
MSH2
MSH6
Recognition
PMS2
MLH1
Nicking
Error-removal
EXO1
POLD
Re-synthesis
LIG1
Ligation
MMR

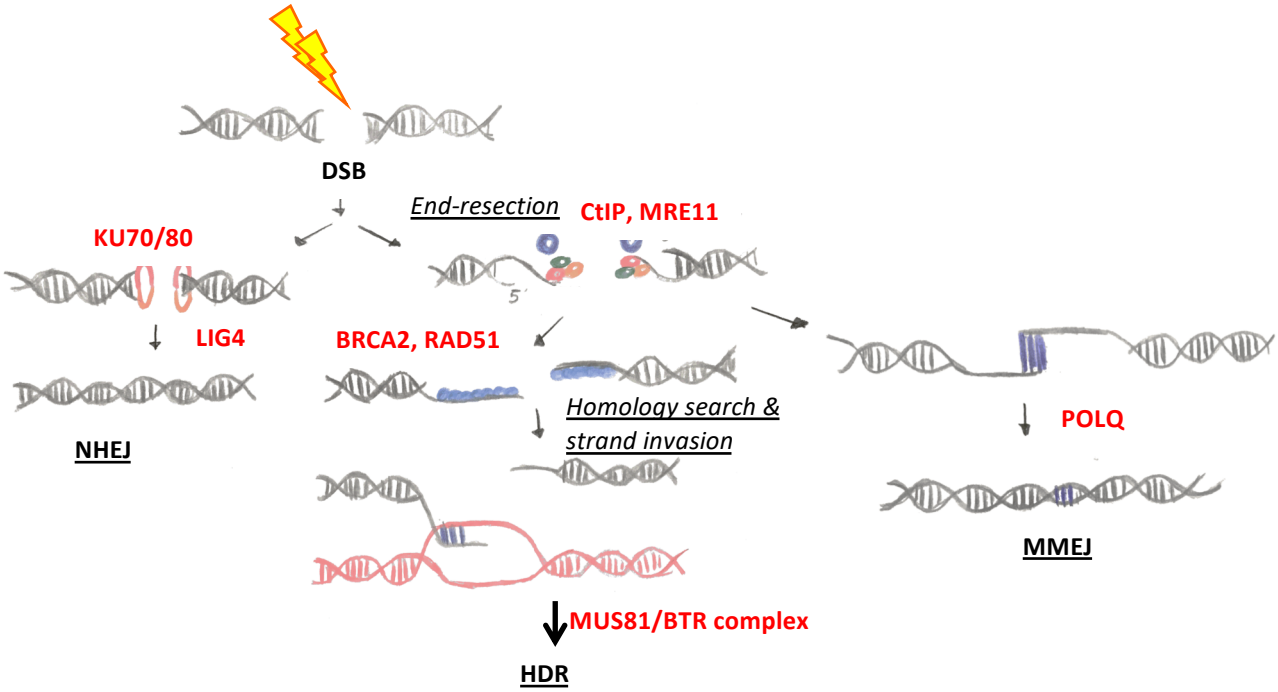
DSB
End-resection
CtIP, MRE11
KU70/80
LIG4
NHEJ
BRCA2, RAD51
Homology search &
strand invasion
POLQ
MMEJ
MUS81/BTR complex
HDR

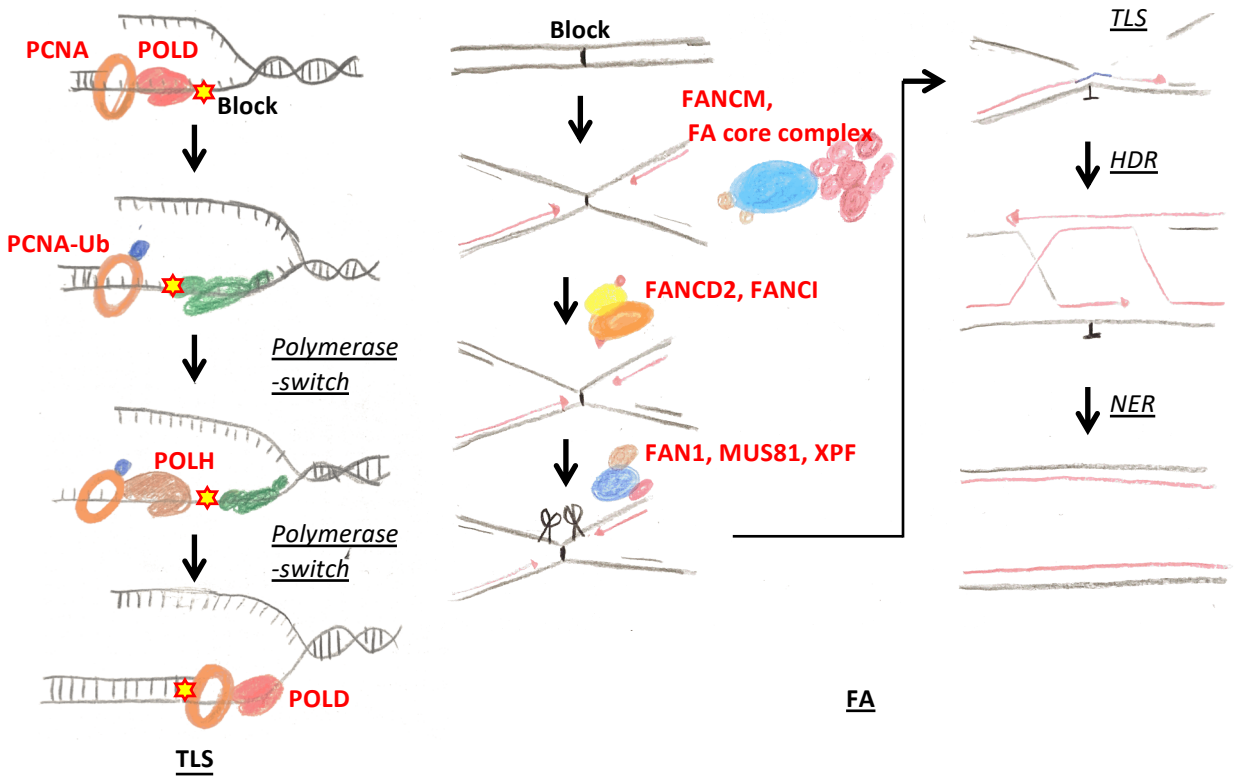

Figure 1.1 Schematics of different DNA repair pathways. See main texts for details.

CHAPTER 2: GENERATION OF A CHEMI-GENETIC INTERACTION MAP OF WELL-CHARACTERIZED DNA DAMAGING AGENTS

2.1 Introduction

Advances in genome sequencing technology are transforming cancer treatment (Hyman et al., 2017). It is now routine to identify genetic and epigenetic changes that differentiate a patient's tumor cells from non-tumor cells. Tumor-specific genetic alterations not only reveal the biological changes driving tumor progression but also uncover genetic vulnerabilities that can be exploited to selectively target the tumor with therapeutics. This means that therapeutic selection can be informed by the genetic variations in a tumor rather than tumor location. This tumor agnostic cancer treatment has the potential to offer individualized, highly specific therapies with fewer side-effects and reduce the overtreatment of tumors. Personalized oncogenomic approaches have had success treating tumors that have failed to respond to standard therapies (Laskin et al., 2015; Stockley et al., 2016; Swanton et al., 2016).

The key to successful tumor agnostic therapeutic selection is understanding how tumor-specific mutations affect the response and resistance to specific chemotherapeutic agents. Each drug or chemotherapeutic has a unique genotypic sensitivity profile and each genetic mutation exhibits a distinctive drug sensitivity profile. Most chemotherapeutic agents target the uncontrolled proliferation of cancer cells, which is often associated with loss of function of DNA replication or repair genes. Many cancer-specific alterations of DNA replication and repair genes have been identified, including *BRCA1*, *BRCA2*, and *TP53* (King et al., 2003; Olivier et al., 2010). Cells harbouring these mutations have been shown to be more responsive to certain chemotherapies (Helleday et al., 2008). While some genotype-chemotherapy connections have been identified, it

is likely that many interactions have not yet been discovered. There is a pressing need to characterize chemi-genetic interactions between chemotherapeutics and tumor-specific DNA replication and repair gene mutations. One approach to this challenge is to generate a chemi-genetic interaction map, in which each gene mutation is exposed to each chemotherapeutic and the effect on viability is quantified. A chemi-genetic interaction map connects specific gene mutations to drug sensitivity and resistance. A chemi-genetic interaction map can link chemotherapeutics to patients based on the mutations in their tumor, and can be used to characterize the mechanisms of action for chemotherapeutics. The map could also be used as a reference, so that one can compare a genotypic sensitivity profile of a less-understood agent to well characterized agents and speculate on its mechanisms of action. Similarly, one can predict the biological function of a DNA damage response gene based on the drug sensitivity profiles of the mutant.

Many efforts have been devoted to generating a genotypic sensitivity profile for DNA damaging agents in yeasts using a comprehensive gene knock-out library (Chang et al., 2002; Hanway et al., 2002). Genome-wide small hairpin RNA (shRNA) screens in cancer cell lines have been developed to uncover genes that are required for drug resistance (O'Connell et al., 2010). More recently, CRISPR-Cas9 genome-wide screens have also identified a number of genetic vulnerabilities for different drugs (Hart et al., 2015; Zimmermann et al., 2018). Although there are discrepancies between screens due to differences in the genetic backgrounds of the cell lines, it is still a useful resource to identify genetic changes that give rise to the drug sensitivity or resistance and provide guidance for potential personalised cancer treatment.

In this chapter, we used *C. elegans* to generate a chemi-genetic interaction map, comprised of DNA replication and repair genes and agents that could induce DNA damage. Since many DNA replication and repair processes are well conserved between *C. elegans* and human, it is likely that these chemi-genetic interactions can be extrapolated to human cancer cells. We included five different well-characterized DNA damaging agents (DDAs): olaparib, camptothecin, etoposide, UVA + trimethylpsoralen, and ultraviolet (UV) C radiation. The agents were chosen to cover of a broad spectrum of DNA damage types. Each agent generates a different type of DNA lesion that should require a specific set of repair mechanism(s) to resolve (summarized in Table 2.1). Specifically, olaparib inhibits PARylation activity, and traps PARP proteins on DNA, which can block DNA replication (Pommier et al., 2016). Olaparib has been approved by FDA to treat breast and ovarian cancer patients with germline *BRCA1/2* mutations (Lord et al., 2015; Tutt et al., 2010). Camptothecin is a Topoisomerase I inhibitor, and it binds to the DNA-Topoisomerase I complex, which prevents normal DNA-religation, resulting in single-strand breaks (SSBs) that can be converted to double-strand breaks (DSBs) upon collision with the replication machinery (Pommier, 2013). Two camptothecin derivative compounds, topotecan and irinotecan, have been approved by FDA to treat different types of cancers (Pommier, 2013). Etoposide is a Topoisomerase II inhibitor, and it binds to DNA-Topoisomerase II complex, which blocks strand re-ligation resulting in DSBs (Nitiss, 2009). Etoposide has been used in combination with other chemotherapeutics as the first-line treatment for small cell lung cancers (Pommier, 2013). UVA + trimethylpsoralen induces interstrand DNA crosslinks that impede DNA replication and transcription (Deans and West, 2011). Crosslinking agents such as the platinum-based cisplatin, carboplatin, and oxaliplatin are commonly used to treat cancer (Huang and Li, 2013). UVC

radiation causes DNA bulky lesions, such as thymine dimers (Rastogi et al., 2010). UVC is not used as an anti-cancer therapeutic.

2.2 Methods

Nematode strains were maintained as described previously (Brenner, 1974). The alleles used in this study were: *atm-1(tm5027)*, *brd-1(dw1)*, *rfs-1(ok1372)*, *cku-80(ok861)*, *lig-4(ok716)*, *hsr-9(ok759)*, *polq-1(tm2026)*, *polh-1(lf31)*, *polk-1(lf29)*, *fcd-2 (tm1298)*, *fan-1*(*tm423)*, *fncm-1(tm3148)*, *msh-2(ok2410)*, *ercc-1(tm1981)*, *xpa-1(ok698), mus-81(tm1937)*, *rcq-5(tm424)*, *rtel-1(tm1866)*, *helq-1 (tm2134)*, *him-6(ok412)*, *dog-1(gk10)*, *wrn-1(gk99)*, *let-418(n3536)*, *him-1(e879)*, *hda-3(ok1991)*, *gld-1(op236)*, *cep-1(gk138)*, *dvc-1(ok260)*, and *rev-3 (gk919715)*. Bristol N2 was used as wild type in all experiments. *rev-3(gk919715)* was Million Mutation Project allele (Thompson et al., 2013) provided by the Moerman lab and outcrossed to N2 six times. Some strains were provided by the Caenorhabditis Genetics Center, which is funded by NIH Office of Research Infrastructure Programs (P40 OD010440), and some knockout alleles were provided by the Shohei Mitani laboratory. Some strains were generated by the International *C. elegans* Gene Knockout Consortium (Consortium, 2012) and by the National Bioresource Project of Japan.

UVA irradiation

UVA Source: predominantly 365 nm, Black-Ray®UV Bench Lamp (Model: XX-15L). Before each UVA exposure, the light source output was determined by a longwave ultraviolet measuring meter (Model: J-221). Different UVA exposures were achieved by varying the exposure times.

Quantitative Acute Assay for olaparib, camptothecin, and etoposide

Synchronized one-day-old adults were incubated in agents (500 μM olaparib, 100 nM camptothecin, 100 μM etoposide) or Dimethyl sulfoxide (DMSO) solvent diluted in M9 buffer containing OP50, carbenicillin (50 μg/ml) and 1X nystatin for ~18 hours. Following treatment, the animals were allowed to recover for 30 to 60 minutes on OP50-containing Nematode growth media (NGM) plates. Next, at least ten worms were transferred in triplicate to NGM plates for a 4-hour interval (18 to 22 hours post-treatment), and then removed. The numbers of arrested embryos and hatched larvae were counted one day later in order to calculate the percentage of embryo survival after treatment (Figure 2.1). For animals that produced few progeny, more treated adult worms were picked to lay embryos in the 4-hour interval.

Quantitative Acute Assay for UVA-Trimethylpsoralen

Synchronized one-day-old adults were washed off plates and resuspended in 10 μg/mL TMP diluted in 500 μL M9 buffer containing 0.1% Triton for one hour in the dark. Following treatment, the animals were washed in M9 and then transferred to two OP50-containing NGM plates. Next, one plate was exposed to 100 J/m^2 UVA irradiation. Both plates were kept in the dark to avoid UVA from light in the laboratory. At least ten worms were transferred in triplicate to NGM plates for a 3-hour interval and then removed. The numbers of arrested embryos and hatched larvae were counted one day later in order to calculate the percentage of embryo survival after treatment. For animals that produced few progeny, more UVA-TMP treated adult worms were picked to lay embryos in the 3-hour interval.

Quantitative Acute Assay for UVC

Synchronized one-day-old adults were exposed to 50 J UVC irradiation (or mock treatment). UVC source was provided by UV-cross-linker (Ultraviolet Translinker TL-2000, ULTRA-

VIOLET PRODUCTS) with 254 nm bulbs (crosslinker). Animals were kept in the dark overnight. At least ten worms were transferred in triplicate to NGM plates for a 2.5-hour interval (18-21 hours post-irradiation) and then removed. The numbers of arrested embryos and hatched larvae were counted one day later in order to calculate the percentage of embryo survival after treatment. For animals that produced few progeny, more irradiated adult worms were picked to lay embryos in the 2.5-hour interval.

Chemi-genetic interaction map generation

The chemi-genetic interaction map is generated by using sensitivity scores, and then color-coded (Figure 2.2). The sensitivity score is the double-normalized embryo survival. The detailed calculation is as followed. For each mutant,

Embryo survival % = $\frac{the\ number\ of\ hatched\ larva}{(the\ number\ of\ hatched\ larva + the\ number\ of\ arrested\ embryos)}$ x100%.

Then, the embryo survival percentage of each mutant treated with DDA is normalized to that with mock treatment. For each mutant,

Normalized embryo survival = $\frac{Embryo\ survival\ \%\ rate\ (treated\ with\ DDA)}{Embryo\ survival\ \%\ (mock)}$.

Next, the sensitivity score is generated by normalizing the normalized embryo survival rate of the mutant to that of wild-type N2. For each mutant,

Sensitivity score = $\frac{Normalized\ embryo\ survival\ (mutant)}{Normalized\ embryo\ survival\ (N2)}$. The higher the score, the less sensitive the mutant is to the DDA, and the lower the score, the more sensitive the mutant is to the DDA. Lastly, the map is color-coded with light blue representing the least sensitive and red representing the most sensitive. The sensitivity score takes the effect of both the DDAs and the genotypes into account.

2.3 Results

2.3.1 Construction of a genome stability mutant panel

As mentioned in Chapter 1, many genes can affect genome stability, ranging from DNA metabolic genes to DNA damage response genes. Here, we constructed a *C. elegans* genome stability mutant panel that covers a wide range of functions involved in safeguarding the genome integrity, especially DNA replication and repair.

The mutant panel consisted of 30 different mutants in total in addition to wild-type N2, which served as a negative control (Figure 2.2). We included a cohesin mutant (*him-1*), chromatin modifier mutants (*let-418* and *hda-3*), an RNA-binding mutant (*gld-1*), checkpoint mutants (*atm-1* and *cep-1*), an endonuclease mutant (*mus-81*), a number of helicase mutants (*dog-1*, *helq-1*, *him-6*, *rcq-5*, *wrn-1* and *rtel-1*), a kinase mutant (*cdk-5*), FA repair pathway mutants (*fncm-1*, *fan-1* and *fcd-2*), NER mutants (*xpa-1* and *ercc-1*), a MMR mutant (*msh-2*), HDR mutants (*brd-1* and *rfs-1*), NHEJ mutants (*cku-80*, *lig-4* and *hsr-9*), a MMEJ mutant (*polq-1*), translesion synthesis mutants (*polh-1*, *rev-3* and *polk-1*) and a protease mutant (*dvc-1*) (Figure 2.2).

2.3.2 Genotypic sensitivity profile of olaparib (Ola)

We first generated the genotypic sensitivity profile of a PARP inhibitor, olaparib. We treated the mutant panel with 500 μM olaparib and scored progeny viability of treated animals. Three out of thirty mutants showed strong sensitivity to olaparib. The DNA damage response checkpoint mutant, *atm-1*, and the endonuclease mutant, *mus-81*, exhibited the greatest sensitivity – about 56% and 67% embryo viability after olaparib treatment (Figure 2.2). To our surprise, the *brd-1* mutant was not sensitive to olaparib. This is in contrast to human cells, where tumors deficient in

BRCA1 or *BARD1* exhibited severe proliferation defects when treated with olaparib (Tutt et al., 2010). Another HDR mutant, *helq-1* had mild olaparib-sensitivity, which produced around 80% viable progeny after olaparib treatment (Figure 2.2).

2.3.3 Genotypic sensitivity profile of camptothecin (CPT)

Next, we generated the genotypic sensitivity profile of the Topoisomerase I inhibitor, camptothecin with the mutant panel. About a third of the mutants we tested exhibited CPT sensitivity. Similar to olaparib, the endonuclease mutant, *mus-81*, and the checkpoint mutant, *atm-1*, were among the most sensitive strains (Figure 2.2). Notably, the cohesin mutant, *him-1*, was also sensitive to CPT, as over 60% progeny were arrested as dead embryos upon CPT treatment. The NHEJ mutants (*cku-80, lig-4* and *hsr-9*) and the MMEJ mutant (*polq-1*) were not sensitive to CPT treatment, whereas HDR mutants (including *brd-1*, *rfs-1* and *helq-1*) were hypersensitive, all of which have reduced embryo viability (>80% arrested embryos) after CPT treatment (Figure 2.2). The mismatch repair mutant, *msh-2*, was also sensitive to CPT (Figure 2.2).

2.3.4 Genotypic sensitivity profile of etoposide (ETOP)

Next, we generated genotypic sensitivity profile of etoposide, an inhibitor of Topoisomerase II. The *mus-81* mutant exhibited the greatest sensitivity to ETOP, and the cohesin mutant *him-1*, was hypersensitive to ETOP (Figure 2.2). Although ETOP and CPT shared many sensitive genotypes, there were clear differences in the sensitivity levels. For instance, HDR mutants (*brd-1*, *rfs-1*, *helq-1*) were less sensitive to ETOP than to CPT. The MMEJ mutant, *polq-1*, which did

not exhibit CPT-sensitivity, was sensitive to ETOP treatment (Figure 2.2). In addition, two helicase mutants, *rtel-1* and *dog-1*, were very sensitive to ETOP treatment (Figure 2.2).

2.3.5 Genotypic sensitivity profile of UVA-trimethylpsoralen (TMP)

Next, we generated the sensitivity profile for UVA-trimethylpsoralen, a DNA interstrand crosslinking (ICL) agent (Deans and West, 2011). TMP exhibited a very different genotypic sensitivity profile compared to other DNA damaging agents. Notably, *C. elegans* animals deficient in Fanconi Anemia (FA) pathways, which repairs ICLs, were sensitive to TMP. The *fan-1* and *fncm-1* mutants produced more than 70% arrested embryos upon UVA-TMP treatment (Figure 2.2). Nucleotide excision repair (NER) mutants, *xpa-1* and *ercc-1*, showed high embryo lethality - ~ 70% and 80%, respectively (Figure 2.2). Mutants that lack translesion synthesis capacity, *polh-1* and *rev-3*, were also extremely sensitive to UVA-TMP, producing more than 85% arrested progeny (Figure 2.2). Among the three major double-strand break (DSB) repair pathways, both MMEJ and HDR were required for TMP-resistance, as *polq-1*, *brd-1* and *rfs-1* single mutants were all sensitive to UVA-TMP (Figure 2.2).

2.3.6 Genotypic sensitivity of ultraviolet C (UVC)

Next, we generated the genotypic sensitivity profile for ultraviolet C exposure. As was expected for UVC-induced DNA damage, the TLS mutants, *polh-1* and *rev-3,* were extremely sensitive to UVC (Figure 2.2). The *polh-1* mutant produced almost no viable progeny (>99% arrested embryos) after UVC exposure. The NER mutants *xpa-1* and *ercc-1* produced more than 60% dead embryos upon UVC exposure (Figure 2.2). Mutants deficient in resolving DSBs, such as HDR, NHEJ and MMEJ mutants, were not sensitive to UVC (Figure 2.2).

2.4 Discussion

2.4.1 Each agent has a distinctive genotypic sensitivity profile

Taking into account the magnitude of sensitivity, each DNA damaging agent has a unique sensitivity profile. DNA damage induced by an agent can be complex consisting of different types of lesions requiring more than one repair mechanism. For example, UVC radiation can cause a range of DNA lesions, such as thymine dimers and bulky (6-4) photoproducts (Cadet et al., 2005). In other cases, the DNA damage requires the coordination of multiple repair pathways to repair the damage, as is the case for ICLs (Youds et al., 2009). These complexities result in sensitivity profiles that touch on multiple repair pathways. In most cases, DNA damage is primarily repaired or resolved by some mechanisms over others. For example, NER pathway mutants (*xpa-1* and *ercc-1*) showed much greater sensitivity to UVA-TMP than HDR mutants (*brd-1* and *rfs-1*) (Figure 2.2), suggesting that repair of TMP-induced lesions is more dependent on NER than HDR in *C. elegans*.

Another way to look at the chemi-genetic interaction map is by comparing the profiles between agents. One can discern the primary repair mechanisms for each lesion induced by different agents. For example, CPT and ETOP are both topoisomerase poisons. Despite the fact that both CPT and ETOP can result in DSBs, the primary mechanism to resolve lesions induced by each agent varies. Three major pathways could resolve DSBs: HDR, MMEJ, and NHEJ. In both CPT and ETOP-induced lesions, NHEJ is dispensable for the repair, as evidenced by the fact that the *cku-80* mutant showed no embryonic death upon either treatment (Figure 2.2). The data also suggest that HDR repair pathway is the primary repair pathway used for CPT-induced lesions because HDR mutants (*brd-1*, and *rfs-1*) were much more sensitive to CPT than the MMEJ

mutant *polq-1* (Figure 2.2), which did not exhibit CPT-sensitivity. By contrast, MMEJ mutant *polq-1* had much stronger ETOP-sensitivity than HDR mutants (Figure 2.2), indicating that MMEJ is primary repair mechanism for resolving ETOP-induced DNA damage. This raises the possibility that the type of DSBs or lesions arising from CPT and ETOP can be different. The interplay between repair pathways is explored further in Chapter 4.

We also identified features for each agent. Compared to human cell line studies, a high concentration of olaparib was needed (500 μM) to generate the sensitivity profile in *C. elegans* and only three mutants were found to be olaparib-sensitive. It is possible that either poor uptake into the worm or detoxification of olaparib required a high initial concentration to achieve an effective concentration in the worm (Johnstone, 1994). Alternatively, it is probable that 18 hours of exposure of adult worms to olaparib was not sufficient to induce DNA damage in the germ lines. In contrast to human counterparts (Min et al., 2013; Walsh, 2015), the HDR mutants (*brd-1* and *rfs-1*) showed no sensitivity to olaparib using quantitative acute assays (Figure 2.2). This could be due to the properties of the assay. The readout for sensitivity is the embryonic survival of progeny (embryo) from the treated animals. The rapid early embryonic cell divisions in *C. elegans* do not utilize HDR pathways and instead rely heavily on TLS (Holway et al., 2006), which could bypass lesions caused by inhibited PARP.

C. elegans had a genotypic sensitivity profile for CPT that was similar to the human cell lines (O'Connell et al., 2010). HDR-deficient human cells are hypersensitive to CPT, and *C. elegans brd-1* and *rfs-1* mutants were extremely sensitive to CPT (Figure 2.2). Furthermore, the mismatch repair gene MSH-2 was required for CPT-resistance likely because of its role in

recombinational repair, similar to its human counterparts (Jacob et al., 2001; Pichierri et al., 2001). The NHEJ pathway has been proposed to antagonize the HDR pathway in response to CPT, and loss of NHEJ factors renders resistance to CPT (Adachi et al., 2004). Consistent with this, none of the *C. elegans* NHEJ mutants (*cku-80*, *lig-4*, and *hsr*-9) were sensitive to CPT (Figure 2.2). Our finding that the cohesin mutant, *him-1*, exhibited CPT-sensitivity was also consistent with a previous report that human glioblastoma H4 cells with a null mutation in the cohesin gene *STAG2* were more sensitive to CPT than H4 cells that had the *STAG2* mutation repaired (Bailey et al., 2014). Although some studies demonstrated that *POLQ*-deficient cells were sensitive to CPT (Wang et al., 2019b; Yousefzadeh et al., 2014), our results did not find the *polq-1* mutant sensitive, indicating that MMEJ is not the primary repair pathway for CPT-induced lesions in *C. elegans*. This could be due to worm-specific differences in repair pathway choice or the result of different genetic backgrounds in the human cell lines.

The genotypic sensitivity profile of ETOP overlapped with that of CPT (Figure 2.2), as many ETOP-sensitive mutants were also sensitive to CPT, albeit with varying degrees. The repair mechanism for ETOP-induced lesions appears to be well conserved between *C. elegans* and humans, as we found *C. elegans* homologs of many human ETOP-sensitive genes were also required for resistance to ETOP. Similar to human counterparts (Treszezamsky et al., 2007; Wang et al., 2019b), both HDR genes and MMEJ genes are required for ETOP-induced DNA damage. Moreover, our data suggested that MMEJ is the primary repair mechanism for ETOP-induced lesions since the MMEJ mutant, *polq-1*, exhibited much stronger sensitivity than HDR mutants (*brd-1* and *rfs-1*) (Figure 2.2). It is as yet uncertain why *C. elegans* favors MMEJ over HDR to counteract ETOP-induced DNA lesions. One possibility is that ETOP did not directly

cause DSBs but instead results in lesions that POLQ-1 could process via its TLS activity (Yoon et al., 2019). This hypothesis is supported by the observation that two *C. elegans FANCJ* helicase family mutants, *dog-1* and *rtel-1* were both sensitive to ETOP but not to CPT. DOG-1 is required to unwind G4 structures during replication (London et al., 2008; Youds et al., 2008), and in the absence of DOG-1, POLQ-1 is needed to bypass these structures (Koole et al., 2014). It is possible that ETOP is generating analogous structures that can be resolved either by DOG-1 helicase activity or POLQ-1-mediated bypass, in a similar manner to G4 structures. Alternatively, loss of FANCJ could result in chromatin re-organization that further impedes the repair of TOP2-induced lesions (Schwab et al., 2013). However, it is unknown whether TOP2 has high affinity towards DNA sequences that tend to form secondary structures, or that trapping of TOP2 by ETOP induces formation of secondary structures in the vicinity.

The genotypic sensitivity profile of UVA-TMP illustrates the requirement for multiple repair processes in the resolution of interstrand crosslinks in *C. elegans*. The canonical interstrand crosslink repair involves cooperation of multiple pathways (Deans and West, 2011). XPA-RPA and MutSβ complexes have been previously shown to function together to recognize ICL, which likely induced structural distortion at the site of damage (Zhao et al., 2009). In support of this, our data showed that both *xpa-1* and *msh-2* mutants were sensitive to UVA-TMP (Figure 2.2). The sensitivity of MMEJ mutant *polq-1* to UVA-TMP is consistent with a recent report showing that MMEJ plays a role in counteracting interstrand crosslink lesions in *C. elegans* (Figure 2.2) (van Schendel et al., 2016). That core FA mutants (*fan-1*, *fcd-2* and *fncm-1*) were only sensitive to UVA-TMP, but not to other agents we tested (Figure 2.2), suggests that the FA pathway is very specific to the resolution of ICLs (Deans and West, 2011). TLS is required for the final step

of ICL-repair to ligate the gap generated by endonucleases. In agreement with a previous report that HDR pathway is required for ICL-repair, such as after treatment with nitrogen mustard (Muzzini et al., 2008), both *brd-1* and *rfs-1* exhibited UVA-TMP-sensitivity (Figure 2.2). There are structural differences between ICLs created by different agents. UVA-TMP generates a specific type of abasic site different from nitrogen mustard and cisplatin after initial incision (Semlow et al., 2016). It has been shown that UVA-TMP-induced ICL-repair did not result in formation of DSBs due to activity of NEIL3 glycosylase (Semlow et al., 2016); however, it does not appear that *C. elegans* has a *NEIL3* homolog that could prevent the formation of DSBs in response to TMP.

The genotypic sensitivity profile of UVC elucidates how bulky lesions are repaired in *C. elegans*. Similar to their human counterparts, mutants deficient in NER and TLS are extremely sensitive to UVC (Figure 2.2). The repair mechanism is likely very similar in both worms and humans. When UVC generates bulky lesions such as thymine dimers, XPA-RPA initiates the recognition process along with RNA polymerase during transcription, XPF-ERCC1 and XPG cleave the lesions, and TLS fills the gap.

2.4.2 Some genes are required for many different DNA damage responses

From our chemi-genetic interaction map, some mutants exhibited sensitivity to all agents tested. This could be that the gene is required for a general response to all DNA damage or that it is a key factor indispensable for many types of DNA repair. For instance, the endonuclease mutant, *mus-81*, showed strong sensitivity to all agents tested (Figure 2.2). MUS81 has multiple roles in the DNA damage response. It has been shown to cleave stalled replication forks to generate a

substrate for HDR (Hanada et al., 2007) and act as a late cell cycle stage fail-safe for resolving unrepaired DNA lesions that block replication to ensure proper cell division (Naim et al., 2013; Ying et al., 2013). Therefore, it would be expected that *mus-81* mutants would be sensitive to many different types of DNA damage. This property makes the *mus-81* mutant a good positive control for testing agents that induce DNA damage.

The DNA damage response checkpoint mutant, *atm-1*, was also sensitive to all agents tested (Figure 2.2). Human *ATM*-deficient cells were also shown to be sensitive to olaparib, CPT, ETOP, UVC and other DNA damaging agents (Bailey et al., 2014; Fedier et al., 2003; Hannan et al., 2002). The ATM checkpoint is activated in DNA damage response and can phosphorylate a number of substrates depending on the type of DNA damage (Marechal and Zou, 2013). These substrates are proteins that are required for removing or resolving the damage. Given the role that ATM-1 plays in the DNA damage checkpoint, it is not surprising that it is sensitive to many different types of DNA lesions.

2.4.3 The chemi-genetic interaction map can be a reference for characterizing new damaging agents and DNA replication and repair genes

The chemi-genetic interaction map can be useful as a reference for understanding how less-understood DNA damaging agents work. New agents can be tested with the same panel of *C. elegans* DNA replication and repair mutants, and new genotypic sensitivity profiles can be generated. Comparing the genotypic sensitivity profile of a less-understood agent with those of well-characterized ones provides a preliminary hypothesis about what type of DNA lesions are induced by the agent under investigation. Agents that induce similar types of lesions require

similar repair mechanism to resolve the lesions, so there will be overlap in the mutants that show sensitivity to the agents.

Conversely, the chemi-genetic interaction map can be used to investigate the biological function of less-understood genes involved in DNA replication and repair. Testing the animals deficient in the gene of interest with all the agents in the chemi-genetic interaction map creates the drug-sensitivity profile for the gene of interest. Drug-sensitivity profile allows us to determine whether the gene of interest is involved in general DNA damage response that is indispensable for repair (such as *mus-81* and *atm-1)*, or is dedicated to repair only certain types of DNA lesions (such as genes involved in Fanconi Anemia pathway).

Although there are differences between how cells repair certain kinds of DNA damage between *C. elegans* and human, the chemi-genetic interaction map here is solely generated using worm data. Even if there are differences between worm and human repair pathway choices for a given lesion, the *C. elegans* panel is still informative because similar types of lesions should require the same pathways for repair or tolerance. The chemi-genetic interaction map is a growing resource that will become even more useful as more mutants and DNA damaging agents are tested and catalogued.

DNA damaging agent	Type(s) of lesions	Known DNA repair pathway(s) to resolve the lesions	Clinical implication
Olaparib	Protein trapping and replication block	HDR	Olaparib is used to treat breast and ovarian cancer patients with germline *BRCA* mutations.
Camptothecin	Replication block, single-strand breaks, and double-stranded breaks	HDR	Camptothecin derivatives (topotecan and irinotecan) are used to treat various types of cancer, including ovarian, cervical and lung cancer.
Etoposide	Replication block, double-strand breaks	HDR	Etoposide is used in combination with other chemotherapy to treat small cell lung cancer and testicular cancer.
UVA + trimethylpsoralen (UVA+TMP)	DNA interstrand crosslinks, replication block	FA, HDR, MMEJ, TLS and NER	UVA+TMP is not used in the clinics. Many platinum-based anticancer drugs (cisplatin, carboplatin, and oxaliplatin), which cause DNA interstrand crosslinks, are used to treat various types of cancer, including ovarian cancer, lung cancer and head and neck cancer.
UVC	DNA bulky lesions, including cyclobutane pyrimidine dimers and [6-4]-photoproducts	NER and TLS	UVC is not used in the clinic.

Table 2.1 Summary of the DNA damaging agents used to generate the chemi-genetic interaction map.

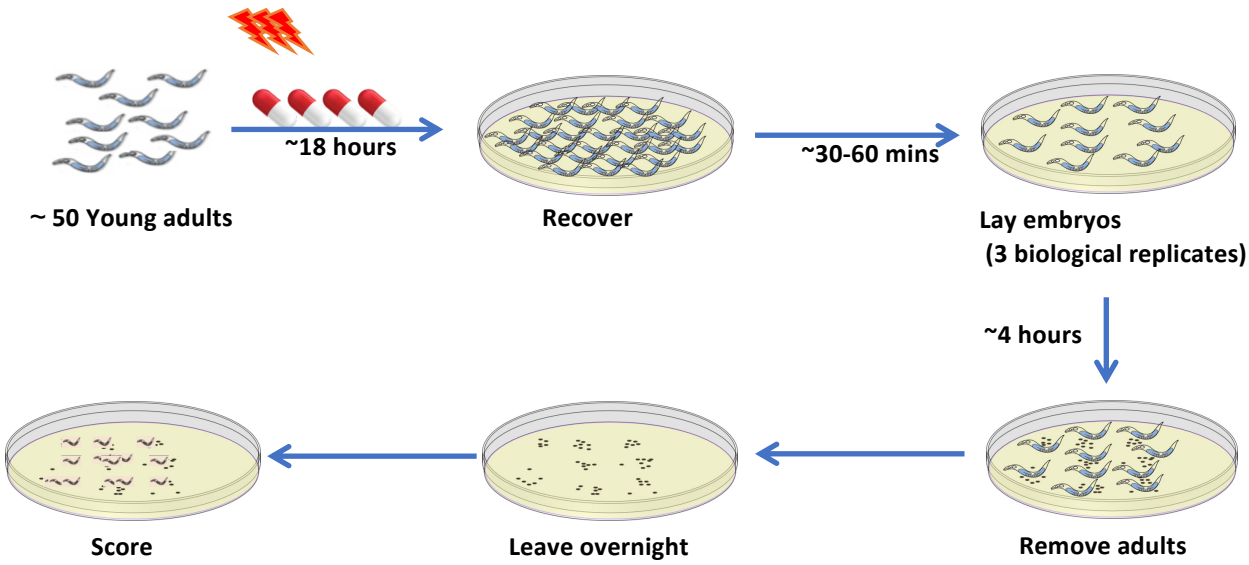

Figure 2.1 A schematic of quantitative acute assay. About 50 young adults were treated with agents for ~ 18 hours (alternatively one hour in trimethylpsoralen followed by UVA irradiation, or transient UVC irradiation). Then treated adults were often transferred to a plate to recover for 30 to 60 minutes, before they were picked to new plates in 3 biological replicates (at least 10 worms on each plate). Adults were given a four-hour interval to lay embryos before they were removed. The numbers of unhatched embryos and new larvae were counted on the following day.

Function	Human homolog	Strain	Ola	CPT	ETOP	UVA + TMP	UVC	CX-5461
///	wild-type	*N2*	1.00	1.00	1.00	1.00	1.00	1.00
Cohesin	SMC1A	*him-1*	1.01	0.33	0.08	0.82	0.74	0.39
Chromatin remodeling	CHD4	*let-418*	1.02	1.00	1.00	0.50	1.04	0.76
	HDAC1	*hda-3*	0.87	1.15	0.83	0.70	0.93	0.96
RNA binding	QKI	*gld-1*	0.95	0.80	0.95	1.04	0.88	0.87
DNA Damage Checkpoint	ATM	*atm-1*	0.56	0.36	0.73	0.67	0.63	0.01
	TP53	*cep-1*	1.03	0.60	0.94	0.96	0.71	0.98
Endonuclease	MUS81	*mus-81*	0.67	0.07	0.06	0.13	0.36	0.03
Helicase	FANCJ	*dog-1*	0.92	0.91	0.50	0.83	0.91	0.95
	HELQ	*helq-1*	0.80	0.12	0.77	0.48	0.79	0.11
	BLM	*him-6*	1.15	0.97	ND	0.86	0.82	ND
	RECQL5	*rcq-5*	1.02	1.09	0.98	1.03	0.94	0.99
	RTEL	*rtel-1*	0.96	0.99	0.49	0.63	1.09	0.79
	WRN	*wrn-1*	0.98	0.92	1.15	0.97	1.14	0.98
	SMARCAL	*smrc-1*	ND	0.12	0.43	0.75	0.70	0.24
Kinase	CDK5	*cdk-5*	1.03	0.84	ND	0.87	0.89	ND
Fanconi Anemia Pathway	FANCM	*fncm-1*	1.00	1.01	1.05	0.28	0.82	0.91
	FAN1	*fan-1*	0.90	1.01	1.07	0.11	0.98	0.95
	FANCD2	*fcd-2*	1.00	1.00	1.13	0.55	0.99	0.87
HDR repair	BARD	*brd-1*	1.04	0.17	0.82	0.52	0.93	0.59
	RAD51C	*rfs-1*	0.96	0.19	0.55	0.49	1.00	0.55
Nucleotide Excision Repair	ERCC1	*ercc-1*	1.07	1.00	1.02	0.19	0.17	0.08
	XPA	*xpa-1*	0.95	0.99	0.92	0.31	0.36	0.27
MMR	MSH2	*msh-2*	1.02	0.42	0.79	0.25	1.12	1.03
NHEJ	TP53BP1	*hsr-9*	0.90	0.92	ND	0.99	0.90	0.98
	KU80	*cku-80*	1.02	1.00	1.05	0.89	1.02	0.99
	LIG4	*lig-4*	0.97	0.93	1.08	1.03	0.98	1.00
MMEJ	POLQ	*polq-1*	1.01	0.95	0.32	0.55	1.06	0.44
Translesion Synthesis (TLS)	POLH	*polh-1*	0.99	0.62	0.69	0.00	0.02	0.09
	REV3	*rev-3*	0.98	0.96	1.02	0.16	0.51	0.01
	POLK	*polk-1*	1.04	1.08	ND	1.01	1.04	ND
Protease	SPRTN	*dvc-1*	ND	1.03	0.91	0.70	0.95	0.85

Not sensitive 0.85 0.75 0.5 0.25 0 Most sensitive

Figure 2.2 The chemi-genetic interaction map of different agents. Indicated mutant animals were treated with corresponding agents, and their embryo survival percentage was calculated. The color range (from blue to red) represent differential sensitivity of mutants as indicated in the scale bar. The calculation of the sensitivity score is detailed in Chapter 2 Method, and raw data are in Table A1. ND, not determined.

CHAPTER 3: UNDERSTANDING THE MECHANISMS OF ACTION OF CX-5461

3.1 Introduction

CX-5461 is a quinolone-containing small molecule with potential anti-cancer properties. It was originally described as an RNA Pol I inhibitor that demonstrated *in vivo* anticancer activity in murine xenograft models (Drygin et al., 2011; Haddach et al., 2012). CX-5461 can trigger ATM/ATR checkpoint activation (Negi and Brown, 2015) and rapamycin-associated signaling (Li et al., 2016). More recently, we contributed to a study that showed that CX-5461 binds and stabilises G-quadruplexes (G4s) and causes selective killing of *BRCA1/2*-deficient tumors (Xu et al., 2017). This has led to a CX-5461 clinical trial in breast cancer patients with homologous recombination-deficient tumors (Hilton et al., 2018). Clinical trials have identified side-effects of CX-5461, including photosensitivity and palmar-plantar erythrodysesthesia (Hilton et al., 2018; Khot et al., 2019). It is imperative to further investigate the mechanism of action of CX-5461 so as to have a better understanding of genotypic sensitivities and resistance, and potential deleterious effects.

3.2 Methods

The alleles used in this study were: BC 2200 *dpy-18(e364)/eT1(III)*; *unc-46(e177)/eT1(V)*, *atm-1(tm5027)*, *brd-1(dw1)*, *rfs-1(ok1372)*, *cku-80(ok861)*, *lig-4(ok716)*, *hsr-9(ok759)*, *polq-1(tm2026)*, *polh-1(lf31)*, *polk-1(lf29)*, *fcd-2 (tm1298)*, *fan-1*(*tm423)*, *fncm-1(tm3148)*, *msh-2(ok2410)*, *ercc-1(tm1981)*, *xpa-1(ok698), mus-81(tm1937)*, *rcq-5(tm424)*, *rtel-1(tm1866)*, *helq-1 (tm2134)*, *him-6(ok412)*, *dog-1(gk10)*, *wrn-1(gk99)*, *let-418(n3536)*, *him-1(e879)*, *hda-3(ok1991)*, *gld-1(op236)*, *cep-1(gk138)*, *dvc-1(ok260)*, *smrc-1(gk176502)*, and *rev-3(gk919715)*. Bristol N2 was used as wild type in all experiments. *smrc-1(gk176502)*, and *rev-3(gk919715)*

were Million Mutation Project (Thompson et al., 2013) alleles provided by the Moerman lab and outcrossed to N2 six times. Some strains were provided by the Caenorhabditis Genetics Center, which is funded by NIH Office of Research Infrastructure Programs (P40 OD010440), and some knockout alleles were provided by the Shohei Mitani laboratory. Some strains were generated by the International *C. elegans* Gene Knockout Consortium (Consortium, 2012) and by the National Bioresource Project of Japan.

UVA irradiation

UVA Source: predominantly 365 nm, Black-Ray®UV Bench Lamp (Model: XX-15L). Before each UVA exposure, the light source output was determined by a longwave ultraviolet measuring meter (Model: J-221). Different UVA exposures were achieved by varying the exposure times.

Quantitative acute assay

Synchronized one-day-old adults were incubated in CX-5461 (in NaH_2PO_4) diluted in M9 buffer containing OP50, carbenicillin (50 μg/ml) and 10 ng/ml nystatin for ~18 hours. Following treatment, the animals were allowed to recover for 30 to 60 minutes on OP50-containing NGM plates before UVA irradiation (if applicable) and then plated ten worms per plate in triplicate on NGM plates for a 4-hour interval (18 to 22 hours post-treatment), and then removed. The numbers of both arrested embryos and hatched larvae were counted one day later in order to calculate the percentage of embryo survival after treatment. For animals that produced few progeny, more treated adult worms were picked to lay embryos in the 4-hour interval.

All results were from at least 30 treated animals (3 plates with at least 10 animals per plate). The calculation of the sensitivity score was detailed in Chapter 2 Method.

Mutagenesis screen for CX-5461

Strain BC2200 *dpy-18/eT1(III);unc-46/eT1(V)* was used in the mutagenesis screen. *dpy-18/eT1(III);unc-46/eT1(V)* hermaphrodites were treated with or without CX-5461 for 18 hours before 150 J/m^2 UVA irradiation, and 200 single *dpy-18/eT1(III);unc-46/eT1(V)* F_1s were picked in each condition. A sterile phenotype at F_1 is considered to indicate the acquisition of a dominant lethal mutation, and lines in which F_2 or later generations that do not have Dpy Unc animals are considered to indicate the acquisition of a recessive lethal mutation in the balanced regions of chromosome III or V.

Genome Sequencing

The lines that acquired recessive lethal mutations were maintained for at least three generations. Worms were rinsed off with deionized water and concentrated by centrifugation. Genomic DNA was purified using Puregene® Core Kit A (Qiagen). Whole-genome sequencing was performed at the Novogene Bioinformatics Institute (Beijing, China). Sequence reads were mapped to the *C. elegans* reference genome version WS230 (http://www.wormbase.org) using the short-read aligner BWA, which gave an average sequencing depth for each sample ranging from 22x to 57x with a median of 34x. Single-nucleotide variants and small insertions/deletions were identified and filtered with the help of the SAMtools toolbox (Li et al., 2009). Candidate variants at genomic locations for which the parental N2 strain had an agreement rate with the reference genome lower than 95% were eliminated from further consideration. Each variant was annotated with a custom Perl script and gene information downloaded from WormBase version WS230. Copy numbers were estimated from the alignments with a procedure analogous to that of Itani *et al.* using 5 kb wide overlapping sliding windows with the alignments from the parental strain used as the reference (Itani et al., 2015).

L1 exposure assay

Gravid animals were bleached to get synchronized L1 larvae by hypochlorite treatment (0.5 M NaOH, 2% hypochlorite). After overnight starvation, about 100 L1 larvae of each mutant strain were incubated in 50 µl of M9 buffer containing OP50, carbenicillin (50 µg/ml), 10 ng/ml nystatin, 500 µM NaH2PO4 with and without 100 µM CX-5461 for ~18 hours. Following treatment, worms were allowed to recover for 0.5 hour on OP50-containing NGM plates before they were irradiated with the indicated amount of UVA exposure. Live animals were imaged after 4 days following UVA exposure to assay developmental defects using EVOS® XL Cell Imaging System.

Reactive oxygen species (ROS) measurement with H_2DCFDA

Adult worms treated in CX-5461 for 18 hours were added with 25 µM 2',7'-dichlorodihydrofluorescein diacetate (H_2DCFDA), and incubated for another hour in the dark before initial fluorescence measurement by a microplate reader. After initial measurement, worms were irradiated with the indicated amount of UVA exposure, and then immediately measured (Yoon et al., 2017).

CX-5461-DNA shifting experiment

PCR products (~40 ng/µL) or sheared 6 kb genomic DNA (~5 ng/µL) were mixed with CX-5461 at room temperature. The CX-5461-DNA mixtures were incubated at 94°C for 25 minutes to denature the dsDNA, and then temperature was monitored and decreased stepwise until the target temperature was reached (if applicable). For the nuclease cleavage experiment, mung bean nuclease (MBN) (BioLabs® M0250S, 10,000 units/ml) was added to the CX-5461-DNA mixtures at room temperature (1.75 µL MBN per 100 µL reaction). Then, the mixture was incubated for one hour at either 25°C or 40°C. The final CX-5461-DNA products were loaded on

1% agarose gel containing SYBR-safe DNA stain for visualization. To note, PCR products were generated using standard PCR protocol, and worm genomic DNA was fragmented with g-tube (Covaris®), which allows genomic DNA to be sheared to a certain size (Kong et al., 2017).

Generational survival assay

Animals were plated individually and maintained at room temperature. Starting with 20 separate lines at P_0 generation, a single L4 stage animal was transferred to a fresh plate for each generation. A line was scored as unsustainable when the parent worm was either sterile or laid only dead embryos.

3.3 Results

3.3.1 The genotypic-sensitivity profile of CX-5461

We used the quantitative acute assay and the mutant panel to generate a genotypic sensitivity profile for CX-5461, as described in previous chapter. Fourteen genotypes demonstrated sensitivity to CX-5461 (Figure 2.2, sensitivity score below 0.85). The translesion synthesis (TLS) mutants *rev-3* and *polh-1*, the checkpoint mutant *atm-1*, and the structure-specific endonuclease mutant *mus-81* were the most sensitive strains to CX-5461. Deficiency in homology-directed repair (HDR) and microhomology-mediated end joining (MMEJ) repair pathways, both of which repair DSBs moderately sensitized worms to CX-5461. Simultaneous loss of MMEJ and HDR repair pathways (*helq-1 polq-1*, *polq-1 brd-1*, and *polq-1 rfs-1*) further sensitized worms to CX-5461 (Figure 3.1B). The *smrc-1* anti-helicase mutants were exquisitely sensitive to CX-5461. NER mutants (*xpa-1*, and *ercc-1*) also showed CX-5461 sensitivity. Taken together, it appears that multiple DNA repair pathways are required for tolerance of CX-5461.

CX-5461 genotypic sensitivity profile resembled those of UVA-TMP, etoposide and camptothecin (Figure 2.2 & 3.1A).

3.3.2 CX-5461 comparison to loss of the G-quadruplex associated helicase *dog-1*

CX-5461 can bind and stabilize G-quadruplexes, which in turn can affect DNA replication (Xu et al., 2017). Loss of the *C. elegans FANCJ* homolog, *dog-1*, was found to result in deletions at replication blocking G-quadruplexes (Cheung et al., 2002; Zhao et al., 2008). These deletions were shown to be the by-product of MMEJ-mediated bypass of *dog-1*-stabilized G-quadruplexes (Koole et al., 2014). The MMEJ POLQ-1 polymerase was also needed for the bypass or repair CX-5461-mediated lesions (Figure 2.2 & 3.1B).

To test whether the effect of CX-5461 treatment phenocopies the loss of *dog-1* activity, we crossed the *dog-1* single mutant to CX-5461-sensitive mutants and generated *dog-1*-containing double mutants, and compared the multigenerational fitness between single and double mutants. As expected, many CX-5461-sensitive mutants exhibited sensitivity to loss of *dog-1*. The *polq-1* and *mus-81* mutant animals were the most sensitive to loss of *dog-1*, as fewer than 50% of the lines survived to the fourth generation and the brood sizes of both *dog-1;polq-1* and *dog-1 mus-81* were significantly reduced at the F_1 generation (Figure 3.2A,B, Table 3.1). HDR mutants, *brd-1* and *rfs-1*, were both mildly sensitive to loss of *dog-1*. In addition, the anti-helicase mutants *smrc-1*, also showed moderate sensitivity to loss of *dog-1*, as no more than 20% of the lines survive at F8 (Figure 3.2B). Nevertheless, not all CX-5461-sensitive mutants were sensitive to loss of *dog-1*. For instance, the TLS mutant *rev-3* was not sensitive to *dog-1*-induced G-quadruplex stabilization, although it was hypersensitive to CX-5461 (Figure 2.2 & 3.2A,B, Table

3.1). This suggests that CX-5461 could cause more than G-quadruplex stabilization.

3.3.3 CX-5461 can intercalate into DNA secondary structures.

The chemi-genetic signature of CX-5461 suggested that CX-5461 could affect DNA replication. *In silico* analysis predicts that the pharmacophore of CX-5461 can intercalate into a crystal structure of DNA (PDB code 1Z3F) (Canals et al., 2005) in a manner similar to the antineoplastic agent ellipticine (Andrews et al., 2013). Therefore, we set out to test whether CX-5461 can intercalate into DNA.

First, we incubated 25 μM CX-5461 with a PCR product (719 bp) and observed a mobility shift on 1% agarose gel. The band shift suggested that CX-5461 could impede double-strand DNA (dsDNA) migration (Figure 3.3A). When dsDNA was denatured and re-annealed in the presence of a high concentration of CX-5461 (>100 μM), the effect was more prominent, with DNA remaining in the well and not migrating into the gel. This suggests that CX-5461 interacts more readily with ssDNA. In addition, we also incubated CX-5461 with genomic DNA that had been sheared to 6 kbp fragments. CX-5461 impeded the migration of genomic DNA with the DNA remaining in the well at high concentrations of CX-5461 (>200 μM). When the genomic DNA was denatured, the single strands could not re-anneal with their complementary partners. We saw no dsDNA bands in the lane without CX-5461 (Figure 3.3B). However, addition of CX-5461 was able to promote the re-annealing of the denatured genomic DNA or prevented the denaturation of the DNA at the denaturation temperature.

Second, we tested whether CX-5461 distorted the DNA structure. Intercalation of ellipticine can

distort the DNA helix (Canals et al., 2005). To test whether CX-5461 intercalation could distort DNA, perhaps by stabilizing G-quadruplexes, we tested whether Mung bean nuclease (MBN), which cleaves ssDNA, could cleave CX-5461-distorted DNA. We incubated 30 μM CX-5461 with a PCR product (890 bp) predicted to form a G-quadruplex and a PCR product (719 bp) without a predicted G-quadruplex, and measured the nuclease activity on the agarose gel. Contrary to our expectation that CX-5461 would expose ssDNA for MBN cleavage, we found that CX-5461 protected DNA from MBN cleavage at both 25°C and 40°C (Figure 3.3C), indicating that CX-5461 reduced the amount of ssDNA available for cleavage, thereby enhancing the thermal stability of DNA.

3.3.4 UVA irradiation enhances CX-5461 cytotoxicity, causing both replication and transcription-associated lesions.

In the course of investigating the properties of CX-5461, we noticed occasional CX-5461-sensitivity in wild-type animals. The varying WT sensitivity was found to be due to light exposure from the light source of the dissection microscope, which emitted UVA radiation. This observation was similar to reports of photosensitivity in the CX-5461 clinical trial (Hilton et al., 2018; Khot et al., 2019). We speculated that CX-5461 might exhibit photosensitivity in a manner similar to other therapeutics.

To re-create the CX-5461-induced photosensitivity in *C. elegans*, young adults were treated with CX-5461 for ~16 hours and then irradiated with UVA. We found that wild-type N2 were not sensitive to CX-5461 or UVA alone, but were sensitive to CX-5461 followed by UVA irradiation (Figure 3.4A). The toxicity is dose-dependent with both increased UVA exposure or

CX-5461 concentration. Importantly, the effect of UVA-induced CX-5461 toxicity is only observed in worms that have been treated with CX-5461 and then exposed to UVA irradiation, but not in worms treated with *in vitro* UVA-irradiated-CX-5461. This demonstrates that UVA is not changing the properties of CX-5461 to create a more toxic compound.

Next, we tested whether the photosensitivity is limited to the germ line by testing the sensitivity of L1 larvae. We synchronized L1 larvae by starvation, exposed the arrested L1 larvae to CX-5461 for 16 hours followed by UVA irradiation and then released the L1 larvae from arrest by feeding. The effect of the exposure was assessed by measuring development 96 hours later. We found that L1 wild-type larvae were not sensitive to CX-5461 or UVA alone, as these animals developed normally and produced F_1 progeny. In contrast, CX-5461 + UVA exposed animals failed to develop to the adult stage (Figure 3.4B). This demonstrated that the CX-5461 photosensitivity also affects somatic cells in *C. elegans*. Similar results were seen in both mammalian cell culture and yeast (Figure 3.4 C,D). We found that most mutants do not exhibit greater sensitivity to CX-5461 + UVA relative to wild-type animals if one takes into account the CX-5461 sensitivity associated with the mutant. The exceptions were the translesion synthesis (TLS) mutant *rev-3* and the nucleotide excision repair (NER) mutant *xpa-1,* which were much more sensitive to CX-5461 + UVA than predicted based on their CX-5461 sensitivity (Figure 3.4E).

Since NER mutants were sensitive to CX-5461 and most NER activity is transcription-coupled, we speculated that CX-5461 could cause transcription-blocking lesions. Replication-arrested NER defective L1 mutant larva fail to re-initiate development after exposure to UVC, which

causes transcription blocking lesions (Astin et al., 2008). To test whether CX-5461 causes transcription blocking lesions, replication-arrested *xpa-1* L1 mutant larvae were treated with CX-5461 followed by UVA irradiation. NER mutant *xpa-1* L1 larvae failed to develop to later larval stages after CX-5461 + UVA treatment (Figure 3.5A), similar to replication-arrested *xpa-1* L1 when exposed to UVC. This suggests that CX-5461 can also cause transcription-blocking lesions upon UVA irradiation. In contrast, the replication-associated CX-5461 hypersensitive mutant, *mus-81*, reinitiated development after L1 CX-5461 exposure and develop into sterile adults, a phenotype associated with defects in post-embryonic cell proliferation. Consistent with this, the TLS mutant *rev-3* had a very similar phenotype as *mus-81* upon CX-5461 treatment (Figure 3.5B). These strong effects of CX-5461 + UVA suggested that replication and transcription blocking lesions were formed. To further investigate the nature of these CX-5461 + UVA -induced lesions, we tested the CX-5461-sensitivity of the *dvc-1* mutant. DVC-1 has been shown to remove DNA-protein adducts (Stingele et al., 2016). The *dvc-1* mutant was completely sterile and exhibited a protruding vulva phenotype when exposed to CX-5461 + UVA treatment at L1, consistent with the possibility that CX-5461 + UVA could cause lesions that block DNA replication and transcription, like by generating DNA-protein adducts.

3.3.5 CX-5461 causes phototoxicity by generating reactive oxygen species

Many phototoxicities of quinolone compounds are due to generation of reactive oxygen species (ROS) after light exposure (de Guidi et al., 2011). To investigate whether CX-5461 generates ROS after UVA exposure, we used an intracellular fluorescent probe, 2',7'-dichlorodihydrofluorescein diacetate (H_2DCFDA) to assay ROS in CX-5461 + UVA exposed *C. elegans* (Yoon et al., 2017). We found that increasing either UVA irradiation or CX-5461

concentration increased the fluorescent signal, indicating the production of more ROS (Figure 3.5C,D).

The increased ROS could explain the increased sensitivity to CX-5461 + UVA of *xpa-1* and *rev-3* mutants, because NER and TLS are needed to repair ROS-generated DNA damage induced by UVA irradiation (van Bostelen and Tijsterman, 2017). Taken together, these data suggest that CX-5461 causes photo-toxicity by generating ROS.

3.3.6 CX-5461 is mutagenic, UVA enhances its mutagenicity

Since CX-5461 could stabilize G-quadruplexes (Xu et al., 2017), it could lead to replication-associated mutagenic events (Cheung et al., 2002; London et al., 2008). This fact taken together with the observation that several DNA repair pathways were required for CX-5461 tolerance, it was probable that CX-5461 was mutagenic. To assay the mutagenicity of CX-5461, we used the genetic balancer strain BC2200 *dpy-18/eT1(III);unc-46/eT1(V)* to measure the frequency of mutagenic events caused by CX-5461 in the absence and presence of UVA irradiation. The *eT1* balancer is a reciprocal translocation of approximately half of chromosome III and half of chromosome V with *dpy-18* and *unc-46* balanced by *eT1(III)* and *eT1(V)*, respectively. It can capture both single nucleotide variants (SNVs) and copy number variants (CNVs) in balanced regions, including terminal deletion events and translocations (Rosenbluth et al., 1985). Two hundred phenotypically wild-type (genotype: *dpy-18/eT1(III);unc-46/eT1(V)*) F_1s from CX-5461-treated BC2200 animals were picked for each condition and scored for phenotypes. Sterility at F_1 is considered to indicate the acquisition of a dominant lethal mutation, and lines

which produce no Dpy Unc animals in F_2 or later generations are considered to indicate the acquisition of a recessive lethal mutation in the balanced regions on chromosome III or V.

UVA alone or buffer did not cause lethal mutations (less than 0.5% based on the screen). CX-5461 alone resulted in 4 recessive lethals out of 200 (2%). UVA exposure increased the mutagenicity of CX-5461 by more than four times, giving rise to 19 recessive lethals out of 200 (9.5%). CX-5461 and CX-5461 + UVA led to 14 and 19 dominant lethals, respectively (Figure 3.6A).

3.3.7 Mutational profile of CX-5461 (-/+ UVA)

Taking advantage of the genetic balancer *eT1*, we were able to maintain and sequence the 23 lines with recessive lethal mutations. The CX-5461-treated lines contained a range of different mutation types, including large copy number variations (CNVs) and single nucleotide variations (SNVs) (Figure 3.6B,C). By analyzing the mutations on the balanced regions of chromosome III and V, we were able to identify the probable cause of recessive lethality in the 23 lines. Many of the lethal mutations were large CNVs on the balanced regions (2/4 and 7/19 for CX-5461 and CX-5461 + UVA, respectively), whereas others were likely due to SNVs on essential genes on the balanced regions (Table 3.2).

<u>CX-5461-induced CNVs</u>

Both MMEJ and HDR pathways are required for tolerance of CX-5461 (Figure 2.2 & 3.1B), and these two pathways respond to double-strand breaks (DSBs). Likewise, the high frequency of CNVs confirmed the necessity of pathways needed for repair of DSBs. The breakpoints of some

of the CNVs were flanked by regions of microhomology, consistent with the MMEJ signature (Figure 3.6B). Many simple, tandem, and inverted repeats were also found surrounding the breakpoints of CNVs. However, we did not find enrichment of any motifs such as G-quadruplex forming sequences around the breakpoints.

CX-5461-induced SNVs

All lines exposed to CX-5461 contained a high frequency of SNVs. Specifically, we focused on homozygous mutations outside balanced regions and heterozygous mutations on balanced regions. CX-5461 + UVA induced more homozygous (mean 84.11+/-8.5 SEM (standard error of the mean)) and balanced heterozygous SNVs (mean 44.21 +/- 5.1 SEM) than CX-5461 alone (homozygous mean 27.25 +/- 6.6 SEM, balanced heterozygous mean 18.25 +/- 7.1 SEM) (Figure 3.6C). This was consistent with a higher frequency of balanced lethals seen in animals exposed to CX-5461 + UVA.

There was no evident difference in the profiles of heterozygous or homozygous SNVs caused by CX-5461 with or without UVA exposure. Taking all the SNVs together, we found that SNVs were distributed throughout the genome with no trend towards coding regions or non-coding regions (Figure 3.6D). Interestingly, we noticed that around 12% SNVs (517 out of 4284) were in multi-nucleotide mutation (MNM) clusters, in which 2 to 13 mutations occur within a 1000 bp region (Figure 3.6E). Most SNVs (>80%) in MNMs were less than 15 bases from the neighboring mutations. MNMs are a common feature in the genomes of many organisms. About 2% of human genetic polymorphisms are MNM events, and clustered mutations are often present in tumors (Roberts et al., 2012). *De novo* MNMs have been observed in model organisms and human (Lynch et al., 2008; Ossowski et al., 2010; Schrider et al., 2013; Schrider et al., 2011). An

analysis of MNMs in human genomes suggested that MNMs can result from error-prone translesion polymerase activity (Harris and Nielsen, 2014), which is consistent with our observation that TLS mutants are very sensitive to CX-5461.

We hypothesized that the SNVs could be the product of repair or bypass of CX-5461-stabilized G-quadruplexes. To test this, we searched for G-quadruplex forming sequences around each SNV using the QuadBase2 webserver (Dhapola and Chowdhury, 2016). By assessing 100 bp 5' and 3' of the SNVs, we found that SNVs were not strongly correlated with G-quadruplex forming sequences. By comparison, only 0.75% of mutation-flanking regions contained predicted G-quadruplexes in CX-5461-treated genomes compared to 0.45% of the mutation-flanking regions in the ethyl methanesulfonate (EMS)-mutated genomes of the Million Mutation Project (Thompson et al., 2013).

CX-5461-induced SNVs exhibited a unique mutational signature. More than 80% of SNVs were A to X mutations, with nearly half of all SNVs being A to T transversions (Figure 3.6F). Examination of the DNA context surrounding the A to X mutations revealed preferences for bases neighboring the mutated adenine. About 70% of the bases immediately 3' (+1) of the mutated adenine were thymine, whereas cytosine and thymine were overrepresented at the 5' (-1) position (Figure 3.6G). Despite the higher frequency in CX-5461 + UVA-treated genome, there is no difference between the types of SNVs, suggesting that the UVA increases the mutagenicity of CX-5461 but does not affect mutational mechanism.

We also looked whether there was any motif that was prone to CX-5461 mutagenesis. Analyzing the flanking regions (-/+ 100 bp) of sites that were mutated in more than one line (47 sites in total), we observed that more than 50% of them contained inverted or tandem repeats (25/47), and that only 3 out of 47 were predicted to form G-quadruplexes. In a control set of EMS-induced mutations from the Million Mutation Project strains, only 20.2% (753/3719) contained inverted or tandem repeats flanking EMS-induced mutations. Based on these data, it appears that CX-5461 is prone to inducing lesions in regions that contain tandem or inverted repeats.

3.4 Discussion: CX-5461 is a multi-modal anticancer drug

Originally identified as RNA polymerase I inhibitor and then proposed to be a more general G-quadruplex stabilizing agent, CX-5461 appears to have other characteristics associated with antineoplastic activity. Our work sheds light on the photosensitivity, chemi-genetic profile, and mutational signature of CX-5461, and suggests that CX-5461 is a complex multimodal anticancer drug that may be more broadly applicable to anti-cancer therapy than previously expected.

3.4.1 Multiple DNA repair pathways are required for CX-5461-induced DNA lesions.

CX-5461 binds or interacts with DNA to generate lesions that block replication and transcription. Our observation that CX-5461 affects dsDNA migration on agarose gel and inhibits nuclease degradation of dsDNA supports the hypothesis that CX-5461 can bind DNA and alter DNA structure. The nature of CX-5461-DNA interactions can also be inferred through the comparison of chemi-genetic signatures between CX-5461 and other better-characterized agents. For instance, many genotypes are also sensitive to UVA-TMP, an inter-crosslinking (ICL) agent, but

CX-5461 is unlikely to result in ICLs, because Fanconi Anemia (FA) genes are not required for CX-5461 tolerance. Most genes required for CPT-tolerance and ETOP-tolerance are also needed for resolution of CX-5461-induced damage, indicating that CX-5461 could result in DNA replication blocks in a manner similar to CPT and ETOP.

The mechanism of CX-5461 can be differentiated from those of CPT and ETOP by the differential requirements for DSB repair pathways in *C. elegans*. HDR rather than MMEJ contributes to the repair of CPT under normal conditions, since HDR mutants (*brd-1* and *rfs-1*) but not MMEJ mutants (*polq-1*) are sensitive to CPT; whereas MMEJ but not HDR is the primary pathway for ETOP-induced lesions (Figure 2.2). In contrast, both HDR and MMEJ contributed to the repair of CX-5461-induced lesions, as HDR single mutants (*brd-1* and *rfs-1*) and MMEJ mutants (*polq-1*) are all sensitive to CX-5461. Moreover, simultaneous loss of HDR and MMEJ leads to greater CX-5461-sensitivity than expected, as seen in *polq-1 brd-1* and *polq-1 rfs-1* double mutants (Figure 3.1B).

3.4.2 CX-5461 can affect non-G4 DNA

CX-5461 can stabilize G-quadruplexes (Xu et al., 2017). MMEJ is needed for the bypass of G-quadruplexes (Koole et al., 2014) and CX-5461 tolerance in *C. elegans* (Figure 2.2 & 3.1B). It is possible that CX-5461 stabilizes G-quadruplexes and other secondary structures that form barriers to replication and transcription. Aspects of the CX-5461 genotypic sensitivity profile are similar to that of the genetic interactions with *dog-1*, the *C. elegans* homolog of *FANCJ* that unwinds G-quadruplexes (Youds et al., 2008). However, if CX-5461 exclusively affects G-quadruplexes, we would expect that loss of *dog-1* should fully phenocopy CX-5461 treatment.

Although many CX-5461-sensitive genotypes are also sensitive to loss of *dog-1*, including *polq-1*, *brd-1*, *rfs-1* and *smrc-1*, all of which have been implicated in resolution of G-tract in the absence of *dog-1* (Koole et al., 2014; Ward et al., 2007; Yang et al., 2019; Youds et al., 2006), the CX-5461-hypersensitive mutant *rev-3* did not exhibit a genetic interaction with the *dog-1* mutant. This suggests that CX-5461 could cause lesions that are not G-quadruplex-associated.

3.4.3 The double-edged sword of therapeutic photosensitivity

We also investigated the phototoxicity of CX-5461. CX-5461 caused photosensitivity in some patients (Hilton et al., 2018; Khot et al., 2019). This is similar to many other therapeutics that exhibit phototoxicity, such as vemurafenib, tamoxifen, and docetaxel (Zuba et al., 2016). We phenocopied CX-5461 photosensitivity in *C. elegans*, and demonstrated that an increase in either UVA irradiation or the concentration of CX-5461 enhanced the cytotoxicity. We also determined that the toxicity enhancement was due to generation of reactive oxygen species (ROS). Despite that, we did not see a ROS-induced mutational signature from genomes treated with CX-5461 + UVA. It is worth noting that either a high amount of UVA irradiation or a high concentration of CX-5461 alone is required to affect the growth and viability of wild-type animals. Worm DNA repair pathways could be sufficient to repair ROS-induced damage from CX-5461 + UVA. This is supported by the observation that the only mutants that were more sensitive to CX-5461 + UVA were TLS and NER mutants, both of which have previously been shown to repair UVA-mediated ROS damage (van Bostelen and Tijsterman, 2017) .

Photosensitivity is a double-edged sword. While phototoxicity is a deleterious side-effect, the ability to generate ROS in response to UVA light could be leveraged for photo-dynamic therapy,

in which targeted light is used to activate a photosensitizer within cancer cells leading to cell death (Banerjee et al., 2017; Yanovsky et al., 2019). Given the strong ROS-mediated phototoxicity and positive drug properties of CX-5461, CX-5461 may be an option for photo-dynamic therapy with fiber-optic light guides to deliver UVA to the tumor site (Mallidi et al., 2016). Since all genotypes of worm animals exhibit photosensitivity to CX-5461, it is likely that many different types of cancer would benefit from CX-5461.

3.4.4 CX-5461 has a complex mutational profile

We showed that CX-5461 is mutagenic and that the mutagenicity increases with UVA irradiation. The mutation frequencies for CX-5461 and CX-5461 + UVA were comparable to exposure to 5 mM and 25 mM Ethyl Methane Sulfonate (EMS), a common alkylating mutagen, or 1000 and 2500 rads gamma radiation (Rosenbluth et al., 1985). Consistent with the complex genotypic sensitivity profile, CX-5461-treated genomes have a complex mutational signature that includes both CNVs and SNVs. Since mutational signatures are characteristic, and dictated by the type of DNA damage and DNA repair process, we can use these signatures to better understand the mechanism of action of CX-5461.

Most CX-5461-treated genomes had CNVs, which are usually associated with formation and resolution of DSBs. This was also supported by the requirement of HDR and MMEJ for CX-5461-tolerance. In addition to CNVs, a high frequency of SNVs was also found in CX-5461-treated genomes. The CX-5461-induced A to X mutations were similar to the mutational signature observed in human urothelial cancers that have been exposed to aristocholic acids (Hoang et al., 2013; Poon et al., 2013). However, the extended sequence context differed

between CX-5461 (CATG) and aristolochic acid (T/CAG). In addition, aristolochic acid results almost exclusively in A-T changes, whereas CX-5461 caused A-X changes. The mutational signature of aristocholic acid shows a strong transcriptional strand bias (Poon et al., 2013), and our data does not support a strand bias for CX-5461 mutagenesis. Despite this, we showed evidence that the NER pathway (which is often transcription-associated) is required for the tolerance of CX-5461, and that CX-5461 + UVA could lead to lesions that arrested L1 development, which has been used as an indirect readout of transcriptional competence (Astin et al., 2008). Given the high frequency of SNVs, the hypersensitivity of TLS mutants, and the presence of MNMs, it is likely that error-prone TLS activity is responsible for the A-X changes in CX-5461-treated genomes in a similar manner as A-T change in tumor cells exposed to aristolochic acids (Hashimoto et al., 2016).

3.4.5 CX-5461 could function in a similar manner as ellipticines

The exact mechanism of how CX-5461 might interact with DNA to form blocking lesions is still unknown. Interestingly, CX-5461 shares a number of characteristics with another antineoplastic compound, ellipticine. Ellipticines have been shown to bind and stabilize G-quadruplexes, and selectively inhibit RNA polymerase I (Wei et al., 2018). A number of studies have also reported that ellipticines intercalate into DNA (Andrews et al., 2013) and lead to inhibition of topoisomerase II upon oxidation by cytochromes P450 (Stiborova et al., 2001). Ellipticines also induce reactive oxygen species (Kim et al., 2011). These characteristics lead us to speculate that CX-5461 acts in a manner similar to ellipticine in causing DNA lesions and activating cellular responses. An *in silico* analysis demonstrated that the pharmacophore of CX-5461 can intercalate into the DNA sequence CGATCG in a similar fashion to ellipticine, resulting in a slight

unwinding of ApT and lengthening of DNA (Andrews et al., 2013). This could account for the propensity of adenine as a substrate for CX-5461 mutagenesis mediated by TLS. The gel shift experiments showed that 25 μM CX-5461 could result in DNA band shift on an agarose gel, suggesting that CX-5461 binds to and distorts DNA migration. This *in vitro* gel shift assay, while not a perfect simulation of the interactions that occur within a cell, can be used to shed light on the interaction between CX-5461 and DNA. Similarly, although the half maximal inhibitory concentration (IC_{50}) for killing *BRCA2*-deficient HCT-116 cells is 4.8 nM, and the IC_{50} for RNA polymerase I inhibition in HCT-116 cells, is 142 nM (Drygin et al., 2011; Xu et al., 2017), CX-5461-induced G4-stabilization was confirmed by an *in vitro* melting assay at the micro-molar level (Xu et al., 2017). It could be that higher concentrations of CX-5461 are required to see measurable effects *in vitro*, and that the effect could be more localized to specific DNA structures at lower concentrations of CX-5461. Additionally, we do not yet know whether CX-5461 forms covalent bonds with DNA, as some ellipticine metabolites have been shown to, or whether metabolic processing of CX-5461 is required for formation of covalent bonds between CX-5461 and DNA.

In summary, CX-5461 is a multimodal DNA damaging agent that shares properties with the antineoplastic agent ellipticine. Ellipticines have failed in stage 1 and 2 clinical trials due to strong adverse side effects (Andrews et al., 2013). It is possible that CX-5461 could provide the anti-cancer properties of ellipticine but with fewer adverse effects.

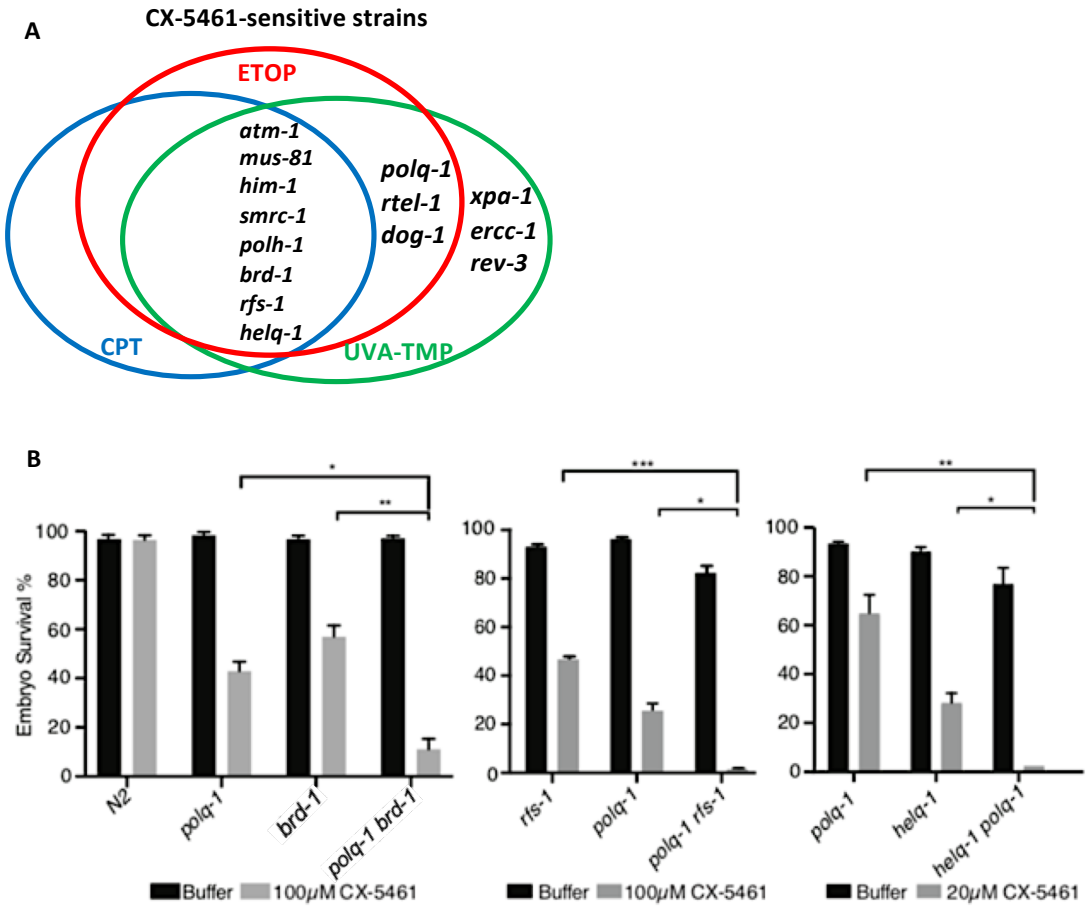

Figure 3.1 Genotypic sensitivity to CX-5461. (A) Genotypic sensitivity profile of CX-5461. Venn diagram shows that the CX-5461-sensitive mutants also exhibited sensitivity to other DNA-damaging agents, including Etoposide (ETOP), Camptothecin (CPT), and UVA-irradiated trimethylpsoralen (UVA-TMP). (B) Loss of *polq-1* sensitizes HDR-associated mutants (*brd-1, rfs-1,* and *helq-1*) to CX-5461. Embryo survival rate of indicated mutants treated with CX-5461. Error bars represent the standard error of the mean. Student t tests were used to compare the embryo survival rates between indicated mutants. *, P <0.05; **, P <0.01; ***, P<0.001.

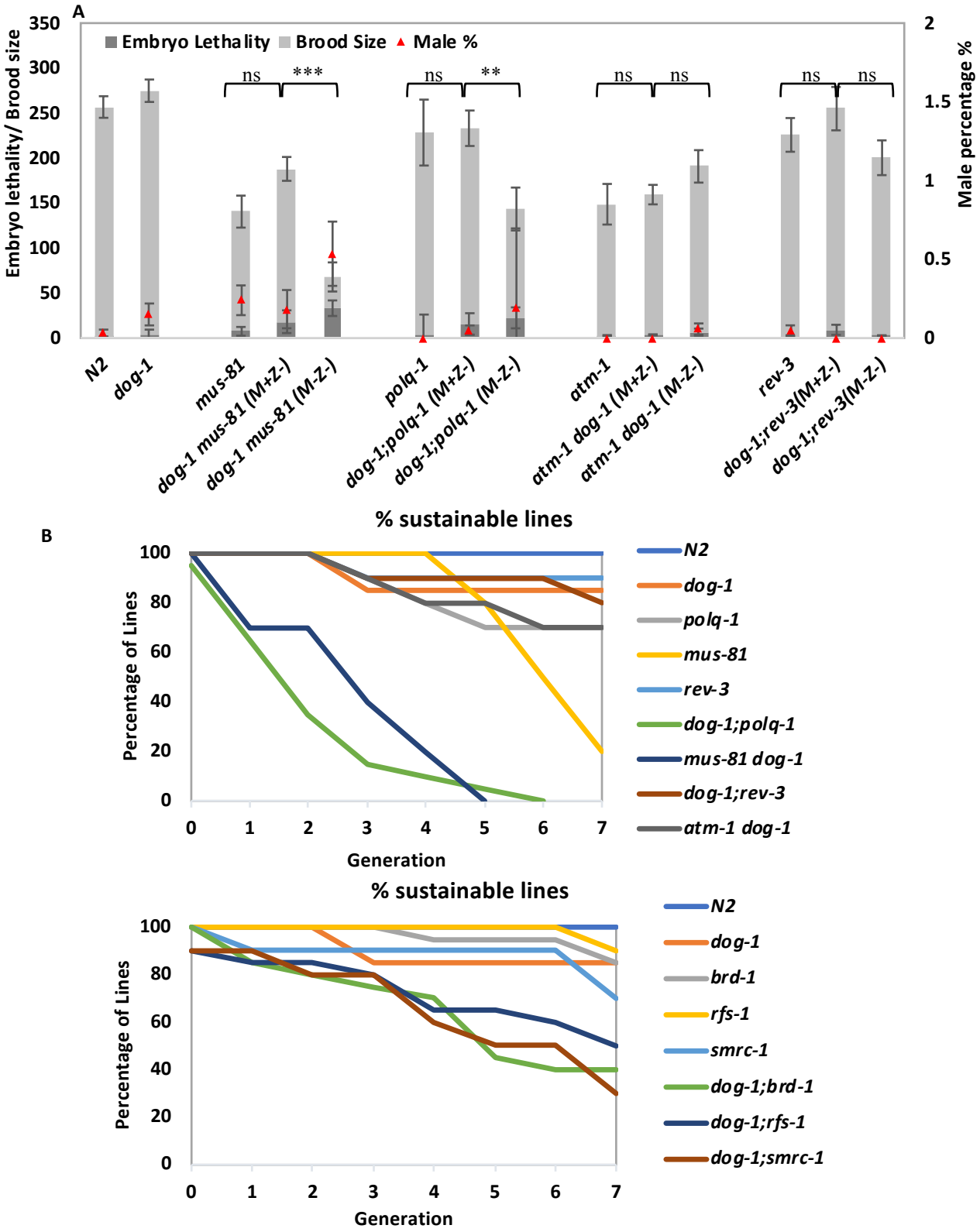

Figure 3.2 Effect of G-quadruplex stabilization on CX-5461-sensitive mutants. (A) Brood size, embryonic lethality and male percentage in *dog-1* and *dog-1*-containing double mutants. Error bars represent the standard error of the mean. Student t tests were used to compare brood sizes between indicated animals. * denotes p value less than 0.05, ** <0.01, ***<0.001. (B) Percentage of sustainable lines by generational fitness assay. M+Z-: maternally positive and zygotically negative. M-Z-: maternally negative and zygotically negative.

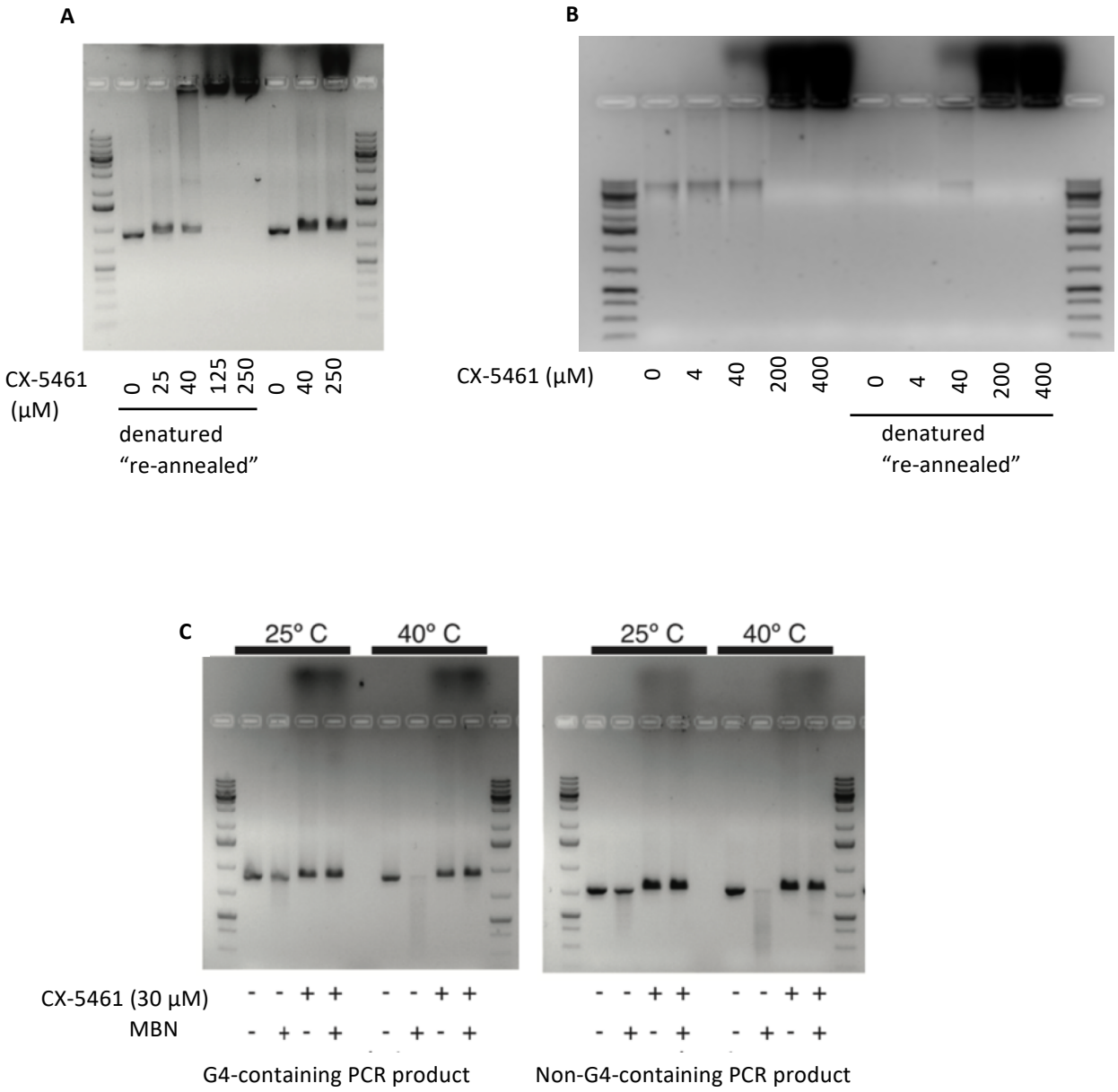

Figure 3.3 CX-5461 stabilizes DNA duplex structures. (A and B) CX-5461 binds to and shifts DNA. CX-5461 binding is enhanced by DNA denaturation and re-annealing. Non G4-containing PCR products (719 bp) were used in A, and sheared worm genomic DNA (about 6 kbp) was used in B. (C) CX-5461 stabilizes PCR products and the complex were more resistant to Mung Bean Nuclease (MBN) cleavage. Two different PCR products were used in the study, G4-containing PCR products (890 bp) and non-G4-containing PCR products (719 bp).

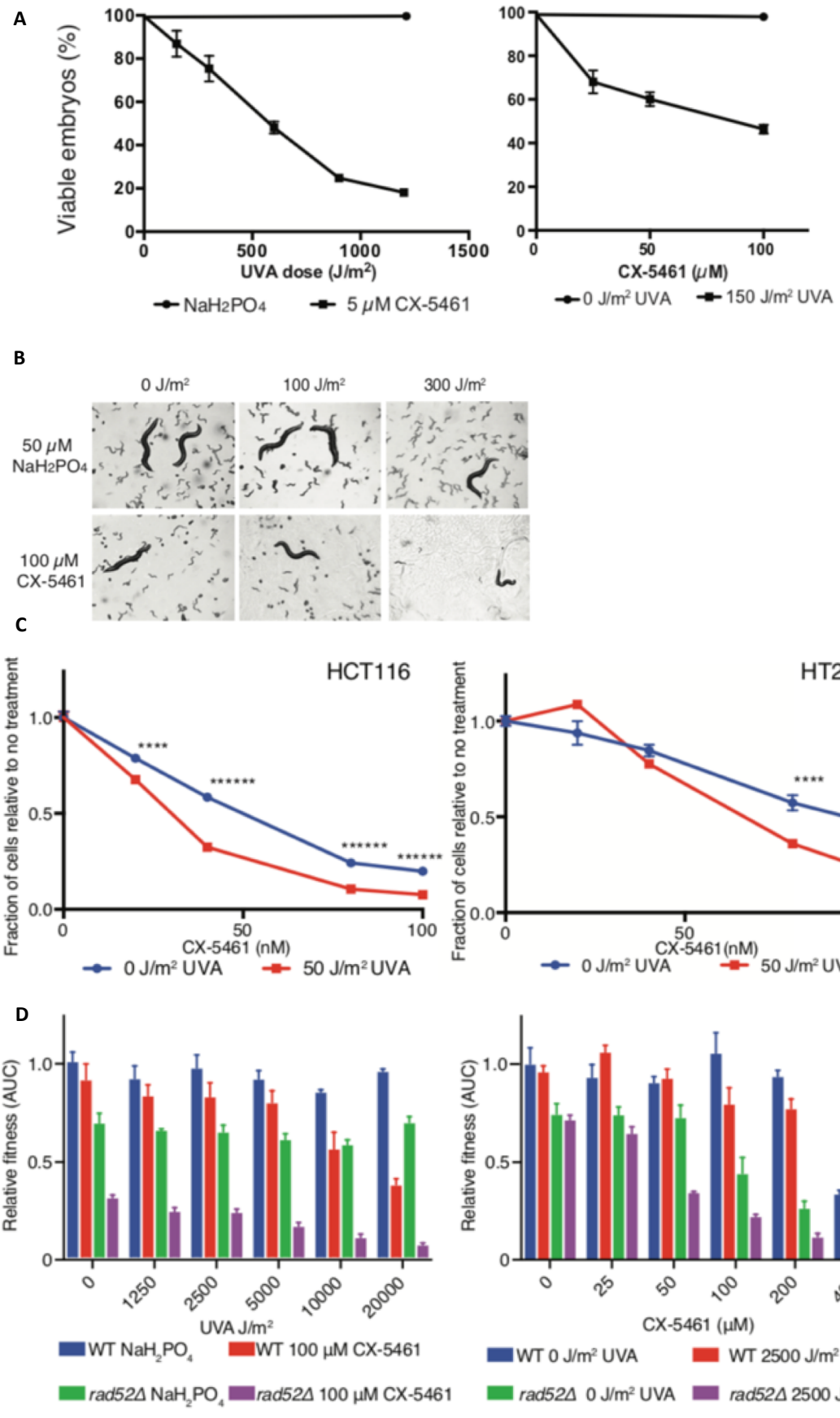
A
Viable embryos (%)
UVA dose (J/m²)
NaH2PO4
5 μM CX-5461
CX-5461 (μM)
0 J/m² UVA
150 J/m² UVA
B
0 J/m²
100 J/m²
300 J/m²
50 μM NaH2PO4
100 μM CX-5461
C
HCT116
HT29
Fraction of cells relative to no treatment
CX-5461 (nM)
0 J/m² UVA
50 J/m² UVA
D
Relative fitness (AUC)
UVA J/m²
WT NaH2PO4
WT 100 μM CX-5461
rad52Δ NaH2PO4
rad52Δ 100 μM CX-5461
CX-5461 (μM)
WT 0 J/m² UVA
WT 2500 J/m² UVA
rad52Δ 0 J/m² UVA
rad52Δ 2500 J/m² UVA

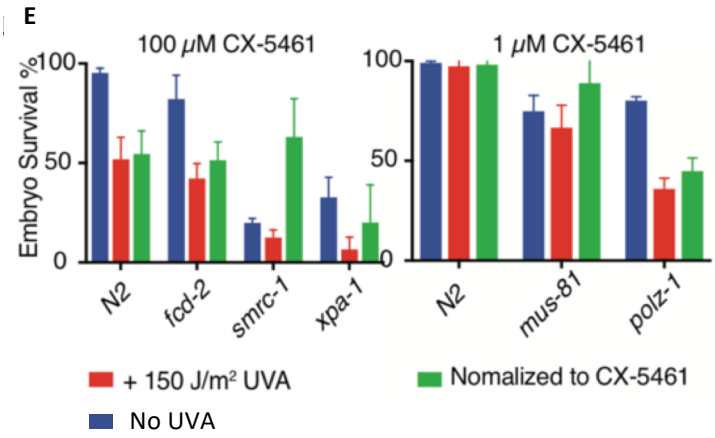

Figure 3.4 CX-5461 is a photosensitizer in *C. elegans*, human cancer cell lines and yeast. (A) Viability of WT *C. elegans* embryos from adult animals exposed to CX-5461 and irradiated with UVA. Left-fixed [CX-5461]; Right-fixed UVA dose. Error bars represent standard error of the mean. (B) Representative images of WT *C. elegans* populations 96 hours after CX-5461 +UVA exposure of synchronized WT L1 larvae. The large animals are the treated P0 individuals. (C) HCT116 and HT29 colorectal cancer cell lines were treated with increasing concentrations of CX-5461 and exposed to UVA irradiation in 96-well format and cell nuclei counted after 96 hours. Student tests were used to compare the fraction of cells under different conditions. ****, P< 0.0005; ******, P<0.000005 . (D) Growth curve analysis of the relative fitness of wild-type and rad52 yeast exposed to CX-5461 + UVA radiation. Left-fixed [CX-5461]; Right-fixed UVA dose. (E) Differential sensitivity of worm mutants upon CX-5461 + UVA.

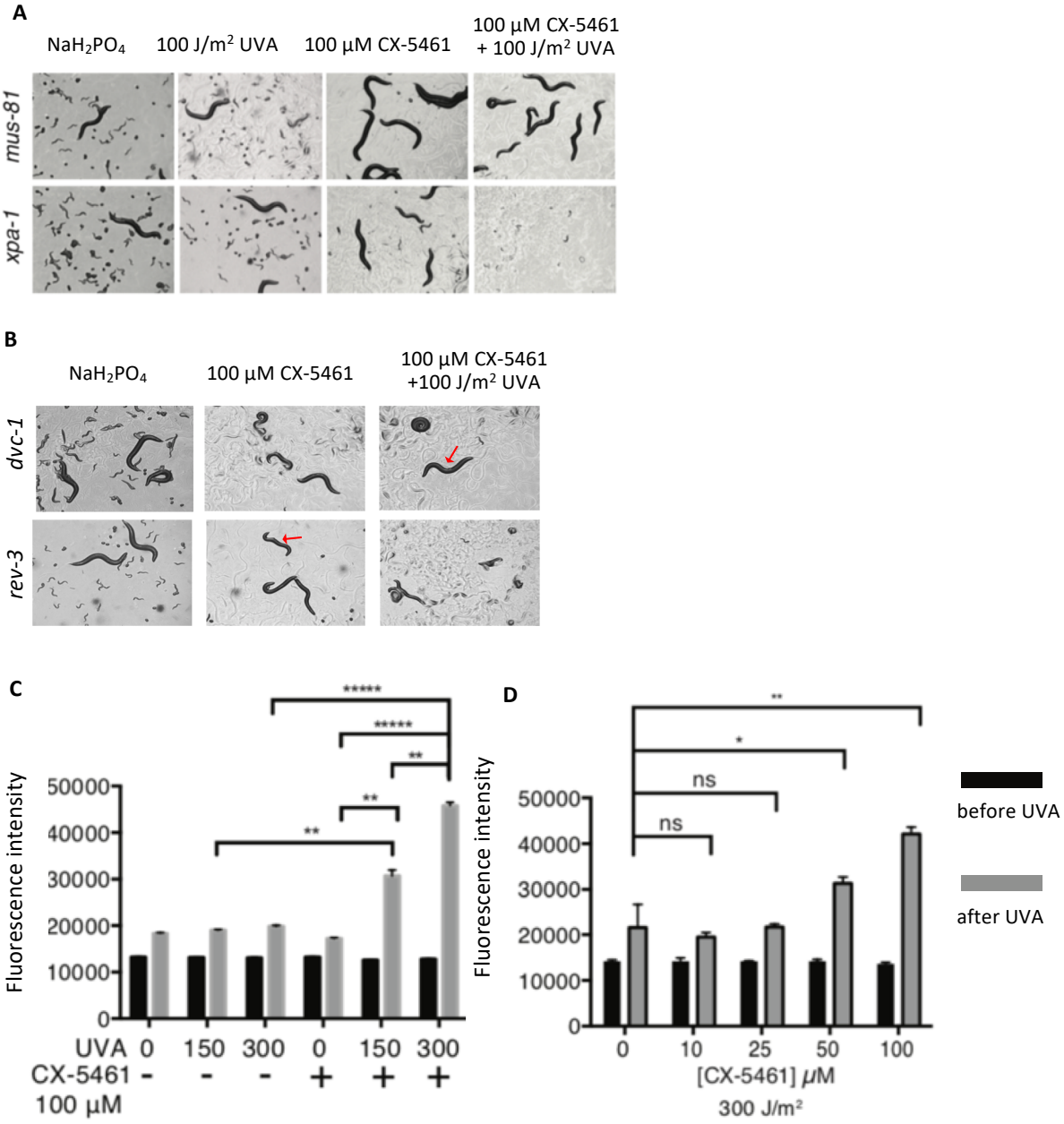

Figure 3.5 CX-5461 + UVA can result in photodamage by generating ROS. (A) UVA enhances the toxicity of CX-5461 that affect replication and transcription. The image shows the growth and development of worms four days after L1 larva-treatment. Upon CX-5461 treatment and UVA irradiation, *mus-81* mutants became completely sterile, whereas *xpa-1* mutants were arrested in L1. (B) CX-5461 could lead to DNA-protein adduct or bulky lesions. Upon CX-5461 treatment and UVA irradiation, *dvc-1* and *rev-3* mutants became mostly sterile and exhibited Pvl (protruding vulva) phenotypes (red arrows). (C) Intracellular ROS levels were measured in CX-5461 + UVA treated wild-type *C. elegans* with constant [CX-5461] and with (D) a constant UVA dose. Student t tests were used to compare the fluorescent intensity of different conditions. *, $P < 0.05$; **, $P < 0.01$; *****, $P < 0.00001$. The black bars represent fluorescent intensity before UVA irradiation, the grey bars represent the fluorescent intensity after UVA irradiation.

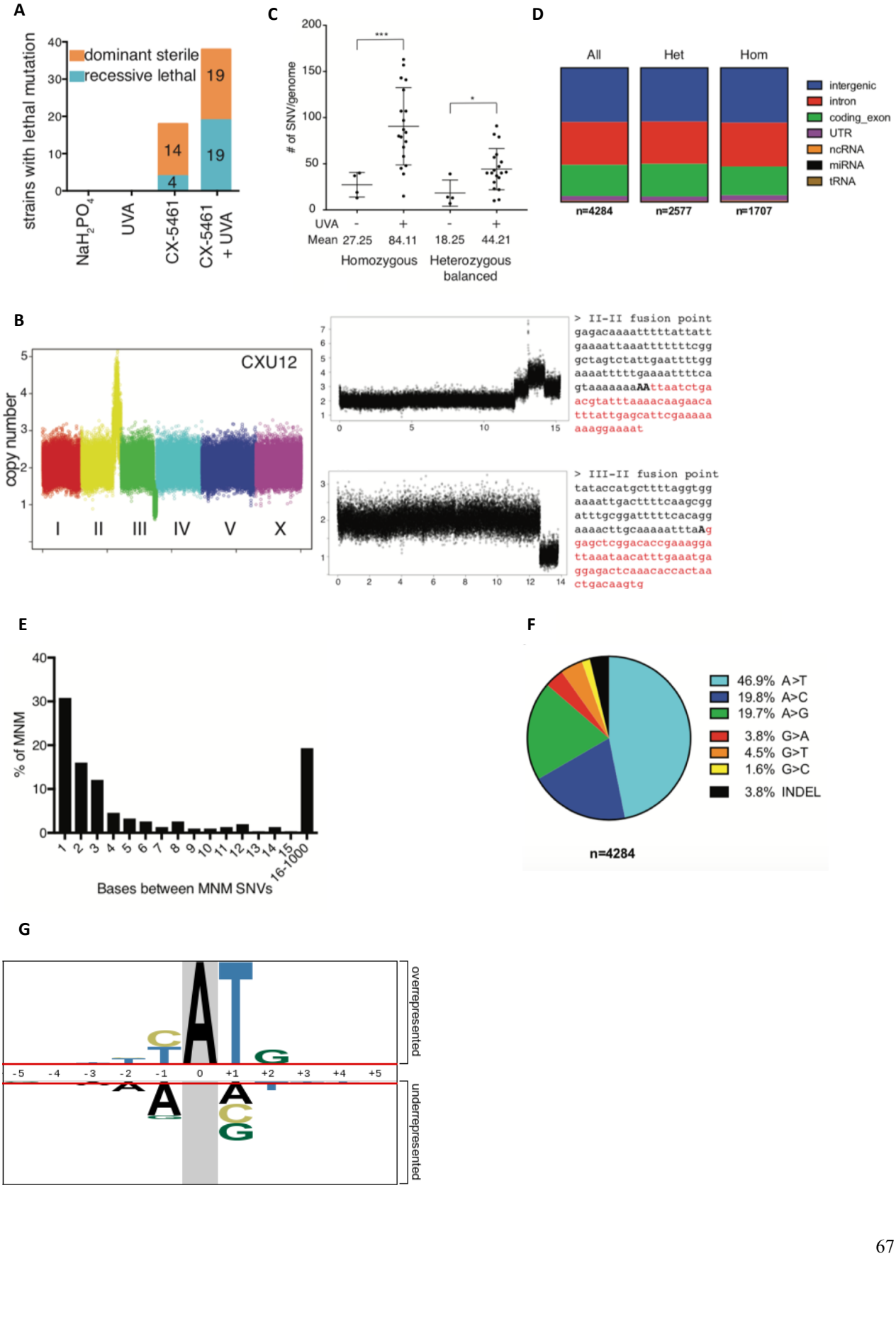
A
strains with lethal mutation
dominant sterile
recessive lethal
19
14
19
4
NaH2PO4
UVA
CX-5461
CX-5461 + UVA
C
# of SNV/genome
***
*
UVA - + - +
Mean 27.25 84.11 18.25 44.21
Homozygous
Heterozygous balanced
D
All
Het
Hom
intergenic
intron
coding_exon
UTR
ncRNA
miRNA
tRNA
n=4284
n=2577
n=1707
B
CXU12
copy number
I II III IV V X
> II-II fusion point
gagacaaaatttttattatt
gaaaattaaatttttttcgg
gctagtctattgaattttgg
aaaatttttgaaaattttca
gtaaaaaaaAAttaatctga
acgtatttaaaacaagaaca
tttattgagcattcgaaaaa
aaaggaaaat
> III-II fusion point
tataccatgcttttaggtgg
aaaattgacttttcaagcgg
atttgcggatttttcacagg
aaaacttgcaaaaatttaAg
gagctcggacaccgaaagga
ttaaataacatttgaaatga
ggagactcaaacaccactaa
ctgacaagtg
E
% of MNM
Bases between MNM SNVs
1 2 3 4 5 6 7 8 9 10 11 12 13 14 15 16-1000
F
46.9% A>T
19.8% A>C
19.7% A>G
3.8% G>A
4.5% G>T
1.6% G>C
3.8% INDEL
n=4284
G
overrepresented
underrepresented
-5 -4 -3 -2 -1 0 +1 +2 +3 +4 +5

Figure 3.6 Exposure to CX-5461 or CX-5461 + UVA results high frequencies of mutations. (A) Number of balanced recessive lethal mutations and dominant sterile mutations. n=200 for each condition. (B) Coverage plot of CX-5461 + UVA-induced genome rearrangements in sample CXU12. Whole genome (Left). Detailed coverage plot of chromosome II (Top right) and chromosome III (bottom right). Sequence at the fusion shown on right. Microhomology in bold. (C) Number of homozygous and heterozygous balanced SNVs/genome. Welch's t-test was used to compare the number of SNV per genome under different conditions. *** $p<0.0005$, * $p<0.05$. (D) Distribution of SNVs in coding and non-coding elements. (E) Distance between SNVs in multi-nucleotide mutations. (F) SNV mutational signature of CX-5461. (G) Extended sequence context of CX-5461-induced SNVs.

Genotypes	Brood size	Embryo Survival Rate %	Male %	n
N2	256.71±12.00	99.58±0.22	0.03±0.02	14
dog-1	274.80±12.47	98.44±1.78	0.15±0.07	20
mus-81	140.40±17.78	94.80±3.47	0.24±0.09	10
mus-81 dog-1 (M+Z-)	187.90±13.25	90.42±6.72	0.18±0.12	10
mus-81 dog-1 (M-Z-)	67.75±16.18	51.29±12.76	0.53±0.20	8
polq-1	228.30±36.64	98.51±9.87	0.00±0.00	10
dog-1;polq-1 (M+Z-)	233.10±19.71	93.39±5.16	0.05±0.03	20
dog-1;polq-1 (M-Z-)	143.29±23.85	84.45±8.12	0.19±0.51	14
atm-1	148.60±22.58	98.52±0.61	0.00±0.00	10
atm-1 dog-1 (M+Z-)	159.30±10.83	97.87±0.35	0.00±0.00	10
atm-1 dog-1 (M-Z-)	190.70±18.04	96.64±2.07	0.06±0.04	10
rev-3	225.70±18.74	99.11±0.39	0.05±0.03	10
dog-1;rev-3(M+Z-)	254.90±24.10	96.47±2.20	0.00±0.00	10
dog-1;rev-3(M-Z-)	200.30±19.32	98.80±0.27	0.00±0.00	10

Table 3.1 Phenotypes of indicated mutants. n denotes the number of parent worms whose progeny were scored. All values are ± standard error of the mean. M+Z-: maternally positive and zygotically negative. M-Z-: maternally negative and zygotically negative.

	Line	SNVs	Balanced heterozygous SNVs	Homozygous SNVs	Balanced CNVs	Putative lethal mutation
CX-5461	1	68	14	52	III Del	
	2	58	5	51	V Del	
	3	348	47	11		chc-1 stop
	4	46	13	19		F54C8.4 stop
CX-5461 + UVA	1	159	38	62		plrg-1 FS
	2	283	52	117	III Del MH	
	3	190	34	107		mrpl-1
	4	241	60	130	III Del	strd-1/mlc-7
	5	144	37	80	V Del MH	
	6	258	57	143	III Dp	multiple
	7	178	45	87		hpo-26
	8	121	35	68	III Del/Inv	
	9	179	52	95	V Del III Inv	multiple
	10	201	33	107		T05H4.10
	11	151	35	74	V Dp	npp-16
	12	138	23	56	III Del	
	13	54	11	15	V Trans	
	14	485	89	157	V Del	let-413
	15	243	43	84		klp-7
	16	154	22	39		pri-1
	17	222	39	79		ncx-2
	18	168	29	43	III Del	
	19	195	10	31		?

Table 3.2 Summary of mutations on CX-5461-treated and CX-5461 + UVA mutants. (SNV, single nucleotide variation. CNV, copy number variation. Del, deletion. MH, microhomology. FS, frameshift. Dp, duplication. Inv, inversion. Trans, translocation.)

CHAPTER 4: GENETIC INTERACTIONS BETWEEN AND WITHIN DOUBLE-STRAND BREAK REPAIR PATHWAYS IN *C. ELEGANS*

4.1 Introduction

Cells are exposed to endogenous and exogenous damage that results in DNA lesions, including double-strand breaks (DSBs), which if not properly resolved can lead to genome instability. Cells have evolved various DNA damage repair pathways to counteract the deleterious effects of DNA damage. As mentioned in Chapter 1, cells can directly ligate DSBs using the non-homologous end joining (NHEJ) pathway, or resect the DSB ends to allow homology-based repair, including the homology-directed repair (HDR) and the microhomology-mediated end joining (MMEJ) (Ceccaldi et al., 2016a) (Figure 1.1 and 4.1). Each pathway has substrate specificity and a set of specific proteins involved. While the mechanisms of DNA repair pathways are well characterized, how these repair pathways interact to ensure error-free repair is less understood. Here, we studied the interplay within and between the different DSB repair pathways in response to endogenous meiotic DSBs and DNA damaging agent-induced DSBs.

Components of the DSB repair process are well conserved across metazoans. Therefore, we used *C. elegans* as a model to investigate genetic interactions among the three DSB repair pathways. The key factors involved in these three DSB repair pathways are fairly well characterized. By assaying and comparing the phenotypes of single, double, triple or quadruple mutants, we are able to shed light on how different DSB repair pathways interact and are regulated in response to intrinsic meiotic DSBs and extrinsic chemical-induced DSBs.

4.1.1 HDR factors

BRC-2 and RAD-51

HDR involves homology-templated repair. RAD51 filaments are essential for homology searching. The loading and stabilization of RAD51 filaments at ssDNA regions, after DSBs have been extensively resected, requires BRCA2 (Prakash et al., 2015) (Figure 4.1). *BRCA2* is the tumor suppressor gene commonly mutated in breast and ovarian cancers (King et al., 2003). The *C. elegans* homologs of *BRCA2* and *RAD51*, *brc-2* and *rad-51* are both emb (embryonic lethal), and therefore cannot be maintained as a viable strain (Alpi et al., 2003; Martin et al., 2005). For this reason, we focused on non-essential HDR factors and their genetic interactions.

BRD-1

BARD1, the interacting partner of the tumor suppressor gene *BRCA1*, has been extensively studied. *BRCA1* is one of the best characterized tumor suppressor genes and is frequently mutated in breast and ovarian cancer (Futreal et al., 1994; King et al., 2003). The BRCA1/BARD1 heterodimer is critical for homologous recombination-mediated repair of DSBs, by promoting DNA break resection and preventing non-homologous end joining (Densham et al., 2016). Loss of *BRCA1/BARD1* is associated with sensitivity to a number of chemotherapeutic agents, including cisplatin and etoposide (Bunting et al., 2012; Treszezamsky et al., 2007). Both *BRCA1*- and *BARD1*-null mutants are embryonic lethal in mammals (Hakem et al., 1996; McCarthy et al., 2003). The *C. elegans BRCA1* and *BARD1* homologs, BRC-1 and BRD-1, are not essential for embryogenesis but are required for repairing DNA lesions caused by camptothecin or ionizing radiation (Boulton et al., 2004; Park et al., 2016). In addition, it was reported that the BRC-1/BRD-1 heterodimer is also needed for non-crossover resolution of meiotic DSBs via an inter-sister pathway (Adamo et al., 2008) (Figure 4.1). More recent studies

showed that BRC-1/BRD-1 promotes stage-specific RAD-51 recruitment in recombination- and synapsis-impaired mutants (Janisiw et al., 2018; Li et al., 2018).

RFS-1

RAD51 paralogs are mediators of HDR repair pathways that act in concert with BRCA2, and RAD51 to facilitate HDR events. RFS-1/RIP-1/SWS-1 is the heterodimeric RAD51 paralog complex in *C. elegans*, and has been shown to physically interact with RAD-51 and BRC-2 (Martin et al., 2005). Unlike BRC-2 and RAD-51 in *C. elegans*, RFS-1 is dispensable for repairing SPO-11-generated and ionizing radiation-induced DSBs. However, RFS-1 is required for RAD-51 recruitment at replication blocking lesions, including those caused by camptothecin or DNA crosslinking agents (Ward et al., 2007). RFS-1/RIP-1/SWS-1 binds and remodels RAD-51 filaments to a flexible conformation that is prone to strand exchange (Taylor et al., 2015; Taylor et al., 2016). It appears that RFS-1/RIP-1/SWS-1 plays multiple roles in regulating RAD-51 filaments, from recruiting to remodeling, from stabilizing to unloading (Figure 4.1). It will be useful to study how RFS-1 interacts with other HDR factors to better understand the biological role of RFS-1/RIP-1/SWS-1.

HELQ-1

HELQ belongs to the HEL308 gene family, and can unwind DNA with a 3' to 5' polarity in an ATP-dependent manner (Han et al., 2016). HELQ mutations are observed in ovarian cancers, however, whether or how HELQ might contribute to tumorigenesis and tumor development is unclear (Pelttari et al., 2016). Mammalian HELQ is recruited to the stalled replication forks and unwind parental strands to recruit repair factors (Tafel et al., 2011). The worm homolog, *helq-1* is required for tolerance of interstrand crosslinking agents (ICLs) (Muzzini et al., 2008), as is *rfs-1*. *helq-1* and *rfs-1* operate redundantly to disassemble RAD-51 filaments from double-strand

breaks in meiosis in *C. elegans* germ line (Ward et al., 2010) (Figure 4.1). Consistent with this observation, *rfs-1* is synthetic lethal with *helq-1*, most likely due to persistent meiotic RAD-51 foci (Ward et al., 2010). More recently, human HELQ has been shown to interact with RAD51 paralogs and function in the ICL repair pathway (Takata et al., 2013). It remains largely unknown how HELQ interacts with other DNA repair factors and how it is regulated.

4.1.2 NHEJ factors

CKU-80

NHEJ directly ligates two broken DNA ends with no need for sequence homology, which can result in the loss of bases or translocations of DNA. KU70 and KU80 are NHEJ factors that form heterodimer that binds to the broken end of a DSB, preventing the broken end from nuclease processing. The KU70/80 heterodimer recruits ligase IV to seal the breaks (Figure 4.1). NHEJ is the predominant DSB repair pathway in non-cycling somatic cells (Ceccaldi et al., 2016a). In *C. elegans,* loss of NHEJ components sensitizes late stage embryos to ionizing radiation, resulting in somatic developmental defects (Clejan et al., 2006). CKU-70/80 activity is normally suppressed in wild type germ cells, but improper CKU-70/80 activity can occur in the absence of the nuclease MRE-11 or COM-1/CtIP (Lemmens et al., 2013; Yin and Smolikove, 2013), which function to resect the broken ends at DSBs (Figure 4.1). It has been shown that the resection of DSBs dictates repair choice between HDR and NHEJ (Ceccaldi et al., 2016a; Panier and Boulton, 2014). To ensure proper repair pathway choice, DSB end resection is a highly regulated process that can be affected by cell stage, the post-translational modifications of the chromatin surrounding DSBs, and a number of accessory factors including 53BP1 and shieldin (Ceccaldi et al., 2016a; Noordermeer et al., 2018). Studies in mammalian cells have shown that knock down

of KU70/80 alleviates sensitivity of *BRCA*-deficient mutants to PARP inhibitors (Bunting et al., 2012). It is not known whether a similar antagonism exists between *cku-70/80* and other HDR factors in *C. elegans*.

4.1.3 MMEJ factors

POLQ-1

POLQ encodes the polymerase theta (Pol θ), which similar to HELQ, belongs to the HEL308 family. Pol θ has a family A DNA polymerase motif at the C-terminus and DNA helicase-like motif at the N-terminus. Pol θ is involved in MMEJ, an end joining DSB repair mechanism that does not involve KU proteins. MMEJ requires DNA end resection and mediates the joining of resected DSBs that harbor microhomology (Figure 4.1). The *C. elegans* homolog, *polq-1*, was first described to be required for tolerance of interstrand crosslinking (ICLs) in a pathway distinct from *helq-1*, another HEL308 family member (Muzzini et al., 2008). POLQ-1 plays an important role in preventing catastrophic chromosomal events at endogenous replication blocking sites (Koole et al., 2014; Roerink et al., 2014). POLQ-1 generates small indels initiated from G4 loci in the absence of *dog-1*, the *C. elegans FANCJ* homolog. POLQ-1 also generates small deletions in EMS and UVA+TMP-treated TLS mutant animals (van Schendel et al., 2016). In mammalian cell lines, loss of *BRCA1/2* and *POLQ* is synthetic lethal, which suggests Pol θ as a potential therapeutic target for tumors carrying mutations in HDR genes (Mateos-Gomez et al., 2015). We used the *C. elegans polq-1* mutant to study the interplay of MMEJ with other DSB repair pathways with respect to different types of DNA lesions.

4.1.4 The *C. elegans* germ line

The *C. elegans* germ line is extremely useful for studying genes involved in DNA replication and repair, particularly DSB repair, because all stage of meiosis can be observed in a spatial-temporal gradient. The germ line starts at the distal tip, where stem germ nuclei undergo mitosis in the mitotic zone. Adjacent to the mitotic zone, nuclei progress to the transition zone, where meiosis begins and at this stage meiotic DSBs are introduced by the SPO-11 endonuclease (Dernburg et al., 1998). After the transition zone, nuclei progress into pachytene which is followed by diplotene and diakinesis, during which DSBs have to be properly resolved. In diakinesis, crossover recombination occurs and condensed chromosomes can be seen as six dumbbell-shaped bivalents. The *C. elegans* germ line allows direct visualization of the effect on chromosomes when DSB repair factors are disrupted.

4.1.5 Genetic interactions

A genetic interaction occurs when the phenotypic effects of one gene are modified by one or several other genes. Negative genetic interactions (NGIs) occurs when mutation of two genes in a double mutant leads to a fitness defect greater than that predicted for the additive effect of the two single gene mutations alone. NGIs can manifest as synthetic lethality (SL) or synthetic sickness (SS). SL is an extreme situation where perturbations of two genes result in loss of viability, while SS is a sub-lethal fitness defect. Positive genetic interactions occur when a double mutant has a less severe fitness defect than expected based on the additive effects of the two single mutants, which could be epistasis or phenotypic suppression.

Complete loss of the HDR pathway leads to inviability in *C. elegans*, because homologous paring and recombination are required for meiosis (Hillers et al., 2017). Loss of NHEJ factors can partially alleviate severe HDR phenotypes, but cannot fully rescue fertility (Lemmens et al., 2013; Macaisne et al., 2018; Yin and Smolikove, 2013). It remains largely unknown how different HDR factors genetically interact to maintain HDR functions in meiosis, and how other non-HDR repair mechanisms (including NHEJ and MMEJ) affect HDR to counteract both endogenous and exogenous DNA lesions. Here in this chapter, we focus on the genetic interactions between and within DSB repair pathways in *C. elegans*.

4.2 Methods

Construction of mutant strains

Alleles used in this chapter include: *atm-1(tm5027)*, *brd-1(dw1)*, *rfs-1(ok1372)*, *cku-80(ok861)*, *polq-1(tm2026),* and *helq-1(tm2134).* Some strains were provided by the Caenorhabditis Genetics Center, which is funded by NIH Office of Research Infrastructure Programs (P40 OD010440), and some knockout alleles were provided by the Shohei Mitani laboratory. Some strains were generated by the International *C. elegans* Gene Knockout Consortium (Consortium, 2012) and by the National Bioresource Project of Japan. Double mutants, triple mutants and quadruple mutants were made by genetic crossing using strains containing the mutant gene(s) of interest. In all cases, mutant genotypes were confirmed by PCR. To maintain mutants with fitness defects, the *hT2* balancer was used to keep mutations as heterozygotes. The *hT2* balancer balances all genes aforementioned except *cku-80* and *helq-1*. The *cku-80* gene is located extremely close to the *hT2 (III)* translocation site but is not covered by *hT2 (III)*. However, since *cku-80* is close to the balanced region where there was very little crossing over between *cku-80*

and *hT2, cku-80* was maintained as a heterozygote. Most homozygous double-, triple- and quadruple mutants used in this chapter were newly isolated segregants from balanced heterozygotes. The *helq-1* single mutant exhibits genomic instability, so it was frequently outcrossed to wild-type N2 and re-segregated to prevent accumulation of background mutations.

Brood Scoring

Single P_0 L4 larvae animals of each genotype were picked to fresh NGM plates and transferred daily. F_1 progeny were scored on the next day for arrested embryos and hatched larvae, and re-scored two days later for adult males and hermaphrodites. The total brood was measured as the sum of arrested embryos and hatched larvae. The embryonic lethality was defined as the percentage of arrested embryos in the total brood. The male percentage was defined as the percentage of adult males in total adults.

DAPI staining diakinesis bodies

Staged 24 hour-old adult worms were picked into 10µl of M9 buffer, and then transferred to 100µl of 150nM 4',6-diamidino-2-phenylindole dihydrochloride (DAPI) in 70% ethanol. The animals were stained in the dark at 4°C overnight. Then they were destained twice by soaking in M9 buffer for one hour each time. DAPI-stained animals were mounted on slides with 3% agarose pads and visualized at 63x magnification on a Zeiss microscope. Stacked images were taken by Digital CMOS camera C11440-42U30 and processed by Zeiss Zen software. DAPI-stained diakinesis bodies were counted in the three oocytes most proximal to the spermatheca in the germ line. A DAPI-stained diakinesis body was defined as a continuous DAPI-stained chromatin structure, regardless of its size.

Generational survival assay

Ten P_0 animals were plated individually and maintained at room temperature. Each generation, a

single L4 stage animal was transferred to a fresh plate. A line was scored as unsustainable when the parent worm was either sterile or produced only arrested embryos.

Quantitative acute assay

Synchronized one-day-old adults were incubated in the DNA damaging agent (CX-5461 in 50mM NaH_2PO_4, etoposide (ETOP) in DMSO, or camptothecin (CPT) in DMSO) diluted in M9 buffer containing OP50, carbenicillin (50 μg/ml) and 10 ng/ml nystatin for ~18 hours. Following treatment, the animals were plated to allow recovery for 30 to 60 minutes on OP50-containing NGM plates, and then plated ten worms per plate in triplicate on NGM plates for a 4-hour interval (18 to 22 hours post-treatment), and then removed. The numbers of both arrested embryos and hatched larvae were counted one day later in order to calculate the percentage of embryo survival after treatment. All results were from at least 30 treated animals. For animals that produced few progeny, more treated adult worms were picked to lay embryos in the 4-hour interval.

4.3 Results

4.3.1 Loss of NHEJ rescues meiotic defects in *helq-1* single mutants but not other HDR mutants.

Previously, *brd-1, helq-1* and *rfs-1* were shown to be involved in HDR repair (Boulton et al., 2004; Ward et al., 2007; Ward et al., 2010), and appeared to function at different steps of HDR in response to different types of DNA lesions requiring HDR. All three HDR genes are not essential. All three deletion mutants *brd-1(dw1)*, *helq-1(tm2314)* and *rfs-1(ok1372)* exhibit a Him (High Incidence of Males) phenotype, which is associated with mis-segregation of the X chromosome. NHEJ and MMEJ mutants, *cku-80(ok681)* and *polq-1(tm2025)*, respectively, have

no apparent Him phenotype.

First, we set out to test for genetic interactions between these three distinct repair pathways, since others have observed that simultaneous loss of two DSB repair pathways result in compromised viability (Mateos-Gomez et al., 2015; Schimmel et al., 2017). Genetic crosses were carried out between single mutants each deficient in one DSB repair pathway: *polq-1(tm2025)* and *cku-80(ok861)* were representatives for MMEJ and NHEJ pathways, and *brd-1(dw1)*, *helq-1(tm2314)* and *rfs-1(ok1372)* were representatives for different aspects of HDR. Surprisingly, no apparent negative genetic interactions were observed in M+Z- (maternally positive and zygotically negative) *cku-80 brd-1* or *cku-80 rfs-1* double mutants (Figure 4.2, Table 4.1). In contrast, loss of *cku-80* significantly reduced the percentage of males in the *helq-1* mutant animals. In order to eliminate the possibility that maternal contribution might be masking genetic interactions, M-Z- double mutants were also scored and no obvious phenotypic difference was observed.

4.3.2 Loss of MMEJ lead to transgenerational sterility in HDR mutants

Although *POLQ* deficiency has been reported to cause extensive chromosomal aberrations and lethality in *BRCA1/2* mutant cells (Mateos-Gomez et al., 2015), we did not observe a strong phenotype in the P_0 generation (M+Z-) of *polq-1 brd-1,* and *polq-1 rfs-1* animals (Figure 4.3A). We did observe a small but statistically significant reduction in brood size and male percentage in *helq-1 polq-1* P_0 animals. We speculate that these M+Z- double mutants had maternal POLQ-1, BRD-1 or RFS-1 proteins that contributed to their development, and that the effect of loss of *polq-1* was ameliorated. Therefore, we tested the phenotypes of double mutants at F_1, which

were M-Z-. In all three cases, the brood sizes of F_1 double mutants were significantly smaller than those of double mutants at P_0 (Figure 4.3A,B, Table 4.1), indicating negative genetic interactions between HDR and MMEJ. To further assess the NGIs, we performed a multigenerational survival assay. The multigenerational survival assay determines whether the mutant can be maintained. The assay can infer whether mutants are accumulating germline DNA damage (Ahmed and Hodgkin, 2000). The generational survival assay found that the *helq-1 polq-1* double mutants exhibited the strongest negative genetic interaction as all ten lines were inviable by the F_6 generation. The *polq-1 brd-1* and *polq-1 rfs-1* double mutants exhibited a weaker but still striking, negative genetic interaction with > 50% of the lines becoming inviable by the F_{10} generation, compared to less than 20 % of the single mutants.

4.3.3 *helq-1 brd-1* double mutants are synthetic lethal

brd-1, helq-1 and *rfs-1* are all involved in HDR. Although loss of any one of these genes results in meiotic defects and sensitivity to DNA damaging agents, these genes are not essential for HDR. This emphasizes the fact that the HDR pathway is complex with many different mechanisms to achieve DSB repair. It is possible that *brd-1, helq-1,* and *rfs-1* act in the same processes or they could represent parallel processes within HDR. The loss of two non-essential HDR genes may be epistatic, or they may be synergistic. A previous study showed that *helq-1* is SL with *rfs-1* due to an overlapping function between HELQ-1 and RFS-1 in unloading of RAD-51 filaments in meiotic DSB repair (Ward et al., 2010). We asked whether simultaneous loss of *helq-1* and *brd-1*, or *brd-1* and *rfs-1* would also lead to exacerbated defective meiotic phenotypes.

Both *helq-1* and *brd-1* single mutants exhibited Him phenotypes (0.79% ± 0.18% and 1.14% ± 0.30%, respectively) but very little embryonic lethality. The homozygous *helq-1 brd-1* double mutants displayed embryonic lethality in 98% of the progeny from P_0, and the 2% that survived likely did so because of maternal contribution (Figure 4.4A), as most hatched F1 failed to reach adulthood. No chromatin bridges were observed in *helq-1 brd-1* double mutants, suggesting that there were no mitotic defects. Next, we asked whether the synthetic lethality was caused by meiotic defects.

We first examined whether there were abnormalities in wild type *N2, helq-1,* and *brd-1* single mutants and *helq-1 brd-1* double mutants at diakinesis. Over 75% of *N2*, *helq-1* and *brd-1* single mutants displayed normal six DAPI-stained dumbbell-shaped bivalents in diakinesis (Figure 4.4B). By contrast, *helq-1 brd-1* double mutants exhibited chromosomal defects with misshapen chromosomes in diakinesis (Figure 4.4B), reminiscent of the phenotype seen in *rad-51* mutants (Alpi et al., 2003; Colaiácovo et al., 2003; Macaisne et al., 2018). Although 64% of *helq-1 brd-1* double mutants contained six DAPI-stained bodies in diakinesis, the DNA in diakinesis that was not organized into discrete bivalents as in *rad-51* mutants. This indicated that synthetic lethality in *helq-1 brd-1* double mutants is likely due to meiotic defects.

Previous studies showed that loss of the NHEJ component *cku-80* partially alleviates the meiotic defects in *rad-51* mutants (Macaisne et al., 2018). Our data demonstrated that *cku-80* loss reduced the Him phenotype in *helq-1* single mutants. We speculated that loss of *cku-80* could alleviate the phenotypes in *helq-1 brd-1* double mutants. To test this, we generated *helq-1 cku-80 brd-1* triple mutants and assayed phenotypes. *cku-80* loss led to a partial suppression of fitness

defects observed in *helq-1 brd-1* double mutants (Figure 4.4A, Table 4.1), as *helq-1 cku-80 brd-1* triple mutants have a survival rate of 30%, significantly higher than *helq-1 brd-1* double mutants. Close examination of diakinesis found a slight improvement in the DAPI-stained body phenotype, as we observed more six-dumbbell shaped diakinesis bodies in *helq-1 cku-80 brd-1* triple mutants (about 80%) (Figure 4.4B,C).

Loss of MMEJ can also alleviate the meiotic defects in *rad-51* single mutants (Macaisne et al., 2018). We tested whether loss of POLQ-1 could alleviate the meiotic defects in *helq-1 brd-1* double mutants. In contrast to loss of *cku-80*, loss of *polq-1* did not improve the embryonic survival. Instead, the brood size of *helq-1 brd-1* reduced by almost 30% upon loss of POLQ-1 (Figure 4.4A, Table 4.1) and the DAPI-stained bodies in *helq-1 polq-1 brd-1* triple mutants were indistinguishable from those of *helq-1 brd-1* double mutants (Figure 4.4B,C), indicating that MMEJ has little contribution to the chromosomal abnormalities in the meiotic DSB repair in *helq-1 brd-1* double mutants. Surprisingly, simultaneous loss of both MMEJ and NHEJ had little effect on *helq-1 brd-1* double mutants (Figure 4.4A,B,C) suggesting that the partial rescue observed in *helq-1 cku-80 brd-1* mutants is dependent on POLQ-1 activity.

4.3.4 *brd-1 rfs-1* double mutants are synthetic sick

brd-1 and *rfs-1* single mutants share many phenotypes, including Him, camptothecin-sensitivity, and UVA-TMP-sensitivity (Figure 2.2). Based on their similar characteristics and chemical sensitivity profiles, we might expect that *brd-1 rfs-1* would be epistatic and thus the *brd-1 rfs-1* double mutants should exhibit similar phenotypes as the single mutants. However, *brd-1 rfs-1* double mutants were synthetic sick. The homozygous double mutants exhibited severe fitness

defects: more than 50% of progeny of P_0 animals were arrested embryos, compared to less than 6% embryonic lethality in the *brd-1* or *rfs-1* single mutants (Figure 4.5A, Table 4.1). Moreover, the *brd-1 rfs-1* double mutants had an extremely high percentage of males (about 14%), whereas the single mutants had less than 2% of males.

We then set out to examine the DAPI-stained bodies in diakinesis. The *brd-1* and *rfs-1* single mutants all exhibited six wild-type bivalents, while the *brd-1 rfs-1* double mutants often had seven or eight DAPI-stained diakinesis bodies (Figure 4.5B). We found that approximately 40% of *brd-1 rfs-1* double mutant oocytes had more than six DAPI-stained diakinesis bodies, which could account for the Him phenotype (Figure 4.5C). In those *brd-1 rfs-1* double mutants that had more than six DAPI-stained bodies at diakinesis, the extra DAPI-stained bodies did not resemble chromosome fragments but rather dissociated univalent(s).

The high frequency of more than six DAPI-stained bodies in diakinesis likely reflects a repair defect in the *brd-1 rfs-1* double mutants. To address whether this abnormality is due to defective meiotic DSB repair, we generated *spo-11; brd-1 rfs-1* triple mutants. SPO-11 is an essential enzyme in the evolutionarily conserved mechanism to induce meiotic DSBs in *C. elegans* germ lines. The *spo-11* mutant lacks meiotic DSBs, and therefore there are no meiotic crossovers or formation of chiasma. The *spo-11* mutant has 12 separate univalents in diakinesis (Dernburg et al., 1998). In contrast to the *brd-1 rfs-1* double mutants, the *spo-11; brd-1 rfs-1* triple mutants displayed the same 12 DAPI-stained bodies as *spo-11* mutants (Figure 4.5B), indicating that the NGI between BRD-1 and RFS-1 is due to defective repair of meiotic DSBs induced by SPO-11.

Next, we asked whether loss of *cku-80* would affect the viability of *brd-1 rfs-1* double mutants. We found that *cku-80 brd-1 rfs-1* triple mutants exhibited very similar phenotypes as *brd-1 rfs-1* double mutants: ~50% arrested embryos, and a high percentage of males (Figure 4.5A, Table 4.1). Cytological analysis also found no difference in DAPI-stained diakinesis bodies between the double and triple mutants (Figure 4.5B,C). This suggested that the meiotic DSB repair defects in *brd-1 rfs-1* were not the result of inappropriate utilization of the NHEJ pathway.

4.3.5 Revisiting the synthetic lethality in *helq-1 rfs-1* double mutants

It appeared that loss of NHEJ factors (e.g. *cku-80*) could partially suppress the chromosomal instability in *helq-1* mutants. We decided to investigate whether NHEJ played a role in causing the meiotic defects in *helq-1 rfs-1*. The previous model for synthetic lethality observed in the *helq-1 rfs-1* double mutants was that simultaneous loss of HELQ-1 and RFS-1 results in failure to unload RAD-51 filaments (Ward et al., 2010). This model proposed that SPO-11-induced meiotic DSBs were committed to HDR repair, and that the inability to resolve the HDR intermediates led to chromosomal aberrations in *helq-1 rfs-1* double mutants. However, the chromosomal aggregates observed in diakinesis in *helq-1 rfs-1* double mutants resembled the phenotype of *com-1* and *mre-11S* mutants (Lemmens et al., 2013; Yin and Smolikove, 2013), both of which are partially rescued by loss of *cku-80*. It is possible that there exists an alternative mechanism for the synthetic lethality in the *helq-1 rfs-1* double mutants. Therefore, we hypothesized that improper end joining events contributed to the chromosomal aggregates and lethality in the *helq-1 rfs-1* double mutants.

To test this hypothesis, we generated *helq-1 cku-80 rfs-1* and *helq-1 polq-1 rfs-1* triple mutants. Surprisingly, both triple mutants have much larger brood sizes (119 ± 10 and 205 ± 13 for *helq-1 cku-80 rfs-1* and *helq-1 polq-1 rfs-1*, respectively), compared to *helq-1 rfs-1* double mutants (23 ± 5) (Figure 4.6A, Table 4.1). This is strong evidence that both NHEJ and MMEJ activities negatively contribute to the brood size in the *helq-1 rfs-1* double mutants. Notably, loss of *cku-80* also partially rescued the embryonic survival rate to 14%, whereas loss of *polq-1* did not significantly reduced embryonic lethality (Figure 4.6A, Table 4.1). We then examined the DAPI-stained bodies in diakinesis in both triple mutants. We found that loss of either NHEJ or MMEJ rescued the aggregated chromosome phenotypes, resulting in distinct bivalents; however, the chromatin morphology in both triple mutants was still different from that of wild-type animals (Figure 4.6B,C). Of note, flocculent chromosomes with long tails were often observed in the *helq-1 polq-1 rfs-1* and *helq-1 cku-80 rfs-1* triple mutants.

Taken together, these data suggest that both end joining pathways contribute to the reduction in brood size and aggregated chromosome phenotypes. We also tested whether simultaneous loss of both NHEJ and MMEJ would further mitigate the defects in the *helq-1 rfs-1* double mutants. Interestingly, elimination of both POLQ-1 and CKU-80 did not result in further increase in either brood size or embryonic viability as compared to single loss of POLQ-1 (Figure 4.6A, Table 4.1). Examination of DAPI-stained diakinesis bodies found no discernable difference between *helq-1 cku-80 polq-1 rfs-1* quadruple mutants and the two triple mutants (Figure 4.6B,C). This implied that there still existed another DSB repair pathway that resolved meiotic DSBs in the quadruple mutants (Macaisne et al., 2018).

4.3.6 Loss of NHEJ rescues the sensitivity to DNA damaging agents in some but not all HDR-compromised mutants

Our results have shown that *cku-80* deficiency was able to partially rescue the meiotic defects in the *helq-1* single mutants, but not the *brd-1* or *rfs-1* single mutants. We set out to determine whether loss of *cku-80* could suppress sensitivity of mutants to DNA damaging agents (DDAs). We tested the Topoisomerase I inhibitor camptothecin (CPT), Topoisomerase II inhibitor etoposide (ETOP) and the G-quadruplex-stabilizing agent CX-5461. Using quantitative acute assays, we determined that NHEJ loss could partially rescue both CPT- and CX-5461-sensitivity in the *helq-1* mutants (Figure 4.7A,B), as the *helq-1 cku-80* double mutants had much higher embryo survival after treatment. By contrast, loss of *cku-80* had no effect on the *rfs-1* single mutants, as the *cku-80 rfs-1* double mutants had similar embryo survival upon CPT or CX-5461 treatment to the *rfs-1* mutants (Figure 4.7A,B). The *cku-80 brd-1* double mutants showed a mild suppression of CPT-sensitivity compared to *brd-1* single mutants (Figure 4.7C). We also observed a partial suppression of CPT-sensitivity in the *atm-1* mutants by loss of *cku-80* (Figure 4.7D). ATM-1 has been shown to activate and regulate HDR pathways (Balmus et al., 2019).

4.3.7 Loss of MMEJ sensitizes HDR mutants to camptothecin (CPT), etoposide (ETOP) and CX-5461.

MMEJ has been considered as a back-up pathway to resolve DSBs in the absence of HDR and NHEJ. Our data showed that MMEJ was required for transgenerational viability of HDR-compromised mutant animals. Next, we determined whether MMEJ was a primary or a backup mechanism for the DSB repair of exogenous DNA damage when other DSB repair pathways were absent.

We first tested the sensitivity of HDR and MMEJ mutants to a Topoisomerase I inhibitor, camptothecin (CPT). HDR mutants all exhibited sensitivity to CPT, whereas MMEJ mutants were not sensitive to CPT (Figure 2.2). HDR single mutants were hypersensitive to CPT (Figure 2.2), so we used a low concentration of CPT. Surprisingly, the loss of POLQ-1 further sensitized all three HDR mutants to CPT, as the *helq-1 polq-1*, *polq-1 rfs-1* and *polq-1 brd-1* mutants all had greater embryonic lethality upon CPT treatment than their respective single mutants (Figure 4.8A,B). Because the *polq-1* single mutants were not sensitive to CPT and deficiency in HDR resulted in a greater sensitivity, it suggested that MMEJ was not a primary repair mechanism for CPT-induced DNA lesions but could repair some lesions in the absence of HDR.

Next, we tested mutants with a Topoisomerase II inhibitor, etoposide (ETOP). Notably, we found that the *polq-1* mutants were much more sensitive to ETOP than HDR-compromised animals (Figure 2.2). At a low dose of ETOP, HDR mutant animals had little embryonic death, whereas the MMEJ mutant *polq-1* was more sensitive to ETOP than *helq-1*, *rfs-1* and *brd-1* mutants (Figure 4.8C). Combined loss of *polq-1* and any one of the three HDR genes resulted in significant reduction in embryo viability upon ETOP treatment (Figure 4.8C). Therefore, HDR deficiency further sensitized MMEJ mutants to ETOP. Taken together, the data suggest there exists a negative genetic interaction between HDR and MMEJ in response to ETOP-induced lesions, and that HDR could repair some ETOP damage in the absence of MMEJ.

Lastly, we also tested the sensitivity of HDR and MMEJ mutants to CX-5461. In contrast to CPT or ETOP, both HDR single mutants and MMEJ single mutants were sensitive to CX-5461,

indicating that both HDR and MMEJ were required for CX-5461 tolerance. Again, loss of POLQ-1 led to greater CX-5461-sensitivity in *helq-1*, *brd-1,* and *rfs-1* mutants (Figure 4.8D,E), suggesting that MMEJ and HDR respond independently to CX-5461-induced DNA damage.

4.4 Discussion

4.4.1 Redundancy between HDR factors

We found NGIs between three factors involved in the HDR pathway. First, HELQ-1 is required for survival in the absence of BRD-1/BRC-1. Second, BRD-1 and RFS-1 work synergistically to maintain genome stability. Third, we analyzed the synthetic lethality observed in the *helq-1 rfs-1* double mutants and suggest a mechanism that may be contributing to SL. All three factors (BRD-1/BRC-1, HELQ-1, and RFS-1) have been shown to play key roles in homologous recombination, including recruiting, influencing or interacting with RAD-51 filaments at the sites of DNA damage (Boulton et al., 2004; Janisiw et al., 2018; Li et al., 2018; Ward et al., 2010; Yousefzadeh et al., 2014). Although they are all involved in HDR of DNA lesions, none is essential for viability in *C. elegans*. Therefore, the NGI (SL and SS) between any two genes uncover the compensating functions of each gene pair.

A. HELQ-1 & BRD-1

Since *helq-1 brd-1* double mutants were synthetic lethal, it is possible that BARD-1 and HELQ-1 share a partially redundant role in meiotic DSB repair. Our data suggest that HELQ-1 is involved in an early step in RAD-51 filament dynamics or resection, since the loss of HELQ-1 resulted in improper NHEJ activity, similar to loss of DNA repair factors that drive DNA resection. This is evidenced by the observation that the *helq-1 cku-80* double mutants had mildly yet significantly

reduced embryonic lethality and male percentage (Figure 4.2), and that loss of CKU-80 suppressed some sensitivity to CPT and CX-5461 in the *helq-1* single mutants (Figure 4.7A,B).

In mammalian cells, BRCA1/BARD1 promotes HDR and counteracts NHEJ activity by presenting end-resected DSBs through its interaction with CtIP and MRN (Chen et al., 2008), and loss of CKU-80 partially alleviated phenotypes in *C. elegans* mutants deficient in CtIP and MRN complex (Girard et al., 2018; Lemmens et al., 2013; Yin and Smolikove, 2013). Taken altogether, one possibility is that there exists a collaborative synergy between BRD-1 and HELQ-1 in promoting HDR in early stage of meiotic DSB repair.

Another possible explanation for SL in *helq-1 brd-1* is co-involvement of HELQ-1 and BRD-1 in late stage of HDR. HELQ-1 affects meiotic recombination by evicting the RAD-51 filaments (Ward et al., 2010). BRC-1/BRD-1, on the other hand, promotes inter-sister repair of SPO-11-induced DSBs (Adamo et al., 2008). In the *brc-1* and *brd-1* single mutants, there is an increase in RAD-51 foci in late pachytene regions compared to wild-type animals (Adamo et al., 2008), whereas no increase of RAD-51 filament is observed in late pachytene in the *helq-1* single mutants despite a proposed role in the disassembly of RAD-51 filaments (Ward et al., 2010). Loss of HELQ-1 further accumulates the RAD-51 filaments in *rtel-1* mutants (Ward et al., 2010), and here it is likely that simultaneous loss of HELQ-1 and BRD-1 also results in excess unloaded RAD-51 filaments in late pachytene, indicative of elevated unrepaired DNA damage that potentially gives rise to lethality.

Close examination of the diakinesis in the *helq-1 brd-1* double mutants revealed a near wild-type number of DAPI-stained diakinesis bodies. However, all DAPI-stained diakinesis bodies in the *helq-1 brd-1* double mutants were misshapen and reminiscent of those observed in *jmjd-5* and *nmad-1* single mutants (Amendola et al., 2017; Wang et al., 2019a). JMJD-5 is a histone demethylase that has been shown to act in the late stage of HDR to promote RAD-51 filament removal in a similar manner as HELQ-1 (Amendola et al., 2017), whereas NMAD-1 is a DNA demethylase that removes methyl groups from DNA; loss of NMAD-1 also resulted in increased RAD-51 foci in the germ line (Wang et al., 2019a). Notably, lack of either JMJD-5 or NMAD-1 could alter the global chromatin methylation level, which could affect DSB repair choice at an early stage. It would be interesting to test whether methylation might be affecting the recruitment of HELQ-1 and BRD-1.

B. BRD-1 & RFS-1

The synthetic sickness in *brd-1 rfs-1* double mutants illustrates the synergy between BRD-1 and RFS-1. The *brd-1 rfs-1* double mutants exhibit greater genome instability phenotypes (Him, and embryonic lethality) than either single mutant, suggesting that co-loss of BRD-1 and RFS-1 compromises meiotic DSB repair likely through affecting HDR. The *brd-1 rfs-1* double mutants displayed a high frequency of more than six DAPI-stained diakinesis bodies, whereas the *spo-11; brd-1 rfs-1* triple mutants displayed a phenotype similar to *spo-11* mutants that have a twelve-univalent phenotype (Figure 4.5B), indicating that the aberrant diakinesis in *brd-1 rfs-1* is dependent on the repair of SPO-11-induced DSBs. From this data, we conclude that that the NGI between BRD-1 and RFS-1 is a consequence of defective meiotic DSB repair.

The *brd-1 rfs-1* mutants frequently contained seven DAPI-stained diakinesis bodies, which is consistent with the extremely high male percentage observed in *brd-1 rfs-1* double mutants. In contrast to the *helq-1 brd-1* double mutants, the *brd-1 rfs*-1 double mutants did not have misshapen DAPI-stained bodies, suggesting a different mechanism leading to meiotic DSB repair defects. Both BRD-1 and RFS-1 promote HDR at different types of lesions (Boulton et al., 2004; Ward et al., 2007). It is possible that loss of both gives rise to insufficient RAD-51 loading and thus compromised HDR activity. However, this is unlikely the case, because CKU-80 loss did not rescue the fitness defects in the *brd-1 rfs-1* double mutants (Figure 4.5B,C), and failure to initiate HDR could result in utilization of NHEJ.

BRC-1/BRD-1 stabilizes RAD-51 filaments on new DSBs in mid- to late pachytene (Li et al., 2018). RFS-1/RIP-1/SWS-1 have been shown to remodel pre-synaptic RAD-51 filaments to a stabilized and flexible confirmation that promote homologous recombination (Taylor et al., 2015). Therefore, this raised another hypothesis that the combined loss of BRD-1 and RFS-1 results in destabilized RAD-51 filaments that weaken HDR competence. This could explain why deficiency in NHEJ did not improve the phenotype of the *brd-1 rfs-1* double mutants, because RAD-51 filaments have already committed repair to HDR, and therefore the DSBs are likely to be resected and not substrates for CKU-80 binding.

Altogether, simultaneous loss of BRD-1 and RFS-1 greatly compromised meiotic DSB repair, and hence caused genome instability phenotypes, such as Him and high embryonic lethality. Future work could assay RAD-51 foci and the state of the synaptonemal complex across

different stages of meiosis in *brd-1 rfs-1* double mutants to further elucidate the basis of NGI between BRD-1 and RFS-1.

C. RFS-1 & HELQ-1

A previous study has characterized the SL in *helq-1 rfs-1* double mutants as excessive unloading of RAD-51 from RAD-51 filaments in late meiotic DSB repair (Ward et al., 2010). Here, we present mechanistic insight into the repair pathways that are used in the absence of both HELQ-1 and RFS-1. Our data suggest that in the *helq-1 rfs-1* double mutants, DSB repair mechanisms other than HDR could take place, such as NHEJ and MMEJ, resulting in chromosomal fusions. Loss of either CKU-80 or POLQ-1 or both, remarkably increased the brood size of *helq-1 rfs-1* double mutants. Moreover, there are no chromosomal fusion phenotypes observed any of the triple mutants *helq-1 cku-80 rfs-1* and *helq-1 polq-1 rfs-1*, or the quadruple mutants *helq-1 cku-80 polq-1 rfs-1*. This suggest that illegitimate end joining may be ligating broken meiotic DSB ends when HDR is defective. Interestingly, CKU-80 loss slightly but significantly increased the embryo viability of the *helq-1 rfs-1* double mutants, whereas loss of POLQ-1 or both POLQ-1 and CKU-80, while rescuing brood size, led to complete embryo lethality, suggesting that MMEJ was needed for viability (discussed more in 4.4.3). These results are reminiscent of the phenotypes observed in *polq-1;rad-51*, *cku-70;rad-51*, and *polq-1 cku70; rad-51* (Yang et al., 2019).

It is still unknown how homologous recombination intermediates in the *helq-1 rfs-1* double mutants would activate or trigger end joining repair. One possibility is that RFS-1 deficiency results in destabilized RAD-51 filaments that are susceptible to nuclease degradation (Taylor et al., 2015). Despite presence of a large quantity of RAD-51 filaments, homologous recombination

is not stimulated. It is also observed in the *brc-1* single mutants that there is high retention of RAD-51 in late pachytene, although the meiotic DSB repair is largely HDR-dependent (Adamo et al., 2008).

4.4.2 MMEJ is both a primary and back-up repair pathway dependent on the nature of the DNA lesion

It has long been thought that MMEJ is a back-up pathway to repair DSB lesions, but recent work has suggested that MMEJ can independently resolve DNA lesions in the presence of both HDR and NHEJ (Koole et al., 2014; Roerink et al., 2014). The activity of MMEJ has been frequently found in the human genome, as many repetitive elements that constitute a large proportion in the genome, have signatures consistent with MMEJ activity (Sfeir and Symington, 2015). Another study demonstrated that POLQ-1 is involved in generating the small indels that are abundantly present in wild isolates of *C. elegans* (Koole et al., 2014). Here, our data also elucidated the versatile role that MMEJ plays in response to different types of DNA lesions in *C. elegans*.

Under normal conditions, when there is no exogenous DNA damage, most DSBs are either SPO-11-induced meiotic DSBs or DSBs formed at hard to replicate regions such as G-quadruplexes or tandem repeats. MMEJ has been shown to initiate the formation of small deletions at endogenous G4 sites when DOG-1 is absent (Koole et al., 2014). It is likely that MMEJ is the primary repair mechanism to resolve DNA lesions formed at G4, compared to other repair pathways such as HDR and TLS, since the *dog-1; polq-1* mutants exhibited a much more severe fitness defect than the *dog-1;brd-1* and *dog-1;rev-3* mutants (Figure 3.2B). It has also been previously reported that POLQ-1 is involved in the repair of the transposon-induced breaks and CRISPR/Cas9-induced

breaks in meiosis (van Schendel et al., 2015). However, POLQ-1 is not required for meiosis under normal conditions, as *polq-1* mutants have a near wild-type phenotype by cytological analysis of the germ line (Figure A4.1).

Our data suggest that POLQ-1 is required for genome integrity when HDR is compromised. Co-depletion of POLQ-1 and HDR factors result in a progressive decline in viability. This is corroborated by the evidence that the brood sizes of the *helq-1 polq-1*, *polq-1 rfs-1* and *polq-1 brd-1* mutants at F_1 (M-Z-) are all significantly smaller than those of their M+Z- counterparts. The reduced brood size could be due to under-proliferated germ lines, or defects in sperm meiosis. Besides, generational survival assay suggests that the double mutants exhibit greater genome instability by accumulating mutations that result in sterility. Additionally, POLQ-1 played a crucial role in chromosomal abnormalities when both HELQ-1 and RFS-1 were absent, because loss of POLQ-1 rescued the chromosomal aggregates and increased the brood size in the *helq-1 rfs-1* double mutants (Figure 4.6A, Table 4.1). This suggested that POLQ-1 could ligate broken DSB ends.

To counteract exogenous DNA damage, we found that MMEJ could be both a back-up repair pathway and a dedicated repair mechanism depending on the type of DNA lesions cells encounter (Figure 4.9). The topoisomerase I inhibitor CPT has been shown to cause replication blocks, which if not repaired could lead to fork collapse and DSB. Our data showed that the *polq-1* mutants were not sensitive to CPT, although some POLQ-/- human cell lines exhibited mild sensitivity upon CPT treatment (Wang et al., 2019b; Yousefzadeh et al., 2014). It is likely that MMEJ is not the primary repair mechanism for CPT-induced lesions in *C. elegans*. We

found that HDR mutants exhibited strong CPT-sensitivity, indicating HDR as the primary repair mechanism for resolving CPT-induced lesions. We also observed increased sensitivity to CPT when both HDR and MMEJ pathways were defective (Figure 4.8A,B), suggesting that POLQ-1 could be used as a back-up pathway for CPT-lesions when HDR pathway is compromised (Figure 4.9). This is possible because both HDR and MMEJ requires end resection, and MMEJ could use resected ends to resolve CPT lesions at a cost of causing small deletions.

The topoisomerase II inhibitor ETOP, however, induces a different type of lesion than CPT. Consistent with that, ETOP utilizes a different repair mechanism than CPT. Our data showed that the *polq-1* mutants exhibited markedly stronger sensitivity even at a low dose of ETOP, compared to HDR mutants (*rfs-1*, *helq-1* and *brd-1*) (Figure 4.8C). This suggests that MMEJ rather than HDR is the primary repair pathway in response to ETOP-induced lesions (as discussed in Chapter 2). Loss of HDR factors further sensitized the *polq-1* mutants to ETOP (Figure 4.8C), demonstrating that HDR could be a back-up repair mechanism to resolve ETOP-induced lesions when the primary MMEJ pathway is not available. This is the converse of CPT, in which HDR is the primary pathway and MMEJ is the backup pathway (Figure 4.9).

CX-5461 induces lesions distinct from CPT or ETOP. It has been shown that CX-5461 stabilizes G-quadruplex and blocks DNA replication (Xu et al., 2017). The G-quadruplex-induced lesions have been shown to be repaired by polymerase theta-mediated MMEJ (Koole et al., 2014), and MMEJ also repaired CX-5461-induced lesions. Based on our data, it appears that HDR is also required for some lesions induced by CX-5461. If HDR and MMEJ are truly redundant pathways for responding to CX-5461-induced lesions, mutants deficient in only one single pathway should

not be sensitive. Simultaneous loss of MMEJ and HDR significantly reduced the embryonic survival in worms exposed to CX-5461 (Figure 4.8D,E), indicating that two pathways work independently to repair CX-5461-induced DNA damage (Figure 4.9). Similarly, a study in A549/DR cancer cells has shown that HDR and MMEJ synergize for cell survival in response to cisplatin (Dai et al., 2016).

4.4.3 Illegitimate NHEJ activity can be toxic in certain HDR-compromised background

Many studies have shown that improper NHEJ activity could lead to deleterious cellular consequences. This is often because NHEJ is an error-prone DSB repair pathway that directly ligates the broken DNA ends, and this can result in deletions or translocations. During meiosis in *C. elegans*, SPO-11-induced meiotic DSBs are processed by the MRN complex and COM-1, which antagonizes CKU-70/80. The meiotic defects of *mre-11S, com-1*, and *nbs-1* mutant animals are partially restored by loss of *cku-80* (Girard et al., 2018; Lemmens et al., 2013; Yin and Smolikove, 2013). We showed that HELQ-1 might also be involved in the early processing of DSB ends to prohibit NHEJ activity. Loss of *cku-80* suppressed the HIM phenotype in *helq-1* single mutants (Figure 4.2). Additionally, the role of HELQ-1 counteracting NHEJ activity appeared not only limited to meiotic DSBs, but also DNA lesions induced by DNA damaging agents, such as CPT and CX-5461 (Figure 4.7A,B). We also observed NHEJ deficiency mildly suppressed the CPT-sensitivity in *brd-1* mutants, similar to human counterparts (Figure 4.7C) (Bunting et al., 2012).

The effect of the loss of NHEJ on the *helq-1* mutants was also visible in genetic interactions. Loss of *cku-80* partially suppressed the lethality in both *helq-1*-containing double mutants, *helq-*

1 brd-1 and *helq-1 rfs-1* (Figure 4.4A, 4.6A). But the *cku-80* suppression of the double mutants was completely ameliorated by additional loss of MMEJ, as both (M+Z-) quadruple mutants *helq-1 cku-80 polq-1 brd-1* and *helq-1 cku-80 polq-1 rfs-1* produced no viable progeny (Figure 4.4A, 4.6A). Taken together, these data indicate a hierarchy for repair mechanisms of meiotic DSBs. Under normal conditions, DSBs are resolved by HDR mechanisms, and end processing factors like MRN and CtIP and other helicases such as HELQ-1 prevent inappropriate NHEJ mechanism. When HDR is defective, NHEJ can act, leading to deleterious effects. When both HDR and NHEJ are defective, MMEJ can join DSBs in a less deleterious manner than NHEJ. Animals lacking all three major DSB repair pathways were unable to resolve meiotic DSBs properly.

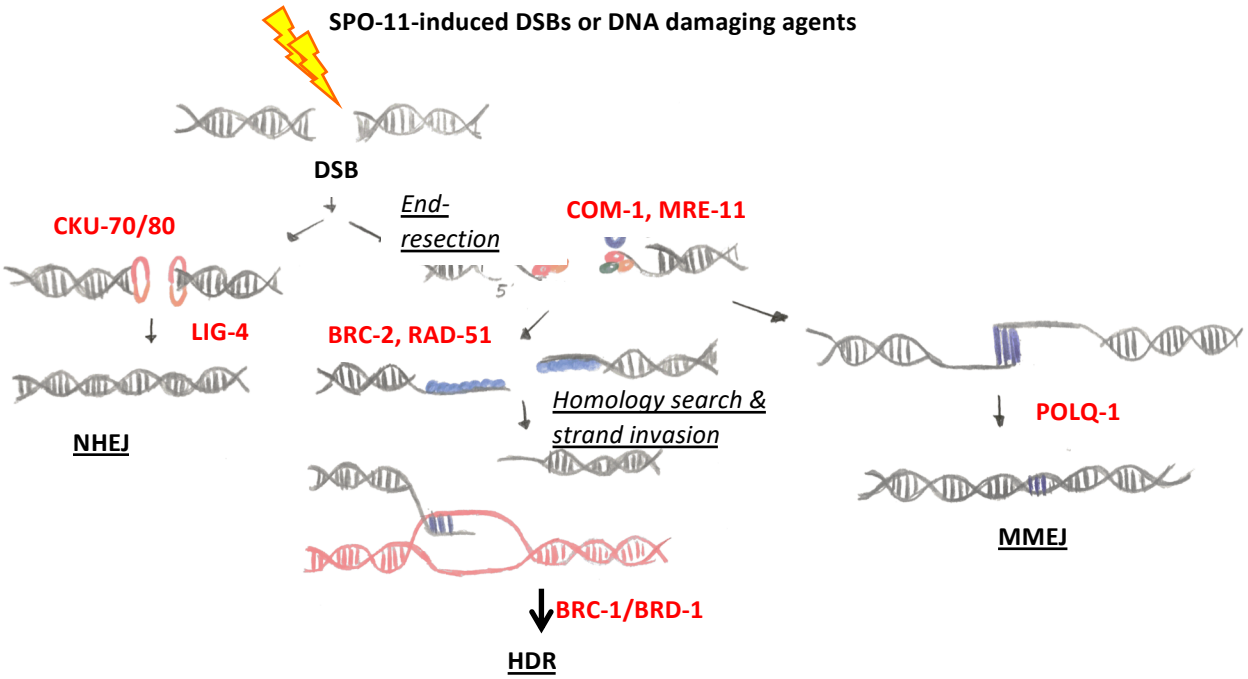

Figure 4.1 A schematic of DSB repair pathways in *C. elegans.* See main texts for details.

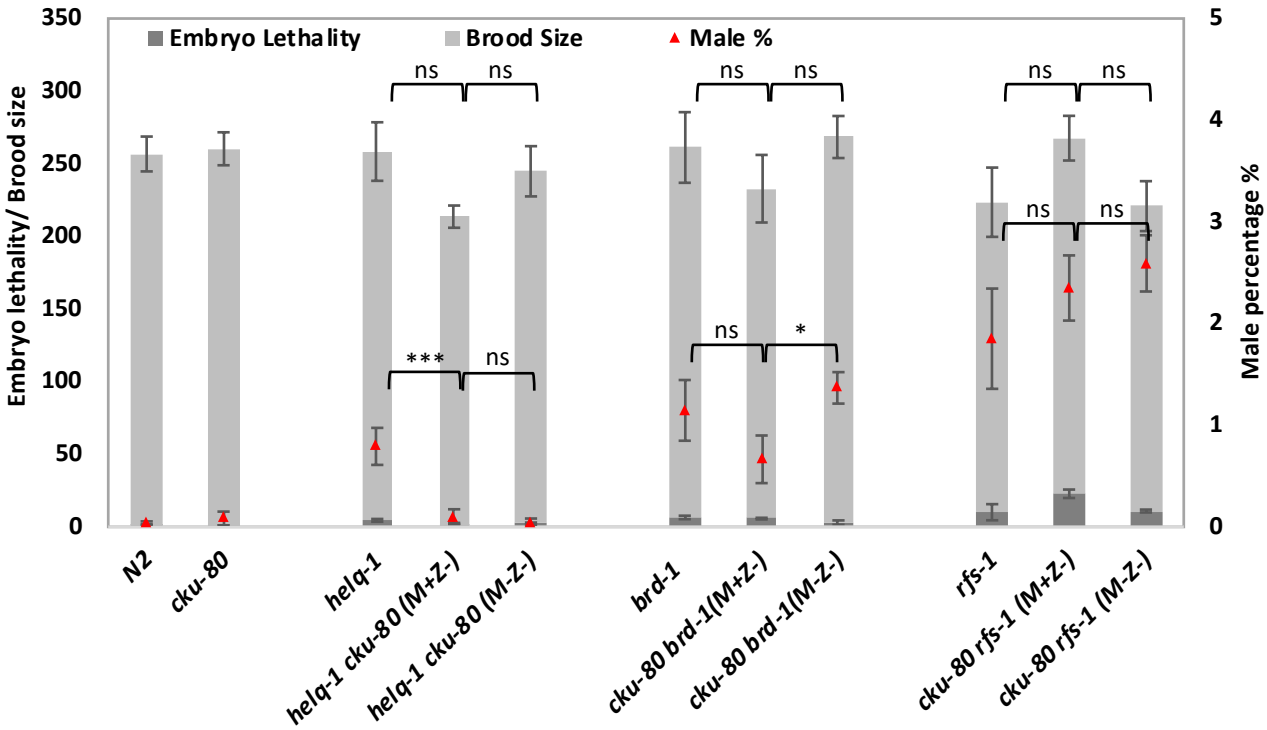

Figure 4.2 *cku-80* genetically interacts *helq-1* single mutants but not other HDR mutants or MMEJ mutants. Brood size, embryonic lethality, and % males in single mutants and *cku-80*-containing double mutants. At least eight hermaphrodites were scored for their progeny. Error bars represent the standard error of the mean. Student t tests were used to compare brood sizes between indicated animals (upper) and male percentage between indicated animals (bottom). Male percentage of cku-80 was no different from that of M+Z- and M-Z- *helq-1 cku-80*, but significantly different from M-Z- *cku-80 brd-1*(***) and M-Z- *cku-80 rfs-1*(***). * denotes p value less than 0.05, ** <0.01, ***<0.001.

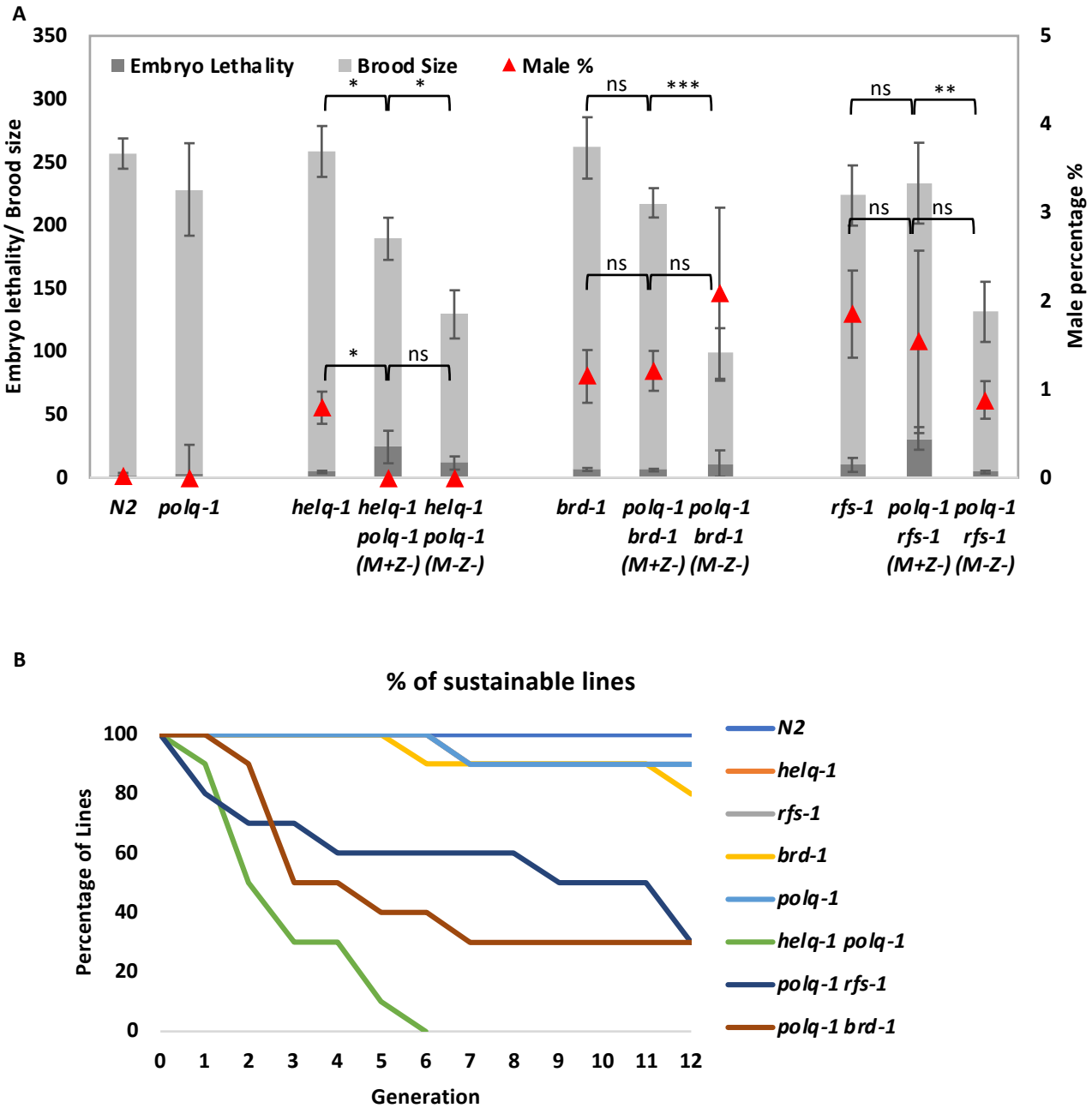

Figure 4.3 *polq-1* genetically interacts with HDR gene/mutants (*helq-1, brd-1,* and *rfs-1*). (A) Brood size, embryonic lethality, and % males in HDR single mutants and *polq-1*-containing double mutants of maternally positive and zygotically negative (M+Z-) P0 and maternally positive and zygotically negative (M-Z-) F1. At least eight hermaphrodites were scored for their progeny. Student t tests were used to compare brood sizes between indicated animals (upper) and male percentage between indicated animals (bottom). To note, the brood size of polq-1 mutant was significantly different from that of M-Z- *polq-1 brd-1*(*), and M-Z- *polq-1 rfs-1*(*). * denotes p value less than 0.05, ** <0.01, ***<0.001. Error bars represent the standard error of the mean. (B) Viability of independent lines of N2, HDR single mutants, and *polq-1*-containing double mutants at 23℃. All starting P0 were M+Z-, and n = 10. The *helq-1*, *rfs-1*, *brd-1*, and *polq-1* lines were largely overlapped between F7 and F11.

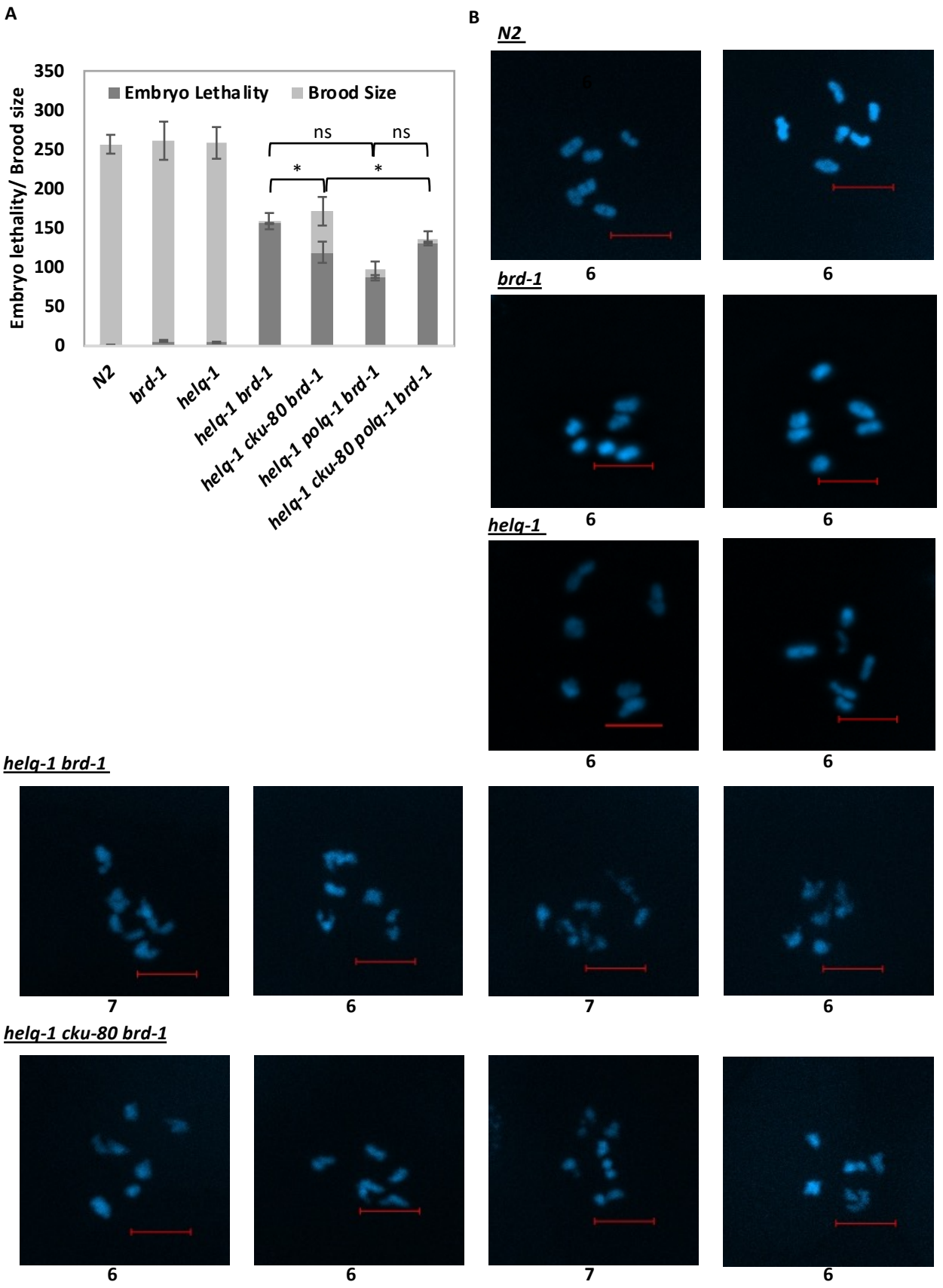
A
B
Embryo Lethality
Brood Size
Embryo lethality/ Brood size
350
300
250
200
150
100
50
0
ns
ns
*
*
N2
brd-1
helq-1
helq-1 brd-1
helq-1 cku-80 brd-1
helq-1 polq-1 brd-1
helq-1 cku-80 polq-1 brd-1
N2
brd-1
helq-1
helq-1 brd-1
helq-1 cku-80 brd-1
6
6
6
6
6
6
7
6
7
6
6
6
7
6

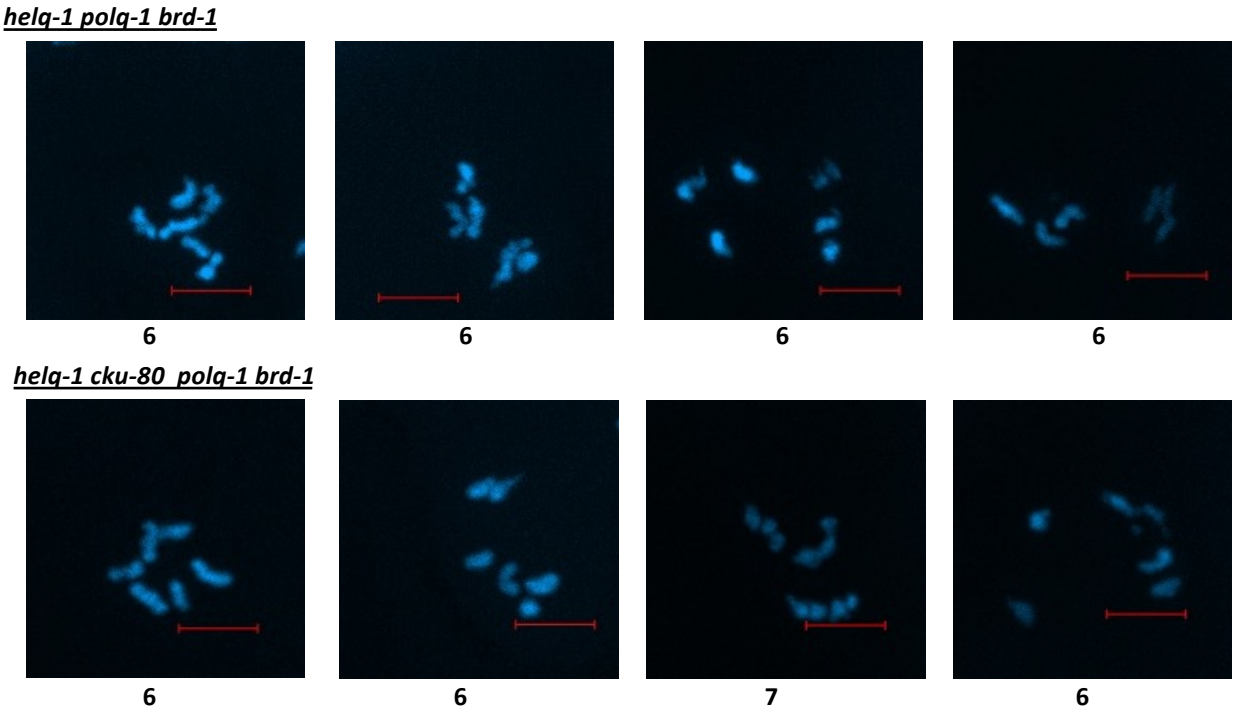

C

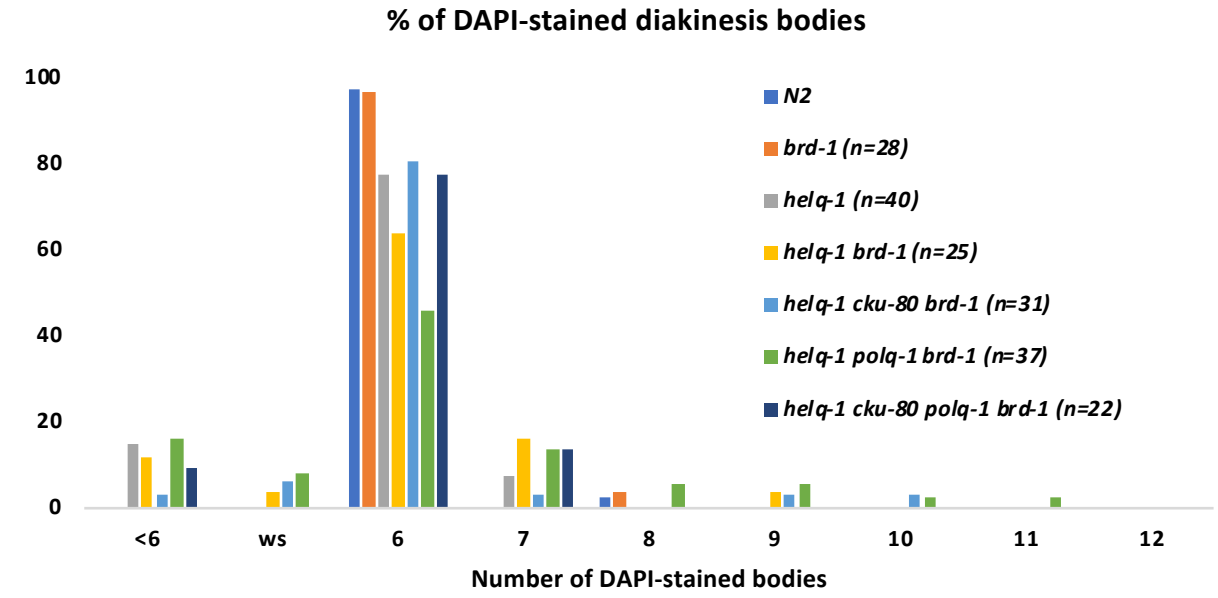

Figure 4.4 *helq-1 brd-1* double mutants are synthetic lethal. (A) Brood size and embryonic lethality in *helq-1* and *brd-1* single mutants*, helq-1 brd-1* double mutants and other associated mutants. The double, triple and quadruple mutants were scored as M+Z- worms. Error bars represent the standard error of the mean. Student t tests were used to compare embryo survival rate between indicated animals. * denotes p value less than 0.05, ** <0.01, ***<0.001. (B) Representative images of DAPI-stained bodies in diakinesis of respective mutants. Numbers below in the brackets indicate the number of DAPI-stained bodies per nuclei. Scale bar denotes 5 µm. (C) Quantification of DAPI-stained bodies at diakinesis from animals of the indicated mutants. ws denotes weird shaped.

A

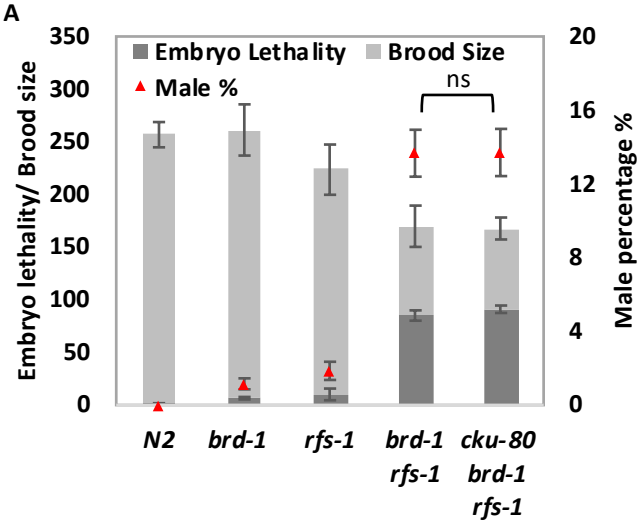
Embryo Lethality
Brood Size
Male %
ns
Embryo lethality/ Brood size
Male percentage %
350
300
250
200
150
100
50
0
20
16
12
8
4
0
N2
brd-1
rfs-1
brd-1 rfs-1
cku-80 brd-1 rfs-1

B

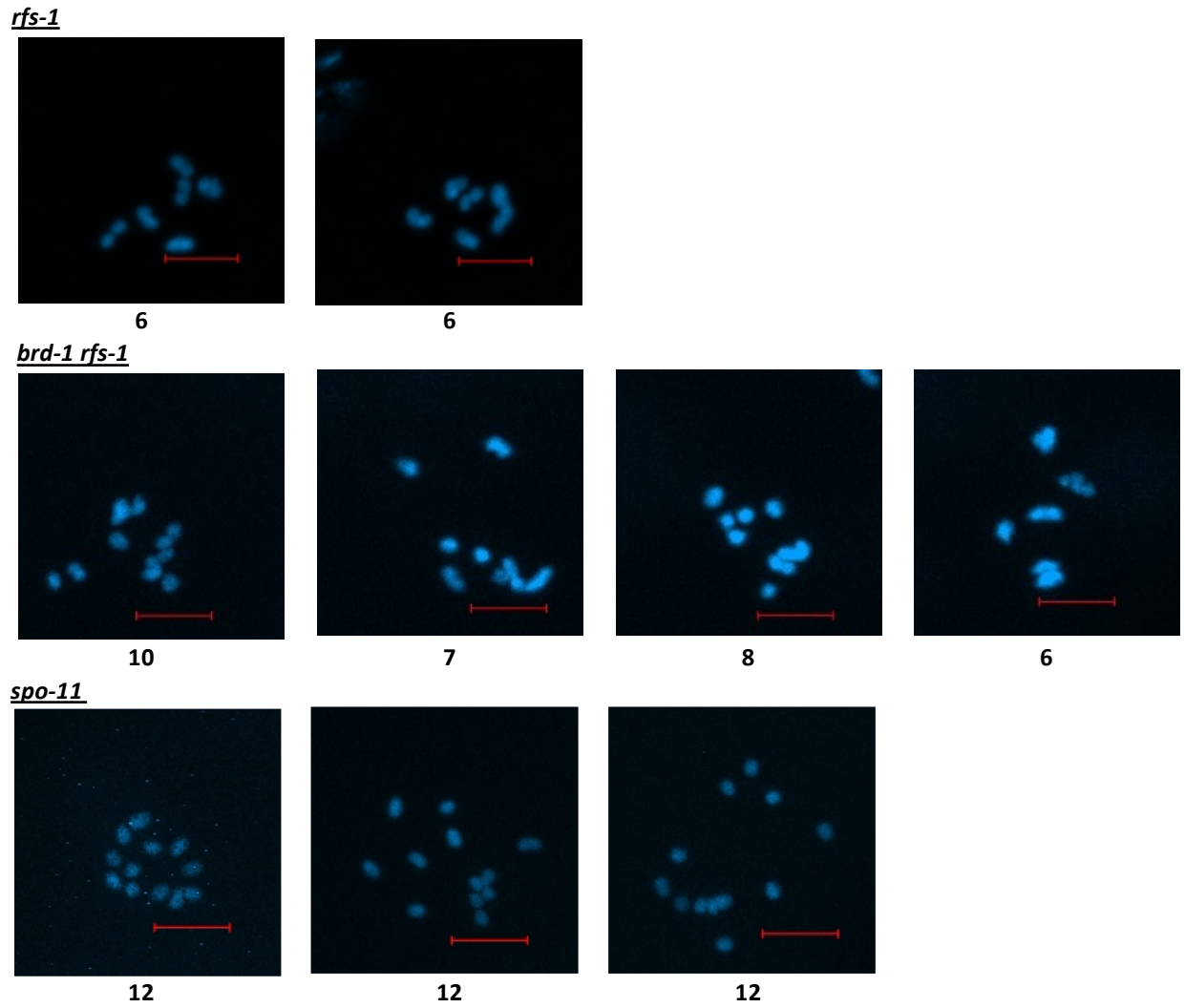
rfs-1
6
6
brd-1 rfs-1
10
7
8
6
spo-11
12
12
12

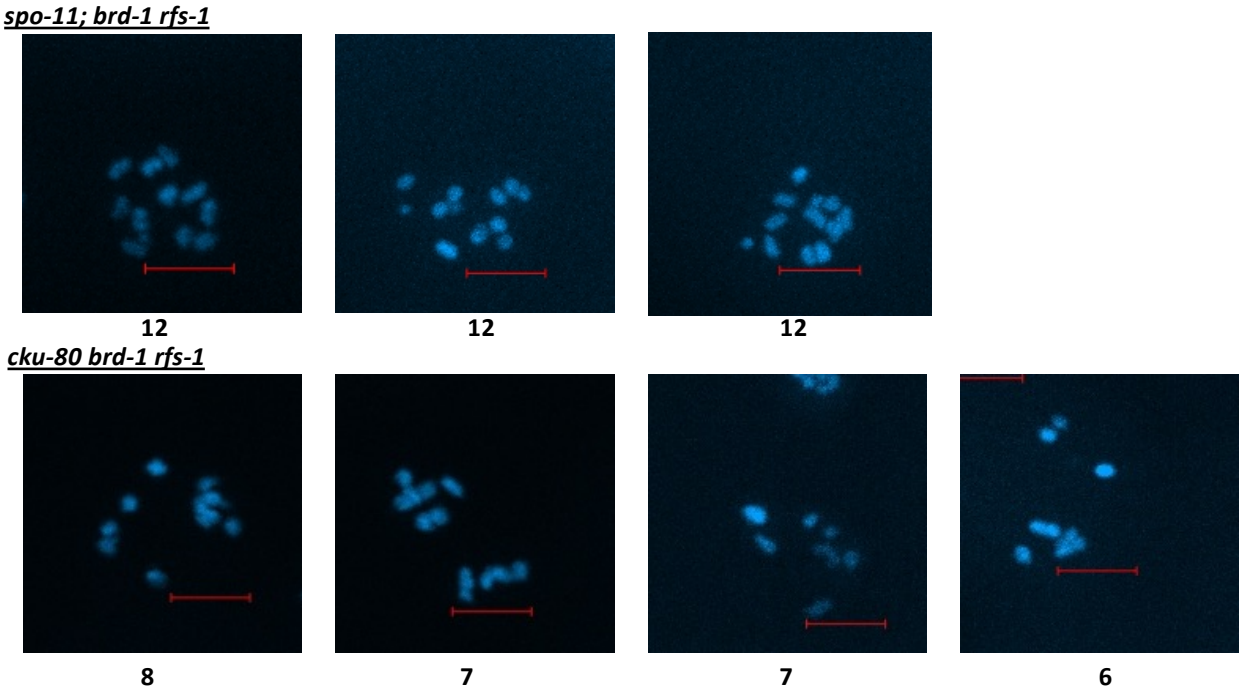

C

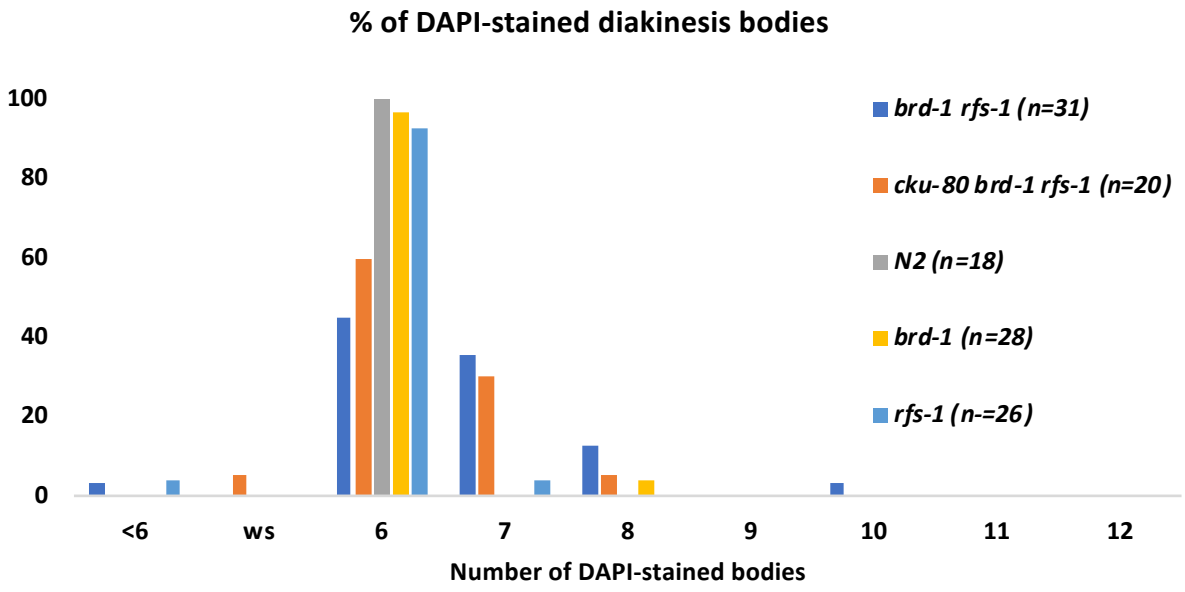

Figure 4.5 *brd-1 rfs-1* double mutants are synthetic sick. (A) Brood size and embryonic lethality in *brd-1* and *rfs-1* single mutants, *brd-1 rfs-1* double mutants and *cku-80 brd-1 rfs-1* triple mutants. The double and triple mutants were scored as M+Z- worms. Student t tests were used to compare the brood size, embryo survival rate and HIM between indicated animals. No statistical significance was found. (B) Representative images of DAPI-stained bodies at diakinesis of respective mutants. Numbers below indicate the number of DAPI-stained bodies per nuclei. Scale bar denotes 5 µm. (C) Quantification of DAPI-stained bodies at diakinesis from animals of the indicated mutants.

A

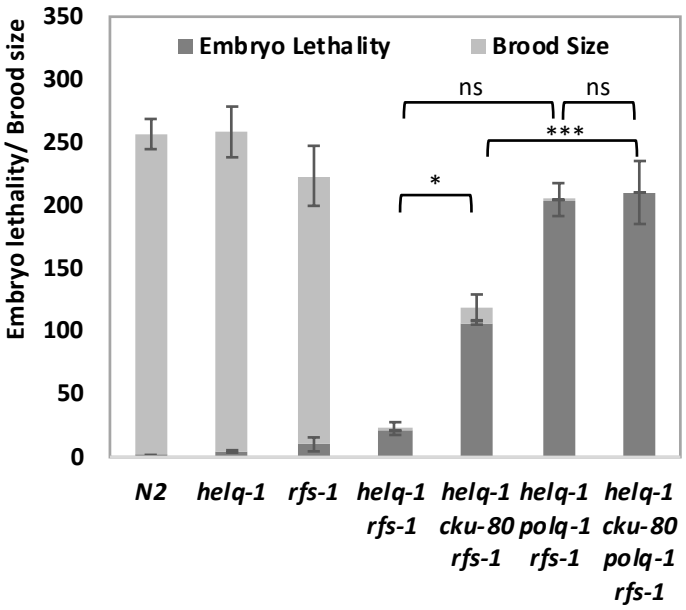
Embryo Lethality
Brood Size
Embryo lethality/ Brood size
350
300
250
200
150
100
50
0
ns
ns
***
*
N2
helq-1
rfs-1
helq-1 rfs-1
helq-1 cku-80 rfs-1
helq-1 polq-1 rfs-1
helq-1 cku-80 polq-1 rfs-1

B

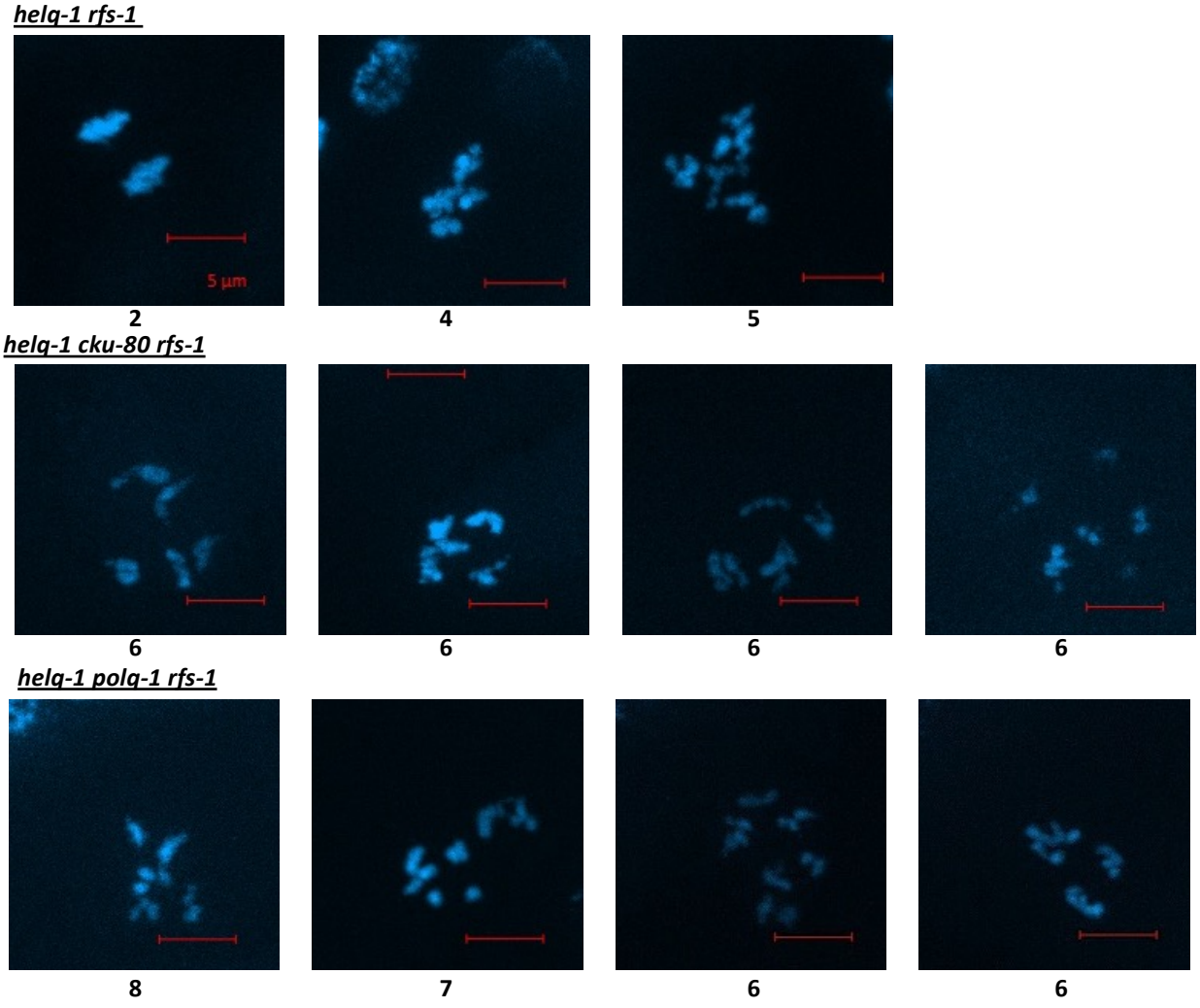
helq-1 rfs-1
5 µm
2
4
5
helq-1 cku-80 rfs-1
6
6
6
6
helq-1 polq-1 rfs-1
8
7
6
6

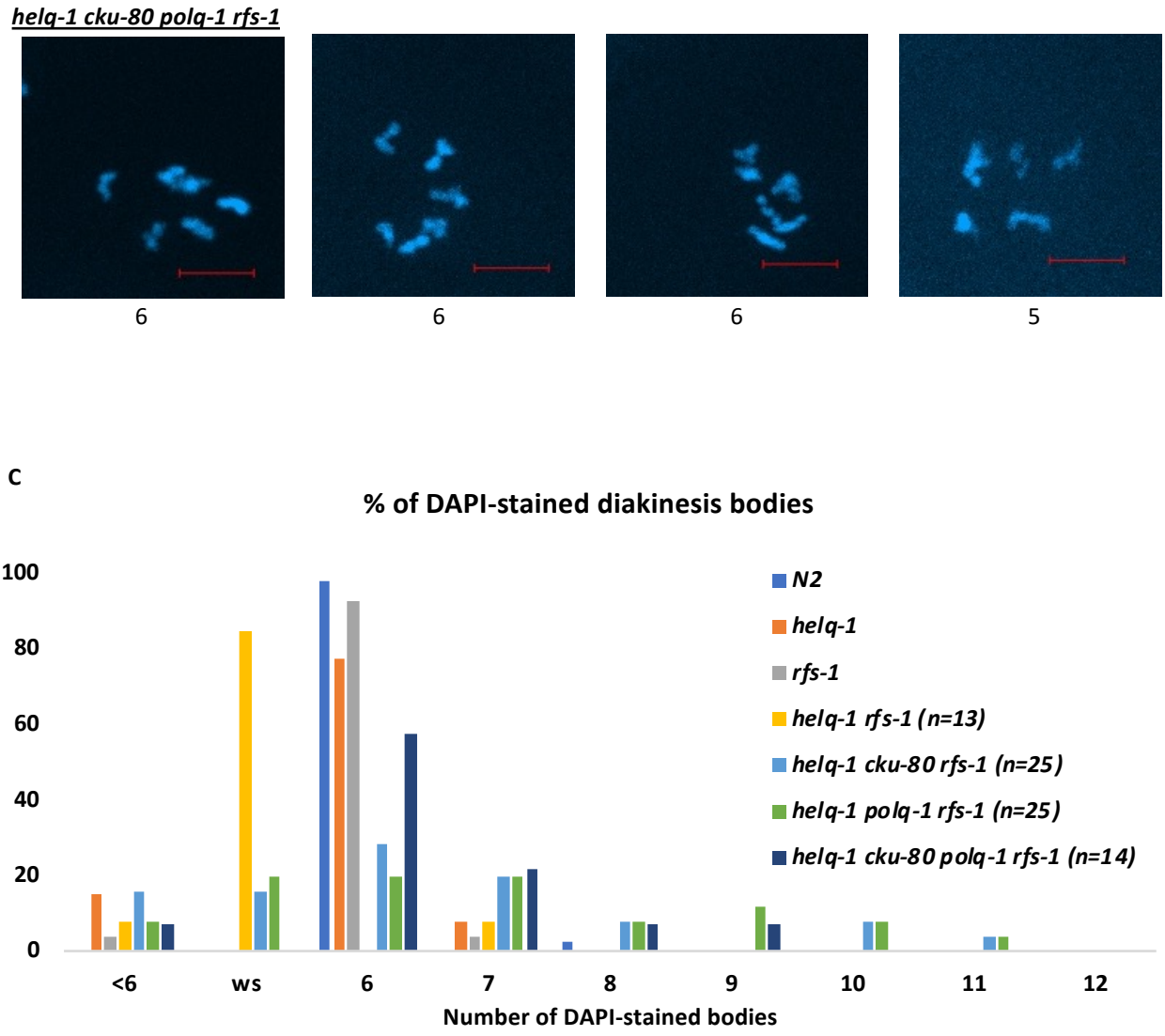

Figure 4.6 *helq-1 rfs-1* double mutants are synthetic lethal. (A) Brood size and embryonic lethality in *helq-1* and *rfs-1* single mutants, *helq-1 rfs-1* double mutants and associated triple and quadruple mutants. The double, triple and quadruple mutants were scored as M+Z- worms. Error bars represent the standard error of the mean. Student t tests were used to compare embryo survival rate between indicated animals. * denotes p value less than 0.05, ** <0.01, ***<0.001. In addition, Student t tests were used to compare brood size between *helq-1 rfs-1* and *helq-1 cku-80 rfs-1*, and *helq-1 rfs-1* and *helq-1 polq-1 rfs-1*. p-value for both was smaller than 0.001. (B) Representative images of DAPI-stained bodies in diakinesis of respective mutants. Numbers below indicate the number of DAPI-stained bodies per nuclei. Scale bar denotes 5 µm. (C) Quantification of DAPI-stained bodies at diakinesis from animals of the indicated mutants.

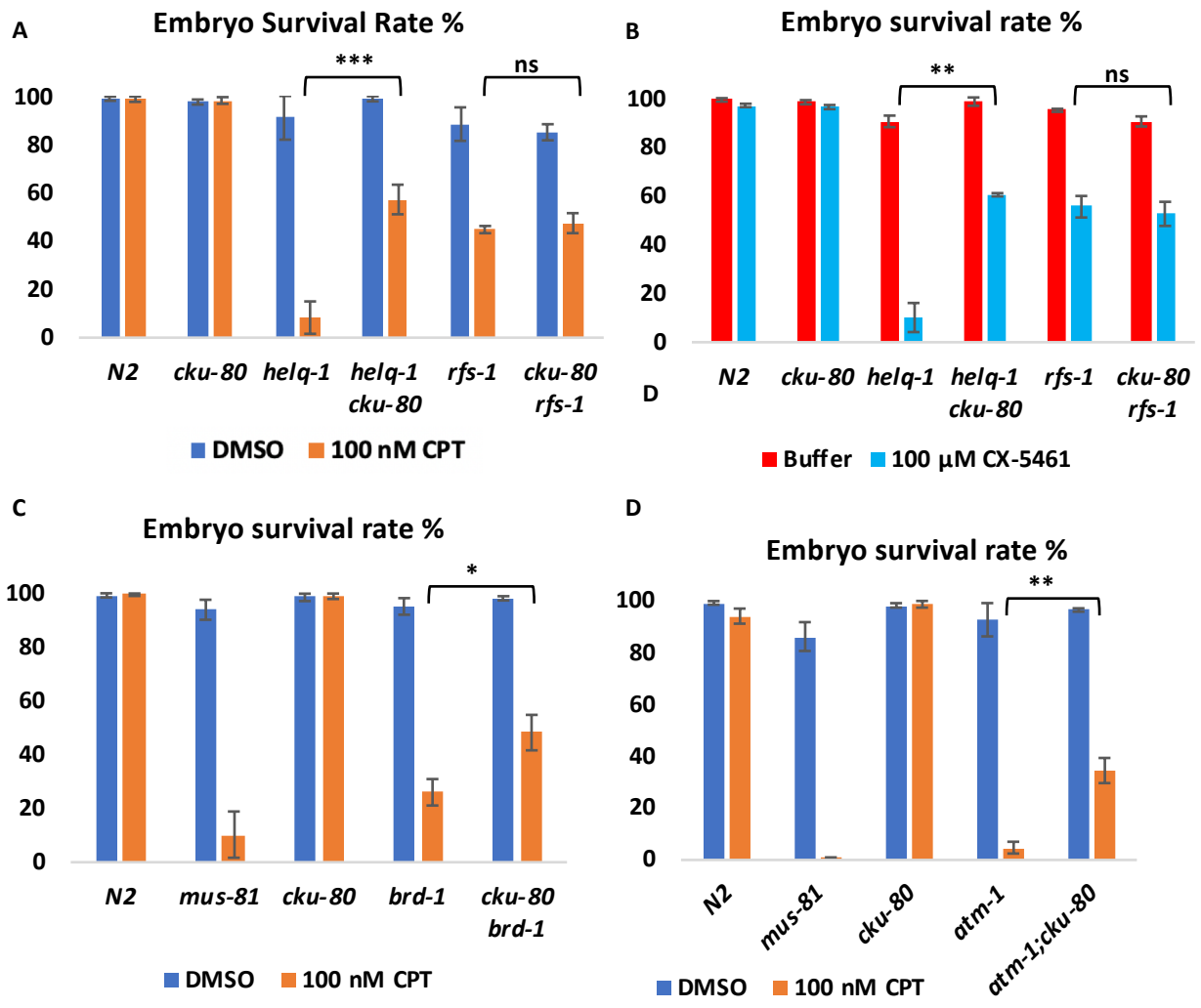

Figure 4.7 Loss of NHEJ rescues the DNA damage agent sensitivity in some but not all HDR-compromised mutants. (A - D) Embryo survival rate of indicated mutants treated with camptothecin (CPT) or CX-5461. CPT was dissolved in DMSO, CX-5461 was dissolved in 50mM Na_2HPO_4. *mus-81* is used as positive control in above experiments. All experiments were conducted in three replicates. Error bars represent the standard error of the mean. P values were calculated using two-tailed student t test. * denotes p value less than 0.05, ** <0.01, ***<0.001.

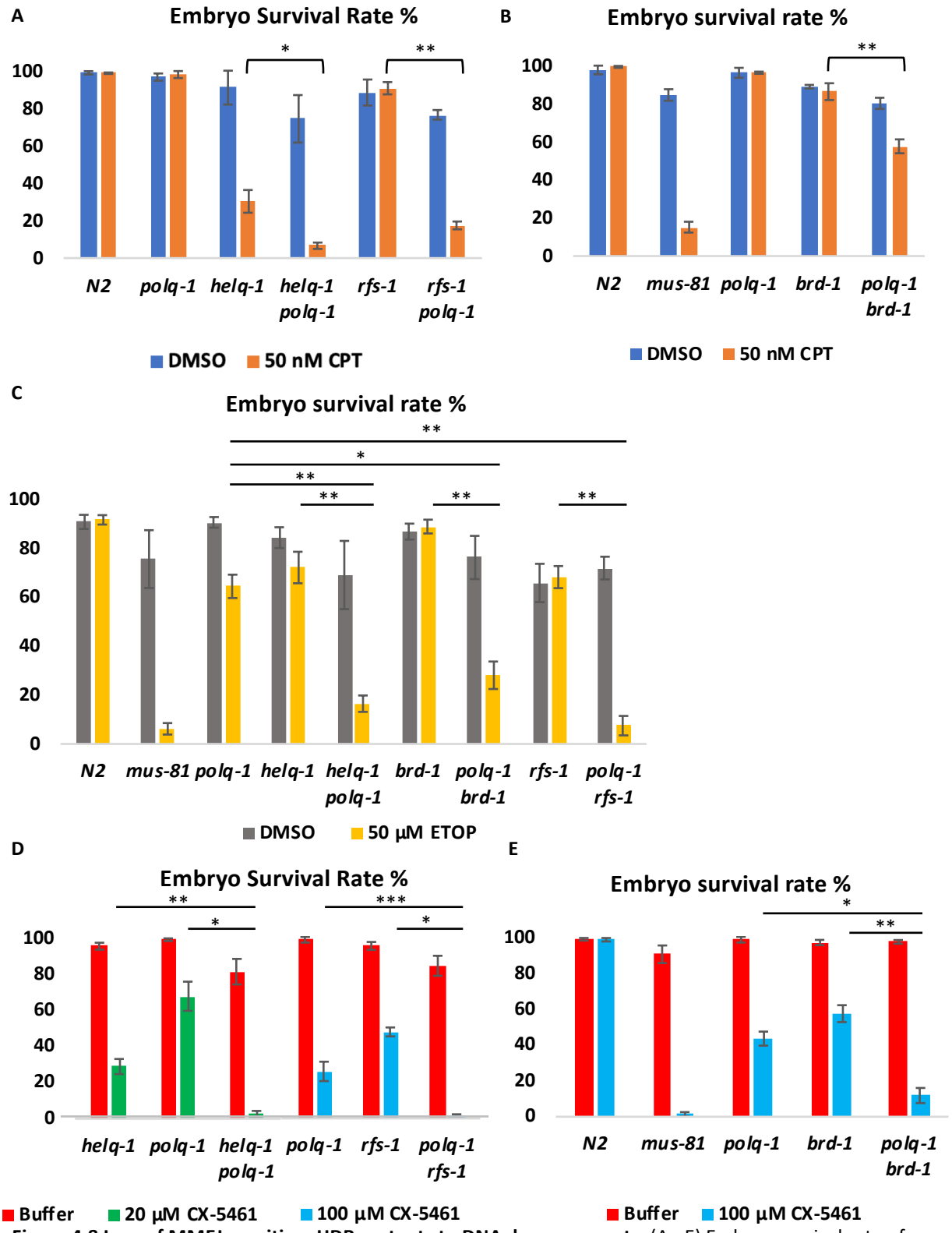

Figure 4.8 Loss of MMEJ sensitizes HDR mutants to DNA damage agents. (A - E) Embryo survival rate of indicated mutants treated with camptothecin (CPT), etoposide (ETOP) or CX-5461. CPT and ETOP were dissolved in DMSO, CX-5461 was dissolved in 50mM Na_2HPO_4. *mus-81* is used as positive control in above experiments. All experiments were conducted in three replicates. Error bars represent the standard error of the mean. P values were calculated using two-tailed student t test. * denotes p value less than 0.05, ** <0.01, ***<0.001.

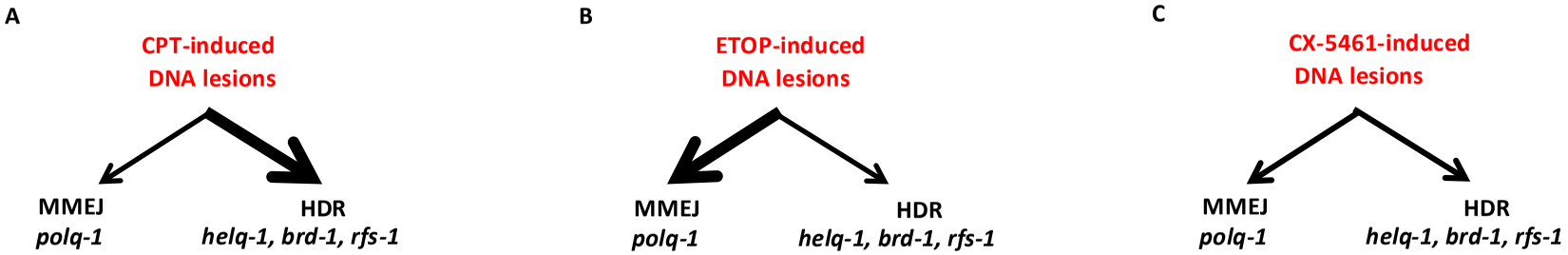

Figure 4.9 Model of different DSB repair pathways required for CPT (A), ETOP (B), and CX-5461 (C). (A) CPT-induced lesions is repaired primarily via HDR pathway (left). In the absence of HDR, MMEJ can be a backup pathway. (B) ETOP-induced lesions is repaired primarily via MMEJ pathway (left). When MMEJ is compromised, HDR can be a backup pathway. (C) CX-5461-induced lesions require both HDR and MMEJ pathways to repair. Thick arrows denote the primary pathway, thin arrows denote the backup pathway when the primary one is overwhelmed or absent, and intermediate arrows in (C) indicate that both pathways are required.

Genotype	Brood Size	Embryo Survival Rate %	Male %	n
N2	256.71±12.00	99.58±0.22	0.03±0.02	14
helq-1	258.40±20.16	98.30±0.37	0.79±0.18	10
brd-1	261.20±24.31	97.55±0.46	1.14±0.30	10
rfs-1	223.50±23.85	95.53±2.48	1.85±0.49	10
cku-80	260.30±11.35	99.77±0.10	0.08±0.07	10
polq-1	228.30±36.64	98.51±9.87	0.00±0.00	10
helq-1 cku-80 (M+Z-)	213.56±7.65	99.27±0.19	0.10±0.07	9
helq-1 cku-80 (M-Z-)	244.80±17.29	99.14±0.31	0.04±0.04	10
cku-80 brd-1 (M+Z-)	232.80±23.26	97.59±0.24	0.66±0.23	10
cku-80 brd-1 (M-Z-)	268.40±14.47	98.92±0.55	1.37±0.15	10
cku-80 rfs-1 (M+Z-)	267.60±15.38	91.52±1.09	2.35±0.32	10
cku-80 rfs-1 (M-Z-)	220.80±17.19	95.10±0.44	2.59±0.28	10
cku-80 polq-1	266.70±11.42	98.65±0.36	0.11±0.06	10
helq-1 polq-1 (M+Z-)	189.20±16.69	87.21±6.81	0.00±0.00	10
helq-1 polq-1 (M-Z-)	129.30±19.09	91.11±4.05	0.00±0.00	10
polq-1 brd-1 (M+Z-)	217.70±11.63	97.29±0.47	1.21±0.23	10
polq-1 brd-1 (M-Z-)	98.30±20.06	88.71±10.62	2.08±0.98	10
polq-1 rfs-1 (M+Z-)	233.30±32.02	86.71±3.84	1.54±0.37	10
polq-1 rfs-1 (M-Z-)	131.30±23.83	96.73±0.83	0.88±0.21	10
helq-1 brd-1 (M+Z-)	158.80±10.36	1.89±0.46	ND	10
helq-1 rfs-1 (M+Z-)	22.56±5.07	7.20±1.28	ND	16
brd-1 rfs-1 (M+Z-)	169.73±19.62	49.96±2.89	13.66±1.27	15
helq-1 brd-1 rfs-1 (M+Z-)	90.80±6.50	0.11±0.20	ND	10
helq-1 cku-80 polq-1 (M+Z-)	228.30±19.51	91.90±5.11	0.00±0.00	10
cku-80 polq-1 rfs-1 (M+Z-)	247.90±29.22	95.93±0.60	0.76±0.15	10
cku-80 polq-1 brd-1 (M+Z-)	193.40±27.80	50.83±10.65	1.36±1.01	10
helq-1 cku-80 brd-1 (M+Z-)	171.40±18.20	30.46±7.87	3.48±5.45	10
helq-1 polq-1 brd-1 (M+Z-)	97.00±10.41	10.62±3.51	0.00±0.00	10
helq-1 cku-80 rfs-1 (M+Z-)	118.93±10.25	10.37±1.17	8.70±2.72	15
helq-1 polq-1 rfs-1 (M+Z-)	204.60±13.09	0.10±0.06	ND	10
cku-80 brd-1 rfs-1 (M+Z-)	167.60±10.42	45.76±2.11	13.70±1.28	10
helq-1 cku-80 polq-1 rfs-1 (M+Z-)	210.25±25.03	0.00±0.00	ND	16
helq-1 cku-80 polq-1 brd-1 (M+Z-)	136.90±8.99	3.80±0.73	ND	10

Table 4.1 Phenotypes of indicated mutants. n denotes the number of parent worms whose progeny were scored. All values are ± standard error of the mean. M+Z-: maternally positive and zygotically negative. M-Z-: maternally negative and zygotically negative. ND: not determined.

CHAPTER 5: CHARACTERIZATION OF THE ANNEALING HELICASE SMRC-1 IN *C. ELEGANS*

5.1 Introduction

SMARCAL1 belongs to the SNF2 family of ATP-dependent chromatin remodeling enzymes that are conserved across species, including worms and humans. SMARCAL1 has been shown to play important roles in maintaining genome integrity. It has a RPA-interacting motif at its N-teminus, and two tandem HARP domains at the protein centre. At its C-terminus, SMARCAL1 has a helicase domain that contains one DEXDc and one HELICc motif. Bi-allelic loss-of-function mutations in *SMARCAL1* cause an autosomal recessive disease called Schimke immune-osseous dysplasia (SIOD) (Boerkoel et al., 2002). The disease is characterized by smaller brain sizes, compromised neuronal development, bone abnormalities, and T-cell immunodeficiency (Deguchi et al., 2008).

It has been shown that SMARCAL1 is required for cell viability under treatment with agents that cause replication stress, including UV, mitomycin, and camptothecin (Bansbach et al., 2009; Ciccia et al., 2009). SMARCAL1 is regulated following hydroxyurea treatment or UV radiation (Bansbach et al., 2009). Biochemical experiments demonstrated that SMARCAL1 can act as an anti-helicase by annealing the nascent ssDNA strands to reverse the fork, forming a four-way DNA structure resembling a chicken foot (Betous et al., 2012). The current model for SMARCAL1 is that it prevents genome instability through the bypass of DNA lesions by catalyzing fork reversal and restoration. It appears that SMARCAL1 maintains genome integrity by preventing ssDNA accumulation at stalled replication forks. Loss of SMARCAL1 leads to

ssDNA that can be a substrate for other repair or resolution mechanisms, which can often be deleterious.

There are many factors that play an important role in guarding the genome stability, including the resolution of substrates arising at stalled replication forks. There are very few confirmed anti-helicases. Other anti-helicases have been identified that are able to reverse replication forks, including HLTF and ZRANB3 (Poole and Cortez, 2017). SMRC-1, the *C. elegans SMARCAL1* homolog, appears to be the only anti-helicase in *C. elegans*, and therefore, the worm may provide a simpler model to characterize the role of anti-helicases in genome stability.

Recently, *smrc-1* mutants have been found to genetically interact with *met-2*, a histone methyltransferase (Yang et al., 2019). Little is known about how SMARCAL1 interacts with other factors at the replication fork. Loss of SMARCAL1 could have an effect on MUS81, a structure-specific endonuclease, which cleaves the stalled forks to create DSBs for HDR-mediated fork restart (Hanada et al., 2007; Regairaz et al., 2011). SMARCAL1 could also play a role in ssDNA maintenance during HDR. The anti-recombinase RTEL1, prevents recombination by disrupting D-loop formations and template switching (Barber et al., 2008; Leon-Ortiz et al., 2018), this process would generate ssDNA that could be a substrate for SMARCAL1. Other helicases play important roles in genome maintenance, such as FANCJ and HELQ. FANCJ can unwind G-quadruplexes, and loss of FANCJ function induces small deletions in *C. elegans* (Cheung et al., 2002; London et al., 2008). HELQ is less understood but has been shown to play a role in regulating D-loops (Ward et al., 2010). In addition, the protease SPRTN/DVC1 safeguards the genome by degrading proteins trapped on DNA (Stingele et al., 2016; Vaz et al.,

2016). If DNA-protein adducts are not resolved, they can act as replication blocks, and SMARCAL1 may be required to mediate the replication fork reversal.

To address these hypotheses, we identified and characterized the genetic interactions between SMARCAL1 and genes involved in DNA metabolism, with an emphasis on those that resolve stalled forks.

5.2 Methods

Construction of mutant strains

Alleles used in this chapter include: *smrc-1 (gk176502)*, *smrc-1 (gk784642)*, *dog-1 (gk10)*, *rtel-1(tm1866)*, *mus-81(tm1937)*, *helq-1 (tm2134)* and *dvc-1 (ok260).* Some strains were provided by the Caenorhabditis Genetics Center, which is funded by NIH Office of Research Infrastructure Programs (P40 OD010440), and some knockout alleles were provided by the Shohei Mitani laboratory. Some strains were generated by the International *C. elegans* Gene Knockout Consortium (Consortium, 2012) and by the National Bioresource Project of Japan. Two *smrc-1* alleles*, gk176502* and *gk784642* were obtained by outcrossing the strains VC20168 and VC40734 from the Million Mutation Project (MMP) collection (Thompson et al., 2013) to N2 six times, and then balancing *the smrc*-1 mutations with the *hT2* balancer to maintain *smrc-1* as a heterozygote to prevent accumulation of mutations. Double mutants were generated by genetic crossing using strains containing the mutant gene(s) of interest. In all cases, mutants were genotyped by PCR. To maintain mutants with strong fitness defects, the *hT2* balancer was used to keep mutations heterozygous. The *hT2* balancer is able to balance most genes studied in this

chapter with the exception of *dog-1* and *helq-1*. Most homozygous double mutants were characterized as fresh segregants from balanced heterozygotes.

Brood Scoring

L4 larvae of each genotype were picked to fresh NGM plates and transferred each day. Progeny were first scored 24 hours later for dead embryos and hatched larvae, and scored two days later for adult males and hermaphrodites. The total brood is measured as the sum of dead embryos and hatched larvae. The embryonic lethality is defined as the percentage of dead embryos in the total brood. The male percentage is defined as the percentage of males in the total adult population.

Generational survival assay

Animals were plated individually and maintained at room temperature. Starting with 10 or 20 separate individuals at the P_0 generation, a single L4 larva was transferred to a fresh plate at each generation. A line was scored as unsustainable when the parent worm was either sterile or produced only dead embryos.

Genome Sequencing

One starting P_0 and all viable F_{10} lines of both *smrc-1* mutants (*gk176502* and *gk784642*) were prepared for sequencing. Worms were rinsed off with deionized water and pelleted by centrifugation. Genomic DNA was purified using Puregene® Core Kit A (Qiagen). Illumina Hi-Seq DNA sequencing was performed at the Novogene Bioinformatics Institute (Beijing, China). Sequence reads were mapped to the *C. elegans* reference genome version WS230 (http://www.wormbase.org) using the short-read aligner BWA, which gave each sample a sequencing depth of a least 20x. Copy numbers were estimated from the alignments with a procedure analogous to that of Itani *et al.* using 5 kb wide overlapping sliding windows with the

alignments from the parental strain used as the reference (Itani et al., 2015). Copy number alterations in F_{10} lines were normalized by subtracting the respective P_0.

DAPI staining

Synchronized animals were picked into 10μl of M9 buffer, and then transferred to 100μl of 150nM 4',6-diamidino-2-phenylindole dihydrochloride (DAPI) in 70% ethanol. The animals were stained in the dark at 4℃ overnight. Then they were destained twice by soaking in M9 buffer for one hour each. DAPI-stained animals were mounted on slides with 3% agarose pads and visualized at 63x magnification on a Zeiss Axioplan microscope using Z-stacking. Stacked images were taken by Hamamatsu ORCA-Flash 4.0 camera and processed by Zeiss Zen software. DAPI-stained diakinesis bodies were counted in the three oocytes most proximal to the spermatheca in the germ line. A DAPI-stained diakinesis body was defined as a continuous DAPI-stained chromatin structure, regardless of its size. Mitotic bridges were defined as unresolved chromatin structures between two distinct nuclei.

Quantitative acute assay

Synchronized one-day-old adults were incubated in the DNA damaging agent (CX-5461 in 50mM NaH_2PO_4, etoposide (ETOP) in DMSO, or camptothecin (CPT) in DMSO) diluted in M9 buffer containing OP50, carbenicillin (50 μg/ml) and 10ng/ml nystatin for ~18 hours. The exception was that adults were incubated in Ethyl methanesulfonate (EMS) for only 4 hours. Following treatment, the animals were plated to allow recovery for 30 to 60 minutes on OP50-containing NGM plates, and then plated ten worms per plate in triplicate on NGM plates for a 4-hour interval (18 to 22 hours post-treatment), and then removed. The numbers of both arrested embryos and hatched larvae were counted one day later in order to calculate the percentage of embryo survival after treatment. All results were from at least 30 treated animals. For animals

that produced few progeny, more treated adult worms were picked to lay embryos in the 4-hour interval. The calculation of the sensitivity score was detailed in Chapter 2 Method.

5.3 Results

5.3.1 SMRC-1 is required for maintaining genome stability

In the course of assembling a panel of *C. elegans* DNA repair mutants, we noticed that two Million Mutation Project (MMP) strains (VC20168 and VC40734) that had a distinct mutational profile. VC20168 and VC40734 both contained many small deletions and duplications (Figure A5.1). Furthermore, both VC20168 and VC40734 exhibited a Him phenotype, which can be indicative of chromosome instability. The MMP strains were generated by EMS (Ethyl methanesulfonate), ENU (N-ethyl-N-nitrosourea), and EMS+ENU mutagenesis followed by 10 generations of self-crossing to homozygose mutations before whole genome sequencing (Thompson et al., 2013). If a mutator homozygosed early in the self-crossing process, this strain would accumulate mutations, which could be distinct from the mutagenesis-induced mutations.

The MMP strains contain many homozygous mutations that could be responsible for these phenotypes. Specifically, VC20168 contained 253 homozygous mutations, of which 93 are predicted to result in non-synonymous protein changes, whereas VC40734 contained 373 homozygous mutations, of which 143 are predicted to result in non-synonymous protein changes. Both strains contained potentially deleterious mutations in the *smrc-1* gene. VC20168 contains *smrc-1 (gk176502),* a point mutation in a conserved residue of the DEXDc helicase domain, and VC40734 contains *smrc-1 (gk784642),* a point mutation that results in a premature stop codon. To test whether the *smrc-1* mutations were the cause of genomic instability, *smrc-1* single

mutants were first outcrossed to N2 six times to remove background mutations. After six times of outcrossing, each of the *smrc-1* alleles (*gk176502* and *gk784642)* was maintained in separate lines using the *hT2* balancer. Then, 10 maternally positive zygotically negative (M+Z-) individual lines (termed as P_0) for both *smrc-1(gk176502)* and *smrc-1(gk784642)* alleles were bottle-necked by picking one L4 in each generation for 10 generations (F_{10}) to re-create the process used to generate the MMP strains. Notably, not all ten lines were viable at F_{10}. Five out of ten lines containing *smrc-1(gk176502)* remained fertile at F_{10}, and seven out of ten of lines containing *smrc-1(gk784642)* had become inviable by F_{10} (Figure 5.1A) The remaining F_{10} (M-Z-) *smrc-1* and starting P_0 (M+Z-) of both alleles were prepared for whole-genome sequencing. In the strains carrying either *smrc-1* allele, comparing genomes at F_{10} to P_0 revealed dramatically more small copy number variations in F_{10} compared to the P_0, supporting the hypothesis that the *smrc-1* mutations were the cause of the copy number variations (Figure 5.1B, Figure A5.2).

Next, we set out to characterize the phenotypes of both M+Z- and M-Z- *smrc-1* mutants. Both M+Z- *smrc-1 (gk176502)* and *smrc-1 (gk784642)* alleles caused a Him (high incidence of males) phenotype and reduced embryonic viability (Figure 5.1C). M-Z- *smrc-1* mutants showed more severe fitness defects than their M+Z- counterparts. In particular, brood size and embryo viability of *smrc-1 (gk784642)* were significantly reduced in M-Z- animals compared to those in M+Z- animals. This is consistent with a recent study that showed SMRC-1 promotes fertility and embryonic viability in *C. elegans* (Yang et al., 2019).

5.3.2 SMRC-1 is required for survival after DDA treatment

Next, we asked whether SMRC-1 was required for tolerance of exogenous DNA damage. To address this, we exposed both *smrc-1* mutants to DNA damaging agents, including ethyl methanesulfonate (EMS, an alkylating agent), camptothecin (CPT, a Topoisomerase I inhibitor), etoposide (ETOP, a Topoisomerase II inhibitor), and CX-5461 (a G4-stabilizing agent), and then scored the viability of the progeny of treated animals. *smrc-1* mutant animals showed reduced viability upon treatment of all these agents (Figure 5.2), suggesting SMRC-1 was required for tolerance to all these DNA damaging agents tested.

5.3.3 Genetic interactions between loss of SMRC-1 and other helicases

Due to the role of SMRC-1 in maintaining genome integrity, we expected that *smrc-1* would have genetic interactions with other genes that maintain genome stability, such as DNA replication and repair genes. A previous report showed that SMRC-1 was required when the chromatin modifier, MET-2 was lost (Yang et al., 2019).

First, we crossed *smrc-1*(*gk176502)* males to *rtel-1(tm1866)* hermaphrodites. RTEL-1 is a helicase that functions as an anti-recombinase. RTEL-1 has been shown to regulate the homeostasis of RAD-51 filaments, and its loss results in increased heterologous and homologous recombination (Barber et al., 2008; Leon-Ortiz et al., 2018). The *rtel-1; smrc-1* double mutants were synthetic lethal. The *rtel-1; smrc-1* double mutants produced 100% arrested embryos, whereas both the *rtel-1* and *smrc-1 (gk176502)* single mutants produced over 90% viable progeny (Figure 5.3A, Table 5.1). In addition, the brood size was severely reduced in the double mutants compared to the *smrc-1* and *rtel-1* single mutants. Cytological analysis of *rtel-1; smrc-1*

(M+Z-) double mutants revealed that the phenotypes of DAPI-stained diakinesis bodies were near wild-type (Figure 5.3C), suggesting that meiosis was grossly normal in *rtel-1; smrc-1* animals. By contrast, many somatic cells in *rtel-1; smrc-1* double mutants showed chromatin bridges (Figure 5.3C), which can be indicative of replication stress and incomplete replication. We also observed chromatin bridges in early embryos produced by double mutants. Taken altogether, simultaneous loss of the anti-helicase *smrc-1* and the anti-recombinase *rtel-1* resulted in profound replication defects in the soma and early embryos.

We also generated *dog-1; smrc-1* and *helq-1 smrc-1* double mutants. The *dog-1;smrc-1* (M+Z-) and *helq-1 smrc-1* (M+Z-) double mutants did not exhibit significantly more genome instability-associated phenotypes than the single mutants (Figure 5.3A, Table 5.1). We speculated that the double mutants may accumulate DNA lesions that lead to fitness defects over successive generations, since loss of SMRC-1 has been shown to cause more G/C-associated deletions (Yang et al., 2019). To test this, we bottle-necked the double mutants and the single mutants by generational survival assay. Both the *helq-1 smrc-1* and *dog-1;smrc-1* double mutants became completely sterile by F_{10} (Figure 5.3B) (Yang et al., 2019), whereas over 40 percent of the *helq-1*, *dog-1*, and *smrc-1* single mutants remain fertile. This indicated that the double mutants exacerbated the accumulation of DNA lesions that were passed down to later generations and resulted in sterility in a much faster manner than the *smrc-1 (gk176502)* single mutants. Overall, *smrc-1* exhibited synthetic lethality or sickness in combination with *rtel-1*, *helq-1,* and *dog-1*.

5.3.4 Genetic interactions between loss of SMRC-1 and other DDR genes

A previous study proposed a model that cells depend on MUS81-mediated repair when SMARCAL1 is absent (Betous et al., 2012). We hypothesized that loss of *smrc-1* would affect the viability of *mus-81* mutants in *C. elegans*. We crossed *smrc-1* (*gk176502)* males to *mus-81* hermaphrodites, and *mus-81;smrc-1* double mutants were maintained as heterozygotes using the *hT2* balancer. Five out of ten M+Z- double mutants scored produced less than 20 progeny, including two that were sterile. On average, the *mus-81;smrc-1* (M+Z-) double mutants had a small brood size, 50% less than the brood size of the *mus-81* (M+Z-) or *smrc-1 (gk176502)* single mutants. The double mutant had a decreased embryo survival rate (50.51% ± 7.78%), compared to more than 90% in the *mus-81* or *smrc-1 (gk176502)* single mutants (Figure 5.3A, Table 5.1). The F_1 *mus-81;smrc-1* double mutants that survived likely did so by maternal rescue, because all F_1 were either sterile or produced no viable progeny (Figure 5.3B). Cytological analysis found similar somatic replication defects in *mus-81; smrc-1* as observed in *rtel-1;smrc-1* double mutants (Figure 5.3C). The DAPI-stained diakinesis bodies in *mus-81; smrc-1* double mutants showed little difference to those in *mus-81* single mutants, both of which had mild meiotic defects (O'Neil et al., 2013).

It has been shown that metalloprotease SPRTN/DVC1 could regulate translesion synthesis as well as degrade DNA-protein crosslink lesions (Ghosal et al., 2012; Mosbech et al., 2012; Stingele et al., 2016; Vaz et al., 2016), and SMARCAL1 mediates fork reversal when the fork encounters DNA lesions. We hypothesized that these two genes could work in concert to counteract DNA lesions. We asked whether simultaneous loss of DVC-1 and SMRC-1 in *C. elegans* would affect animal survival by generating *dvc-1;smrc-1* double mutants. The *dvc-*

1;smrc-1 double mutants exhibited more severe fitness defects than either the *dvc-1* or *smrc-1* single mutants (Figure 5.3A, Table 5.1). The double mutants had approximately one third the brood size of either single mutants, and two out of 10 lines of *dvc-1;smrc-1* (M+Z-) double mutants were sterile. In addition, the double mutants showed reduced embryo viability (76.61% ± 11.49%) than that of the *dvc-1* mutants (98.41 ± 0.68%).

5.4 Discussion

SMRC-1 is required for genome integrity. Biallelic mutation of *SMARCAL1* in humans is linked to the etiology of Schimke immuno-osseous dysplasia (SIOD). Little is known about how SMARCAL1 interacts with other replication fork stabilizing proteins. Using *C. elegans,* we investigated the *in vivo* role of SMRC-1 and studied the genetic interactions between *smrc-1* and other genes involved in genome maintenance.

5.4.1 SMRC-1 is required for genome integrity.

Close examination of mutational signatures of the two original MMP strains that contain SMRC-1 mutations raised a hypothesis that SMRC-1 loss induced chromosomal abnormalities. Accumulation of these chromosomal alterations over successive generations could eventually lead to sterility or lethality.

Recently, Yang and colleagues have showed that CRISPR-edited *smrc-1* nonsense and frame-shift alleles could cause reduced fertility and increased embryo lethality (Yang et al., 2019). We found similar genome instability-associated phenotypes using independent nonsense and missense *smrc-1* alleles. To further support that SMRC-1 plays a key role in maintaining genome

integrity, we bottle-necked *smrc-1* mutants for 10 generations and sequenced the genome of F_{10} (M-Z-) and P_0 (M+Z-) *smrc-1* mutants. Our data indicated that SMRC-1 deficiency resulted in a mutator phenotype characterized by the accumulation of small copy number variations. In addition, generational sterility occurred in later generations confirmed that accumulation of chromosomal alteration events had deleterious effects on viability.

It has been previously shown that SMARCAL1 was part of the DNA damage response by its recruitment to mediate the regression of stalled replication forks via interaction with RPA (Bansbach et al., 2009; Ciccia et al., 2009), a protein complex that coats and protects ssDNA. DNA damage is often associated with the presence of ssDNA-RPA complex, which triggers the DNA damage response (Zou et al., 2006). Lack of SMRC-1 could lead to inability to repair certain type of DNA lesions. Therefore, when SMRC-1 is defective, animals could accumulate unresolved endogenous DNA lesions and develop dysfunctional germ lines that produce fewer progeny; or alternatively, if the lesions were tolerable and passed to the next generation, the next generation animals would continue to accumulate unresolved lesions, which could eventually lead to embryonic lethality or sterility.

The sensitivity of *smrc-1* mutants to various types of exogenous DNA damage demonstrates that SMRC-1 plays a vital role in preserving genome stability. For example, EMS induces methylated guanines that are usually resolved by O^6-methylguanine-DNA methyltransferase (MGMT) or the mismatch repair pathway. In the course of repair, single stranded DNA is generated, which is susceptible to further damage in the form of DNA breaks. Our data showed that *smrc-1* mutants were extremely sensitive to EMS treatment, indicating that annealing ability of SMRC-1 could

be critical for resolution of EMS-induced DNA lesions in *C. elegans*. Likewise, treatment with the topoisomerase poisons camptothecin and etoposide can generate ssDNA intermediates, which might require SMRC-1 to prevent the spreading of ssDNA and DNA breakage. Taken together, SMRC-1 is required for protecting genome integrity from both endogenous and exogenous DNA damage *in vivo*.

5.4.2 SMRC-1 is required for genome integrity in the absence of RTEL-1

The synthetic lethality between *smrc-1* and *rtel-1* emphasizes the role of SMRC-1 in maintaining genome integrity. Previous studies showed that loss of SMRC-1 increased meiotic recombination frequency by five-fold (Yang et al., 2019), and that loss of RTEL-1 could elevate meiotic recombination frequency by 2.5-fold (Barber et al., 2008; Yang et al., 2019). It is unknown whether a similar mechanism underlies these increases in meiotic crossover rates. In addition, loss of RTEL1 has been shown to cause increase in heterologous recombination and lead to duplication of genomic regions inserted at some distance from its original copies in mammalian cells (Leon-Ortiz et al., 2018). We have also identified a similar pattern of duplications in *smrc-1*-deficient mutants (Figure 5.1B, Figure A5.2). It appears that loss of SMRC-1 or RTEL-1 increases the frequency of CNVs. In light of the annealing activity of SMRC-1 and anti-recombination activity of RTEL-1, we propose a speculative model in which the loss of SMRC-1 causes ssDNA accumulation upon replication fork stalling, which becomes a substrate for homology-directed recombination, eventually giving rise to templated-duplications. These duplications are the by-product of an error-prone tolerance mechanism needed for *smrc-1* mutant survival. However, additional loss of RTEL-1 further promotes inappropriate recombination and

template switching, potentially resulting in massive amount of recombination intermediates that could not be resolved.

5.4.3 SMRC-1 is required for genome integrity in the absence of MUS-81

A previous study showed that *SMARCAL1*-deficient cells rely on MUS81-catalyzed cleavage of damaged forks to prevent DNA lesions (Betous et al., 2012). In agreement with this, we showed that loss of SMRC-1 function is synthetic lethal with the absence of MUS-81. In human cells, MUS81, together with its interacting partners (EME1 or EME2), is able to cleave a variety of DNA structure substrates, and its activity is tightly regulated by WEE1/CDK and other kinases (Duda et al., 2016; Wyatt et al., 2013). Since MUS81 is required for cutting persistent replication intermediates at common fragile sites in mitosis, it is often the backup mechanism to safeguard chromosome segregation (Minocherhomji et al., 2015; Naim et al., 2013; Ying et al., 2013). Similar to *mus-81* mutants, *smrc-1* mutants exhibited broad sensitivity to many DNA damaging agents tested (Figure 5.2). This suggests that SMRC-1 could be involved in different repair mechanisms to counteract DNA damage, or that SMRC-1 is essential to regulate ssDNA which is a common intermediate for many repair pathways (Zellweger et al., 2015). Mechanistically, Mus81 has been shown to cleave the stalled forks to form DSBs to restart replication (Hanada et al., 2007) as well as to limit Pol32-dependent error prone synthesis in break-induced repair (Mayle et al., 2015). This raises the possibility that MUS-81 and SMRC-1 represent two alternate repair/bypass mechanisms at stalled replication forks.

It is worth noting that both *mus-81* and *rtel-1* exhibit synthetic lethality with *smrc-1*, and that *mus-81 rtel-1* double mutants are also synthetic lethal due to accumulated replication intermediates that fail to be resolved in meiosis (Barber et al., 2008). It has also been shown in yeast that Mus81 removes toxic Holliday junctions in the absence of Srs2, the yeast helicase analogous to RTEL1 (Elango et al., 2017). Therefore, it appears that there are distinct mechanisms behind the SL observed *mus-81;smrc-1*, *rtel-1;smrc-1* and *mus-81 rtel-1*. The next step will be to look for phenotypes that could differentiate the three pairs of synthetic lethal double mutants to elucidate distinctive roles of each gene.

5.4.4 *smrc-1* genetically interacts with factors required for DNA metabolism

The *helq-1 smrc-1*, *dog-1;smrc-1,* and *dvc-1;smrc-1* double mutants were all synthetic sick, indicating that *smrc-1* negatively interacts with *helq-1, dog-1*, and *dvc-1*, all of which are factors involved in very different aspects of DNA metabolism.

DOG-1 is the *C. elegans FANCJ* homolog that has been shown to unwind G-quadruplexes (Youds et al., 2008). Loss of DOG-1 induces a mutator phenotype that primarily causes G-tract deletions that are mediated by MMEJ repair (Cheung et al., 2002; Koole et al., 2014). It has been recently reported that additional loss of SMRC-1 increases the frequency of G-tract deletions in the *dog-1* mutant background (Yang et al., 2019). We found that, similar to *dog-1* mutants, the loss of SMRC-1 results in a distinctive mutator phenotype characterized by small copy number variations (Figure 5.1B, Figure A5.2). It remains to be determined if the *smrc-1* mutator phenotype is catalysed by MMEJ as is the case with *dog-1*. However, *smrc-1*-induced rearrangements are frequently small local duplications which are distinct from the small

deletions flanked by microhomology. It remains to be determined if these small duplications contain microhomology at the breakpoints. One model for *dog-1*-induced small deletions involves persistence of ssDNA through mitosis (Koole et al., 2014), which could also be a substrate for *smrc-1*. It is likely that loss of SMRC-1 changes the mutational nature of *dog-1* or increases the mutations to an intolerable level. This is consistent with the observation that *dog-1;smrc-1* double mutant lines became inviable much faster than *dog-1* and *smrc-1* single mutant lines (Figure 5.3B). In human cells, a recent study demonstrated that FANCJ and helicase-like transcription factor (HLTF, another fork reversal remodeler) work in opposing roles to keep fork remodeling and replication progression in check (Peng et al., 2018). Combined loss of FANCJ and HLTF results in severe replication stress in cells. Our data suggest there is a synergy between DOG-1 and SMRC-1 in protecting genome integrity.

helq-1 is the *C. elegans* homolog of human *HELQ*, which is involved in repairing interstrand crosslink (ICL) damage. It has been shown that HELQ interacts with RAD51C to promote efficient homologous recombination (Adelman et al., 2013; Ward et al., 2010). We found that *helq-1* mutant animals exhibited sensitivity to a number of DNA damaging agents, including topoisomerase poisons and CX-5461 (See Chapter 2 and 3), and that *helq-1* is synthetic lethal with *brd-1* (Chapter 4). Little is known about how *helq-1* genetically interacts with other helicases. M+Z- *helq-1 smrc-1* double mutants did not show strong fitness defects when compared to *smrc-1* single mutants. It appears that HELQ-1 deficiency exacerbated the negative effect of the mutator phenotype due to loss of SMRC-1, since *helq-1 smrc-1* lost fertility much faster than respective single mutants. The next step would be to look into how HELQ-1 contributes to DNA repair in the absence of SMRC-1.

dvc-1 is the *C. elegans* homolog of human *SPRTN* metalloprotease. SPRTN regulates the switch between replicative polymerases and translesion synthesis (TLS) polymerases (Ghosal et al., 2012; Mosbech et al., 2012), and removes protein-DNA adducts (Stingele et al., 2016; Vaz et al., 2016). The *dvc-1;smrc-1* double mutants were synthetic sick, with a reduced brood size and reduced embryo viability compared to respective single mutants. The negative genetic interaction between *dvc-1* and *smrc-1* raised two possibilities due to two distinctive roles of DVC-1. One possibility is that TLS and fork remodeling represent two separate repair mechanisms to bypass endogenous DNA lesions without actually resolving the lesions, and that simultaneous loss of TLS regulators and SMRC-1 lead to cell death. The other possibility would involve a role for SMRC-1 in bypassing DNA-protein adducts when they are not degraded by DVC-1. It is noted that both TLS regulation and protease activity can play a role in managing protein adducts trapped on DNA, thus making SMRC-1 a potential target in some genetic backgrounds for anticancer therapeutics that result in protein trapping on DNA.

We have identified genetic interactions between SMRC-1 and multiple genes involved in DNA metabolism and confirmed the distinct mutator phenotype that occurs when SMRC-1 is lost. More detailed analysis of the *smrc-1*-induced rearrangements could shed light on the mechanisms that cause the rearrangements in the absence of SMRC-1. Unfortunately, the complex nature of the rearrangements, which contain multiple small duplications and breakpoints, confound analysis using the standard short reads of Illumina sequencing. To further characterize how SMRC-1 contributes to maintaining genome stability, we could use long-read Nanopore sequencing to identify breakpoints of CNVs in *smrc-1* mutant animals to elucidate

whether there are sequence motifs or structural preferences in the genome where chromosomal abnormality events are likely to occur in the absence of SMRC-1.

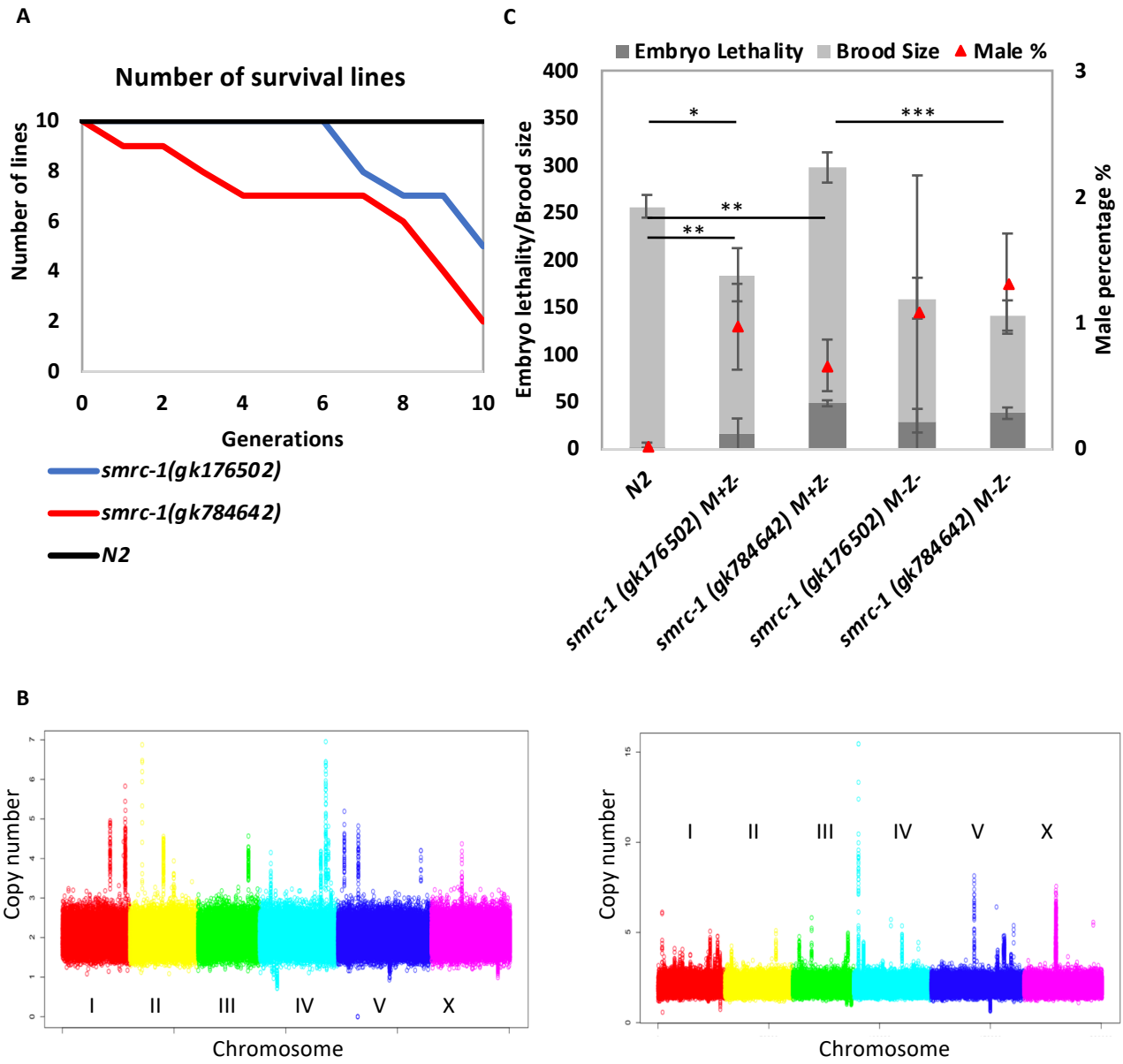

Figure 5.1 SMRC-1 is required for maintaining genome stability. (A) Viability of independent lines of N2, *smrc-1* mutants at 23°C. Both *smrc-1* mutants were M+Z-. (B) Coverage plot of genome rearrangements of F10 *gk176502* (Left). Coverage plot of genome rearrangements of F10 *gk784642* (Right). (C) Brood size and embryonic lethality in *smrc-1(gk176502)* and *smrc-1(gk784642)* single mutants, both *smrc-1* mutants have been outcrossed to N2 six times, and maintained heterozygous by hT2 balancer before scoring. Error bars represent the standard error of the mean. Student t tests were used to compare brood sizes between indicated animals (upper) and male percentage between indicated animals (bottom). * denotes p value less than 0.05, ** <0.01, ***<0.001.

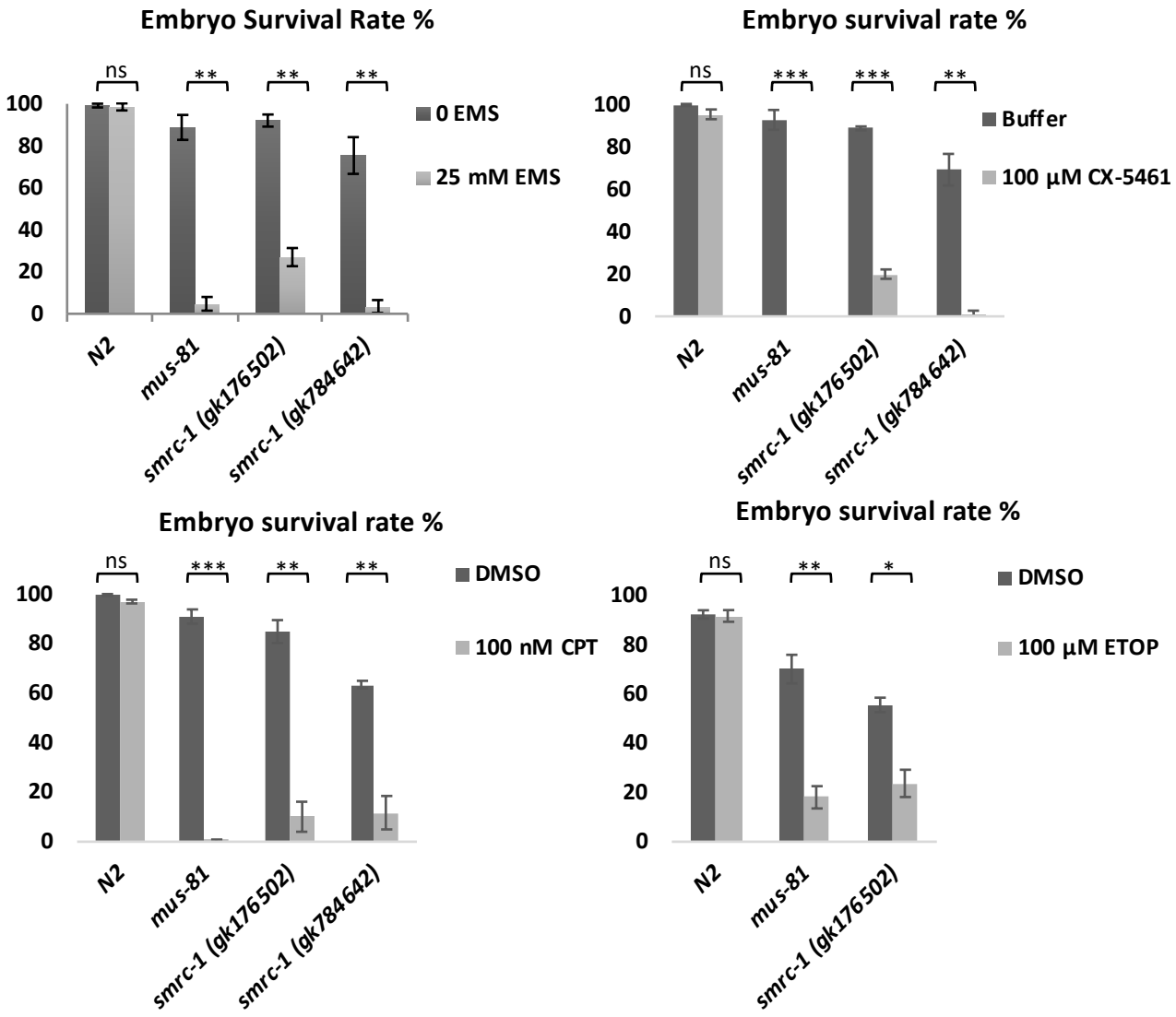

Figure 5.2 SMRC-1 is required for tolerance of genotoxins. Embryo survival rate of *smrc-1* mutants treated with ethyl methanesulfonate (EMS), CX-5461, camptothecin (CPT), and etoposide (ETOP). CPT and ETOP were dissolved in DMSO solution. *mus-81* mutant was used as a positive control in all experiments above. All experiments were conducted in at least three replicates. Error bars represent the standard error of the mean. P values were calculated using two-tailed student t test. The embryo survival rates of mutants treated with DDAs were all significantly from that of N2 treated with DDAs. * denotes p value less than 0.05, ** <0.01, ***<0.001.

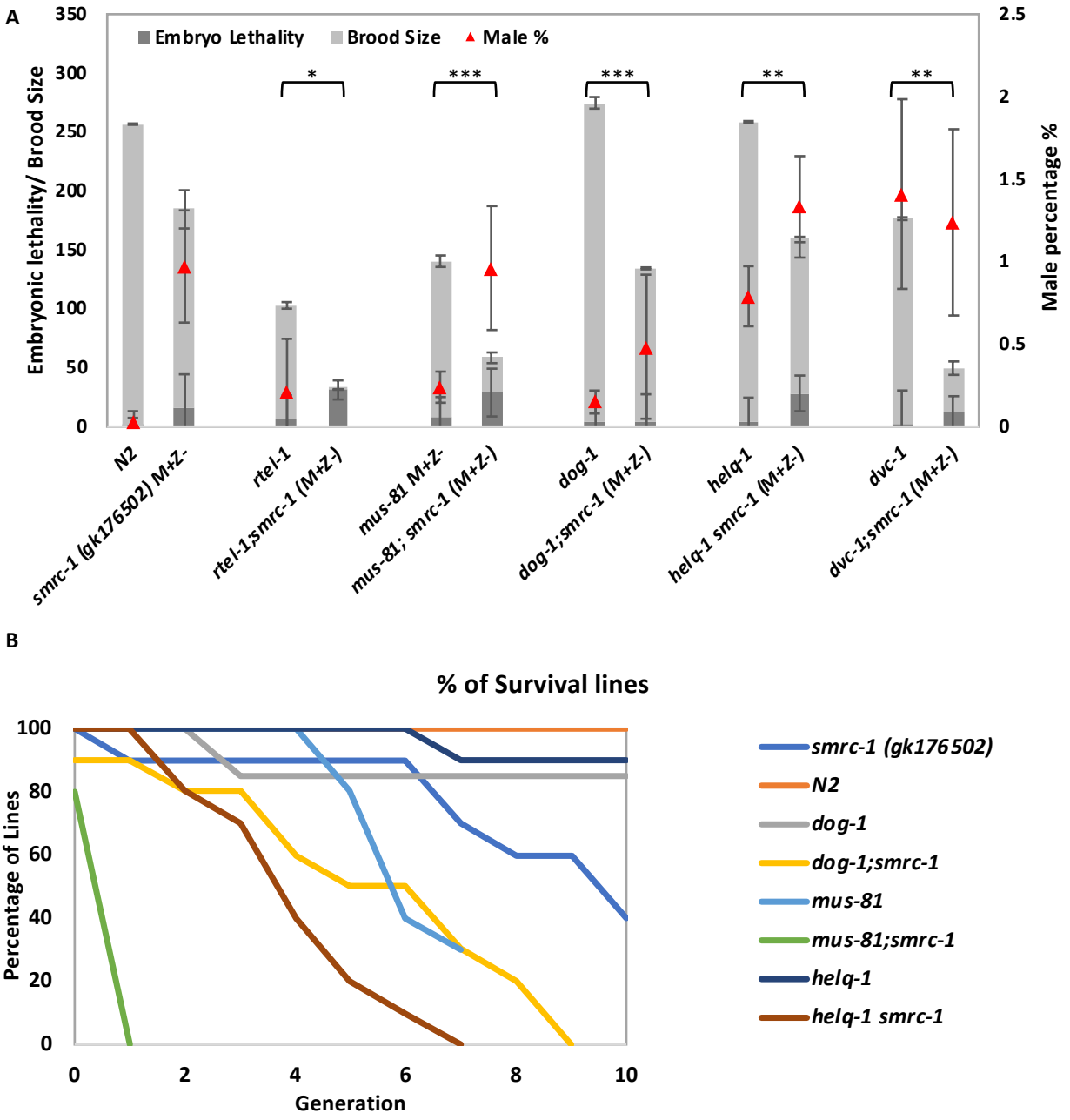
A
Embryo Lethality
Brood Size
Male %
Embryonic lethality/ Brood Size
Male percentage %
350
300
250
200
150
100
50
0
2.5
2
1.5
1
0.5
0
*
***
***
**
**
N2
smrc-1 (gk176502) M+Z-
rtel-1
rtel-1;smrc-1 (M+Z-)
mus-81 M+Z-
mus-81; smrc-1 (M+Z-)
dog-1
dog-1;smrc-1 (M+Z-)
helq-1
helq-1 smrc-1 (M+Z-)
dvc-1
dvc-1;smrc-1 (M+Z-)
B
% of Survival lines
Percentage of Lines
100
80
60
40
20
0
0
2
4
6
8
10
Generation
smrc-1 (gk176502)
N2
dog-1
dog-1;smrc-1
mus-81
mus-81;smrc-1
helq-1
helq-1 smrc-1

C

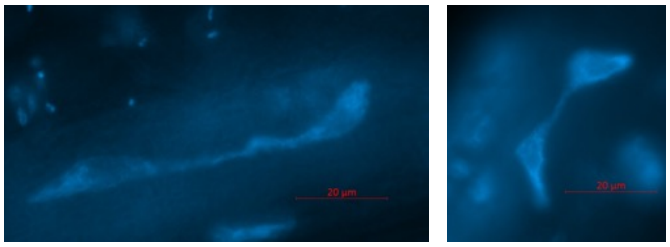

Chromatin bridges between intestinal cells in *rtel-1;smrc-1*

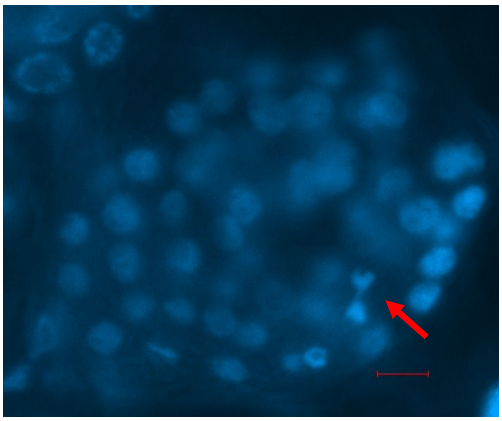

Chromatin bridges in early embryos in *rtel-1;smrc-1*

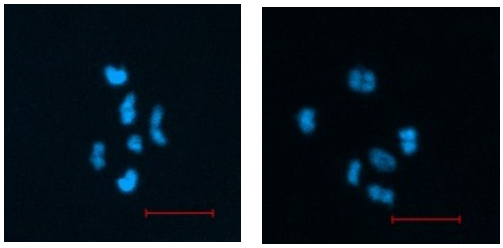

Diakinesis bodies in *rtel-1;smrc-1*

D

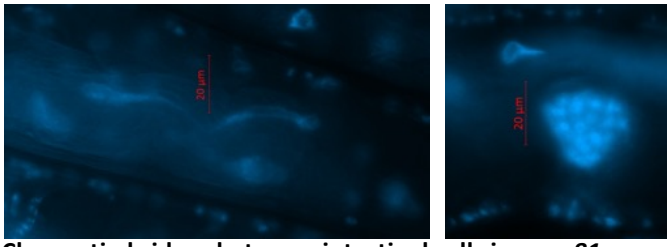

Chromatin bridges between intestinal cells in *mus-81;smrc-1*

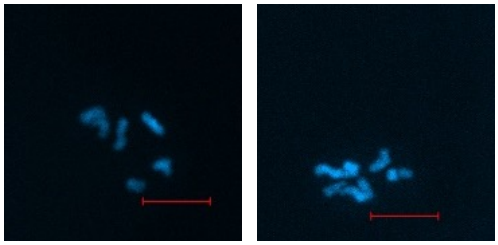

Diakinesis bodies in *mus-81;smrc-1*

Figure 5.3 Genetic interactions with loss of SMRC-1. (A) Brood size and embryonic lethality and male percentage single mutants, and *smrc-1(gk176502)*-containing double mutants. Student t tests were used to compare brood sizes between indicated animals. The brood size of *smrc-1(gk176502)* was significantly different from *rtel-1;smrc-1*(*), *mus-81;smrc-1*(**), and *dvc-1;smrc-1*(**). * denotes p value less than 0.05, ** <0.01, ***<0.001. Error bars represent the standard error of the mean. (B) Viability of independent lines of N2, *smrc-1, rtel-1*, *helq-1*, *dog-1* single mutants and *smrc-1*-containing double mutants at 23°C. (C) Representative images of somatic cells, early embryos and DAPI-stained diakinesis bodies of *rtel-1;smrc-1.* (D) Representative images of somatic cells and DAPI-stained diakinesis bodies of *mus-81;smrc-1* double mutants . Scale bar denotes 5 µm if not indicated.

Genotypes	Brood Size	Embryo Survival Rate %	Male %	n
N2	256.71±12.00	99.58±0.22	0.03±0.02	14
smrc-1 (gk176502) M+Z-	184.40±28.08	91.16±8.80	0.97±0.34	10
smrc-1 (gk784642) M+Z-	297.70±15.97	83.67±1.06	0.67±0.20	10
smrc-1 (gk176502) M-Z-	159.60±21.59	81.08±7.82	1.08±1.09	10
smrc-1 (gk784642) M-Z-	141.30±15.99	73.04±4.28	1.31±0.40	10
rtel-1	102.90±20.49	94.17±2.71	0.21±0.32	10
mus-81 (M+Z-)	140.40±17.78	94.80±3.47	0.24±0.09	10
helq-1	258.40±20.16	98.30±0.37	0.79±0.18	10
dog-1	274.80±12.47	98.44±1.78	0.15±0.07	20
dvc-1	176.50±27.84	98.41±0.68	1.41±0.57	10
rtel-1;smrc-1 (M+Z-)*	31.50±8.13	1.27±0.82	ND	10
mus-81; smrc-1 (M+Z-)*	58.40±20.29	50.51±7.78	0.96±0.38	10
helq-1 smrc-1 (M+Z-)*	158.80±15.13	82.24±1.44	1.33±0.31	10
dog-1;smrc-1 (M+Z-)*	134.30±23.31	96.95±0.63	0.48±0.44	10
dvc-1;smrc-1 (M+Z-)*	49.60±14.19	76.61±11.49	1.24±0.56	10

Table 5.1 Phenotypes of indicated mutants. n denotes the number of parent worms whose progeny were scored. All values are ± standard error of the mean. * indicates the *smrc-1* allele *gk176502*. M+Z-: maternally positive and zygotically negative. M-Z-: maternally negative and zygotically negative. ND: not determined.

CHAPTER 6: CONCLUSION

6.1 Anticancer drugs have complex, multimodal mechanisms of action.

The promise of genotype targeted anti-cancer therapies raises new challenges. Previously, anti-proliferative drugs targeting the hyper-proliferation of cancer cells were the front line of tumor treatment. Now, genome sequencing technologies are uncovering new actionable biomarkers in tumors, thereby facilitating the development of new highly selective therapeutics. This new wave of therapeutics requires extensive testing not only to assess efficacy but also to confirm their target specificity. It has been recently suggested that off-target toxicity could be the main mechanism of action for many new anticancer drugs undergoing clinical trial (Lin et al., 2019). The efficacy of these drugs was not affected even when their putative targets (genes) were knocked out (Lin et al., 2019). Therefore, understanding the mechanisms of action of new drugs is critical for the effective adoption of new anticancer therapeutics. Using the model metazoan *C. elegans,* we were able to characterize a new anticancer chemotherapeutic, CX-5461, in a whole live organism.

CX-5461 is an example of a therapeutic for which our understanding of the mechanism of action is evolving. CX-5461 was first identified as an RNA polymerase I inhibitor (Drygin et al., 2011). A more recent study showed that the mechanism of action was likely through stabilization of G-quadruplexes, a mechanism that could also account for the RNA polymerase I inhibition (Xu et al., 2017). It is probable that G4-stabilization at sites other than the rDNA-associated G4 was responsible for the selective killing of *BRCA*-deficient cancer cells, as the concentration of CX-5461 required to kill *BRCA*-deficient cells was not high enough to inhibit RNA polymerase I (Xu et al., 2017). Interestingly, a wide-range of breast cancer cells were sensitive to CX-5461, some

of which were *BRCA*-proficient (Xu et al., 2017), suggesting that a broader range of genotypes may be sensitive to CX-5461 treatment. This led us to test a panel of DNA replication and repair mutants to determine if CX-5461 sensitivity was linked to mutations associated with G4 repair. We also sequenced CX-5461-induced mutations to see if the mutations were at sites that could form G4 DNA structures. In light of our data (as discussed in Chapter 3), it is likely that the mechanism of action of CX-5461 extends beyond G4-stabilization, and may be due, at least in part, to DNA intercalation. CX-5461 could be similar to the anthracycline class of intercalating agents. Anthracyclines, such as daunorubicin and doxorubicin, intercalate into DNA, poison topoisomerases, generate reactive oxygen species, and form covalent DNA adducts (Kizek et al., 2012). Our data strongly supports a model in which CX-5461 intercalates into DNA, resulting in a range of lesions requiring several different repair pathways for tolerance.

The therapeutic mechanisms of action and efficacy can be affected by both genetic and environmental factors. Often the effect of environmental factors on therapeutic efficacy is overlooked. For example, the efficacy of some drugs can be affected by the consumption of grapefruit, which contains compounds that can increase the activity and expression of cytochrome P450 CYP1A1 and enhance drug metabolism and detoxification (Hahn-Obercyger et al., 2005). In the case of the antineoplastic ellipticine, P450 metabolism of ellipticine generates metabolites that can covalently bind DNA and result in nucleotide substitution mutations (Stiborova et al., 2004). The metabolism of drugs is primarily performed in the liver (Almazroo et al., 2017). P450-mediated drug metabolism in cell culture is variable depending on the cell line. The importance of P450-mediated metabolism in analyzing DNA damaging agents was demonstrated in a recent study, which showed that some compounds, including ellipticine, were

only mutagenic after metabolism by rat liver extracts (Kucab et al., 2019). *C. elegans* is remarkably efficient in P450-mediated metabolism of compounds, and this process is similar to that observed in the human liver (Harlow et al., 2018). It is possible that testing the effects of drugs in *C. elegans* would also test the effect of drug metabolites, a capacity that would not be available in cultured mammalian cell lines. This could explain differences in CX-5461 genotypic sensitivities observed between human cell lines and *C. elegans* (Xu et al., 2017). Other environmental factors such as sunlight can also play a role affecting the drug efficacy. The CX-5461 clinical trial resulted in some cases of photosensitivity (Hilton et al., 2018; Khot et al., 2019). We used *C. elegans* to show that UVA potentiates CX-5461 toxicity by generating ROS (Figure 3.4 and 3.5).

To summarize, mechanisms of action for anticancer therapeutics can be complex and dependent on physiological and environmental factors, such as light and diet. Therefore, it is imperative to use *in vivo* platforms to identify the targeted biological processes and to assess the efficacy and off-target effects. We have demonstrated that *C. elegans* is a powerful tool with which to investigate the effects of chemotherapeutics in an *in vivo* model organism.

6.2 *C. elegans* is a good platform with which to study factors affecting genome stability

Maintaining genome integrity is essential for all organisms and the processes that maintain genome stability tend to be evolutionarily conserved. While not all components are conserved at the gene level, the overall repair processes are conserved. For example, the Fanconi anemia (FA) pathway, which repairs interstrand crosslinks (ICLs), is only partially conserved between humans and *C. elegans* at the protein level. However, mutation of FA pathway genes sensitizes

C. elegans specifically to ICL agents (Figure 2.2), in a similar fashion as the human counterpart (Deans and West, 2011). Although the *C. elegans* FA pathway contains fewer components than the human FA pathway, it could represent the minimal requirements for functional ICL repair and simplify the study of the core FA repair processes (Youds et al., 2009). This is also true for other DNA repair pathways in *C. elegans*. *C. elegans* has fewer RecQ helicases, PARPs, homologous recombination proteins, and annealing helicases. The smaller number of repair genes in *C. elegans* makes it easier to investigate the role of specific genes in response to anticancer therapeutics and to dissect the interplay between repair pathways. *C. elegans* provides a simplified *in vivo* platform for studying human diseases such as cancer.

The simpler DNA replication and repair pathways in *C. elegans* make it a great model in studying the biology of genes involved in genome maintenance. SMRC-1 is the only annealing helicase known in *C. elegans*, making it a simple model to investigate the role of annealing helicases. Loss of SMRC-1 has been shown to induce genome instability. Examination of the genome from late generation *smrc-1* mutants revealed many small CNVs (Figure 5.1B & Figure A5.2). Despite that, the *smrc-1* mutants were still viable at F_{10}, indicating that these chromosomal duplications or deletions may be the byproducts of repair or bypass pathways that are needed in the absence of SMRC-1 for survival.

The simpler DNA repair pathways in *C. elegans* also benefit the dissection of interplay between different repair proteins. This thesis has illustrated the overlapping and competing roles of different repair mechanisms using *C. elegans*. For instance, MMEJ repair pathway can act as an alternate repair mechanism to repair DNA lesions that are normally repaired by HDR (Figure

4.9). Even within the HDR repair pathway, there are many proteins that show functional redundancy. In HDR-compromised mutants (such as *helq-1*), improper NHEJ activity could occur and lead to genome destabilizing effects. Such scenarios are common in a tumor, that the redundancies and alleviation in different repair mechanisms could allow a tumor to survive and evolve through accumulating more mutations that favor survival, making anticancer treatment more complicated (Nickoloff et al., 2017).

In addition to the advantages of a simpler repertoire of DNA damage response genes, there is a suite of tools and phenotypic readouts in *C. elegans* that can be exploited to query the effects of genome stability. For instance, brood size, embryo viability, and the frequency of spontaneous males can be used to assess whether a gene mutation leads to genome instability. The well characterized development of *C. elegans* allows one to study the effects of genome instability in different tissue types or under different growth conditions. For example, the quantitative acute assay measures the effect of genome instability in embryos, which undergo rapid division and contain no DNA damage checkpoints, whereas the L1 exposure assay measures genome instability affecting post-embryonic somatic cell development and can be used to determine if a DNA damaging agent affects transcription (Astin et al., 2008). In addition, the *C. elegans* germline nuclei are arranged in a spatio-temporal gradient in which sequential meiotic stages are easily differentiated, making *C. elegans* a great platform to investigate meiotic events, such as meiotic DSB repair (Lui and Colaiacovo, 2013). Genetic balancers in *C. elegans* provide tools with which to measure the mutagenicity of the factors of interest (Rosenbluth et al., 1983) and allow for the capture and stable propagation of induced mutations, which is necessary for whole genome sequencing to delineate mutational signatures (Edgley et al., 2006).

In this thesis, we have demonstrated how *C. elegans* can be exploited to investigate the phenotypic effects of internal and external factors that affect genome stability. One could use the same strategies that we used to characterize CX-5461 in *C. elegans* to study other genome-destabilizing agents, whether they are chemical agents or anticancer therapeutics. We have also generated a chemi-genetic interaction map that is a useful reference for the study of new DNA damaging agents or DNA repair mutants. By generating and comparing the genotypic sensitivity profile of the agent of interest, it is possible to form a hypothesis on the mechanism of action of the agent.

In summary, the emergence of sequencing technology has revolutionized our understanding of cancer and is changing how cancer is treated. An explosion of tumor sequencing has identified tumor-specific genetic variations that can be exploited for treatment. High-throughput screens in model organisms and cancer cell lines are elucidating the connections between mutations and therapeutic targets at an amazing pace. Now the main challenge for personalized medicine is to link the genetic alterations and therapeutic agents, as well as to untangle their interplay between the constellation of mutations found in tumors and their effect on therapeutic efficacy. Here, *C. elegans* provides a sophisticated model to investigate the complex interactions between the genes, environmental factors, and anticancer therapeutic agents.

Reference list

Adachi, N., So, S., and Koyama, H. (2004). Loss of nonhomologous end joining confers camptothecin resistance in DT40 cells. Implications for the repair of topoisomerase I-mediated DNA damage. J Biol Chem *279*, 37343-37348.

Adamo, A., Montemauri, P., Silva, N., Ward, J.D., Boulton, S.J., and La Volpe, A. (2008). BRC-1 acts in the inter-sister pathway of meiotic double-strand break repair. EMBO Rep *9*, 287-292.

Adelman, C.A., Lolo, R.L., Birkbak, N.J., Murina, O., Matsuzaki, K., Horejsi, Z., Parmar, K., Borel, V., Skehel, J.M., Stamp, G.*, et al.* (2013). HELQ promotes RAD51 paralogue-dependent repair to avert germ cell loss and tumorigenesis. Nature *502*, 381-384.

Aguilera, A., and Garcia-Muse, T. (2013). Causes of genome instability. Annu Rev Genet *47*, 1-32.

Ahmed, S., and Hodgkin, J. (2000). MRT-2 checkpoint protein is required for germline immortality and telomere replication in C. elegans. Nature *403*, 159-164.

Alexandrov, L.B., Nik-Zainal, S., Wedge, D.C., Aparicio, S.A., Behjati, S., Biankin, A.V., Bignell, G.R., Bolli, N., Borg, A., Borresen-Dale, A.L.*, et al.* (2013). Signatures of mutational processes in human cancer. Nature *500*, 415-421.

Allan, J.M., and Travis, L.B. (2005). Mechanisms of therapy-related carcinogenesis. Nat Rev Cancer *5*, 943-955.

Almazroo, O.A., Miah, M.K., and Venkataramanan, R. (2017). Drug Metabolism in the Liver. Clin Liver Dis *21*, 1-20.

Alpi, A., Pasierbek, P., Gartner, A., and Loidl, J. (2003). Genetic and cytological characterization of the recombination protein RAD-51 in Caenorhabditis elegans. Chromosoma *112*, 6-16.

Amendola, P.G., Zaghet, N., Ramalho, J.J., Vilstrup Johansen, J., Boxem, M., and Salcini, A.E. (2017). JMJD-5/KDM8 regulates H3K36me2 and is required for late steps of homologous recombination and genome integrity. PLoS Genet *13*, e1006632.

Ames, B.N., Lee, F.D., and Durston, W.E. (1973). An improved bacterial test system for the detection and classification of mutagens and carcinogens. Proc Natl Acad Sci U S A *70*, 782-786.

Andor, N., Maley, C.C., and Ji, H.P. (2017). Genomic Instability in Cancer: Teetering on the Limit of Tolerance. Cancer Res *77*, 2179-2185.

Andrews, W.J., Panova, T., Normand, C., Gadal, O., Tikhonova, I.G., and Panov, K.I. (2013). Old drug, new target: ellipticines selectively inhibit RNA polymerase I transcription. J Biol Chem *288*, 4567-4582.

Arlt, V.M., Stiborova, M., and Schmeiser, H.H. (2002). Aristolochic acid as a probable human cancer hazard in herbal remedies: a review. Mutagenesis *17*, 265-277.

Astin, J.W., O'Neil, N.J., and Kuwabara, P.E. (2008). Nucleotide excision repair and the degradation of RNA pol II by the Caenorhabditis elegans XPA and Rsp5 orthologues, RAD-3 and WWP-1. DNA Repair (Amst) *7*, 267-280.

Bailey, M.L., O'Neil, N.J., van Pel, D.M., Solomon, D.A., Waldman, T., and Hieter, P. (2014). Glioblastoma cells containing mutations in the cohesin component STAG2 are sensitive to PARP inhibition. Mol Cancer Ther *13*, 724-732.

Balmus, G., Pilger, D., Coates, J., Demir, M., Sczaniecka-Clift, M., Barros, A.C., Woods, M., Fu, B., Yang, F., Chen, E.*, et al.* (2019). ATM orchestrates the DNA-damage response to counter toxic non-homologous end-joining at broken replication forks. Nature communications *10*, 87.

Banerjee, S.M., MacRobert, A.J., Mosse, C.A., Periera, B., Bown, S.G., and Keshtgar, M.R.S. (2017). Photodynamic therapy: Inception to application in breast cancer. Breast (Edinburgh, Scotland) *31*, 105-113.

Bansbach, C.E., Betous, R., Lovejoy, C.A., Glick, G.G., and Cortez, D. (2009). The annealing helicase SMARCAL1 maintains genome integrity at stalled replication forks. Genes Dev *23*, 2405-2414.

Barber, L.J., Youds, J.L., Ward, J.D., McIlwraith, M.J., O'Neil, N.J., Petalcorin, M.I., Martin, J.S., Collis, S.J., Cantor, S.B., Auclair, M.*, et al.* (2008). RTEL1 maintains genomic stability by suppressing homologous recombination. Cell *135*, 261-271.

Barretina, J., Caponigro, G., Stransky, N., Venkatesan, K., Margolin, A.A., Kim, S., Wilson, C.J., Lehar, J., Kryukov, G.V., Sonkin, D.*, et al.* (2012). The Cancer Cell Line Encyclopedia enables predictive modelling of anticancer drug sensitivity. Nature *483*, 603-607.

Basu, A., Bodycombe, N.E., Cheah, J.H., Price, E.V., Liu, K., Schaefer, G.I., Ebright, R.Y., Stewart, M.L., Ito, D., Wang, S.*, et al.* (2013). An interactive resource to identify cancer genetic and lineage dependencies targeted by small molecules. Cell *154*, 1151-1161.

Betous, R., Mason, A.C., Rambo, R.P., Bansbach, C.E., Badu-Nkansah, A., Sirbu, B.M., Eichman, B.F., and Cortez, D. (2012). SMARCAL1 catalyzes fork regression and Holliday junction migration to maintain genome stability during DNA replication. Genes Dev *26*, 151-162.

Blackford, A.N., and Jackson, S.P. (2017). ATM, ATR, and DNA-PK: The Trinity at the Heart of the DNA Damage Response. Mol Cell *66*, 801-817.

Boerkoel, C.F., Takashima, H., John, J., Yan, J., Stankiewicz, P., Rosenbarker, L., André, J.-L., Bogdanovic, R., Burguet, A., Cockfield, S.*, et al.* (2002). Mutant chromatin remodeling protein SMARCAL1 causes Schimke immuno-osseous dysplasia. Nat Genet *30*, 215-220.

Boulton, S.J., Martin, J.S., Polanowska, J., Hill, D.E., Gartner, A., and Vidal, M. (2004). BRCA1/BARD1 Orthologs Required for DNA Repair in Caenorhabditis elegans. Curr Biol *14*, 33-39.

Bouwman, P., Aly, A., Escandell, J.M., Pieterse, M., Bartkova, J., van der Gulden, H., Hiddingh, S., Thanasoula, M., Kulkarni, A., Yang, Q.*, et al.* (2010). 53BP1 loss rescues BRCA1 deficiency and is associated with triple-negative and BRCA-mutated breast cancers. Nat Struct Mol Biol *17*, 688-695.

Brenner, S. (1974). The genetics of Caenorhabditis elegans. Genetics *77*, 71-94.

Bridge, W.L., Vandenberg, C.J., Franklin, R.J., and Hiom, K. (2005). The BRIP1 helicase functions independently of BRCA1 in the Fanconi anemia pathway for DNA crosslink repair. Nat Genet *37*, 953-957.

Bunting, S.F., Callen, E., Kozak, M.L., Kim, J.M., Wong, N., Lopez-Contreras, A.J., Ludwig, T., Baer, R., Faryabi, R.B., Malhowski, A.*, et al.* (2012). BRCA1 functions independently of homologous recombination in DNA interstrand crosslink repair. Mol Cell *46*, 125-135.

Bunting, S.F., Callen, E., Wong, N., Chen, H.T., Polato, F., Gunn, A., Bothmer, A., Feldhahn, N., Fernandez-Capetillo, O., Cao, L.*, et al.* (2010). 53BP1 inhibits homologous recombination in Brca1-deficient cells by blocking resection of DNA breaks. Cell *141*, 243-254.

Cadet, J., Sage, E., and Douki, T. (2005). Ultraviolet radiation-mediated damage to cellular DNA. Mutat Res *571*, 3-17.

Canals, A., Purciolas, M., Aymami, J., and Coll, M. (2005). The anticancer agent ellipticine unwinds DNA by intercalative binding in an orientation parallel to base pairs. Acta Crystallogr D Biol Crystallogr *61*, 1009-1012.

Ceccaldi, R., Rondinelli, B., and D'Andrea, A.D. (2016a). Repair Pathway Choices and Consequences at the Double-Strand Break. Trends Cell Biol *26*, 52-64.

Ceccaldi, R., Sarangi, P., and D'Andrea, A.D. (2016b). The Fanconi anaemia pathway: new players and new functions. Nat Rev Mol Cell Biol *17*, 337-349.

Chan, D.A., and Giaccia, A.J. (2011). Harnessing synthetic lethal interactions in anticancer drug discovery. Nat Rev Drug Discov *10*, 351-364.

Chang, M., Bellaoui, M., Boone, C., and Brown, G.W. (2002). A genome-wide screen for methyl methanesulfonate-sensitive mutants reveals genes required for S phase progression in the presence of DNA damage. Proceedings of the National Academy of Sciences *99*, 16934-16939.

Chen, L., Nievera, C.J., Lee, A.Y., and Wu, X. (2008). Cell cycle-dependent complex formation of BRCA1.CtIP.MRN is important for DNA double-strand break repair. J Biol Chem *283*, 7713-7720.

Cheung, I., Schertzer, M., Rose, A., and Lansdorp, P.M. (2002). Disruption of dog-1 in Caenorhabditis elegans triggers deletions upstream of guanine-rich DNA. Nat Genet *31*, 405-409.

Cheung-Ong, K., Giaever, G., and Nislow, C. (2013). DNA-damaging agents in cancer chemotherapy: serendipity and chemical biology. Chem Biol *20*, 648-659.

Ciccia, A., Bredemeyer, A.L., Sowa, M.E., Terret, M.E., Jallepalli, P.V., Harper, J.W., and Elledge, S.J. (2009). The SIOD disorder protein SMARCAL1 is an RPA-interacting protein involved in replication fork restart. Genes Dev *23*, 2415-2425.

Ciccia, A., and Elledge, S.J. (2010). The DNA damage response: making it safe to play with knives. Mol Cell *40*, 179-204.

Clejan, I., Boerckel, J., and Ahmed, S. (2006). Developmental modulation of nonhomologous end joining in Caenorhabditis elegans. Genetics *173*, 1301-1317.

Colaiácovo, M.P., MacQueen, A.J., Martinez-Perez, E., McDonald, K., Adamo, A., La Volpe, A., and Villeneuve, A.M. (2003). Synaptonemal Complex Assembly in C. elegans Is Dispensable for Loading Strand-Exchange Proteins but Critical for Proper Completion of Recombination. Dev Cell *5*, 463-474.

Consortium, T.C.e.D.M. (2012). large-scale screening for targeted knockouts in the Caenorhabditis elegans genome. G3 (Bethesda, Md) *2*, 1415-1425.

Corsi, A.K., Wightman, B., and Chalfie, M. (2015). A Transparent Window into Biology: A Primer on Caenorhabditis elegans. Genetics *200*, 387-407.

Craig, A.L., Moser, S.C., Bailly, A.P., and Gartner, A. (2012). Methods for studying the DNA damage response in the Caenorhabdatis elegans germ line. Methods Cell Biol *107*, 321-352.

Dai, C.H., Chen, P., Li, J., Lan, T., Chen, Y.C., Qian, H., Chen, K., and Li, M.Y. (2016). Co-inhibition of pol theta and HR genes efficiently synergize with cisplatin to suppress cisplatin-resistant lung cancer cells survival. Oncotarget *7*, 65157-65170.

de Guidi, G., Bracchitta, G., and Catalfo, A. (2011). Photosensitization reactions of fluoroquinolones and their biological consequences. Photochem Photobiol *87*, 1214-1229.

Deans, A.J., and West, S.C. (2011). DNA interstrand crosslink repair and cancer. Nat Rev Cancer *11*, 467-480.

Degtyareva, N.P., Greenwell, P., Hofmann, E.R., Hengartner, M.O., Zhang, L., Culotti, J.G., and Petes, T.D. (2002). Caenorhabditis elegans DNA mismatch repair gene msh-2 is required for microsatellite stability and maintenance of genome integrity. Proc Natl Acad Sci U S A *99*, 2158-2163.

Deguchi, K., Clewing, J.M., Elizondo, L.I., Hirano, R., Huang, C., Choi, K., Sloan, E.A., Lucke, T., Marwedel, K.M., Powell, R.D., Jr*., et al.* (2008). Neurologic phenotype of Schimke immuno-

osseous dysplasia and neurodevelopmental expression of SMARCAL1. J Neuropathol Exp Neurol *67*, 565-577.

Densham, R.M., Garvin, A.J., Stone, H.R., Strachan, J., Baldock, R.A., Daza-Martin, M., Fletcher, A., Blair-Reid, S., Beesley, J., Johal, B.*, et al.* (2016). Human BRCA1-BARD1 ubiquitin ligase activity counteracts chromatin barriers to DNA resection. Nat Struct Mol Biol *23*, 647-655.

Denver, D.R., Feinberg, S., Estes, S., Thomas, W.K., and Lynch, M. (2005). Mutation rates, spectra and hotspots in mismatch repair-deficient Caenorhabditis elegans. Genetics *170*, 107-113.

Deriano, L., and Roth, D.B. (2013). Modernizing the nonhomologous end-joining repertoire: alternative and classical NHEJ share the stage. Annu Rev Genet *47*, 433-455.

Dernburg, A.F., McDonald, K., Moulder, G., Barstead, R., Dresser, M., and Villeneuve, A.M. (1998). Meiotic recombination in C. elegans initiates by a conserved mechanism and is dispensable for homologous chromosome synapsis. Cell *94*, 387-398.

Dhapola, P., and Chowdhury, S. (2016). QuadBase2: web server for multiplexed guanine quadruplex mining and visualization. Nucleic Acids Res *44*, W277-283.

Drygin, D., Lin, A., Bliesath, J., Ho, C.B., O'Brien, S.E., Proffitt, C., Omori, M., Haddach, M., Schwaebe, M.K., Siddiqui-Jain, A.*, et al.* (2011). Targeting RNA polymerase I with an oral small molecule CX-5461 inhibits ribosomal RNA synthesis and solid tumor growth. Cancer Res *71*, 1418-1430.

Duda, H., Arter, M., Gloggnitzer, J., Teloni, F., Wild, P., Blanco, M.G., Altmeyer, M., and Matos, J. (2016). A Mechanism for Controlled Breakage of Under-replicated Chromosomes during Mitosis. Dev Cell *39*, 740-755.

Duffy, S., Fam, H.K., Wang, Y.K., Styles, E.B., Kim, J.H., Ang, J.S., Singh, T., Larionov, V., Shah, S.P., Andrews, B.*, et al.* (2016). Overexpression screens identify conserved dosage chromosome instability genes in yeast and human cancer. Proc Natl Acad Sci U S A *113*, 9967-9976.

Edgley, M.L., Baillie, D.L., Riddle, D.L., and Rose, A.M. (2006). Genetic balancers. WormBook, 1-32.

Elango, R., Sheng, Z., Jackson, J., DeCata, J., Ibrahim, Y., Pham, N.T., Liang, D.H., Sakofsky, C.J., Vindigni, A., Lobachev, K.S.*, et al.* (2017). Break-induced replication promotes formation of lethal joint molecules dissolved by Srs2. Nature communications *8*, 1790.

Fedier, A., Schlamminger, M., Schwarz, V.A., Haller, U., Howell, S.B., and Fink, D. (2003). Loss of atm sensitises p53-deficient cells to topoisomerase poisons and antimetabolites. Ann Oncol *14*, 938-945.

Fong, P.C., Boss, D.S., Yap, T.A., Tutt, A., Wu, P., Mergui-Roelvink, M., Mortimer, P., Swaisland, H., Lau, A., O'Connor, M.J*., et al.* (2009). Inhibition of poly(ADP-ribose) polymerase in tumors from BRCA mutation carriers. N Engl J Med *361*, 123-134.

Friedberg, E.C., Lehmann, A.R., and Fuchs, R.P. (2005). Trading places: how do DNA polymerases switch during translesion DNA synthesis? Mol Cell *18*, 499-505.

Futami, K., Ogasawara, S., Goto, H., Yano, H., and Furuichi, Y. (2010). RecQL1 DNA repair helicase: A potential tumor marker and therapeutic target against hepatocellular carcinoma. Int J Mol Med *25*, 537-545.

Futreal, P.A., Liu, Q., Shattuck-Eidens, D., Cochran, C., Harshman, K., Tavtigian, S., Bennett, L.M., Haugen-Strano, A., Swensen, J., Miki, Y*., et al.* (1994). BRCA1 mutations in primary breast and ovarian carcinomas. Science *266*, 120-122.

Garcia-Muse, T., and Boulton, S.J. (2005). Distinct modes of ATR activation after replication stress and DNA double-strand breaks in Caenorhabditis elegans. EMBO J *24*, 4345-4355.

Garnett, M.J., Edelman, E.J., Heidorn, S.J., Greenman, C.D., Dastur, A., Lau, K.W., Greninger, P., Thompson, I.R., Luo, X., Soares, J*., et al.* (2012). Systematic identification of genomic markers of drug sensitivity in cancer cells. Nature *483*, 570-575.

Ghosal, G., Leung, J.W., Nair, B.C., Fong, K.W., and Chen, J. (2012). Proliferating cell nuclear antigen (PCNA)-binding protein C1orf124 is a regulator of translesion synthesis. J Biol Chem *287*, 34225-34233.

Gilbert, E.S., Stovall, M., Gospodarowicz, M., Van Leeuwen, F.E., Andersson, M., Glimelius, B., Joensuu, T., Lynch, C.F., Curtis, R.E., Holowaty, E*., et al.* (2003). Lung cancer after treatment for Hodgkin's disease: focus on radiation effects. Radiat Res *159*, 161-173.

Girard, C., Roelens, B., Zawadzki, K.A., and Villeneuve, A.M. (2018). Interdependent and separable functions of Caenorhabditis elegans MRN-C complex members couple formation and repair of meiotic DSBs. Proc Natl Acad Sci U S A *115*, E4443-E4452.

Goldstein, B. (2016). Sydney Brenner on the Genetics of Caenorhabditis elegans. Genetics *204*, 1-2.

Gordon, D.J., Resio, B., and Pellman, D. (2012). Causes and consequences of aneuploidy in cancer. Nat Rev Genet *13*, 189-203.

Gupta, R., Somyajit, K., Narita, T., Maskey, E., Stanlie, A., Kremer, M., Typas, D., Lammers, M., Mailand, N., Nussenzweig, A*., et al.* (2018). DNA Repair Network Analysis Reveals Shieldin as a Key Regulator of NHEJ and PARP Inhibitor Sensitivity. Cell *173*, 972-988 e923.

Haddach, M., Schwaebe, M.K., Michaux, J., Nagasawa, J., O'Brien, S.E., Whitten, J.P., Pierre, F., Kerdoncuff, P., Darjania, L., Stansfield, R*., et al.* (2012). Discovery of CX-5461, the First Direct and Selective Inhibitor of RNA Polymerase I, for Cancer Therapeutics. ACS Med Chem Lett *3*, 602-606.

Hahn-Obercyger, M., Stark, A.H., and Madar, Z. (2005). Grapefruit and oroblanco enhance hepatic detoxification enzymes in rats: possible role in protection against chemical carcinogenesis. J Agric Food Chem *53*, 1828-1832.

Hakem, R., de la Pompa, J.L., Sirard, C., Mo, R., Woo, M., Hakem, A., Wakeham, A., Potter, J., Reitmair, A., Billia, F.*, et al.* (1996). The tumor suppressor gene Brca1 is required for embryonic cellular proliferation in the mouse. Cell *85*, 1009-1023.

Han, X., Zhao, L., and Li, X. (2016). HELQ in cancer and reproduction. Neoplasma *63*, 825-835.

Hanada, K., Budzowska, M., Davies, S.L., van Drunen, E., Onizawa, H., Beverloo, H.B., Maas, A., Essers, J., Hickson, I.D., and Kanaar, R. (2007). The structure-specific endonuclease Mus81 contributes to replication restart by generating double-strand DNA breaks. Nat Struct Mol Biol *14*, 1096-1104.

Hanahan, D., and Weinberg, R.A. (2011). Hallmarks of cancer: the next generation. Cell *144*, 646-674.

Hannan, M.A., Hellani, A., Al-Khodairy, F.M., Kunhi, M., Siddiqui, Y., Al-Yussef, N., Pangue-Cruz, N., Siewertsen, M., Al-Ahdal, M.N., and Aboussekhra, A. (2002). Deficiency in the repair of UV-induced DNA damage in human skin fibroblasts compromised for the ATM gene. Carcinogenesis *23*, 1617-1624.

Hanway, D., Chin, J.K., Xia, G., Oshiro, G., Winzeler, E.A., and Romesberg, F.E. (2002). Previously uncharacterized genes in the UV- and MMS-induced DNA damage response in yeast. Proceedings of the National Academy of Sciences *99*, 10605-10610.

Harlow, P.H., Perry, S.J., Stevens, A.J., and Flemming, A.J. (2018). Comparative metabolism of xenobiotic chemicals by cytochrome P450s in the nematode Caenorhabditis elegans. Sci Rep *8*, 13333.

Harris, K., and Nielsen, R. (2014). Error-prone polymerase activity causes multinucleotide mutations in humans. Genome Res *24*, 1445-1454.

Hart, T., Chandrashekhar, M., Aregger, M., Steinhart, Z., Brown, K.R., MacLeod, G., Mis, M., Zimmermann, M., Fradet-Turcotte, A., Sun, S.*, et al.* (2015). High-Resolution CRISPR Screens Reveal Fitness Genes and Genotype-Specific Cancer Liabilities. Cell *163*, 1515-1526.

Hashimoto, K., Bonala, R., Johnson, F., Grollman, A.P., and Moriya, M. (2016). Y-family DNA polymerase-independent gap-filling translesion synthesis across aristolochic acid-derived adenine adducts in mouse cells. DNA Repair (Amst) *46*, 55-60.

Helleday, T. (2010). Homologous recombination in cancer development, treatment and development of drug resistance. Carcinogenesis *31*, 955-960.

Helleday, T., Petermann, E., Lundin, C., Hodgson, B., and Sharma, R.A. (2008). DNA repair pathways as targets for cancer therapy. Nat Rev Cancer *8*, 193-204.

Higgins, G.S., Harris, A.L., Prevo, R., Helleday, T., McKenna, W.G., and Buffa, F.M. (2010). Overexpression of POLQ confers a poor prognosis in early breast cancer patients. Oncotarget *1*, 175-184.

Hillers, K.J., Jantsch, V., Martinez-Perez, E., and Yanowitz, J.L. (2017). Meiosis. WormBook *2017*, 1-43.

Hilton, J., Cescon, D.W., Bedard, P., Tu, D., Ritter, H., Soong, J., Gelmon, K., Aparicio, S., and Seymour, L. (2018). 44OCCTG IND.231: A phase 1 trial evaluating CX-5461 in patients with advanced solid tumors. Ann Oncol *29*.

Hoang, M.L., Chen, C.H., Sidorenko, V.S., He, J., Dickman, K.G., Yun, B.H., Moriya, M., Niknafs, N., Douville, C., Karchin, R.*, et al.* (2013). Mutational signature of aristolochic acid exposure as revealed by whole-exome sequencing. Sci Transl Med *5*, 197ra102.

Holway, A.H., Kim, S.H., La Volpe, A., and Michael, W.M. (2006). Checkpoint silencing during the DNA damage response in Caenorhabditis elegans embryos. J Cell Biol *172*, 999-1008.

Hopkins, T.A., Shi, Y., Rodriguez, L.E., Solomon, L.R., Donawho, C.K., DiGiammarino, E.L., Panchal, S.C., Wilsbacher, J.L., Gao, W., Olson, A.M.*, et al.* (2015). Mechanistic Dissection of PARP1 Trapping and the Impact on In Vivo Tolerability and Efficacy of PARP Inhibitors. Mol Cancer Res *13*, 1465-1477.

Huang, Y., and Li, L. (2013). DNA crosslinking damage and cancer - a tale of friend and foe. Translational cancer research *2*, 144-154.

Hustedt, N., and Durocher, D. (2016). The control of DNA repair by the cell cycle. Nat Cell Biol *19*, 1-9.

Hyman, D.M., Taylor, B.S., and Baselga, J. (2017). Implementing Genome-Driven Oncology. Cell *168*, 584-599.

Itani, O.A., Flibotte, S., Dumas, K.J., Moerman, D.G., and Hu, P.J. (2015). Chromoanasynthetic Genomic Rearrangement Identified in a N-Ethyl-N-Nitrosourea (ENU) Mutagenesis Screen in Caenorhabditis elegans. G3 (Bethesda, Md) *6*, 351-356.

Jacob, S., Aguado, M., Fallik, D., and Praz, F. (2001). The role of the DNA mismatch repair system in the cytotoxicity of the topoisomerase inhibitors camptothecin and etoposide to human colorectal cancer cells. Cancer Res *61*, 6555-6562.

Janisiw, E., Dello Stritto, M.R., Jantsch, V., and Silva, N. (2018). BRCA1-BARD1 associate with the synaptonemal complex and pro-crossover factors and influence RAD-51 dynamics during Caenorhabditis elegans meiosis. PLoS Genet *14*, e1007653.

Jeggo, P.A., Pearl, L.H., and Carr, A.M. (2016). DNA repair, genome stability and cancer: a historical perspective. Nat Rev Cancer *16*, 35-42.

Johnson, G.E. (2012). Mammalian cell HPRT gene mutation assay: test methods. Methods Mol Biol *817*, 55-67.

Johnstone, I.L. (1994). The cuticle of the nematode Caenorhabditis elegans: a complex collagen structure. Bioessays *16*, 171-178.

Jones, M.R., Huang, J.C., Chua, S.Y., Baillie, D.L., and Rose, A.M. (2012). The atm-1 gene is required for genome stability in Caenorhabditis elegans. Mol Genet Genomics *287*, 325-335.

Kavanaugh, G., Ye, F., Mohni, K.N., Luzwick, J.W., Glick, G., and Cortez, D. (2015). A whole genome RNAi screen identifies replication stress response genes. DNA Repair (Amst) *35*, 55-62.

Khot, A., Brajanovski, N., Cameron, D.P., Hein, N., Maclachlan, K.H., Sanij, E., Lim, J., Soong, J., Link, E., Blombery, P.*, et al.* (2019). First-in-Human RNA Polymerase I Transcription Inhibitor CX-5461 in Patients with Advanced Hematologic Cancers: Results of a Phase I Dose-Escalation Study. Cancer Discov *9*, 1036-1049.

Kim, J.Y., Lee, S.G., Chung, J.Y., Kim, Y.J., Park, J.E., Koh, H., Han, M.S., Park, Y.C., Yoo, Y.H., and Kim, J.M. (2011). Ellipticine induces apoptosis in human endometrial cancer cells: the potential involvement of reactive oxygen species and mitogen-activated protein kinases. Toxicology *289*, 91-102.

King, M.C., Marks, J.H., and Mandell, J.B. (2003). Breast and ovarian cancer risks due to inherited mutations in BRCA1 and BRCA2. Science *302*, 643-646.

Kizek, R., Adam, V., Hrabeta, J., Eckschlager, T., Smutny, S., Burda, J.V., Frei, E., and Stiborova, M. (2012). Anthracyclines and ellipticines as DNA-damaging anticancer drugs: recent advances. Pharmacol Ther *133*, 26-39.

Kong, N., Ng, W., Thao, K., Agulto, R., Weis, A., Kim, K.S., Korlach, J., Hickey, L., Kelly, L., Lappin, S.*, et al.* (2017). Automation of PacBio SMRTbell NGS library preparation for bacterial genome sequencing. Standards in genomic sciences *12*, 27.

Koole, W., van Schendel, R., Karambelas, A.E., van Heteren, J.T., Okihara, K.L., and Tijsterman, M. (2014). A Polymerase Theta-dependent repair pathway suppresses extensive genomic instability at endogenous G4 DNA sites. Nature communications *5*, 3216.

Kucab, J.E., Zou, X., Morganella, S., Joel, M., Nanda, A.S., Nagy, E., Gomez, C., Degasperi, A., Harris, R., Jackson, S.P.*, et al.* (2019). A Compendium of Mutational Signatures of Environmental Agents. Cell.

Kunkel, T.A., and Erie, D.A. (2015). Eukaryotic Mismatch Repair in Relation to DNA Replication. Annu Rev Genet *49*, 291-313.

Laskin, J., Jones, S., Aparicio, S., Chia, S., Ch'ng, C., Deyell, R., Eirew, P., Fok, A., Gelmon, K., Ho, C.*, et al.* (2015). Lessons learned from the application of whole-genome analysis to the treatment of patients with advanced cancers. Cold Spring Harbor molecular case studies *1*, a000570.

Lemee, F., Bergoglio, V., Fernandez-Vidal, A., Machado-Silva, A., Pillaire, M.J., Bieth, A., Gentil, C., Baker, L., Martin, A.L., Leduc, C.*, et al.* (2010). DNA polymerase theta up-regulation is associated with poor survival in breast cancer, perturbs DNA replication, and promotes genetic instability. Proc Natl Acad Sci U S A *107*, 13390-13395.

Lemmens, B.B., Johnson, N.M., and Tijsterman, M. (2013). COM-1 promotes homologous recombination during Caenorhabditis elegans meiosis by antagonizing Ku-mediated non-homologous end joining. PLoS Genet *9*, e1003276.

Leon-Ortiz, A.M., Panier, S., Sarek, G., Vannier, J.B., Patel, H., Campbell, P.J., and Boulton, S.J. (2018). A Distinct Class of Genome Rearrangements Driven by Heterologous Recombination. Mol Cell *69*, 292-305.e296.

Li, H., Handsaker, B., Wysoker, A., Fennell, T., Ruan, J., Homer, N., Marth, G., Abecasis, G., and Durbin, R. (2009). The Sequence Alignment/Map format and SAMtools. Bioinformatics *25*, 2078-2079.

Li, L., Li, Y., Zhao, J., Fan, S., Wang, L., and Li, X. (2016). CX-5461 induces autophagy and inhibits tumor growth via mammalian target of rapamycin-related signaling pathways in osteosarcoma. Onco Targets Ther *9*, 5985-5997.

Li, Q., Saito, T.T., Martinez-Garcia, M., Deshong, A.J., Nadarajan, S., Lawrence, K.S., Checchi, P.M., Colaiacovo, M.P., and Engebrecht, J. (2018). The tumor suppressor BRCA1-BARD1 complex localizes to the synaptonemal complex and regulates recombination under meiotic dysfunction in Caenorhabditis elegans. PLoS Genet *14*, e1007701.

Li, W., and Yanowitz, J.L. (2019). ATM and ATR Influence Meiotic Crossover Formation Through Antagonistic and Overlapping Functions in Caenorhabditis elegans. Genetics *212*, 431-443.

Lin, A., Giuliano, C.J., Palladino, A., John, K.M., Abramowicz, C., Yuan, M.L., Sausville, E.L., Lukow, D.A., Liu, L., Chait, A.R.*, et al.* (2019). Off-target toxicity is a common mechanism of action of cancer drugs undergoing clinical trials. Sci Transl Med *11*, eaaw8412.

London, T.B., Barber, L.J., Mosedale, G., Kelly, G.P., Balasubramanian, S., Hickson, I.D., Boulton, S.J., and Hiom, K. (2008). FANCJ is a structure-specific DNA helicase associated with the maintenance of genomic G/C tracts. J Biol Chem *283*, 36132-36139.

Lord, C.J., Tutt, A.N., and Ashworth, A. (2015). Synthetic lethality and cancer therapy: lessons learned from the development of PARP inhibitors. Annu Rev Med *66*, 455-470.

Lui, D.Y., and Colaiacovo, M.P. (2013). Meiotic development in Caenorhabditis elegans. Adv Exp Med Biol *757*, 133-170.

Lynch, M., Sung, W., Morris, K., Coffey, N., Landry, C.R., Dopman, E.B., Dickinson, W.J., Okamoto, K., Kulkarni, S., Hartl, D.L.*, et al.* (2008). A genome-wide view of the spectrum of spontaneous mutations in yeast. Proc Natl Acad Sci U S A *105*, 9272-9277.

Macaisne, N., Kessler, Z., and Yanowitz, J.L. (2018). Meiotic Double-Strand Break Proteins Influence Repair Pathway Utilization. Genetics *210*, 843-856.

Mallidi, S., Anbil, S., Bulin, A.L., Obaid, G., Ichikawa, M., and Hasan, T. (2016). Beyond the Barriers of Light Penetration: Strategies, Perspectives and Possibilities for Photodynamic Therapy. Theranostics *6*, 2458-2487.

Marechal, A., and Zou, L. (2013). DNA damage sensing by the ATM and ATR kinases. Cold Spring Harb Perspect Biol *5*.

Marteijn, J.A., Lans, H., Vermeulen, W., and Hoeijmakers, J.H. (2014). Understanding nucleotide excision repair and its roles in cancer and ageing. Nat Rev Mol Cell Biol *15*, 465-481.

Martin, J.S., Winkelmann, N., Petalcorin, M.I., McIlwraith, M.J., and Boulton, S.J. (2005). RAD-51-dependent and -independent roles of a Caenorhabditis elegans BRCA2-related protein during DNA double-strand break repair. Mol Cell Biol *25*, 3127-3139.

Mateos-Gomez, P.A., Gong, F., Nair, N., Miller, K.M., Lazzerini-Denchi, E., and Sfeir, A. (2015). Mammalian polymerase theta promotes alternative NHEJ and suppresses recombination. Nature *518*, 254-257.

Mayle, R., Campbell, I.M., Beck, C.R., Yu, Y., Wilson, M., Shaw, C.A., Bjergbaek, L., Lupski, J.R., and Ira, G. (2015). Mus81 and converging forks limit the mutagenicity of replication fork breakage. Science *349*, 742.

McCarthy, E.E., Celebi, J.T., Baer, R., and Ludwig, T. (2003). Loss of Bard1, the heterodimeric partner of the Brca1 tumor suppressor, results in early embryonic lethality and chromosomal instability. Mol Cell Biol *23*, 5056-5063.

McLellan, J.L., O'Neil, N.J., Barrett, I., Ferree, E., van Pel, D.M., Ushey, K., Sipahimalani, P., Bryan, J., Rose, A.M., and Hieter, P. (2012). Synthetic lethality of cohesins with PARPs and replication fork mediators. PLoS Genet *8*, e1002574.

Meier, B., Cooke, S.L., Weiss, J., Bailly, A.P., Alexandrov, L.B., Marshall, J., Raine, K., Maddison, M., Anderson, E., Stratton, M.R.*, et al.* (2014). C. elegans whole-genome sequencing reveals mutational signatures related to carcinogens and DNA repair deficiency. Genome Res *24*, 1624-1636.

Meier, B., Volkova, N.V., Hong, Y., Schofield, P., Campbell, P.J., Gerstung, M., and Gartner, A. (2018). Mutational signatures of DNA mismatch repair deficiency in C. elegans and human cancers. Genome Res *28*, 666-675.

Min, A., Im, S.A., Yoon, Y.K., Song, S.H., Nam, H.J., Hur, H.S., Kim, H.P., Lee, K.H., Han, S.W., Oh, D.Y.*, et al.* (2013). RAD51C-deficient cancer cells are highly sensitive to the PARP inhibitor olaparib. Mol Cancer Ther *12*, 865-877.

Minocherhomji, S., Ying, S., Bjerregaard, V.A., Bursomanno, S., Aleliunaite, A., Wu, W., Mankouri, H.W., Shen, H., Liu, Y., and Hickson, I.D. (2015). Replication stress activates DNA repair synthesis in mitosis. Nature *528*, 286-290.

Mortelmans, K., and Zeiger, E. (2000). The Ames Salmonella/microsome mutagenicity assay. Mutat Res *455*, 29-60.

Mosbech, A., Gibbs-Seymour, I., Kagias, K., Thorslund, T., Beli, P., Povlsen, L., Nielsen, S.V., Smedegaard, S., Sedgwick, G., Lukas, C*., et al.* (2012). DVC1 (C1orf124) is a DNA damage-targeting p97 adaptor that promotes ubiquitin-dependent responses to replication blocks. Nat Struct Mol Biol *19*, 1084-1092.

Muzzini, D.M., Plevani, P., Boulton, S.J., Cassata, G., and Marini, F. (2008). Caenorhabditis elegans POLQ-1 and HEL-308 function in two distinct DNA interstrand cross-link repair pathways. DNA Repair (Amst) *7*, 941-950.

Naim, V., Wilhelm, T., Debatisse, M., and Rosselli, F. (2013). ERCC1 and MUS81-EME1 promote sister chromatid separation by processing late replication intermediates at common fragile sites during mitosis. Nat Cell Biol *15*, 1008-1015.

Negi, S.S., and Brown, P. (2015). rRNA synthesis inhibitor, CX-5461, activates ATM/ATR pathway in acute lymphoblastic leukemia, arrests cells in G2 phase and induces apoptosis. Oncotarget *6*, 18094-18104.

Negrini, S., Gorgoulis, V.G., and Halazonetis, T.D. (2010). Genomic instability--an evolving hallmark of cancer. Nat Rev Mol Cell Biol *11*, 220-228.

Nickoloff, J.A., Jones, D., Lee, S.H., Williamson, E.A., and Hromas, R. (2017). Drugging the Cancers Addicted to DNA Repair. J Natl Cancer Inst *109*.

Nitiss, J.L. (2009). Targeting DNA topoisomerase II in cancer chemotherapy. Nat Rev Cancer *9*, 338-350.

Noordermeer, S.M., Adam, S., Setiaputra, D., Barazas, M., Pettitt, S.J., Ling, A.K., Olivieri, M., Alvarez-Quilon, A., Moatti, N., Zimmermann, M*., et al.* (2018). The shieldin complex mediates 53BP1-dependent DNA repair. Nature *560*, 117-121.

Nowsheen, S., and Yang, E.S. (2012). The intersection between DNA damage response and cell death pathways. Exp Oncol *34*, 243-254.

O'Connell, B.C., Adamson, B., Lydeard, J.R., Sowa, M.E., Ciccia, A., Bredemeyer, A.L., Schlabach, M., Gygi, S.P., Elledge, S.J., and Harper, J.W. (2010). A genome-wide camptothecin sensitivity screen identifies a mammalian MMS22L-NFKBIL2 complex required for genomic stability. Mol Cell *40*, 645-657.

O'Neil, N.J., Bailey, M.L., and Hieter, P. (2017). Synthetic lethality and cancer. Nat Rev Genet *18*, 613-623.

O'Neil, N.J., Martin, J.S., Youds, J.L., Ward, J.D., Petalcorin, M.I., Rose, A.M., and Boulton, S.J. (2013). Joint molecule resolution requires the redundant activities of MUS-81 and XPF-1 during Caenorhabditis elegans meiosis. PLoS Genet *9*, e1003582.

Olivier, M., Hollstein, M., and Hainaut, P. (2010). TP53 mutations in human cancers: origins, consequences, and clinical use. Cold Spring Harb Perspect Biol *2*, a001008.

Ossowski, S., Schneeberger, K., Lucas-Lledo, J.I., Warthmann, N., Clark, R.M., Shaw, R.G., Weigel, D., and Lynch, M. (2010). The rate and molecular spectrum of spontaneous mutations in Arabidopsis thaliana. Science *327*, 92-94.

Panier, S., and Boulton, S.J. (2014). Double-strand break repair: 53BP1 comes into focus. Nat Rev Mol Cell Biol *15*, 7-18.

Park, S., Choi, S., and Ahn, B. (2016). DNA Strand Breaks in Mitotic Germ Cells of Caenorhabditis elegans Evaluated by Comet Assay. Mol Cells *39*, 204-210.

Paulsen, R.D., Soni, D.V., Wollman, R., Hahn, A.T., Yee, M.C., Guan, A., Hesley, J.A., Miller, S.C., Cromwell, E.F., Solow-Cordero, D.E.*, et al.* (2009). A genome-wide siRNA screen reveals diverse cellular processes and pathways that mediate genome stability. Mol Cell *35*, 228-239.

Pelttari, L.M., Kinnunen, L., Kiiski, J.I., Khan, S., Blomqvist, C., Aittomaki, K., and Nevanlinna, H. (2016). Screening of HELQ in breast and ovarian cancer families. Fam Cancer *15*, 19-23.

Pena-Diaz, J., and Jiricny, J. (2012). Mammalian mismatch repair: error-free or error-prone? Trends Biochem Sci *37*, 206-214.

Peng, M., Cong, K., Panzarino, N.J., Nayak, S., Calvo, J., Deng, B., Zhu, L.J., Morocz, M., Hegedus, L., Haracska, L.*, et al.* (2018). Opposing Roles of FANCJ and HLTF Protect Forks and Restrain Replication during Stress. Cell reports *24*, 3251-3261.

Pichierri, P., Franchitto, A., Piergentili, R., Colussi, C., and Palitti, F. (2001). Hypersensitivity to camptothecin in MSH2 deficient cells is correlated with a role for MSH2 protein in recombinational repair. Carcinogenesis *22*, 1781-1787.

Pollard, M.O., Gurdasani, D., Mentzer, A.J., Porter, T., and Sandhu, M.S. (2018). Long reads: their purpose and place. Hum Mol Genet *27*, R234-r241.

Pommier, Y. (2013). Drugging topoisomerases: lessons and challenges. ACS Chem Biol *8*, 82-95.

Pommier, Y., O'Connor, M.J., and de Bono, J. (2016). Laying a trap to kill cancer cells: PARP inhibitors and their mechanisms of action. Sci Transl Med *8*, 362ps317.

Poole, L.A., and Cortez, D. (2017). Functions of SMARCAL1, ZRANB3, and HLTF in maintaining genome stability. Crit Rev Biochem Mol Biol *52*, 696-714.

Poon, S.L., Pang, S.T., McPherson, J.R., Yu, W., Huang, K.K., Guan, P., Weng, W.H., Siew, E.Y., Liu, Y., Heng, H.L.*, et al.* (2013). Genome-wide mutational signatures of aristolochic acid and its application as a screening tool. Sci Transl Med *5*, 197ra101.

Prakash, R., Zhang, Y., Feng, W., and Jasin, M. (2015). Homologous recombination and human health: the roles of BRCA1, BRCA2, and associated proteins. Cold Spring Harb Perspect Biol *7*, a016600.

Rastogi, R.P., Richa, Kumar, A., Tyagi, M.B., and Sinha, R.P. (2010). Molecular mechanisms of ultraviolet radiation-induced DNA damage and repair. Journal of nucleic acids *2010*, 592980.

Regairaz, M., Zhang, Y.W., Fu, H., Agama, K.K., Tata, N., Agrawal, S., Aladjem, M.I., and Pommier, Y. (2011). Mus81-mediated DNA cleavage resolves replication forks stalled by topoisomerase I-DNA complexes. J Cell Biol *195*, 739-749.

Roberts, S.A., Lawrence, M.S., Klimczak, L.J., Grimm, S.A., Fargo, D., Stojanov, P., Kiezun, A., Kryukov, G.V., Carter, S.L., Saksena, G.*, et al.* (2013). An APOBEC cytidine deaminase mutagenesis pattern is widespread in human cancers. Nat Genet *45*, 970-976.

Roberts, S.A., Sterling, J., Thompson, C., Harris, S., Mav, D., Shah, R., Klimczak, L.J., Kryukov, G.V., Malc, E., Mieczkowski, P.A.*, et al.* (2012). Clustered mutations in yeast and in human cancers can arise from damaged long single-strand DNA regions. Mol Cell *46*, 424-435.

Roerink, S.F., Koole, W., Stapel, L.C., Romeijn, R.J., and Tijsterman, M. (2012). A broad requirement for TLS polymerases eta and kappa, and interacting sumoylation and nuclear pore proteins, in lesion bypass during C. elegans embryogenesis. PLoS Genet *8*, e1002800.

Roerink, S.F., van Schendel, R., and Tijsterman, M. (2014). Polymerase theta-mediated end joining of replication-associated DNA breaks in C. elegans. Genome Res *24*, 954-962.

Rosenbluth, R.E., Cuddeford, C., and Baillie, D.L. (1983). Mutagenesis in Caenorhabditis elegans: I. A rapid eukaryotic mutagen test system using the reciprocal translocation, eTI(III;V). Mutation Research/Fundamental and Molecular Mechanisms of Mutagenesis *110*, 39-48.

Rosenbluth, R.E., Cuddeford, C., and Baillie, D.L. (1985). Mutagenesis in Caenorhabditis elegans. II. A spectrum of mutational events induced with 1500 r of gamma-radiation. Genetics *109*, 493-511.

Rosenquist, T.A., and Grollman, A.P. (2016). Mutational signature of aristolochic acid: Clue to the recognition of a global disease. DNA Repair (Amst) *44*, 205-211.

Saito, T.T., and Colaiacovo, M.P. (2017). Regulation of Crossover Frequency and Distribution during Meiotic Recombination. Cold Spring Harb Symp Quant Biol *82*, 223-234.

Sale, J.E. (2013). Translesion DNA synthesis and mutagenesis in eukaryotes. Cold Spring Harb Perspect Biol *5*, a012708.

Schafer, B., Neffgen, A., and Klinner, U. (2008). A novel yeast-based tool to detect mutagenic and recombinogenic effects simultaneously. Mutat Res *652*, 20-29.

Schimmel, J., Kool, H., van Schendel, R., and Tijsterman, M. (2017). Mutational signatures of non-homologous and polymerase theta-mediated end-joining in embryonic stem cells. EMBO J *36*, 3634-3649.

Schrider, D.R., Houle, D., Lynch, M., and Hahn, M.W. (2013). Rates and genomic consequences of spontaneous mutational events in Drosophila melanogaster. Genetics *194*, 937-954.

Schrider, D.R., Hourmozdi, J.N., and Hahn, M.W. (2011). Pervasive multinucleotide mutational events in eukaryotes. Curr Biol *21*, 1051-1054.

Schwab, R.A., Nieminuszczy, J., Shin-ya, K., and Niedzwiedz, W. (2013). FANCJ couples replication past natural fork barriers with maintenance of chromatin structure. J Cell Biol *201*, 33-48.

Segovia, R., Shen, Y., Lujan, S.A., Jones, S.J., and Stirling, P.C. (2017). Hypermutation signature reveals a slippage and realignment model of translesion synthesis by Rev3 polymerase in cisplatin-treated yeast. Proc Natl Acad Sci U S A *114*, 2663-2668.

Semlow, D.R., Zhang, J., Budzowska, M., Drohat, A.C., and Walter, J.C. (2016). Replication-Dependent Unhooking of DNA Interstrand Cross-Links by the NEIL3 Glycosylase. Cell *167*, 498-511 e414.

Serero, A., Jubin, C., Loeillet, S., Legoix-Ne, P., and Nicolas, A.G. (2014). Mutational landscape of yeast mutator strains. Proc Natl Acad Sci U S A *111*, 1897-1902.

Sfeir, A., and Symington, L.S. (2015). Microhomology-Mediated End Joining: A Back-up Survival Mechanism or Dedicated Pathway? Trends Biochem Sci *40*, 701-714.

Shin, N., Cuenca, L., Karthikraj, R., Kannan, K., and Colaiacovo, M.P. (2019). Assessing effects of germline exposure to environmental toxicants by high-throughput screening in C. elegans. PLoS Genet *15*, e1007975.

Sieber, O.M., Lipton, L., Crabtree, M., Heinimann, K., Fidalgo, P., Phillips, R.K., Bisgaard, M.L., Orntoft, T.F., Aaltonen, L.A., Hodgson, S.V.*, et al.* (2003). Multiple colorectal adenomas, classic adenomatous polyposis, and germ-line mutations in MYH. N Engl J Med *348*, 791-799.

Stiborova, M., Bieler, C.A., Wiessler, M., and Frei, E. (2001). The anticancer agent ellipticine on activation by cytochrome P450 forms covalent DNA adducts. Biochem Pharmacol *62*, 1675-1684.

Stiborova, M., Sejbal, J., Borek-Dohalska, L., Aimova, D., Poljakova, J., Forsterova, K., Rupertova, M., Wiesner, J., Hudecek, J., Wiessler, M.*, et al.* (2004). The anticancer drug ellipticine forms covalent DNA adducts, mediated by human cytochromes P450, through metabolism to 13-hydroxyellipticine and ellipticine N2-oxide. Cancer Res *64*, 8374-8380.

Stingele, J., Bellelli, R., Alte, F., Hewitt, G., Sarek, G., Maslen, S.L., Tsutakawa, S.E., Borg, A., Kjaer, S., Tainer, J.A*., et al.* (2016). Mechanism and Regulation of DNA-Protein Crosslink Repair by the DNA-Dependent Metalloprotease SPRTN. Mol Cell *64*, 688-703.

Stirling, P.C., Bloom, M.S., Solanki-Patil, T., Smith, S., Sipahimalani, P., Li, Z., Kofoed, M., Ben-Aroya, S., Myung, K., and Hieter, P. (2011). The complete spectrum of yeast chromosome instability genes identifies candidate CIN cancer genes and functional roles for ASTRA complex components. PLoS Genet *7*, e1002057.

Stockley, T.L., Oza, A.M., Berman, H.K., Leighl, N.B., Knox, J.J., Shepherd, F.A., Chen, E.X., Krzyzanowska, M.K., Dhani, N., Joshua, A.M*., et al.* (2016). Molecular profiling of advanced solid tumors and patient outcomes with genotype-matched clinical trials: the Princess Margaret IMPACT/COMPACT trial. Genome Med *8*, 109.

Stratton, M.R., Campbell, P.J., and Futreal, P.A. (2009). The cancer genome. Nature *458*, 719-724.

Su, Y., Meador, J.A., Calaf, G.M., Proietti De-Santis, L., Zhao, Y., Bohr, V.A., and Balajee, A.S. (2010). Human RecQL4 helicase plays critical roles in prostate carcinogenesis. Cancer Res *70*, 9207-9217.

Sugasawa, K., Okamoto, T., Shimizu, Y., Masutani, C., Iwai, S., and Hanaoka, F. (2001). A multistep damage recognition mechanism for global genomic nucleotide excision repair. Genes Dev *15*, 507-521.

Swanton, C., Soria, J.C., Bardelli, A., Biankin, A., Caldas, C., Chandarlapaty, S., de Koning, L., Dive, C., Feunteun, J., Leung, S.Y*., et al.* (2016). Consensus on precision medicine for metastatic cancers: a report from the MAP conference. Ann Oncol *27*, 1443-1448.

Tafel, A.A., Wu, L., and McHugh, P.J. (2011). Human HEL308 localizes to damaged replication forks and unwinds lagging strand structures. J Biol Chem *286*, 15832-15840.

Takata, K., Reh, S., Tomida, J., Person, M.D., and Wood, R.D. (2013). Human DNA helicase HELQ participates in DNA interstrand crosslink tolerance with ATR and RAD51 paralogs. Nature communications *4*, 2338.

Taylor, M.R.G., Spirek, M., Chaurasiya, K.R., Ward, J.D., Carzaniga, R., Yu, X., Egelman, E.H., Collinson, L.M., Rueda, D., Krejci, L*., et al.* (2015). Rad51 Paralogs Remodel Pre-synaptic Rad51 Filaments to Stimulate Homologous Recombination. Cell *162*, 271-286.

Taylor, M.R.G., Spirek, M., Jian Ma, C., Carzaniga, R., Takaki, T., Collinson, L.M., Greene, E.C., Krejci, L., and Boulton, S.J. (2016). A Polar and Nucleotide-Dependent Mechanism of Action for RAD51 Paralogs in RAD51 Filament Remodeling. Mol Cell *64*, 926-939.

Thompson, O., Edgley, M., Strasbourger, P., Flibotte, S., Ewing, B., Adair, R., Au, V., Chaudhry, I., Fernando, L., Hutter, H*., et al.* (2013). The million mutation project: a new approach to genetics in Caenorhabditis elegans. Genome Res *23*, 1749-1762.

Tijsterman, M., Pothof, J., and Plasterk, R.H. (2002). Frequent germline mutations and somatic repeat instability in DNA mismatch-repair-deficient Caenorhabditis elegans. Genetics *161*, 651-660.

Treszezamsky, A.D., Kachnic, L.A., Feng, Z., Zhang, J., Tokadjian, C., and Powell, S.N. (2007). BRCA1- and BRCA2-deficient cells are sensitive to etoposide-induced DNA double-strand breaks via topoisomerase II. Cancer Res *67*, 7078-7081.

Truong, L.N., Li, Y., Shi, L.Z., Hwang, P.Y., He, J., Wang, H., Razavian, N., Berns, M.W., and Wu, X. (2013). Microhomology-mediated End Joining and Homologous Recombination share the initial end resection step to repair DNA double-strand breaks in mammalian cells. Proc Natl Acad Sci U S A *110*, 7720-7725.

Tutt, A., Robson, M., Garber, J.E., Domchek, S.M., Audeh, M.W., Weitzel, J.N., Friedlander, M., Arun, B., Loman, N., Schmutzler, R.K.*, et al.* (2010). Oral poly(ADP-ribose) polymerase inhibitor olaparib in patients with BRCA1 or BRCA2 mutations and advanced breast cancer: a proof-of-concept trial. Lancet *376*, 235-244.

van Bostelen, I., and Tijsterman, M. (2017). Combined loss of three DNA damage response pathways renders C. elegans intolerant to light. DNA Repair (Amst) *54*, 55-62.

van Schendel, R., Roerink, S.F., Portegijs, V., van den Heuvel, S., and Tijsterman, M. (2015). Polymerase Theta is a key driver of genome evolution and of CRISPR/Cas9-mediated mutagenesis. Nature communications *6*, 7394.

van Schendel, R., van Heteren, J., Welten, R., and Tijsterman, M. (2016). Genomic Scars Generated by Polymerase Theta Reveal the Versatile Mechanism of Alternative End-Joining. PLoS Genet *12*, e1006368.

Vaz, B., Popovic, M., Newman, J.A., Fielden, J., Aitkenhead, H., Halder, S., Singh, A.N., Vendrell, I., Fischer, R., Torrecilla, I.*, et al.* (2016). Metalloprotease SPRTN/DVC1 Orchestrates Replication-Coupled DNA-Protein Crosslink Repair. Mol Cell *64*, 704-719.

Verma, P., and Greenberg, R.A. (2016). Noncanonical views of homology-directed DNA repair. Genes Dev *30*, 1138-1154.

Walsh, C.S. (2015). Two decades beyond BRCA1/2: Homologous recombination, hereditary cancer risk and a target for ovarian cancer therapy. Gynecol Oncol *137*, 343-350.

Wang, L., Wang, S., Yin, J.J., Fu, P.P., and Yu, H. (2009). Light-Induced Toxic Effects of Tamoxifen: A Chemotherapeutic and Chemopreventive Agent. J Photochem Photobiol A Chem *201*, 50-56.

Wang, S.Y., Mao, H., Shibuya, H., Uzawa, S., O'Brown, Z.K., Wesenberg, S., Shin, N., Saito, T.T., Gao, J., Meyer, B.J.*, et al.* (2019a). The demethylase NMAD-1 regulates DNA replication and repair in the Caenorhabditis elegans germline. PLoS Genet *15*, e1008252.

Wang, T., Wei, J.J., Sabatini, D.M., and Lander, E.S. (2014). Genetic screens in human cells using the CRISPR-Cas9 system. Science *343*, 80-84.

Wang, Z., Song, Y., Li, S., Kurian, S., Xiang, R., Chiba, T., and Wu, X. (2019b). DNA polymerase theta (POLQ) is important for repair of DNA double-strand breaks caused by fork collapse. J Biol Chem *294*, 3909-3919.

Ward, J.D., Barber, L.J., Petalcorin, M.I., Yanowitz, J., and Boulton, S.J. (2007). Replication blocking lesions present a unique substrate for homologous recombination. EMBO J *26*, 3384-3396.

Ward, J.D., Muzzini, D.M., Petalcorin, M.I., Martinez-Perez, E., Martin, J.S., Plevani, P., Cassata, G., Marini, F., and Boulton, S.J. (2010). Overlapping mechanisms promote postsynaptic RAD-51 filament disassembly during meiotic double-strand break repair. Mol Cell *37*, 259-272.

Wei, T., Najmi, S.M., Liu, H., Peltonen, K., Kucerova, A., Schneider, D.A., and Laiho, M. (2018). Small-Molecule Targeting of RNA Polymerase I Activates a Conserved Transcription Elongation Checkpoint. Cell reports *23*, 404-414.

Wilson, D.M., 3rd, Rieckher, M., Williams, A.B., and Schumacher, B. (2017). Systematic analysis of DNA crosslink repair pathways during development and aging in Caenorhabditis elegans. Nucleic Acids Res *45*, 9467-9480.

Wright, W.D., Shah, S.S., and Heyer, W.D. (2018). Homologous recombination and the repair of DNA double-strand breaks. J Biol Chem *293*, 10524-10535.

Wyatt, H.D., Sarbajna, S., Matos, J., and West, S.C. (2013). Coordinated actions of SLX1-SLX4 and MUS81-EME1 for Holliday junction resolution in human cells. Mol Cell *52*, 234-247.

Xu, H., Di Antonio, M., McKinney, S., Mathew, V., Ho, B., O'Neil, N.J., Santos, N.D., Silvester, J., Wei, V., Garcia, J.*, et al.* (2017). CX-5461 is a DNA G-quadruplex stabilizer with selective lethality in BRCA1/2 deficient tumours. Nature communications *8*, 14432.

Yang, B., Xu, X., Russell, L., Sullenberger, M.T., Yanowitz, J.L., and Maine, E.M. (2019). A DNA repair protein and histone methyltransferase interact to promote genome stability in the Caenorhabditis elegans germ line. PLoS Genet *15*, e1007992.

Yang, J., Yu, Y., Hamrick, H.E., and Duerksen-Hughes, P.J. (2003). ATM, ATR and DNA-PK: initiators of the cellular genotoxic stress responses. Carcinogenesis *24*, 1571-1580.

Yanovsky, R.L., Bartenstein, D.W., Rogers, G.S., Isakoff, S.J., and Chen, S.T. (2019). Photodynamic therapy for solid tumors: A review of the literature. Photodermatol Photoimmunol Photomed *35*, 295-303.

Yin, Y., and Smolikove, S. (2013). Impaired resection of meiotic double-strand breaks channels repair to nonhomologous end joining in Caenorhabditis elegans. Mol Cell Biol *33*, 2732-2747.

Ying, S., Minocherhomji, S., Chan, K.L., Palmai-Pallag, T., Chu, W.K., Wass, T., Mankouri, H.W., Liu, Y., and Hickson, I.D. (2013). MUS81 promotes common fragile site expression. Nat Cell Biol *15*, 1001-1007.

Yoon, D.S., Choi, Y., Cha, D.S., Zhang, P., Choi, S.M., Alfhili, M.A., Polli, J.R., Pendergrass, D., Taki, F.A., Kapalavavi, B.*, et al.* (2017). Triclosan Disrupts SKN-1/Nrf2-Mediated Oxidative Stress Response in C. elegans and Human Mesenchymal Stem Cells. Sci Rep *7*, 12592.

Yoon, J.H., McArthur, M.J., Park, J., Basu, D., Wakamiya, M., Prakash, L., and Prakash, S. (2019). Error-Prone Replication through UV Lesions by DNA Polymerase theta Protects against Skin Cancers. Cell *176*, 1295-1309 e1215.

Youds, J.L., Barber, L.J., and Boulton, S.J. (2009). C. elegans: a model of Fanconi anemia and ICL repair. Mutat Res *668*, 103-116.

Youds, J.L., Barber, L.J., Ward, J.D., Collis, S.J., O'Neil, N.J., Boulton, S.J., and Rose, A.M. (2008). DOG-1 is the Caenorhabditis elegans BRIP1/FANCJ homologue and functions in interstrand cross-link repair. Mol Cell Biol *28*, 1470-1479.

Youds, J.L., O'Neil, N.J., and Rose, A.M. (2006). Homologous recombination is required for genome stability in the absence of DOG-1 in Caenorhabditis elegans. Genetics *173*, 697-708.

Yousefzadeh, M.J., Wyatt, D.W., Takata, K., Mu, Y., Hensley, S.C., Tomida, J., Bylund, G.O., Doublie, S., Johansson, E., Ramsden, D.A.*, et al.* (2014). Mechanism of suppression of chromosomal instability by DNA polymerase POLQ. PLoS Genet *10*, e1004654.

Yuen, K.W., Warren, C.D., Chen, O., Kwok, T., Hieter, P., and Spencer, F.A. (2007). Systematic genome instability screens in yeast and their potential relevance to cancer. Proc Natl Acad Sci U S A *104*, 3925-3930.

Zalevsky, J., MacQueen, A.J., Duffy, J.B., Kemphues, K.J., and Villeneuve, A.M. (1999). Crossing over during Caenorhabditis elegans meiosis requires a conserved MutS-based pathway that is partially dispensable in budding yeast. Genetics *153*, 1271-1283.

Zellweger, R., Dalcher, D., Mutreja, K., Berti, M., Schmid, J.A., Herrador, R., Vindigni, A., and Lopes, M. (2015). Rad51-mediated replication fork reversal is a global response to genotoxic treatments in human cells. The Journal of Cell Biology *208*, 563.

Zhao, J., Jain, A., Iyer, R.R., Modrich, P.L., and Vasquez, K.M. (2009). Mismatch repair and nucleotide excision repair proteins cooperate in the recognition of DNA interstrand crosslinks. Nucleic Acids Res *37*, 4420-4429.

Zhao, L., and Washington, M.T. (2017). Translesion Synthesis: Insights into the Selection and Switching of DNA Polymerases. Genes (Basel) *8*.

Zhao, Y., Tarailo-Graovac, M., O'Neil, N.J., and Rose, A.M. (2008). Spectrum of mutational events in the absence of DOG-1/FANCJ in Caenorhabditis elegans. DNA Repair *7*, 1846-1854.

Zheng, H., Wang, X., Warren, A.J., Legerski, R.J., Nairn, R.S., Hamilton, J.W., and Li, L. (2003). Nucleotide excision repair- and polymerase eta-mediated error-prone removal of mitomycin C interstrand cross-links. Mol Cell Biol *23*, 754-761.

Zimmermann, M., Murina, O., Reijns, M.A.M., Agathanggelou, A., Challis, R., Tarnauskaite, Z., Muir, M., Fluteau, A., Aregger, M., McEwan, A.*, et al.* (2018). CRISPR screens identify genomic ribonucleotides as a source of PARP-trapping lesions. Nature *559*, 285-289.

Zou, Y., Liu, Y., Wu, X., and Shell, S.M. (2006). Functions of human replication protein A (RPA): from DNA replication to DNA damage and stress responses. J Cell Physiol *208*, 267-273.

Zuba, E.B., Koronowska, S., Osmola-Mankowska, A., and Jenerowicz, D. (2016). Drug-induced Photosensitivity. Acta dermatovenerologica Croatica : ADC *24*, 55-64.

APPENDIX

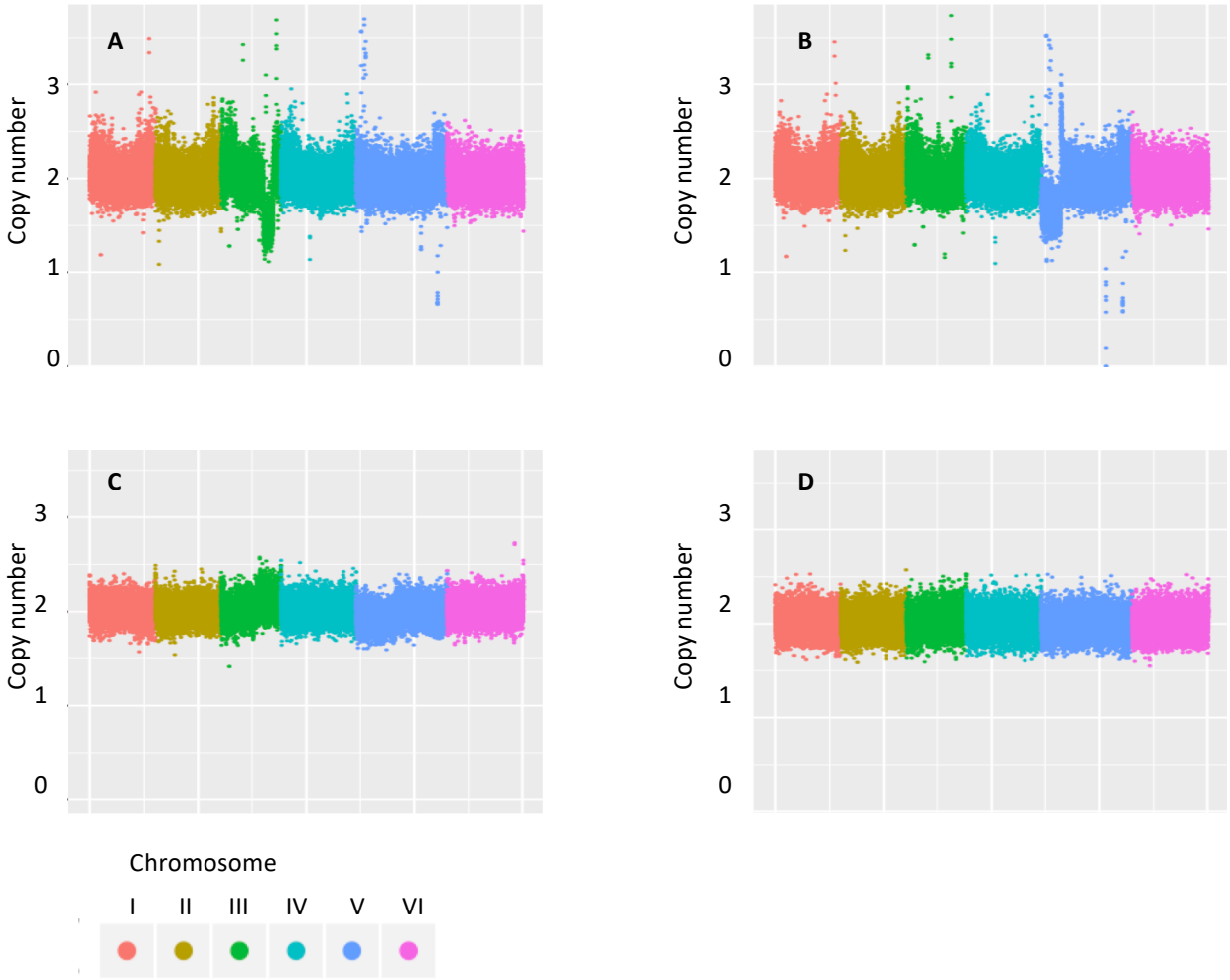

Figure A3.1 Coverage plot of CX-5461-induced genome rearrangements (A-D, 4 in total)

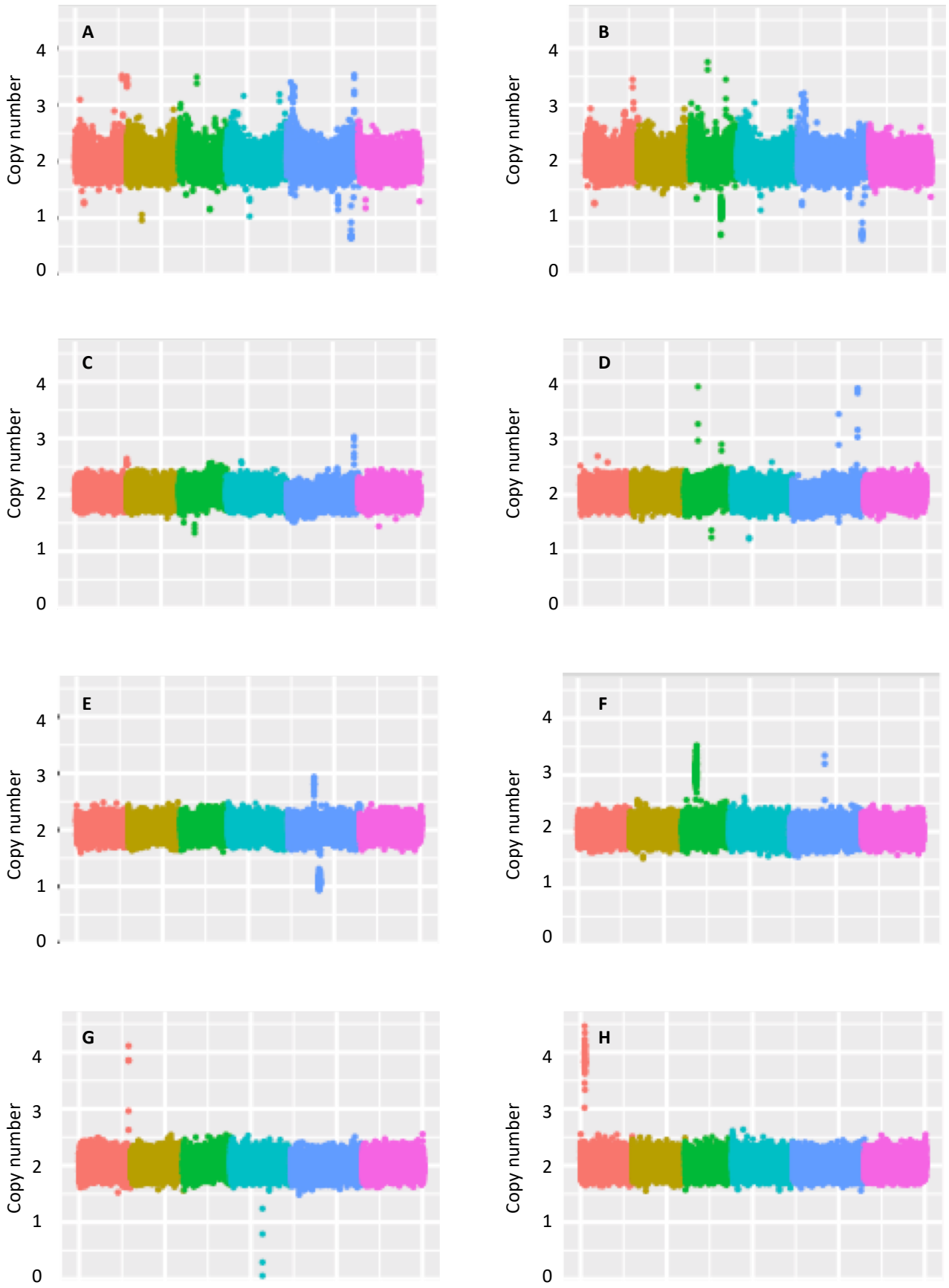
A
B
C
D
E
F
G
H
Copy number
0
1
2
3
4

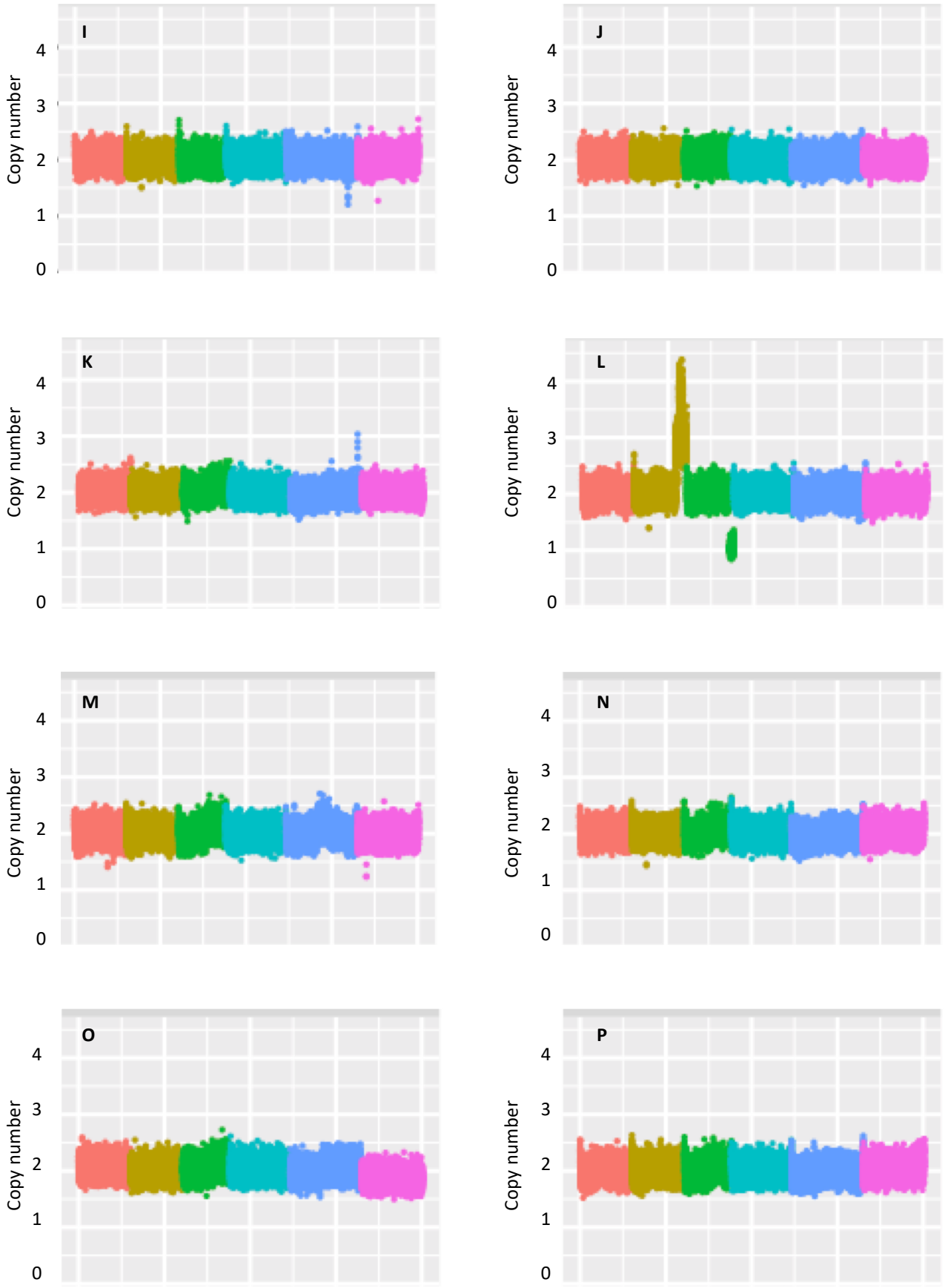
I
J
K
L
M
N
O
P
Copy number
0
1
2
3
4

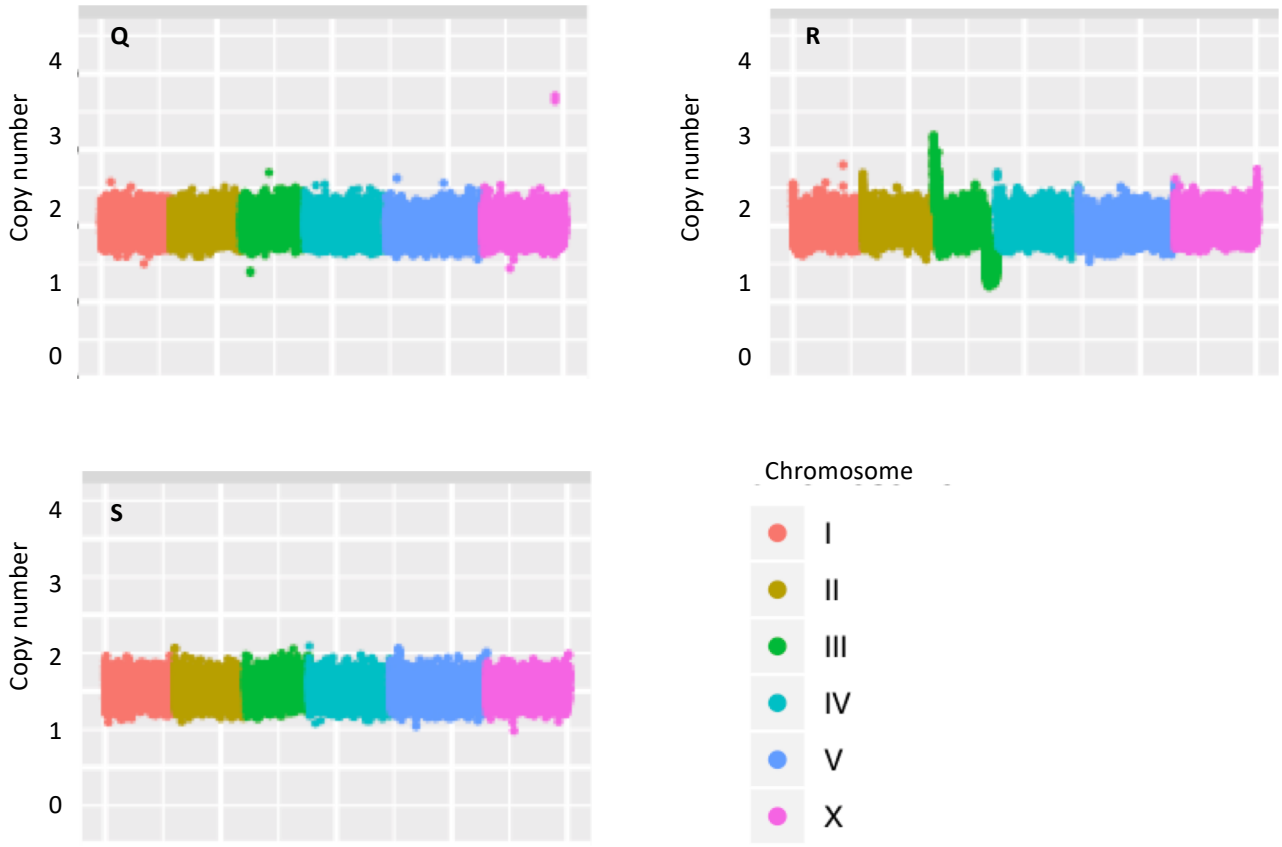

Figure A3.2 Coverage plot of CX-5461 + UVA-induced genome rearrangements (A-S, 19 in total)

cku-80

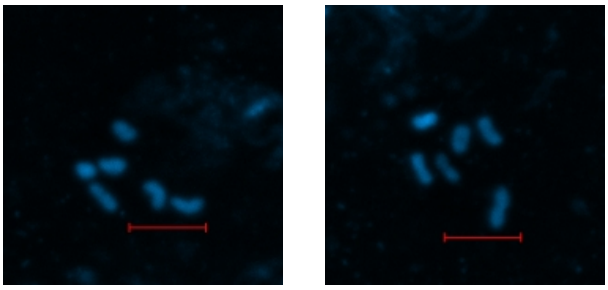

6 6

polq-1

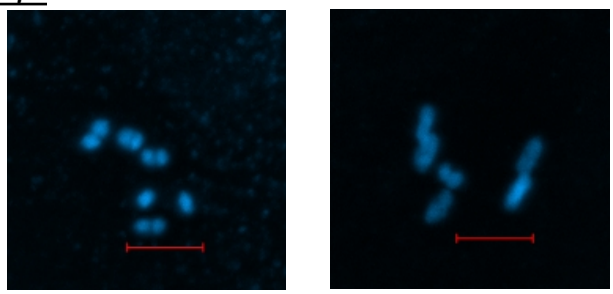

6 6

Figure A4.1 Representative images of DAPI-stained bodies in diakinesis of *cku-80* and *polq-1* single mutants. Both mutants have a near wild-type phenotype that displays six DAPI-stained bodies in diakinesis. Numbers below indicate the number of DAPI-stained bodies per nuclei. Scale bar denotes 5 μm.

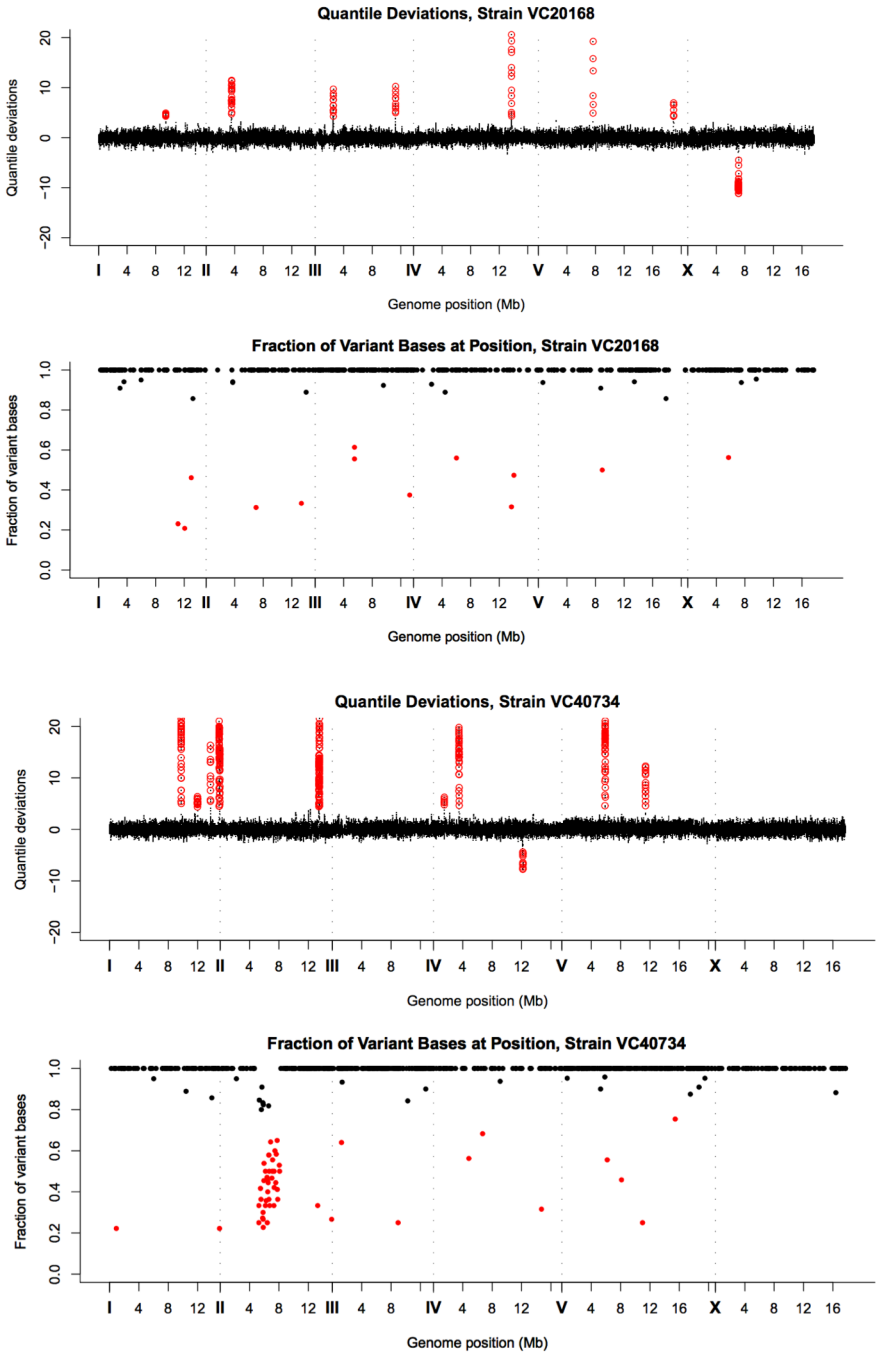

Figure A5.1 Coverage plot of quantile deviations and fractions of variant basis of Million Mutation Project collection strains VC20168 and VC40734. Pictures were screenshotted from http://genome.sfu.ca/mmp/. (Thompson et al., 2013)

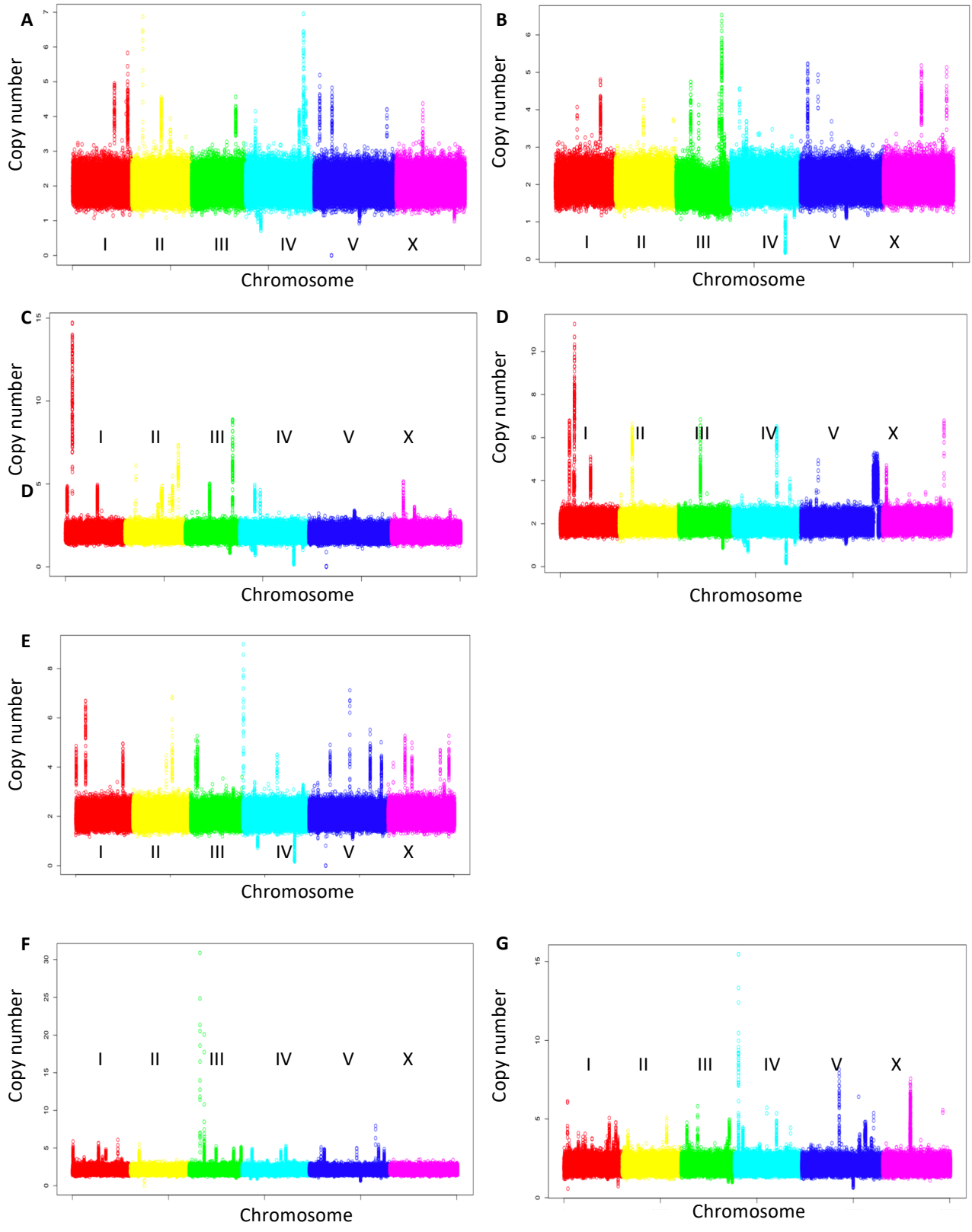

Figure A5.2 Coverage plot of genome rearrangements of F_{10} *gk176502* (A - E) and F_{10} *gk784642* (F - G).

Genotype	DMSO		500 µM Ola		Sensitivity score	P-value (in t-test with mock treatment)	P-value (in t-test with N2)
	Embryo survival rate %	Number of progeny counted	Embryo survival rate %	Number of progeny counted			
N2	99.83±0.29	522	98.25±1.97	411	1.00	0.3392	
mus-81	90.74±4.62	436	59.80±0.99	345	0.67	0.0046	0.0009
atm-1	79.64±6.27	330	44.10±9.61	352	0.56	0.0250	0.0097
polq-1	98.52±1.03	479	97.47±1.72	433	1.01	0.5155	0.7388
him-1	99.81±0.33	465	99.40±0.59	464	1.01	0.5107	0.4651
cku-80	99.07±0.30	533	99.10±0.79	442	1.02	0.9233	0.5217
gen-1	99.30±0.64	422	99.78±0.38	414	1.02	0.3478	0.3653
fncm-1	77.71±7.04	490	76.38±11.73	499	1.00	0.9097	0.0780
fan-1	99.65±0.61	269	88.08±2.74	343	0.90	0.0113	0.0029
rfs-1	92.47±4.37	489	87.17±1.91	477	0.96	0.1397	0.0590
dog-1	99.73±0.47	318	90.26±8.64	416	0.92	0.2123	0.1588
rtel-1	99.77±0.41	398	99.77±0.41	409	1.02	1.0000	0.3618
N2	98.62±0.88	501	96.73±1.69	429	1.00	0.3222	
mus-81	91.77±6.12	306	63.70±7.63	252	0.71	0.0096	0.0207
him-6	40.15±2.17	475	45.14±4.79	306	1.15	0.0876	0.0014
ercc-1	68.09±2.94	396	71.63±3.98	467	1.07	0.1503	0.0112
helq-1	88.22±7.79	399	69.42±2.88	372	0.80	0.0829	0.0044
fcd-2	99.61±0.68	485	97.66±0.97	424	1.00	0.1667	0.5232
let-418	96.70±2.88	188	96.29±3.40	234	1.02	0.8362	0.8156
N2	97.75±2.04	454	94.87±4.75	243	1.00	0.5383	
mus-81	91.12±3.23	130	35.83±9.27	274	0.41	0.0118	0.0113
rcq-5	99.46±0.47	374	98.61±0.86	307	1.02	0.1833	0.2989
cdk-5	99.22±0.71	424	99.25±0.66	267	1.03	0.9721	0.2558
polk-1	98.47±0.87	403	99.05±0.89	299	1.04	0.3957	0.2015
cep-1	98.89±0.40	296	98.90±1.91	288	1.03	0.9969	0.3993
brd-1	97.92±3.61	279	99.16±0.87	371	1.04	0.6243	0.2372
N2	99.73±0.47	394	98.41±0.36	441	1.00	0.0638	
mus-81	90.46±8.13	197	33.19±3.59	186	0.37	0.0135	0.0012
msh-2	83.85±9.81	364	84.64±2.05	292	1.02	0.9043	0.0093
N2	99.43±0.50	356	98.48±0.77	269	1.00	0.1332	
mus-81	92.96±7.18	117	55.94±5.46	223	0.61	0.0069	0.0046
rev-3	90.45±3.85	216	87.82±3.88	200	0.98	0.4479	0.0302
polh-1	93.88±2.96	390	91.59±10.68	454	0.99	0.6592	0.3936
N2	98.08±0.43	364	99.33±0.58	314	1.00	0.0349	
mus-81	90.24±3.62	218	38.45±12.26	263	0.42	0.0138	0.0131
lig-4	99.65±0.60	289	98.01±1.05	305	0.97	0.0393	0.1837
xpa-1	98.72±1.24	287	95.18±2.42	295	0.95	0.1400	0.0808
wrn-1	98.77±1.07	332	98.10±1.42	300	0.98	0.3981	0.3982
hsr-9	65.94±7.68	304	60.28±12.76	326	0.90	0.6756	0.0365
N2	99.71±0.51	341	99.23±0.79	401	1.00	0.4856	
mus-81	90.62±2.18	247	39.84±13.47	232	0.44	0.0296	0.0175
gld-1	94.43±1.95	261	89.30±1.85	247	0.95	0.0606	0.0226
hda-3	93.45±0.91	341	80.84±2.31	343	0.87	0.0398	0.0156

Table A1.1 Raw data for generating the sensitivity scores for Olaparib.

Genotype	DMSO		100 nM CPT		Sensitivity score	P-value (in t-test with mock treatment)	P-value (in t-test with N2)
	Embryo survival rate %	Number of progeny counted	Embryo survival rate %	Number of progeny counted			
N2	98.55±0.57	547	98.30±1.30	485	1.00	0.6284	
mus-81	94.27±3.34	433	6.63±1.68	312	0.07	0.0001	0.0001
fncm-1	97.49±1.67	485	98.24±0.75	385	1.01	0.6404	0.9284
fan-1	99.07±0.80	241	99.59±0.70	267	1.01	0.3492	0.3593
rfs-1	93.99±1.52	381	17.42±7.96	308	0.19	0.0048	0.0033
dog-1	97.58±1.51	284	88.83±10.94	326	0.91	0.3344	0.2839
rtel-1	99.23±0.87	407	98.09±1.07	385	0.99	0.2244	0.8237
N2	99.78±0.37	407	97.12±0.76	309	1.00	0.0260	
mus-81	91.07±2.88	389	0.32±0.56	362	0.00	0.0005	0.0001
him-1	80.55±7.22	216	25.80±3.13	218	0.33	0.0047	0.0009
smrc-1	84.98±4.64	362	10.10±6.07	331	0.12	0.0054	0.0015
N2	98.62±0.88	501	98.43±0.92	397	1.00	0.8329	
mus-81	91.77±6.12	306	3.21±4.73	266	0.04	0.0025	0.0008
him-6	40.15±2.17	475	39.05±8.25	334	0.97	0.8690	0.0059
ercc-1	68.09±2.94	396	67.68±1.88	388	1.00	0.5749	0.0026
helq-1	88.22±7.79	399	10.43±2.87	362	0.12	0.0060	0.0006
atm-1	82.60±2.55	406	29.59±4.23	479	0.36	0.0046	0.0013
fcd-2	99.61±0.68	485	99.25±0.75	399	1.00	0.5945	0.4357
let-418	96.70±2.88	188	96.53±0.61	346	1.00	0.9114	0.1411
polq-1	96.94±2.19	445	92.28±8.14	367	0.95	0.4335	0.3330
cku-80	99.32±0.04	444	99.39±0.06	496	1.00	0.3350	0.2295
N2	97.75±2.04	454	56.39±1.81	203	1.00	0.0000	
mus-81	91.12±3.23	130	1.47±1.45	214	0.03	0.0007	0.0001
rcq-5	99.46±0.47	374	62.26±1.50	172	1.09	0.0005	0.0620
polk-1	98.47±0.87	403	61.34±8.30	203	1.08	0.0186	0.4625
N2	99.73±0.47	394	96.15±1.22	298	1.00	0.0232	
mus-81	90.46±8.13	197	0.95±0.82	242	0.01	0.0032	0.0001
msh-2	83.85±9.81	364	33.67±12.08	300	0.42	0.0151	0.0110
brd-1	97.85±2.35	370	16.28±3.02	308	0.17	0.0001	0.0009
cep-1	96.50±1.49	364	56.05±10.23	218	0.60	0.0263	0.0201
N2	99.43±0.50	356	99.33±0.58	278	1.00	0.8655	
mus-81	92.96±7.18	117	1.66±1.88	176	0.02	0.0002	0.0002
rev-3	90.45±3.85	216	86.79±5.68	138	0.96	0.1302	0.0726
polh-1	93.88±2.96	390	58.29±9.59	273	0.62	0.0354	0.0161
N2	98.08±0.43	364	87.93±7.60	335	1.00	0.1373	
mus-81	90.24±3.62	218	1.09±1.89	196	0.01	0.0007	0.0038
lig-4	99.65±0.60	289	83.22±0.28	262	0.93	0.0004	0.3913
wrn-1	98.77±1.07	332	81.84±4.78	246	0.92	0.0158	0.4779
cdk-5	99.08±0.81	237	74.92±7.96	210	0.84	0.0396	0.1438
N2	99.71±0.51	341	77.70±11.64	288	1.00	0.0819	
mus-81	90.62±2.18	247	0.34±0.60	254	0.00	0.0002	0.0068
gld-1	94.43±1.95	261	58.70±18.38	251	0.80	0.0650	0.0960
hda-3	93.45±0.91	341	83.56±2.31	310	1.15	0.2314	0.1622
N2	98.10±1.24	368	97.82±2.05	288	1.00	0.6607	
mus-81	88.92±5.45	131	6.86±6.95	158	0.08	0.0075	0.0014
xpa-1	96.07±1.73	321	94.46±1.60	326	0.99	0.2465	0.0109
N2	99.28±0.69	393	95.75±3.75	357	1.00	0.2023	
hsr-9	78.32±9.18	307	69.32±16.32	310	0.92	0.5990	0.1282
dvc-1	89.60±7.96	346	88.90±2.88	256	1.03	0.8351	0.0169

Table A1.2 Raw data for generating the sensitivity scores for Camptothecin.

Genotype	DMSO		100 μM ETOP		Sensitivity score	P-value (in t-test with mock treatment)	P-value (in t-test with N2)
	Embryo survival rate %	Number of progeny counted	Embryo survival rate %	Number of progeny counted			
N2	90.75±2.88	454	82.93±9.38	316	1.00	0.1980	
mus-81	75.56±11.80	268	4.24±2.61	273	0.06	0.0126	0.0068
polq-1	90.56±2.17	519	26.38±6.32	363	0.32	0.0018	0.0203
helq-1	84.31±4.25	519	59.32±5.38	465	0.77	0.0090	0.0677
brd-1	86.79±3.26	479	65.12±5.40	491	0.82	0.0490	0.1016
rfs-1	65.79±7.82	453	32.89±6.03	511	0.55	0.0496	0.0195
N2	91.76±7.59	462	83.98±8.70	386	1.00	0.1954	
mus-81	89.81±3.39	304	5.53±0.28	326	0.07	0.0005	0.0042
gld-1	94.01±3.26	272	81.36±6.01	311	0.95	0.0656	0.3420
polh-1	91.88±4.89	252	58.25±3.87	309	0.69	0.0004	0.0265
fan-1	98.13±1.14	471	96.34±0.44	466	1.07	0.1848	0.1437
fcd-2	91.84±1.40	405	94.78±2.34	424	1.13	0.2582	0.1228
fncm-1	94.69±1.79	453	91.33±3.73	418	1.05	0.1977	0.4132
N2	97.57±1.83	305	80.10±3.88	331	1.00	0.0230	
mus-81	88.84±3.41	292	7.76±5.00	268	0.11	0.0003	0.0002
wrn-1	97.82±1.33	316	92.09±4.43	405	1.15	0.0912	0.1102
lig-4	97.27±1.31	392	86.32±0.37	380	1.08	0.0047	0.1004
msh-2	84.72±7.18	228	55.11±5.75	270	0.79	0.0477	0.0374
cep-1	92.51±3.05	389	71.52±5.90	374	0.94	0.0068	0.0201
N2	98.98±0.36	384	85.26±6.23	347	1.00	0.0681	
mus-81	81.53±9.15	354	11.60±4.67	323	0.17	0.0022	0.0064
him-1	85.33±2.23	293	5.89±2.33	271	0.08	0.0003	0.0022
let-418	90.36±2.86	340	78.01±12.55	357	1.00	0.2923	0.2976
hda-3	84.84±3.67	338	60.62±9.55	338	0.83	0.0199	0.0342
ercc-1	63.96±3.72	299	56.16±4.66	366	1.02	0.1630	0.0055
dvc-1	89.25±1.72	357	70.02±12.73	280	0.91	0.1078	0.2374
N2	92.26±1.70	580	91.65±2.37	452	1.00	0.7306	
mus-81	70.07±5.81	447	18.03±4.52	346	0.26	0.0058	0.0026
xpa-1	89.20±1.32	484	81.33±8.81	374	0.92	0.2898	0.1761
rtel-1	80.70±4.84	240	39.32±1.62	326	0.49	0.0066	0.0008
smrc-1	55.54±2.93	365	23.68±5.54	450	0.43	0.0207	0.0041
rcq-5	91.60±3.65	551	89.23±5.91	441	0.98	0.3896	0.6569
N2	98.66±0.44	371	89.75±6.76	483	1.00	0.1634	
mus-81	74.27±7.88	292	8.89±2.58	342	0.13	0.0053	0.0021
atm-1	92.17±2.70	391	60.95±12.57	344	0.73	0.0443	0.0836
rev-3	95.62±1.71	449	89.03±6.15	320	1.02	0.2823	0.9236
dog-1	95.10±4.40	368	43.63±8.32	325	0.50	0.0174	0.0336
cku-80	95.99±4.62	538	92.01±5.76	422	1.05	0.5307	0.3488

Table A1.3 Raw data for generating the sensitivity scores for Etoposide.

Genotype	TMP		TMP + UVA		Sensitivity score	P-value (in t-test with mock treatment)	P-value (in t-test with N2)
	Embryo survival rate %	Number of progeny counted	Embryo survival rate %	Number of progeny counted			
N2	99.82±0.32	506	97.64±1.85	449	1.00	0.1333	
mus-81	91.42±5.51	247	11.73±10.20	146	0.13	0.0027	0.0032
ercc-1	69.87±2.88	516	12.73±2.56	506	0.19	0.0010	0.0007
him-6	46.32±6.52	392	39.06±4.62	452	0.86	0.1856	0.0040
him-9	77.39±3.17	354	11.45±2.63	359	0.15	0.0000	0.0001
cep-1	99.72±0.25	691	93.69±5.28	522	0.96	0.1761	0.2231
gld-1	95.24±1.91	192	97.31±2.46	217	1.04	0.4814	0.9037
N2	98.11±0.97	791	95.42±0.41	832	1.00	0.0221	
mus-81	82.86±0.63	375	25.42±13.53	418	0.32	0.0194	0.2547
polq-1	98.98±0.98	775	52.93±6.79	648	0.55	0.0077	0.0098
brd-1	98.98±0.18	681	49.69±6.63	644	0.52	0.0062	0.0089
rfs-1	91.26±2.89	608	43.15±8.42	588	0.49	0.0166	0.0279
N2	99.44±0.55	541	98.05±0.77	523	1.00	0.2004	
mus-81	87.70±5.36	459	14.74±6.45	397	0.17	0.0029	0.0016
hda-3	96.61±1.35	441	66.61±3.11	442	0.70	0.0013	0.0027
N2	99.22±0.76	369	93.95±2.74	286	1.00	0.0443	
mus-81	87.44±6.10	250	3.97±2.88	275	0.05	0.0014	0.0000
lig-4	98.47±0.52	327	96.02±2.45	308	1.03	0.2444	0.1371
wrn-1	99.36±0.66	454	91.56±6.20	608	0.97	0.1839	0.3684
xpa-1	97.37±2.47	734	28.76±11.75	726	0.31	0.0132	0.0160
N2	99.80±0.35	517	95.39±0.63	574	1.00	0.0162	
mus-81	96.57±0.09	175	19.07±4.39	173	0.21	0.0010	0.0008
hsr-9	95.31±1.81	482	90.22±3.08	452	0.99	0.0507	0.1330
N2	98.73±0.36	704	85.17±11.55	786	1.00	0.1707	
mus-81	91.97±1.10	223	7.14±6.84	171	0.09	0.0026	0.0033
him-1	72.16±7.42	482	51.06±2.62	332	0.82	0.0547	0.0438
fcd-2	97.45±1.53	760	46.19±16.82	655	0.55	0.0334	0.0175
N2	98.88±1.52	570	99.62±0.33	511	1.00	0.4604	
mus-81	92.88±4.20	351	17.13±10.90	287	0.18	0.0119	0.0058
rev-3	93.88±3.02	249	15.42±6.41	239	0.16	0.0031	0.0021
cku-80	99.00±0.68	710	88.69±11.14	635	0.89	0.1114	0.1067
cdk-5	99.62±0.40	838	87.09±14.76	620	0.87	0.2707	0.2759
let-418	92.58±8.29	279	46.85±3.71	242	0.50	0.0208	0.0015
N2	99.71±0.25	702	96.35±3.23	679	1.00	0.2331	
mus-81	89.69±8.15	331	22.82±8.83	314	0.26	0.0039	0.0025
dog-1	98.07±1.38	470	78.28±14.62	547	0.83	0.1609	0.1709
polk-1	99.86±0.25	794	97.20±2.13	830	1.01	0.1511	0.8029
polh-1	73.08±12.52	395	0.00±0.00	390	0.00	0.0096	0.0004
rcq-5	99.63±0.34	792	98.76±1.26	582	1.03	0.2822	0.4365
msh-2	88.38±3.24	671	21.20±3.27	483	0.25	0.0018	0.0007
N2	99.82±0.32	831	94.83±1.78	798	1.00	0.0341	
mus-81	91.42±5.51	375	5.10±1.72	376	0.13	0.0222	0.0002
rtel-1	69.87±2.88	277	50.40±13.74	297	0.63	0.0566	0.0367
atm-1	46.32±6.52	691	55.11±9.97	534	0.67	0.0061	0.0212
fncm-1	77.39±3.17	589	26.31±2.99	647	0.28	0.0004	0.0004
fan-1	99.72±0.25	615	10.67±7.37	621	0.11	0.0019	0.0039
helq-1	95.24±1.91	504	40.01±2.09	699	0.48	0.0068	0.0012
N2	84.51±1.80	687	50.40±13.74	615	1.00	0.0540	
mus-81	40.19±12.91	424	1.62±2.81	309	0.01	0.0003	0.0005
dvc-1	86.63±8.82	709	55.11±9.97	658	0.70	0.0075	0.0203
smrc-1	97.74±0.65	663	26.31±2.99	641	0.75	0.0484	0.0171

Table A1.4 Raw data for generating the sensitivity scores for UVA-Trimethylpsoralen.

Genotype	0J UVC		50J UVC		Sensitivity score	P-value (in t-test with mock treatment)	P-value (in t-test with N2)
	Embryo survival rate %	Number of progeny counted	Embryo survival rate %	Number of progeny counted			
N2	99.19±0.75	582	81.35±5.10	631	1.00	0.0335	
mus-81	91.73±6.97	256	27.05±4.68	205	0.36	0.0007	0.0062
smrc-1	70.73±9.86	382	40.57±3.81	401	0.70	0.0285	0.0007
hsr-9	91.46±0.88	452	67.77±1.42	523	0.90	0.0003	0.0370
polh-1	92.73±3.79	172	1.46±1.30	163	0.02	0.0007	0.0008
N2	99.49±0.89	192	70.51±2.50	606	1.00	0.0041	
mus-81	87.26±2.39	203	18.56±3.77	338	0.30	0.0022	0.0036
xpa-1	91.52±7.83	541	23.53±6.12	328	0.36	0.0062	0.0090
gld-1	88.02±2.08	241	54.69±6.38	205	0.88	0.0067	0.0765
cep-1	99.44±0.97	336	50.01±4.70	797	0.71	0.0026	0.0089
cku-80	100.00±0.00	591	72.33±3.85	528	1.02	0.0064	0.6684
wrn-1	99.22±0.37	521	80.34±3.81	600	1.14	0.0116	0.0151
N2	99.86±0.25	693	72.71±3.27	719	1.00	0.0051	
mus-81	94.45±3.34	558	28.51±1.20	378	0.41	0.0014	0.0021
let-418	85.42±13.68	350	64.70±2.55	305	1.04	0.0951	0.0383
rtel-1	98.69±0.53	390	78.11±2.34	244	1.09	0.0059	0.0364
fncm-1	99.48±0.48	574	59.73±3.39	551	0.82	0.0030	0.0277
fan-1	99.05±1.65	222	70.90±5.76	616	0.98	0.0080	0.6628
fcd-2	99.72±0.49	324	72.24±4.28	511	0.99	0.0066	0.6917
polk-1	99.60±0.40	752	75.37±3.33	693	1.04	0.0071	0.4493
polq-1	99.33±1.16	476	76.95±3.60	490	1.06	0.0043	0.0545
N2	100.00±0.00	222	85.20±6.12	256	1.00	0.0526	
mus-81	90.58±5.53	346	28.34±6.86	308	0.37	0.0043	0.0072
helq-1	91.29±4.36	392	61.62±4.63	448	0.79	0.0117	0.0625
rev-3	91.14±3.49	230	39.33±7.01	233	0.51	0.0132	0.0262
ercc-1	65.80±2.41	464	9.38±2.97	210	0.17	0.0001	0.0031
him-9	83.78±0.97	443	13.03±10.85	117	0.18	0.0085	0.0035
cdk-5	99.59±0.35	487	75.22±7.87	457	0.89	0.0311	0.3152
rfs-1	94.19±3.59	382	80.24±5.56	355	1.00	0.0206	0.1475
N2	100.00±0.00	203	82.30±8.22	169	1.00	0.0650	
mus-81	89.27±6.37	136	26.69±1.88	232	0.36	0.0055	0.0066
dog-1	98.38±1.10	272	73.62±5.16	379	0.91	0.0188	0.3470
rcq-5	99.76±0.42	418	77.30±5.07	467	0.94	0.0162	0.1350
msh-2	86.27±4.60	454	79.55±2.51	450	1.12	0.1432	0.4963
him-6	47.74±4.04	378	32.22±0.97	447	0.82	0.0242	0.0098
brd-1	97.94±1.90	484	74.97±1.42	471	0.93	0.0020	0.3092
N2	99.08±0.80	419	89.49±1.32	546	1.00	0.0159	
mus-81	81.10±6.15	413	31.23±6.17	450	0.43	0.0061	0.0029
him-1	84.42±6.05	385	56.37±1.41	573	0.74	0.0124	0.0018
N2	99.84±0.28	613	77.79±8.06	390	1.00	0.1681	
mus-81	85.24±10.63	251	23.14±6.64	233	0.35	0.0226	0.0036
atm-1	93.68±5.89	263	46.00±4.86	228	0.63	0.0013	0.0107
N2	98.98±0.89	405	89.34±3.06	397	1.00	0.0165	
mus-81	94.60±3.31	236	38.66±9.18	292	0.45	0.0129	0.0162
dvc-1	90.40±10.93	436	77.58±2.39	532	0.95	0.1234	0.0636
N2	99.81±0.33	542	79.05±4.12	508	1.00	0.0150	
mus-81	87.82±7.00	351	23.81±9.06	238	0.34	0.0008	0.0047
hda-3	99.03±1.01	336	73.17±6.99	413	0.93	0.0174	0.4487
N2	98.51±1.37	347	76.77±5.44	651	1.00	0.0286	
mus-81	94.00±3.97	470	28.74±3.95	293	0.39	0.0047	0.0113
lig-4	99.38±0.58	452	75.53±6.87	610	0.98	0.0259	0.8420

Table A1.5 Raw data for generating the sensitivity scores for UVC.

Genotype	Phosphate Buffer		100 µM CX-5461		Sensitivity score	P-value (in t-test with mock treatment)	P-value (in t-test with N2)
	Embryo survival rate %	Number of progeny counted	Embryo survival rate %	Number of progeny counted			
N2	99.70±0.52	388	99.08±0.94	322	1.00	0.4325	
mus-81	93.92±1.01	338	3.24±4.82	270	0.03	0.0006	0.0008
cep-1	99.68±0.56	284	96.62±3.12	196	0.98	0.1902	0.3803
N2	99.79±0.37	407	99.05±0.94	311	1.00	0.3319	
mus-81	90.57±2.62	344	2.50±4.33	239	0.03	0.0012	0.0007
hda-3	99.83±0.30	528	94.72±3.16	345	0.96	0.0976	0.1973
hsr-9	99.75±0.44	435	97.23±3.64	413	0.98	0.3081	0.5068
N2	99.81±0.33	449	94.87±1.68	340	1.00	0.0264	
atm-1	91.57±5.89	154	1.11±1.92	133	0.01	0.0014	0.0001
him-1	89.55±3.60	317	32.94±6.17	202	0.39	0.0096	0.0049
gld-1	97.52±1.73	202	81.05±2.75	148	0.87	0.0151	0.0437
N2	99.22±0.02	384	90.12±8.66	292	1.00	0.2106	
mus-81	92.50±5.10	265	5.58±4.83	196	0.07	0.0038	0.0064
dvc-1	96.09±5.35	178	74.41±5.67	142	0.85	0.0642	0.0885
N2	99.17±0.82	351	96.17±2.42	237	1.00	0.0850	
mus-81	92.23±3.95	298	1.79±3.09	174	0.02	0.0017	0.0000
xpa-1	98.69±1.51	368	25.49±5.22	369	0.27	0.0011	0.0006
ercc-1	55.28±10.11	232	4.18±1.22	415	0.08	0.0160	0.0001
N2	99.32±0.71	465	0.70±300.00	300	1.00	0.0918	
mus-81	86.31±5.57	363	1.72±290.00	290	0.02	0.0019	0.0001
msh-2	96.35±4.51	271	1.80±339.00	339	1.03	0.8917	0.8930
N2	98.84±2.01	389	88.45±0.89	390	1.00	0.0089	
mus-81	87.43±4.64	248	1.45±1.36	206	0.02	0.0016	0.0000
let-418	92.71±4.04	248	63.18±10.21	233	0.76	0.0334	0.0434
polh-1	98.39±1.76	566	7.80±6.89	171	0.09	0.0011	0.0025
N2	99.75±0.43	398	99.67±0.57	312	1.00	0.8932	
mus-81	86.36±8.55	277	0.44±0.77	269	0.01	0.0034	0.0000
lig-4	99.72±0.49	378	99.72±0.49	293	1.00	0.4226	0.9408
rcq-5	98.75±0.42	316	98.15±2.04	251	0.99	0.5868	0.3519
wrn-1	95.96±7.00	449	94.44±5.30	379	0.98	0.2645	0.2486
N2	99.29±0.73	438	99.03±0.96	298	1.00	0.7918	
mus-81	90.91±4.93	339	1.38±1.20	263	0.02	0.0013	0.0000
cku-80	98.79±1.31	349	97.34±0.81	218	0.99	0.2183	0.2307
brd-1	97.49±1.46	315	57.68±4.73	343	0.59	0.0058	0.0028
polq-1	99.07±1.61	451	43.69±3.93	283	0.44	0.0033	0.0025
rfs-1	95.04±0.62	402	55.53±4.41	344	0.59	0.0048	0.0027
helq-1	90.51±2.36	406	10.13±5.96	380	0.11	0.0034	0.0011
N2	99.22±0.77	375	97.38±2.28	154	1.00	0.3074	
dog-1	95.33±3.98	277	89.23±4.65	187	0.95	0.3428	0.2383
N2	99.72±0.49	302	95.30±2.31	273	1.00	0.0521	
mus-81	92.70±4.67	316	0.00±0.00	202	0.00	0.0008	0.0002
fncm-1	97.94±0.43	430	85.23±2.88	295	0.91	0.0124	0.0406
fan-1	98.96±0.96	255	90.27±3.40	266	0.95	0.0593	0.1273
fcd-2	98.21±3.10	416	82.10±11.99	295	0.87	0.2058	0.1755
smrc-1	88.68±0.93	353	19.92±2.21	207	0.24	0.0001	0.0011
rev-3	97.71±10.11	332	1.37±1.22	179	0.01	0.0002	0.0014

Table A1.6 Raw data for generating the sensitivity scores for CX-5461.

Notes for Table A1.1-A1.6. These are the raw data for generating chemi-genetic interaction map of Olaparib (Ola), Camptothecin (CPT), Etoposide (ETOP), UVA-TMP (Trimethylpsoralen), UVC and CX-5461. Different sub-sections in each table indicate different batches of experiments. N2 animals were used as positive control, whereas *mus-81* mutants were often used as a negative control. The calculation of sensitivity score is detailed in Chapter 2 Method.

Worm Strain	Genotype
WPH90	*smrc-1(gk176502)/hT2*
WPH91	*smrc-1(gk784642)/hT2*
WPH92	*dvc-1(ok260);smrc-1(gk176502)*
WPH103	*helq-1(tm2134) cku-80(ok861)*
WPH108	*cku-80(ok861) rfs-1(ok1372)*
WPH114	*cku-80(ok861) polq-1(tm2026)*
WPH124	*helq-1(tm2134) rfs-1(ok1372)/helq-1(tm2134) hT2*
WPH125	*helq-1(tm2134) cku-80(ok861) rfs-1(ok1372)/helq-1(tm2134) + hT2*
WPH132	*polq-1(tm2026) rfs-1(ok1372)*
WPH134	*cku-80(ok861) polq-1(tm2026) rfs-1(ok1372)*
WPH140	*helq-1(tm2134) cku-80(ok861) polq-1(tm2026)*
WPH142	*helq-1(tm2134) polq-1(tm2026)*
WPH145	*helq-1(tm2134) polq-1(tm2026)/helq-1(tm2134) hT2*
WPH147	*polq-1(tm2026) rfs-1(ok1372)/hT2*
WPH148	*cku-80(ok861) polq-1(tm2026) rfs-1(ok1372)/+ hT2*
WPH168	*mus-81(tm1937) dog-1(gk10)*
WPH169	*mus-81(tm1937) dog-1(gk10)/hT2 dog-1(gk10)*
WPH172	*atm-1(tm5027) dog-1(gk10)*
WPH176	*dog-1(gk10);polq-1(tm2026)/hT2(III)*
WPH179	*atm-1(tm5027) dog-1(gk10)/hT2 dog-1(gk10)*
WPH181	*dog-1(gk10);rev-3(gk919715)*
WPH189	*helq-1(tm2134) polq-1(tm2026) rfs-1(ok1372)/helq-1(tm2134) hT2*
WPH191	*helq-1(tm2134) cku-80(ok861) polq-1(tm2026) rfs-1(ok1372)/helq-1(tm2134) + hT2*
WPH201	*brd-1(dw1) rfs-1(ok1372)/hT2*
WPH202	*cku-80(ok861) brd-1(dw1)*
WPH205	*polq-1(tm2026) brd-1(dw1)*
WPH217	*polq-1(tm2026) brd-1(dw1)/hT2*
WPH221	*cku-80(ok861) brd-1(dw1) rfs-1(ok1372)/+ hT2*
WPH222	*cku-80(ok861) brd-1(dw1)/+ hT2*
WPH228	*cku-80(ok861) polq-1(tm2026) brd-1(dw1)/+ hT2*
WPH229	*helq-1(tm2134) brd-1(dw1)/hT2*
WPH229	*dog-1(gk10);smrc-1(gk176502)/hT2*
WPH231	*helq-1(tm2134) polq-1(tm2026) brd-1(dw1)/helq-1(tm2134) hT2*
WPH233	*mus-81(tm1937)/hT2; smrc-1(gk176502)/hT2*
WPH236	*rtel-1(tm1866)lhT2;smrc-1(gk176502)/T2*
WPH243	*helq-1(tm2134) smrc-1(gk176502)/helq-1(tm2134) hT2*
WPH244	*helq-1(tm2134) cku-80(ok861) brd-1(dw1)/helq-1(tm2134) + hT2*
WPH248	*cku-80(ok861) polq-1(tm2026)/+ hT2*
WPH249	*smrc-1 (gk176502)*
WPH250	*smrc-1 (gk784642)*
WPH251	*helq-1(tm2134) brd-1(dw1) rfs-1(ok1372)/helq-1(tm2134) hT2*
WPH279	*spo-11(me44)/+;brd-1(dw1) rfs-1(ok1372)*
WPH281	*rev-3(gk919715)*
WPH282	*helq-1(tm2134) cku-80(ok861) polq-1(tm2026) brd-1(dw1)/helq-1(tm2134) + hT2*

Table A2. Worm strains generated in this thesis. WPH is the Hieter Lab worm collection.